SBORNÍK GEOLOGICKÝCH VĚD
JOURNAL OF GEOLOGICAL SCIENCES

užitá geofyzika

applied geophysics

24

Publikace s. p. Geofyzika, Brno

Vědecký redaktor

RNDr. KAREL CIDLINSKÝ, CSc.

Diskuse o pracích se konala na vědecké radě s. p. Geofyzika,
Brno, dne 7. září 1988

SBORNÍK GEOLOGICKÝCH VĚD
JOURNAL OF GEOLOGICAL SCIENCES

užitá geofyzika

applied geophysics

24

VYDAL ÚSTŘEDNÍ ÚSTAV GEOLOGICKÝ
PRAHA 1990

ISBN 80-7075-011-1

OBSAH

Sbor. geol. věd	Užitá geofyz., 24	Pages 9–49	6 figs.	3 tabs.	– pl.	Praha 1990 ISSN 0036-5319

Airborne geophysical survey in southwest Bohemia (Šumava Mts. piedmont) and its interpretation

Letecké geofyzikální měření v jihozápadních Čechách (Pošumaví) a jeho interpretace

Karel Dědáček[1]–Jan Mašín[2]–Naděžda Šťovíčková[2]–Zdeněk Vejnar[3]–Václav Veselý[4]

Received September 22, 1988

1 : 50 000
21–22, 24, 42
22–11–14, 23, 31–34, 41, 43

Airborne methods
Interpretation
Petrophysics
Magnetic properties
Petrology

Dědáček, K.–Mašín, J.–Šťovíčková, N.–Vejnar, Z.–Veselý, V. (1990): Airborne geophysical survey in southwest Bohemia (Šumava Mts. piedmont) and its interpretation. – Sbor. geol. Věd, užitá Geofyz., 24, *9–49*. Praha.

Abstract: In southwest Bohemia an area of approx. 3 400 km^2 was covered by new airborne magnetometric and gamma spectrometric survey on the scale of 1 : 25 000. In the Barrandian Proterozoic of the surveyed area an expressive zone of magnetic anomalies has been observed over the belts of the products of paleobasalt volcanism, corresponding with the zones of decreased concentration of K, U and Th. Petrological and petrophysical studies proved pyrrhotite as the main carrier of magnetization in the paleobasalts. The surveyed parts of the Central Bohemian Pluton do not exhibit magnetic anomalies. The north-western boundaries of the partial apophyses of the Pluton are distinctly marked in the field of K, U and Th concentrations. In the islets of the Pluton crystalline mantle, the striking magnetic anomalies are associated with products of mafic and also felsic volcanism, containing magnetite. The radiometric anomalies indicate great variability of the rocks of the islet-zone. The Moldanubian part of the study area is characterized by the regional magnetic zones, trending NE–SW. The sources of these zones are metamorphosed volcanics of contrast chemism, containing magnetite. The anomalies of radioactivity, trending E–W, can be traced several tens of kilometers. They are associated with the system of dykes of porphyries and porphyrites.

[1] *Geofyzika, s. p., Brno, Ječná 29a, 612 46 Brno*
[2] *Geofyzika, s. p., závod Praha, Geologická 2, 152 00 Praha 5*
[3] *Ústřední ústav geologický, Malostranské nám. 19, 118 21 Praha 1*
[4] *Uranový průzkum, k. p., Liberec, Tř. 1. máje 108, 460 00 Liberec*

Introduction

In 1982 a new stage of airborne geophysical measurements (magnetometric and gamma spectrometric) and geological interpretation of selected areas in the Bohemian Massif has stard. teln each selected area (approx. of 3 500 km^2) the project is going on in a three-year cycle. The first year is devoted to airborne measurements. The results, i.e. contour maps of ΔT anomalies, total gamma activity and K, U and Th concentrations, are used for planning of the ground verification and selecting anomalies for a detailed survey. These works are carried out during the second year and serve as a basis for geophysical interpretation. The maps of primary data processing are verified and the set of airborne maps is enhanced by the derived magnetic maps (continuation upward to 200 and 750 m above the flight elevation, vertical gradient) and derived gamma spectrometric maps (ratios of Th/U, Th/K concentrations). During the third year, the verified and derived maps are used for complex geophysical and geological interpretation.

The area in southwest Bohemia (Šumava Mts. piedmont) where the airborne survey and the subsequent geological interpretation were accomplished in 1985, includes the southern part of the Central Bohemian Pluton and the adjoining part of the Moldanubicum and Barrandian (approx. 3 400 km^2).

Geological review

The study area includes the following regional-geological units (from W to E): 1. The Domažlice crystalline complex, 2. The Barrandian basin, 3. The Central Bohemian Pluton, 4. The Šumava section of the Moldanubicum (cf. Fig. 1).

The studied area covers the eastern part of the Domažlice crystalline complex, consisting of the Kdyně basic complex and of the Stod granitoid massif. The Kdyně complex is represented by its north-eastern part where the Kdyně massif proper is built of quartz diorite and its crystalline mantle of metabasites represented by various types ol amphibolites whose mafic components are Fe, Mg silicates of the amphibole group and the main accessories are ilmenite and pyrrhotite. Crystalline pelitic-psammitic schists are less abundant. Among them various types of contact hornfelses, sometimes cordieritic, prevail. The Stod massif is built up mainly of biotite granite in which numerous enclaves of quartz diorite and pyroxene-amphibole hornfels occur at the contact with the Kdyně massif.

The study area includes the south-western part of the Barrandian, which with increasing regional metamorphism passes into the rocks of the Domažlice crystalline complex. The boundary between the both units is indistinct and can be defined by the conventional boundary of the biotite isograde.

The lithofacial development of the pelitic-psammitic sediments changes from NW to SE. In this direction the frequency and amount of black (graphitic) schist

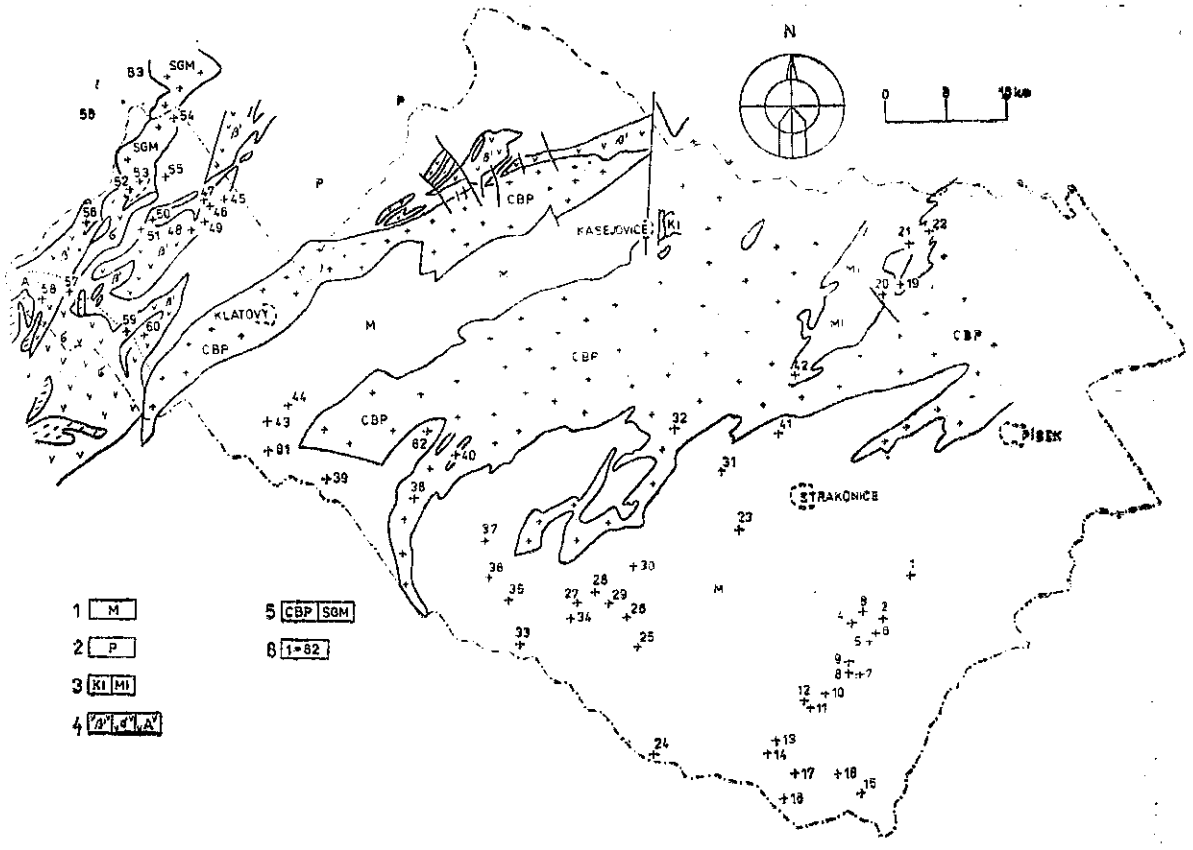

1. Scheme of geological units and sample collection localities

1 – Moldanubicum, *2* – Proterozoic, *3* – KI – Kasejovice islet, MI – Mirovice islet, *4* – mafic volcanics and plutonites: *β'* – Proterozoic basalts ("spilites"), *σ* – Kdyně massif, A – amphibolites, *5* – acid and intermediate plutonites, CBM – Central Bohemian Pluton, SGM – Stod granitoid massif, *6* – sample collection localities (*PŠ* symbol in text)

intercalations increase similarly as the number of pyrite shists and lydites. The greywackes are separated into individual layers and lenses, between Klatovy and Švihov attaining the thickness of hundreds of meters. The mineral association of metapelites in this area is locally enriched with amphibole.

Facial changes can also be observed in belts of metabasites. The number of bodies primarily corresponding to basalts increases also in the NW–SE direction. Their chemical composition is that of tholeiites. Alkaline basalts of the Domažlice crystalline complex occur westwards, outside the study area.

The rocks, between Blovice and Nepomuk, belong also to the Barrandian, and, similarly as in the environs of Klatovy, they are metamorphosed due to the thermal effects of the Central Bohemian Pluton into various types of hornfelses. The lithofacial development of metapelites is very similar to that between Klatovy and Švihov. Strikingly different, however, is the development of paleovolcanites which, besides tholeiitic basalts, include types ranging to andesite.

The Central Bohemian Pluton occupies the prevailing part of the studied area. It is represented by the Klatovy apophysis and by its south-western and southern branched out parts (Kolinec, Hory Matky Boží and Střelské Hoštice apophyses).

The Klatovy apophysis is composed of the Nýrsko biotite granite, the Klatovy biotite-hornblende granodiorite, the Kozlovice biotite-cordierite granodiorite and of marginal-type biotite granite. The petrography of the south-western part of the Pluton is relatively monotonous, composed of the Blatná biotite granodiorite and of the Červená biotite-amphibole granodiorite. In the southern part the Kozárovice (Sázava) biotite-amphibole granodiorite and the porphyritic biotite-amphibole melanocratic granite of Čertovo břemeno occur.

The more important enclaves of the Pluton crystalline mantle in our study area, are represented by the Kasejovice islet, by the Mirovice islet, mainly its southern part formed by the Mirotice orthogneisses, and finally by the southern margin of the Sedlčany–Krásná Hora islet, also composed of the Mirotice orthogneisses.

The Moldanubian part of the study area consists of a lithologically varied complex of rocks. Migmatized paragneisses, sometimes with sillimanite and cordierte, prevail. Intercalations of different rocks comprise quartzites, erlans, crystalline limestones, and amphibolites. Leptynites and orthogneisses can be observed locally.

The local accumulations of various intercalations create in the Šumava section of the Moldanubicum several regional-geological units. From W to E these are: the Strážov varied unit south of Klatovy, the Sušice varied unit, and the Strakonice varied unit. The above mentioned occurrences of migmatites of orthogneises can be ranged to the Podolsko complex.

Local intrusions of granitoid rocks in the Moldanubicum, abundant especially along the contact with the Central Bohemian Pluton, are represented by different types of leucocratic granites, granodiorites and tonalites of the Červená type, and

in the eastern part of the area by porphyritic melanocratic Rastenberg granite, which is equivalent to the Čertovo břemeno type of the Central Bohemian Pluton.

Minor Tertiary relics ranged to the South Bohemian basins, occur near Horaždovice, Strakonice and Písek, in a greater extent in the environs of Protivín and Vodňany where they are more or less associated with the Budějovice basin.

As regards Quaternary sedimentation, this is an area of predominant denudation with minor local deposits, chiefly deluviums and alluviums. In the Otava valley, only relatively thin terraces can be observed.

Outline of previous geophysical measurements

Regional geophysical measurements

At the end of the 1950s the entire area of interest was covered by reconnaissance airborne mapping 1 : 200 000. Much more detailed, however, was the airborne geophysical mapping 1 : 25 000 conducted during the 1960s. Measurements of the total magnetic field were carried out using flux-gate magnetometer with the accuracy ranging between 8 and 13 nT. For radiometric measurements scintillation counter was used.

The entire area of interest was also covered by gravity mapping 1 : 200 000, some parts on the scale of 1 : 50 000.

Physical properties of rocks

The previous petrophysical studies in the area concentrated on the Kdyně-Štěnovice magnetic anomaly. Physical properties of so called spilites in the area were studied by Čejchanová (1971).

Krsová (1976) measured magnetic properties of a set of rock samples from the so called Přeštice zone of the Kdyně-Štěnovice anomaly.

Chlupáčová (1984) studied magnetic properties of rocks in a gallery and in a horizontal drillhole at the locality Struhadlo in the Přeštice magnetic zone. She found out that the magnetic susceptibility characterized the pyrrhotite distribution. The study of magnetic anisotropy implies that magnetic and metamorphic foliations are interrelated and presumably formed by the same deformation. It implies that the pyrrhotite mineralization was pre-deformational or perhaps syndeformational owing to the forming of metamorphic foliation.

In other parts of the area of interest physical properties of rocks were studied separately at individual localities. Physical properties of rocks of the Kasejovice islet were examined by Hron (1963), who collected 75 samples from anomalous magnetic zones and measured their susceptibility and density. Samples described

as quartzitic hornfelses exhibited large values – susceptibility 20.5×10^{-3} to 431×10^{-3} SI units, density 2.82 to 3.03 g . cm^{-3}. Amphibolites were strongly magnetic – susceptibility 12.6×10^{-3} to 80×10^{-3} SI units. Orthogneisses exhibited susceptibility values 3.4×10^{-3} to 23.3×10^{-3} SI units. Other rock samples from the Kasejovice islet did not show increased susceptibility.

Physical properties of rocks of the Kasejovice islet and of the Proterozoic spilite series between Sedliště and Starý Smolivec were studied by Krsová and Šťovíčková (1975). Their results show relatively high susceptibility and remanent magnetization of Proterozoic spilitic rocks. The chief carrier of magnetization was found to be pyrrhotite, in places magnetite. The northern part of the Kasejovice islet is characterized by the presence of magnetite in amphibolites, quartzites, and orthogneisses. On the contrary, in the southern part of the islet some amphibolites contain also pyrrhotite. This is what they have in common with the spilite series. It is also manifested by higher mineralogical densities.

Hron (1963) studied the susceptibilities of various types of Moldanubian orthogneisses from the area of Hartmanice. The obtained values ranged from 0.2×10^{-3} (two-mica sillimanite paragneiss) to 9.2×10^{-3} SI (biotite feldspathized paragneiss).

Local geophysical measurements

The relatively large area of approx. 45 km^2 between Sedliště and Starý Smolivec where the Proterozoic spilite series contacts on the Klatovy apophysis was surveyed by Benda (1973). The network of profiles at 100 m intervals and points at 20 m intervals made it possible to delimit with sufficient accuracy the individual magnetic anomalies. Results can serve for comparison of ground and airborne measurements.

Ground radiometric measurements

Almost the entire study area was covered by a systematic radiometric survey carried out by Uranový průzkum Liberec. Emanometry prevailed namely in the 1950s when it was applied on the scale of 1 : 25 000 (with 250 m intervals between profiles) and in more perspective area on the scale of 1 : 5 000, in places on even more detailed scales. Since the 1970s the survey concentrated on selected localities (1 : 5 000), radiometric sounding moved to greater depths and the gamma method spread. Attention focused mainly on the Klatovy apophysis in the Central Bohemian Pluton, on its north-western exocontact and on the Chanovice apophysis.

Since the 1970s ground gamma spectrometry has been applied on parametric profiles in order to verify the distribution of radioactive elements in the Central Bohemian Pluton and in adjoining geological units, and to estimate the known

anomalies of total radioactivity and emanation. At first the measurements were executed in dug holes, later on in drilled holes 150 mm in diameter, predominantly in eluvial-deluvial covers.

New airborne geophysical survey

Airborne magnetometric and gamma spectrometric survey was carried out using the proton magnetometer G 801/3 B (Geometrics) and the difference four-channel gamma spectrometer DiGRS 3001 (Exploranium).

The magnetometer detector is mounted at the edge of the right wing of the aircraft. Detectors of the gamma spectrometer are eight NaI(Tl) crystals of the total volume of 14 830 cm^3 which are placed inside the aircraft.

The equipment comprises electronic navigation system Mini Ranger III, Motorola, which enables navigation of the aircraft along the planned path, digital recording of the local coordinates of the points of measurements and calculation of the real flight path. Owing to the accurate location the quality of the resultant geophysical maps is greatly increased. A limiting factor of the electronic navigation, however, is the condition of direct visibility between the aircraft and two ground reference stations. Where this is impossible, the aircraft must be navigated by the navigator and the coordinates are interpolated using orientation points that he has chosen. Then, of course, the accuracy of locating the measured data is decreased.

Of basic importance for the airborne survey is the field verification system which was used together with the desk-computer Olivetti M 20. The system enables immediate processing of daily measurements on test profiles, processing of diurnal variations and their introduction to the measured values, subtraction of the background and reduction for altitude.

Furthermore, in all channels on all measured profiles the obtained data were tested for gross errors. Simultaneously, flight paths were checked. The system as a whole enabled daily checks of the quality of measurements.

The entire area was surveyed on the scale of 1 : 25 000, i.e. the flight lines were parallel, at 250 m intervals. Moreover, so called tie lines, perpendicular to the flight lines at 2.5 km intervals, were flown. Measurements on both flight and tie lines were conducted at a ground clearance between 60 and 100 m (the average was 80 m). The velocity of the aircraft ranged from 130 to 140 km per hour. The azimuth of the flight lines was 145° (325°).

Measurements in calibration zones with known concentrations of radio-elements were used to calculate the sensitivities for the given system and altitude of 80 m:

50.0 c.p.s./1 % K (in K-window)
6.0 c.p.s./1 ppm U (in U-window)
2.5 c.p.s./1 ppm Th (in Th-window)
20.0 c.p.s./1 Ur (in TC-window)

The evaluation of daily measurements of the natural gamma spectrometer background showed that in 1983 the variability of radioactivity in atmosphere was favourably low.

Every day the system was checked during flight on a test line. Nevertheless, the accuracy of individual measurements in the study area can be better evaluated by a new method of adjustment of field values on the basis of a network of basic and tie lines. In the point of intersection of a basic and a tie line the obtained values should be equal. The difference between these values is given by the sum of errors of both measurements. By evaluating several tens of thousands of differences obtained at the points of intersection throughout the study area we get the mean error of one measurement as shown in Table 1.

Table 1

Mean error of measurement

Channel	Mean error of measurement	
	measured quantity	processed quantity
Magnetometry	1.1–2.1 nT	1.10–2.1 nT
Potassium	4.5–6.2 c.p.s.	0.09–0.12 % K
Uranium	1.8–2.5 c.p.s.	0.30–0.4 ppm U
Thorium	1.2–1.8 c.p.s.	0.50–0.7 ppm Th
Total count	11–18 c.p.s.	0.60–0.9 Ur

The presented range of mean errors follows from the fact that in some parts of the study area the variability of the measured quantity is small, while elsewhere anomalies are more abundant and thus, naturally, the error of one measurement increases.

To process the results of measurements and compile contour maps we applied a new method, making full use of navigation data and of an accurate location of the points of measurement.

Observing the planned flight velocity, we take measurements at 35–40 m intervals on profiles 250 m apart. The obtained values of magnetic channels are corrected for geomagnetic field diurnal variations, reduced for the normal geomagnetic field and adjusted according to points of intersection of flight and tie lines. Gamma spectrometric values are corrected for natural backgrounds and adjusted according to the points of intersection.

Another important step was evaluating the secular variation between the time of measurement and the epoch 1981. The presented magnetic maps of contour lines are related to the normal field for the epoch 1981.0 for which was used the

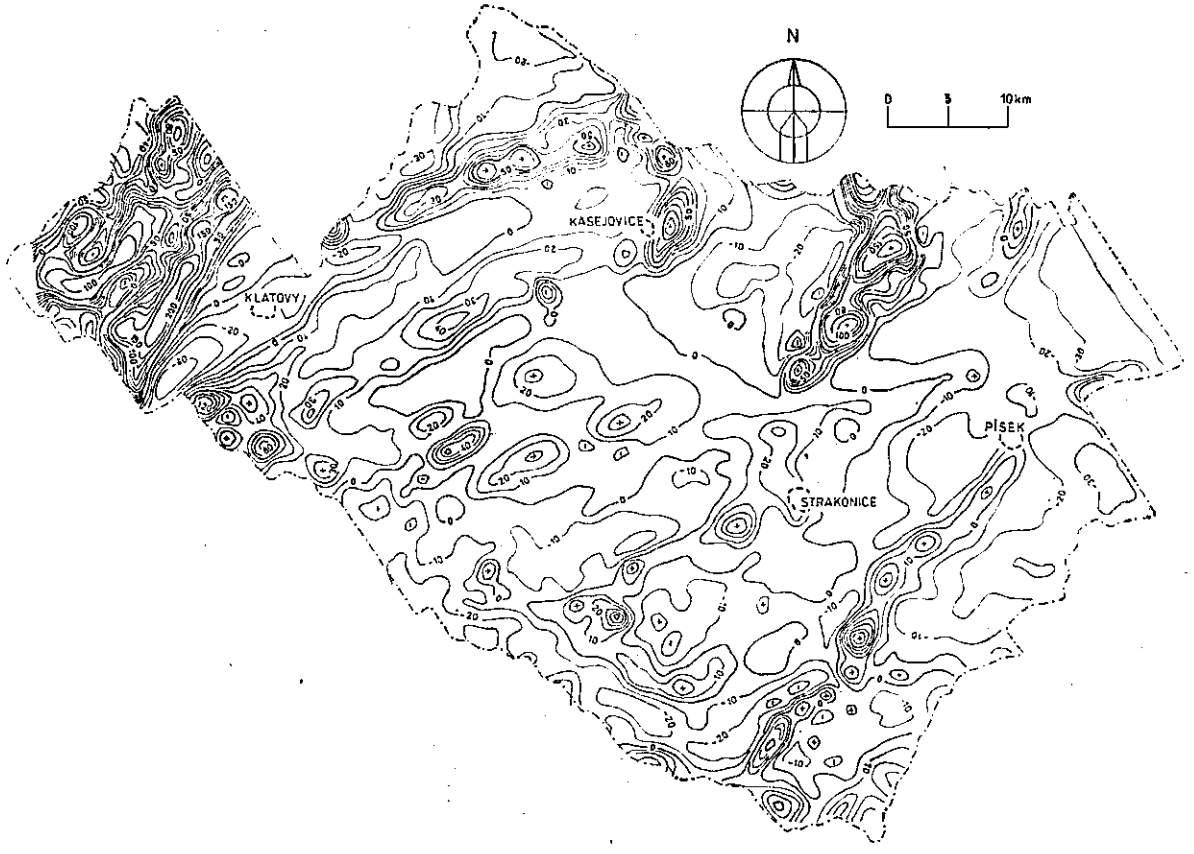

2. Airborne magnetometry, analytical continuation of ΔT to the level of 200 m above the flight altitude

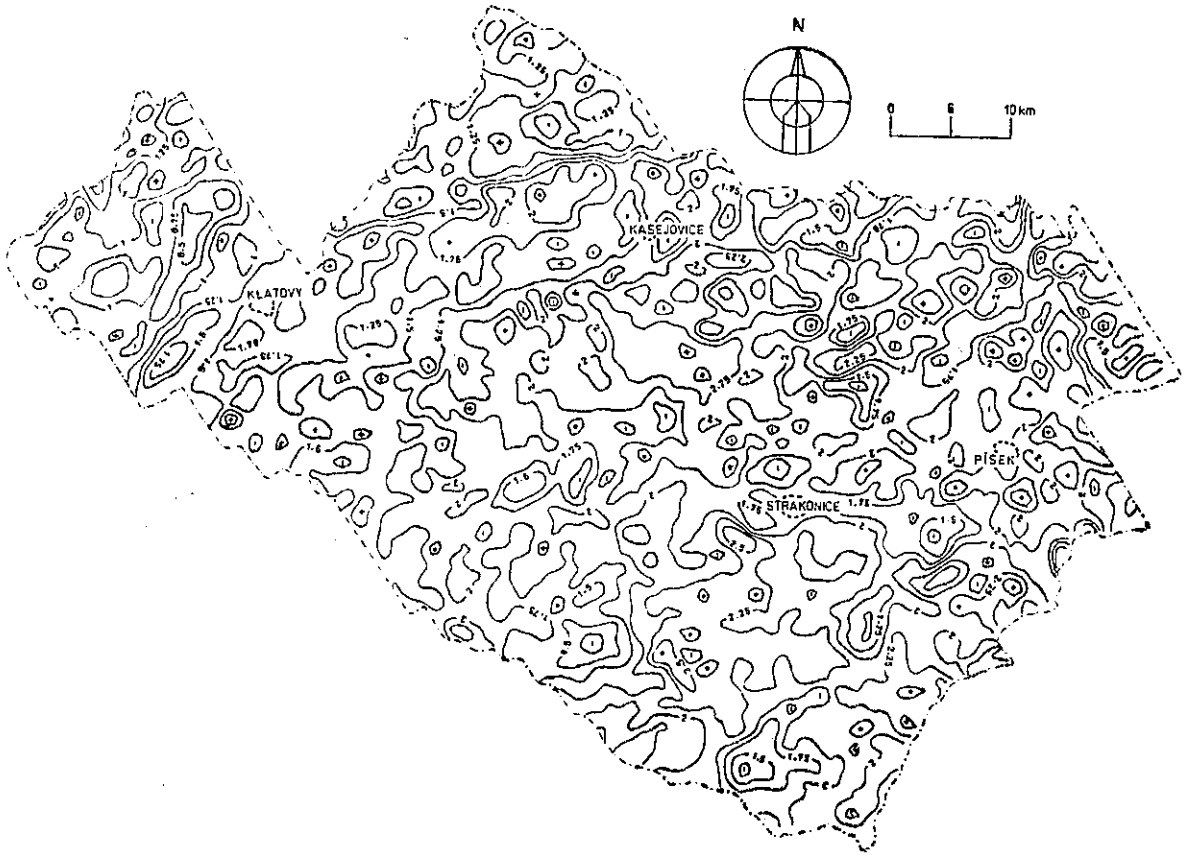

3. Airborne gamma spectrometry, concentration of potassium

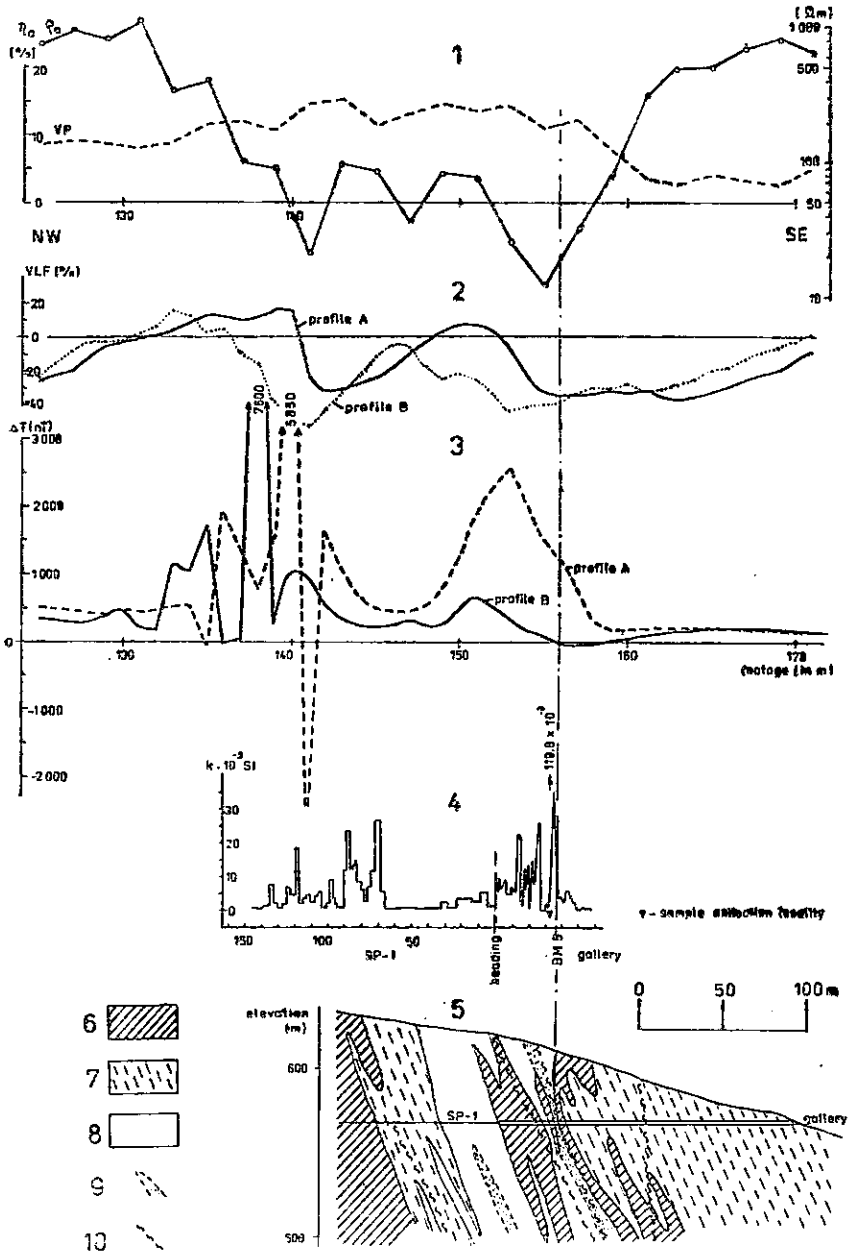

4. Geophysical profiles above Tetětice gallery

1 – profile A – apparent specific resistivity and induct polarization, *2* – VLF method, *3* – magnetometry, *4* – susceptibility measured in gallery and borehole SP-1, *5* – geological profile, *6* – basalts and metabasites, *7* – greywacke schists and aleurolites, *8* – grafitic schists with metabasite intercalations, *9* – stratiform ore mineralization, *10* – mylonite zones

relation

$$T_{1981.0}(\lambda, \varphi) = 48\,012 + 66.7(\lambda - 15) + 262.6(\varphi - 50),$$

where λ is longitude and φ latitude in degrees.

This particular way of data processing employs all the obtained values including location data of the navigation system in order to construct the resultant maps. Thus reliability of results is guaranteed.

The airborne geophysical survey yielded contour maps of the measured parameters and derived magnetic and isoradiation contour maps. Also the maps of analytical continuation of magnetic field upwards to 200 and 750 m above the flight level and the vertical gradient of the analytical continuation of magnetic field at 200 m above the flight level. Radiometric data are presented in the form of contour maps of total count, K, U, and Th concentrations. The K, U, and Th concentrations were used to calculate maps of Th/U, Th/K ratios.

The scale of maps was 1 : 50 000, in some cases 1 : 200 000. The contour map of magnetic field continued upward 200 m above the flight level is in Fig. 2. As an example of radiometric map the contour map of K concentration is shown in Fig. 3.

Ground verification of airborne data

Interpretation of aeromagnetic measurements was based on previous geophysical works, namely reports of Šalanský and Manová (1966, 1974, 1976) and on available geological material. Moreover, to obtain more information we carried out detailed ground geophysical measurements at some anomalies and collected rock samples for petrographic studies and measurements of physical parameters. Interesting results yielded ground measurements over the so called Přeštice anomalous zone near Tetětice (cf. Fig. 4) in the Kdyně-Štěnovice anomaly whose interpretations by various authors differed a great deal.

Geophysical measurements at the locality Tetětice (Struhadlo)

West of Tetětice over the Velký Bítov ridge, measurements were carried out along two parallel profiles A and B situated at a distance of 100 m over a gallery and an underground horizontal borehole SP-1 (Uranový průzkum). The applied methods were magnetometry, the VLF method, symmetric resistivity profiling (SOP), and the IP method. Results of measurements on both profiles projected in the axes of the gallery and of the borehole are in Fig. 4 together with a geological section and with the results of susceptibility measurements by kappameter in the gallery and on cores from the horizontal borehole. The data are taken from the report of Chlupáčová et al. (1984).

According to the geological profile, two high susceptibility zones (Fig. 4) correspond with zones of spilites. The samples collected by Chlupáčová in the high susceptibility zone in the gallery, mostly hornstones and metabasites, have an average Q-coefficient 3.25. The highest susceptibility of approx. 120×10^{-3} SI units was exhibited by a sample of dark metatuff, collected 4 m to the NW of point BM5. Samples from the high susceptibility zone in borehole SP-1, described as hornstones, tuffs and spilitic rocks, have an average Q-coefficient 2.77 and the highest susceptibility is approx. 60×10^{-3} SI units.

The distinct magnetic anomalies detected above the gallery and horizontal borehole were shifted by approx. 30 m to the NW of both increased susceptibility zones, obviously, due to dipping of the strata. The smooth shape of the magnetic anomaly over the increased susceptibility zone in the gallery indicates that the zone does not reach the surface. On the contrary, the increased susceptibility zone in the borehole, approx. 70 m wide, comes out at the surface, as it can be seen from the gradient of the magnetic field which changes from −2 500 nT to +5 850 nT over a short distance (on profile A).

Resistivity and IP measurements were carried out on profile A only, with AB/2 = = 50 m. Both magnetic zones are manifested by decreased resistivity (below 30 Ωm) and by a continuous increased polarization zone (up to 15 %). It shows that the carrier of magnetization is a sulphidic mineralization, i.e. pyrrhotite.

Kovalová and Mrázek (1986) determined the contents of minority elements in the horizontal borehole SP-1. In the high susceptibility zone (66 to 135 m from the face) the contents of economic elements, except for Ag, were lower. It can be said that the pyrrhotite mineralization is basically monomineral.

A comparison of ground geophysical data, petrophysical data from the borehole and from the gallery, and the petrographic descriptions of rocks shows that the source of the anomaly are paleovolcanites (metabasites) with a high content of pyrrhotite.

Ground radiometric verification

In the past few years ground preliminary verification of airborne geophysical maps became an essential part of airborne geophysical mapping. The verification is aimed at better reliability of airborne radiometric maps and at obtaining information about the distribution of radio-elements in eluvial-deluvial covers which is necessary for geological interpretation. Detailed ground verification is carried out by the users of airborne geophysical maps according to their own prospection tasks.

In the course of the airborne survey in Pošumaví we accomplished preliminary verification on 34 ground gamma spectrometry profiles. Moreover, to evaluate the contour maps of K, U and Th concentrations we used data obtained by Uranový průzkum from their own prospection.

On certain parts of the profiles we used ground spectrometers to measure K, U and Th concentrations in boreholes 150 mm in diameter at a depth of 1 m at most, in dependence on local conditions. In this way obtained values mostly represent the concentrations of radio-elements in the eluvial cover.

Some profiles, aimed at verification of the airborne spectrometric data in the cases when preliminary processing cast doubt on its reality, were measured continuously. The detector was carried 50 cm above the ground and apparent concentration values were read at 80 m intervals. In case of disproportions the maps were corrected. In this way obtained concentrations were close to the airborne values.

The ground verification showed a good agreement between airborne and ground measurements in a majority of profiles. In a number of cases ground measurements revealed great variability of concentrations which could not be recorded by airborne measurements. Airborne maps show the shielding effect of forests which must be taken into account in interpretation.

Comparison of K, U and Th concentrations on ground profiles with airborne gamma spectrometric data provided valuable information for geological interpretation of airborne maps.

Ground data were statistically processed (Tab. 2). Average concentrations and other statistical parameters were calculated, characterizing the radiogeochemical distribution in eluvial-deluvial covers, ranging to the main rock types of the study area. Fig. 5 shows radioactive anomalies classified in the following groups:

a) Anomalies without geological foundation (Group V) comprise anomalies due to devastation of natural radioactivity field by civilization effects.
b) Anomalies caused by known objects due to spoil material from prospected or exploited localities (Group X).
c) Regional anomalies of concentrations (Group Y) indicate extensive geological units with primary radiogeochemical distribution different from the distribution in neighbouring geological units (e.g. granitoids of the Klatovy apophysis where the concentration of radioelements is increased compared with the surrounding Moldanubian and Barrandian Proterozoic complexes – Y8 or, on the contrary, paleobasalts and crystalline limestones with low contents of radio-elements). Often, the contours of these anomalies do not coincide with the delimited geological boundaries.
d) Regional gradients of concentration (Group Z) indicate important boundaries of rocks with different radiogeochemical distribution (e.g. the north-western boundary of the Chanovice apophysis of the Central Bohemian Pluton with the Moldanubicum – Z1).
e) Local anomalies (Group L) indicate less extensive geological bodies, often of not well defined genesis, with an anomalous radiogeochemical distribution. Some of them can be significant as indications for prospecting for non-radioactive raw materials.

Table 2
Results of statistical evaluation of ground gamma spectrometry

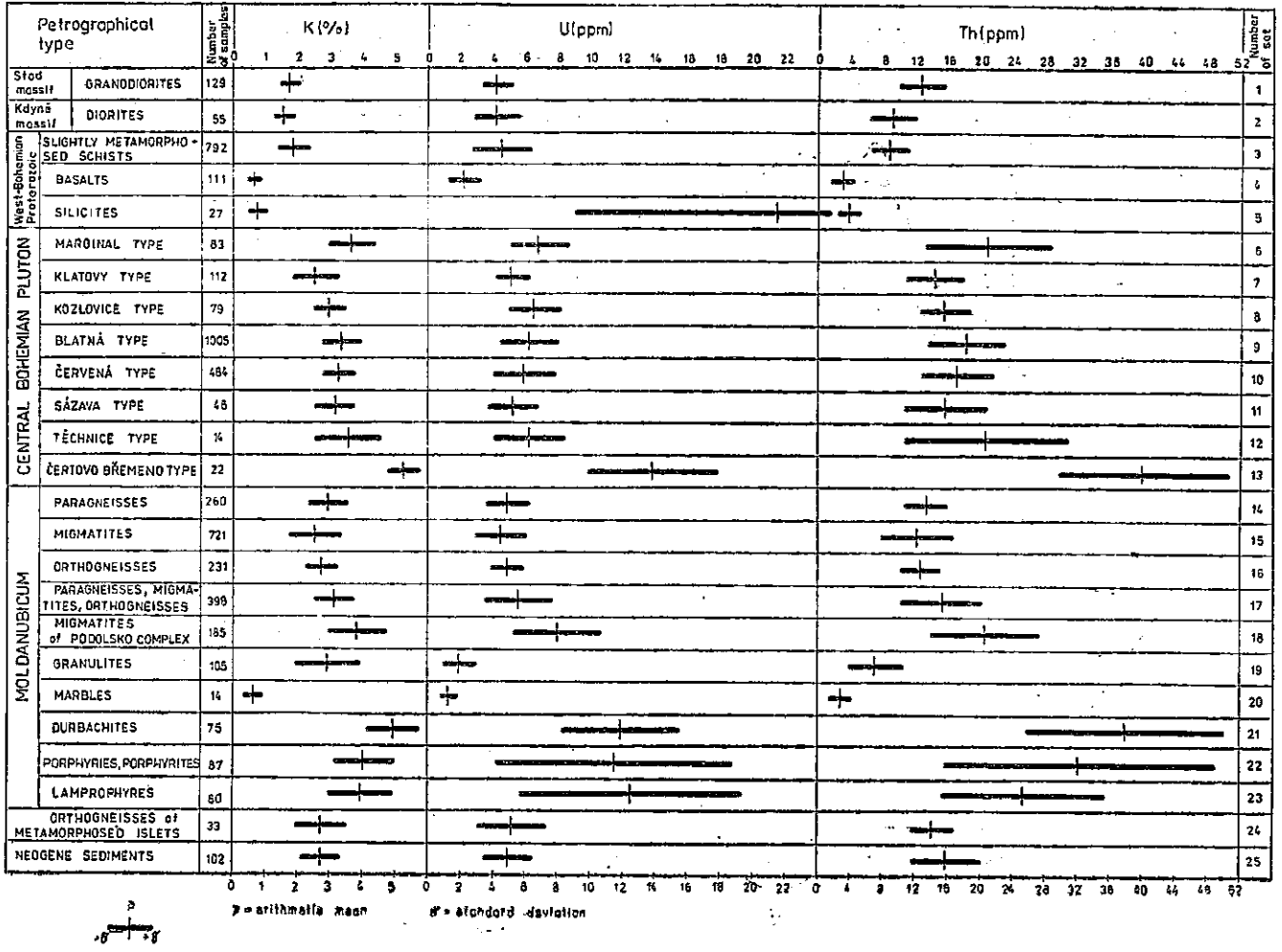

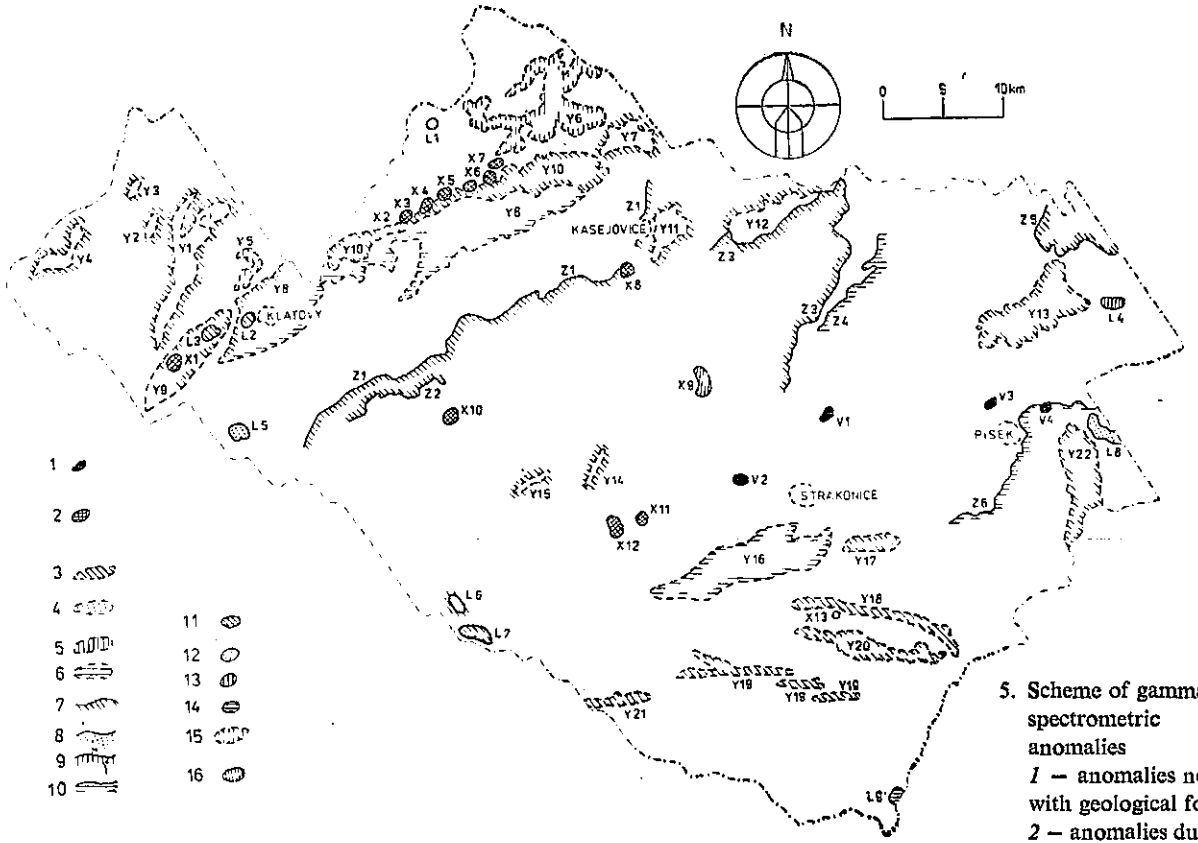

5. Scheme of gamma spectrometric anomalies
1 – anomalies not connected with geological foundation, *2* – anomalies due to the known artificial objects, *3* – multicomponental anomalies, *4* – regional anomalies of K, *5* – regional anomalies of U, *6* – regional anomalies of Th, *7* – regional gradient of concentrations multicomponent, *8* – regional gradient of K, *9* – regional gradient of U, *10* – regional gradient of Th, *11* – local multicomponent anomalies, *12* – local anomalies of K, *13* – local anomalies of U, *14* – local anomalies of Th, *15* – regional anomalies of low values of Th/U ratio, *16* – local anomalies of low values of Th/U ratio. Contours are hatched on the side of higher concentration

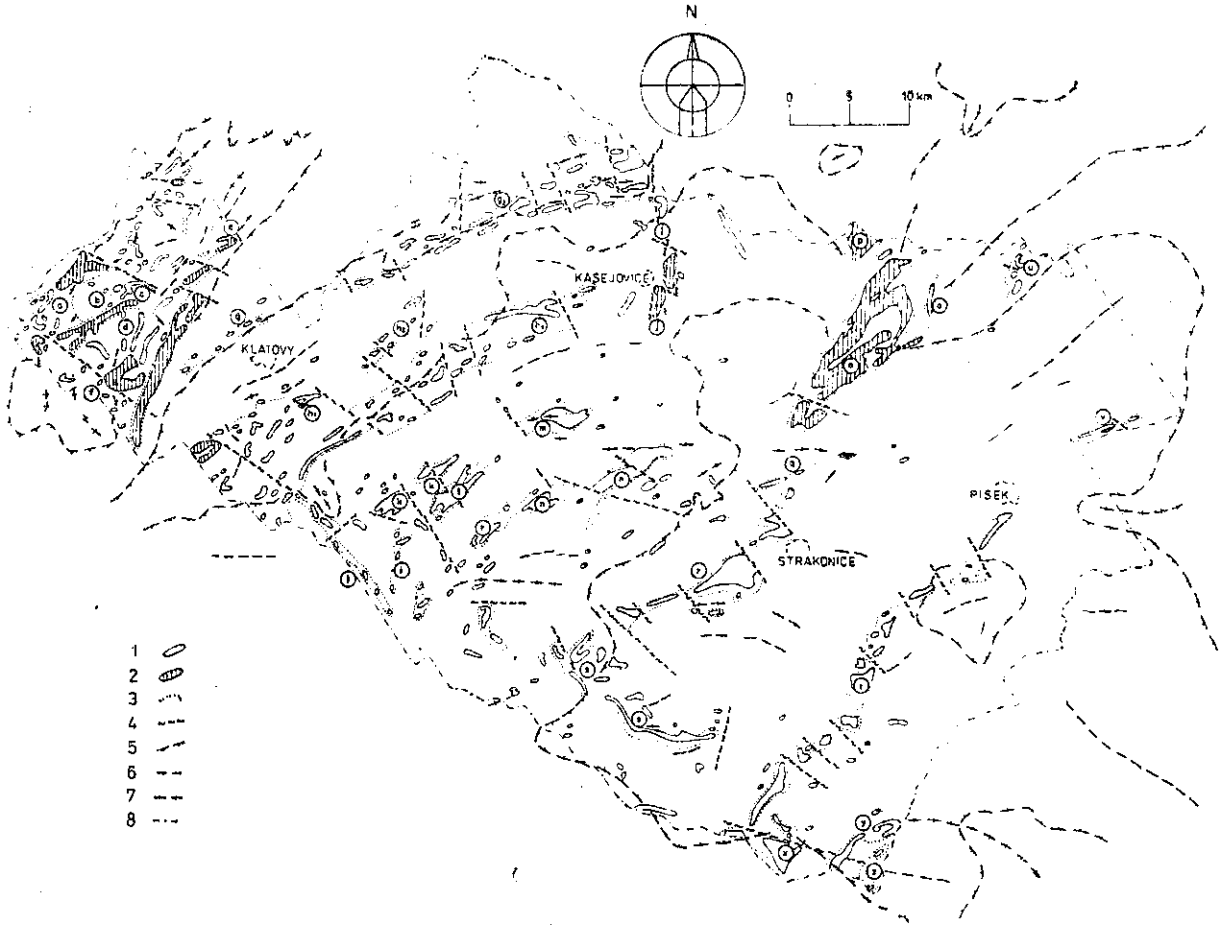

6. Scheme of magnetic structures *1* – magnetic anomalies – $\Delta T < 200$ nT, *2* – magnetic anomalies – $\Delta T > 200$ nT, *3* – boundaries of respective magnetic zones, *4* – interpreted tectonic lines, *5* – contours of gravity field, *6* – axes of negative gravity anomalies, *7* – axes of positive gravity anomalies, *8* – boundary of measured area

Interpretation of airborne geophysical survey

Magnetic anomalies

On the basis of magnetic contour maps we constructed a scheme of magnetic structures (see Fig. 6). According to maps of analytical continuation of magnetic field upward to 200 and 750 m we delimited zones including anomalies of the same type. The scheme also shows some important contours of gravity field with indicated directions of the gradients and axes of positive and negative gravity anomalies to make possible comparison of gravity and magnetic data for easier interpretation.

The magnetic field in the surveyed area is greatly varied. The individual geological formations differ by magnetic anomalies, each having a specific character. Distinct in the westernmost part of the study area is the so called Kdyně-Štěnovice anomaly. This area of intensive magnetic anomalies is accompanied by a gravity high and is divided into several partial zones (*a* to *f*). The most distinct and most continuous one is the so called Přeštice zone (*e*) in the east, fringing the Kdyně-Štěnovice anomaly. Results of geophysical measurements and petrographical verification of some anomalies in this area prove that the magnetic anomalies are associated with Proterozoic metabasalts, so called "spilites" with a high content of pyrrhotite, or with rocks of similar genesis, e.g. tuffs and tuffites.

The distinct Žinkovy magnetic zone (g_1, g_2) in the Proterozoic closely follows the north-western margin of the Klatovy apophysis. Occurrences of magnetic metabasites were found in the north-eastern part of the Žinkovy zone (g_2).

The rocks of the Central Bohemian Pluton are practically non-magnetic, some minor anomalies within the Pluton, e.g. zone (*m*) in the vicinity of Březany, were most probably caused by mantle relics or by younger dyke rocks, or by amphibolite enclaves [zone (*l*) near Hrádek].

Striking anomalies are associated with rocks of the Mirovice islet zone (*o*). The Kasejovice islet zone (*i*) and Staré Sedlo orthogneisses in the southernmost part of the Sedlčany-Krásná Hora islet zone (*u*) are very clearly manifested too.

Approximately NE–SW trending zone of magnetic anomalies can be observed in the Moldanubicum. In Fig. 6 they are designated *h*, *k*, *n*, *q*, *r* and *t*. It can be assumed that they coincide with occurrences of migmatized paragneisses in the Moldanubicum. They do not substantially differ in lithology, but contain more magnetic minerals, presumably of volcanic origin. Most striking of them is the Písek zone (*t*), the northern part of which between Písek and Ražice follows the boundary (Z-6) in Fig. 5 of low K, U and Th concentrations in the northwest and high concentrations in the southeast. Farther to the southwest this boundary can only be assumed because the field of concentrations is disturbed by the presence of other anomalies. This implies that the Písek zone most probably represents zone of metamorphic volcanic rocks, fringing the Podolsko complex, the radioactivity of which is higher compared with the surrounding Moldanubian rocks.

The W–E striking radioactivity anomalies Y-18, Y-19 and Y-20 (Fig. 5) in the area east and south of Volyně are believed to be due to accumulations of dykes of anomalously radioactive porphyries or porphyrites (see below). These radioactivity anomalies fill the gaps in the zone (*t*) magnetic anomalies. The older suite of volcanic rocks of the Písek zone is disturbed by younger E–W striking dykes.

Anomalies of different directions can be observed in the southern part of the study area. They follow mostly the foliation of the Moldanubicum. An exception is the anomalous zone (*s*) whose western part forms a kind of knot from which the anomalies strike in various directions. Obviously, both older and younger tectonic activity left traces there. In the anomalous zone (*x*) submeridional and subequatorial directions play a part besides the NE–SW strike.

As mentioned above, the Central Bohemian Pluton is composed of non-magnetic rocks. However, its tectonic position evidently influences the distribution of anomalies in the area. Magnetic and radioactivity anomalies clearly mark the north-western margin of the Klatovy apophysis. Its south-eastern margin can be traced only in the field of Th-concentrations (anomaly Y-8 in Fig. 5) and does not affect the magnetic field.

An analogy is the Chanovice apophysis from both sides bordered by the Moldanubicum. The magnetic anomalies in the south-eastern margin of zone (h_1) fringe the Chanovice apophysis. It seems that they are linked with the Pluton contact zone. In the field of concentrations of radio-elements as well the north-western margin of the Chanovice apophysis is indicated by the distinct boundary Z-1. The south-eastern margin has not been traced by airborne mapping.

Magnetic anomalies occur also south of Horažďovice in the north-western margin of the Střelské Hoštice apophysis of the Pluton. It suggests that the north-western boundaries of the Pluton are well defined in physical fields and petrophysical properties of rocks change there. On the contrary, south-eastern boundaries cannot be definitely traced by geophysical measurements in the study area. Since, there are practically no petrophysical contrasts between the rocks of the Pluton and of the Moldanubicum.

These facts presumably reflect the tectonic features of the Pluton. It is not easy to explain this asymmetry from geophysical viewpoint. It may be associated with the emplacement of the Pluton which obviously was not vertical. The anomalies of the Petrovice zone (*j*) also delimit the zone of the emplacement of granodiorite bodies, in this case in NW–SE direction.

In the south-eastern corner of the study area near Husinec the arcuate zones of magnetic anomalies (*y*, *z*) follow the margin of a granulite body.

Results of gamma-ray spectrometry

Radioactivity of the rocks in the investigated area is much varied. The geological units there mutually differ in the distribution of radio-elements. The different concentrations are due to the different origins of geological units and to the primary contrasts in composition of prevailing types of rocks. While a majority of magmatites of the Central Bohemian Pluton belong to felsic rocks with relatively high K-concentrations and associated Th and U-concentrations, the weakly metamorphic Proterozoic sediments and volcanites range to rocks with low concentrations of these elements. Then, radioactivity of the metamorphites of the Šumava Moldanubicum is on average lower compared with granitoids of the Central Bohemian Pluton and higher compared with sediments and volcanics of the Proterozoic. Radioactivity of the Moldanubian rocks on average increases from NW to SE. According to Matolín (1970) it is apparently associated with increased K, U and Th concentrations in the metatect component of some migmatized complexes. The generally increased concentrations in the southern part of the Moldanubicum are also due to porphyric and porphyritic dykes with anomalous radioactivity.

In the Proterozoic there prevail rocks with low K and Th concentrations. The average U-concentration is lower than in the Moldanubicum and in the Central Bohemian Pluton. The distribution of radio-elements in both investigated parts of the Proterozoic in the western neighbourhood of Klatovy and in the vicinity of Blovice is rather different, though.

The western neighbourhood of Klatovy between the Klatovy apophysis of the Central Bohemian Pluton, the Kdyně and Stod massifs exhibit the lowest K, U and Th concentrations (zones Y-1, Y-2 and Y-4 in Fig. 5). The relatively monotonous concentrations in weakly metamorphic Proterozoic schists and in the diorite apophysis of the Kdyně massif are contrasted by extremely low values in mafic Proterozoic volcanites. An almost continuous zone of low concentrations Y-1 coincides with the Kdyně-Štěnovice magnetic anomaly and indicates a large body of mafic paleovolcanites. Increased K, U and Th-concentrations, without contrasts however, can be observed in the southern part of the Stod massif (zone Y-3).

Several local anomalies occur in low K- and Th-concentrations in the vicinity of Blovice. Greater differences can be observed between U-concentrations where numerous local anomalies (X-2, X-1) occur. It can be assumed that the generally increased and varied U-concentrations were affected by numerous inclusions of rocks with anomalous U-concentrations (particularly silicites) and by secondary redistribution of U.

Majority of granodiorites in the Central Bohemian Pluton exhibit similar K, U and Th-concentrations. Therefore, also their indications in airborne maps are analogous. In the area of the Klatovy apophysis marginal type granites and granodiorites (Y-9 and Y-10) differ from the remaining granitoids (Y-8) by higher K,

U and Th-concentrations. As it can be seen in radiometric maps, the contours of the anomalies deviate from the geological boundaries of these rocks, namely where the Klatovy apophysis links with the Central Bohemian Pluton. According to airborne maps the marginal granites do not occur there.

Both contacts of the Klatovy apophysis and the south-western contact of the Chanovice apophysis (Z-1) relatively distinctly differ from their neighbourhood. Similarly as in the magmatites of the Klatovy apophysis, the K, U and particularly Th-concentrations in the Blatná granodiorite are higher than in the surrounding rocks and compared with the Moldanubicum their contrasts are big enough to enable drawing of the boundary. On the contrary, the south-eastern boundary of the Central Bohemian Pluton, cannot be easily interpreted on the basis of concentrations because of a gradual decrease of concentrations in the Central Bohemian Pluton towards its southern margin. Moreover, interpretation of the southern margin of the Pluton is influenced by random locations of shielding forests. The Blatná granodiorite contrasts with the metamorphic islets of Kasejovice (Y-11) and Mirovice (Z-3). The highest concentrations of radioactive elements within the Blatná type coincides with its porphyric facies in the vicinity of Blatná.

East of the Mirovice islet high concentrations are exhibited by durbachite of the type of Čertovo břemeno near Sobědraž (Z-5). The occurrence of this type near Vráž (Y-13) is also manifested by anomalous K, U and Th-concentrations. According to airborne maps these concentrations outcome the extent of the assumed geological body.

Concentrations of radio-elements in most of Moldanubian rocks are very similar. Therefore in airborne radiometric maps it is impossible to distinguish paragneisses from orthogneisses. From NW to SE the radioactivity of both para- and ortho-series gradually increases. In the eastern part the high concentrations (Z-6) are obviously associated with migmatites of orthogneiss appearance of the Podolsko complex. Extremely high concentrations in the vicinity of Písek indicate a durbachite body (Y-22).

As seen in radiometric maps, the lowest concentrations in the Moldanubicum coincide with occurrences of crystalline marbles (Y-14, Y-14), e.g. the well known bodies in the vicinity of Rábí. A total decrease of concentrations can be observed in some parts of the varied group with numerous marble occurrences. Striking E–W trending linear anomalies (Y-17 to Y-20) in the area delimited by Kašperské Hory, Volyně, Bavorov and Vimperk are due to accumulations of parallel dykes of porphyries and porphyrites. They indicate disjunctive tectonic structures of regional significance. Some of them can be traced in airborne radiometric maps at a length of several tens of kilometers. According to the magnetic contour map we can assume that they dislocate the Písek metavolcanic zone. On the contrary, partial discontinuities may indicate younger disjunctions, presumably striking to the NE. Results of statistical evaluation of the ground spectrometric survey are given in Tab. 2.

Petrophysical and petrological characteristics of aeromagnetic anomalies

Field samples were collected during the summer and autumn of 1984. Owing to the large extent and to geological diversity of the study area we were not able to carry out field reconnaissance of all detected magnetic anomalies. Therefore we focused on expressive anomalous zones and on some significant anomalies, regardless of previous studies. We did so in an effort for overall understanding, also taking into account the preceding stage of airborne measurements, namely in regard to the original petrophysical interpretation of important aeromagnetic anomalies. Measurements by KT-5 kappameter were taken in the broader surroundings of the anomalous maxima on all rocks from outcrops and artificial exposures, from skeletons in fields, pastures and forests, and on loose boulders and blocks which presumably had not undergone transport. We executed tens to hundreds of measurements at every locality and collected representative samples of autochthonous maximally magnetized rocks and for comparison samples of less magnetic or non-magnetic rocks. At 62 localities (Fig. 1) we collected 148 samples for laboratory studies – determination of bulk and mineralogical density (σ_o and σ_m), porosity (p), magnetic susceptibility ($\varkappa$), remanent magnetization intensity (J_r) and calculation of the Koenigsberger ratio (Q-coefficient). The values of physical properties of respective samples (*PŠ 1-62*) of microscopically identified rocks are listed in Table 3. At another 23 localities we did not found either any rock material at all (because of thick, either Quaternary or Tertiary, cover), or only non-magnetic rocks.

Subsequently, we microscopically examined all samples with the aim to identify rocks types and carriers of anomalous magnetization. We believe that this very approach to interpretation of anomalies with evidently surface sources yields realistic results. Of 148 samples collected at 62 localities we made 83 thin sections for qualitative petrographic analysis.

Anomalous rocks will be described from W to E, similarly as in the chapter of geology.

1. In the westernmost part the attention was paid to rocks within the Kdyně-Štěnovice anomaly where individual NE – SW striking zones of magnetic anomalies precisely coincide with morphologically apparent belts of Proterozoic basalts (so-called spilites). These basalts are almost non-metamorphosed in the southwestern part of the Barrandian and both regionally and thermally metamorphosed in the Domažlice crystalline complex. We attempted to elucidate this zone, one of the most significant magnetic zones in the Bohemian Massif, whose previous interpretations had been somehow confused.

In the major metabasalt belt contoured by the Přeštice anomaly in the area Zdeslav – Chudenice – Ježovy the predominant magnetized rocks are weakly regionally metamorphosed basalts (metaspilites) – *PŠ 45, 46, 47, 48, 50* and *51*

(of Table 3). They are identified as greenschists with chlorite and actinolite often with striking relic structure of original basalts and their tuffs (with clearly recognizable compressed pyroclastic clasts, maybe plastic at the time of deposition, partly dynamometamorphosed). They contain actinolite, chlorite, clinozoisoite, albite, calcite. Lava equivalents contain phenocryst palimpsests. An ore-component is ilmenite, but the predominating ferromagnetic mineral is pyrrhotite, often forming macroscopically recognizable impregnations. It is present in the form of small grains in the ground mass, they often mobilize and create tiny veinlets.

We have never observed that it would originate from pyrite. Magnetic susceptibility of metaspilites in this zone attains $0.82-5.12\times10^{-3}$ SI. The Q-coefficient is generally more than 20. The maximum remanent magnetization value is 9 871 nT. The north-western belt of metabasalts between Kdyně and Koloveč which underwent intensive regional and contact metamorphism is the source of linear, though dispersed, anomalies. The collected magnetized samples *PŠ 52, 53, 56, 57* and *58* are metabasalts metamorphosed, however, even to pyroxene-amphibole hornfelses with mosaic or poikiloblastic structure almost without relics of original lava or pyroclastic structures. The association comprises green amphibole, brown or orange granoblastic or nematoblastic amphibole, pyroxene of salite nature, fresh non-lamellar plagioclases, titanite, apatite, ilmenite, and above all pyrrhotite. Magnetic susceptibility ranges from 0.67 to 6.11×10^{-3} SI. The Q-coefficient is mostly high. Remanent magnetization values attain up to 29 000 nT. This belt also includes the diorite bodies of the Kdyně complex which, sporadically, are the sources of anomalies. It is e.g. amphibole-pyroxene-biotite diorite up to quartz diorite (*PŠ 52b* – $\varkappa = 2.22\times10^{-3}$ SI, Q = 5.94) where the only ore mineral found was ilmenite (or titanomagnetite), similarly, in the southernmost belt between Libkov, Loučim and Tetětice (including the locality Struhadlo studied by Chlupáčová et al. 1984) metaspilites (greenschists – *PŠ 59a*) strongly impregnated with pyrrhotite ($\varkappa = 7.42\times10^{-3}$ SI, $I_{rn} = 15\,864$ nT) as well as pyroxene-amphibole diorites with titanomagnetite (*PŠ 60b* – $\varkappa = 11.61\times10^{-3}$ SI, Q = 4.5) occur. A reliable identification property of all metabasites is their high mineralogical density, mostly around $3.0\ g.cm^{-3}$. It can be concluded that the magnetic anomalies in the south-eastern margin of the extensive Kdyně-Štěnovice zone are presumably due to pyrrhotite primarily associated with Proterozoic basaltic volcanism regardless of the degree to which it had been affected by younger regional and/or contact metamorphic processes as it is evidenced by high remanent magnetization values of almost all paleobasalt samples of various metamorphic degrees.

2. The rocks of the Central Bohemian Pluton in the study area do not reveal anomalous magnetization. An exception is e.g. foliated amphibole-biotite granodiorite, containing magnetite, in the Střelské Hoštice apophysis (*PŠ* 32 – $\varkappa = 25.44\times10^{-3}$ SI). It is presumably an assimilated remnant of the mantle, i.e.

Table 3

Review of anomalously magnetized rocks and of their petrophysical properties

Number of sample (*PŠ*)	Locality	$\varkappa$ (10^{-3} SI)	Q coef.	σ_m (g.cm^{-3})	Lithology	Carrier of magnetization
1a	Cehnice	24.32	0.19	2.69	amphibole-biotite orthogneiss	magnetite
1b	Cehnice	28.83	0.27	2.68	leucocratic biotite gneiss	magnetite
1d	Cehnice	16.79	0.21	2.69	leucocratic biotite gneiss	magnetite
1e	Cehnice	68.90	0.11	3.00	diopside amphibolite	magnetite
2a	Kváskovice	24.02	0.19	2.69	amphibole-pyroxene leptynite	magnetite
2b	Kváskovice	24.42	0.26	2.68	leucocratic biotite-amphibole orthogneiss	magnetite
2c	Kváskovice	87.36	0.07	2.89	amphibolite	magnetite
4a	Střítež	59.96	0.26	2.83	amphibole-biotite paragneiss	magnetite
4b	Střítež	40.53	1.10	2.87	biotitic amphibolite	magnetite
4c	Střítež	22.76	0.16	2.41	biotite-plagioclase paragneiss arteritic migmatitized	magnetite
5b	Litochovice	30.47	0.30	2.70	biotitic arteritic migmatite	magnetite
6b	Kobylence	44.91	0.19	2.89	migmatitized amphibolite	magnetite
6d	Kobylence	19.41	0.13	2.76	quartz-amphibolite	magnetite
6e	Kobylence	18.50	0.32	2.69	biotite orthogneiss	magnetite
7	Volyně (Bohunice)	60.94	0.10	2.76	magnetitic biotite paragneiss	magnetite
10a	Bušanovice	46.66	4.92	2.96	amphibolite	magnetite Q > 1
11c	Beneda (Zálezly)	7.22	0.38	2.65	leucocratic biotite orthogneiss to leptynite	magnetite

12b	Beneda	52.74	0.49	2.85	migmatitic amphibolite	magnetite
12c	Beneda	111.14	0.20	2.96	altered pyroxene amphibolite	magnetite
13a	Vlachovo Březí	0.38	0.36	2.78	biotite-cordierite paragneiss (mobilizate portion)	pyrrhotite
13c	Vlachovo Březí	203.60	1.30	2.89	biotite-cordierite gneiss	magnetite
15b	Husinec	3.24	2.08	3.44	garnet-amphibole skarn	pyrrhotite
17b	Žárovná	5.49	20	2.67	leucocratic biotite orthogneiss	unknown
17c	Žárovná	2.50	1.62	2.67	biotite orthogneiss	
17e	Žárovná	35.29	0.70	2.74	quartz amphibolite with biotite and garnet	magnetite
18	Šumavské Hoštice	5.88	1.28	2.74	biotite porphyrite up to kersantite	magnetite
19b	Mirotice	27.513	0.16	2.66	biotitic orthogneiss (Mirotice type)	magnetite
20a	Stráž	5.39	0.13	2.64	leucocratic biotite orthogneiss	magnetite
20b	Stráž	55.75	0.11	2.78	biotite metaporphyrite	magnetite
20c	Stráž	57.58	0.12	2.97	granitized amphibolite	magnetite
20d	Stráž	96.58	0.29	2.82	two-mica paragneiss	magnetite
21a	N of Mirotice	21.72	0.26	2.68	amphibole-biotite quartz diorite	magnetite
21c	N of Mirotice	6.47	0.36	2.66	muscovite-biotite aplite	magnetite
21d	N of Mirotice	37.85	0.32	2.75	biotite-amphibole quartz porphyrite (dacite)	magnetite
25a	Přečín	7.44	0.17	2.73	pyroxene-amphibole-biotite erlan gneiss	magnetite
25b	Přečín	27.26	0.11	2.69	biotite quartzitic gneiss with garnet	magnetite
25c	Přečín	31.99	0.26	2.71	biotite-amphibole-pyroxene quartzitic erlan gneiss	magnetite
25d	Přečín	14.82	0.10	2.75	pyroxene-amphibole quartzitic gneiss	magnetite
26a	Vacov (Kůstrý)	43.04	3.35	2.81	quartz amphibolite with biotite	magnetite Q > 1
26b	Vacov (Kůstrý)	19.48	2.87	2.79	cordierite-biotite-sillimanite paragneiss	magnetite Q > 1
26d	Vacov (Kůstrý)	69.57	0.10	2.74	biotite migmatitic gneiss	

Table 3 (continued)

Number of sample (*PŠ*)	Locality	$\varkappa$ (10^{-3} SI)	Q coef.	σ_m (g.cm^{-3})	Lithology	Carrier of magnetization
27a	Nahořánky	35.31	1.00	2.80	cordierite-biotite-sillimanite gneiss muscovitized	magnetite
27b	Nahořánky	21.88	0.13	2.72	migmatitic amphibole	magnetite
27d	Nahořánky	16.80	0.22	2.80	cordierite-biotite-sillimanite migmatitic gneiss	magnetite
27e	Nahořánky	9.45	0.16	2.77	biotite-sillimanite gneiss altered and migmatitized (mobilizate)	magnetite
29b	Parýzek	67.28	2.23	2.79	two-mica sillimanite paragneiss with garnet migmatitized and cataclastic	magnetite Q > 1
29c	Parýzek	71.05	0.19	2.77	biotite-sillimanite paragneiss migmatitized	magnetite
30a	Soběšice	56.13	0.40	2.70	biotite migmatite of orthogneiss appearance	magnetite
30b	Soběšice	82.61	0.29	2.77	biotite-cordierite gneiss migmatitized	magnetite
30c	Soběšice	3.70	0.08	2.75	sillimanite-cordierite-biotite paragneiss	magnetite
30d	Soběšice	47.18	0.08	2.74	amphibole-biotite orthogneiss	magnetite
32	Zádušní les	25.44	0.24	2.67	amphibole-biotite leptynite granitized	magnetite
33	Kašperské Hory	15.80	0.10	2.88	sillimanite-biotite paragneiss with hercynite and garnet	magnetite
35a	Ostružná (Sedlo)	11.13	0.23	2.75	diopside-amphibole leptynite up to erlan with garnet and biotite	magnetite
35b	Ostružná (Sedlo)	24.33	0.08	2.71	amphibole-biotite migmatite of orthogneiss appearance	magnetite
35c	Ostružná (Sedlo)	44.40	0.33	2.74	sillimanite-biotite-migmatitic gneiss	magnetite
36	Albrechtice	14.25	0.94	2.82	sillimanite-biotite paragneiss	magnetite
37b	Sušice (Rok)	13.17	2.86	2.76	cordierite-sillimanite-biotite paragneiss	magnetite Q > 1
37d	Sušice (Rok)	24.10	0.16	2.80	cordierite-sillimanite-biotite paragneiss	magnetite

38	Lešišov	16.66	0.08	2.92	diopside amphibolite	magnetite
39a	Nemilkov	1.30	8.21	2.84	biotite-amphibole-diopside erlan	pyrrhotite
40a	Nalžovské Hory	16.26	0.30	2.67	leucocratic biotite orthogneiss	magnetite
40b	Nalžovské Hory	9.78	0.17	2.70	amphibole epidotic quartzitic erlan	magnetite
40c	Nalžovské Hory	64.81	0.10	3.02	amphibolite	magnetite
41a	Radomyšl	5.65	0.31	2.62	leucocratic amphibole orthogneiss	magnetite
42c	Doubravice	41.25	0.26	2.94	amphibolite	magnetite
42d	Doubravice	35.24	0.14	2.94	amphibolite	magnetite
44a	Radimovy	38.16	0.11	2.62	leucocratic aplitic biotite orthogneiss	magnetite
45a	Chlumsko	5.12	20	3.04	chlorite-actinolite greenschist (spilitic metatuff)	pyrrhotite
47	Krušce	2.39	18.50	3.05	altered metabasalt	pyrrhotite
49	Bělýšov	2.51	20	3.03	amphibolite metabasalt with relic texture	pyrrhotite
52a	Koloveč (Zíchov)	3.09	20	3.01	amphibole hornfels (metabasalt)	pyrrhotite ilmenite
52b	Koloveč (Zíchov)	2.22	5.94	2.91	amphibole-pyroxene-biotite diorite up to quartz diorite	ilmenite
53a	Koloveč (Suková hora)	0.85	0.96	3.03	pyroxene-amphibole hornfels	pyrrhotite
53b	Koloveč (Suková hora)	3.88	20	3.01	diopside-amphibole hornfels	pyrrhotite
56d	Koloveč	4.65	14.93	2.96	actinolite contact greenschist (basaltic metatuff)	pyrrhotite
57	Němčice	6.21	20	2.98	pyroxene-amphibole hornfels	pyrrhotite ilmenite
59a	Libkov	7.41	20	3.11	chlorite-actinolite greenschist (metabasalt)	pyrrhotite
60b	Libkov	11.47	4.58	3.02	pyroxene-amphibole diorite	ilmenite titanomagnetite
62	Kolinec (Vidhošť)	7.67	20	2.88	diopside-amphibole erlan	pyrrhotite

original leptynite. Sample PŠ 38 from the Hory Matky Boží apophysis belongs to an enclave of pyroxene amphibolite with magnetite ($\varkappa = 16.66 \times 10^{-3}$ SI), similarly as numerous rocks from locality PŠ 40 near Čejkovy (Table 3) are mantle enclosures in surrounding plutonites, in this case leucocratic biotite orthogneisses, quartzitic erlans and amphibolites, all of them containing accessoric up to abundant magnetite.

3. Islets zone rocks constitute one of the most important sources of anomalies in the study area. In many cases they were the subject of previous petrographical-petrophysical studies. For instance, in the Kasejovice metamorphic islet (Krsová–Šťovíčková 1975) various types of rocks exhibit anomalous magnetic values: quartzites with magnetite, biotite-muscovite orthogneisses, leucocratic orthogneisses, hornfels paragneisses, various types of amphibolites mostly containing magnetite, often, particularly in the southern parts of the Kasejovice islet, containing pyrrhotite.

The southern part of the Mirovice islet fringed by striking anomalies has recently been studied (*PŠ 19, 20, 21, 22*). Not only the mentioned Mirotice orthogneisses, but also the rocks of diorite to gabbrodiorite composition exhibit anomalous magnetization. Thy typical Mirotice orthogneisses are of the nature of leucocratic biotite or non-mica orthogneisses in association with biotite, acid plagioclases, quartz, orthite, titanite and magnetite (*PŠ 19b* – $\varkappa = 27.51 \times 10^{-3}$ SI, Q = 0.16; *PŠ 20a* – $\varkappa = 5.39 \times 10^{-3}$ SI, Q = 0.13). Biotite metaporphyrite *PŠ 20b* contains altered phenocrysts of plagioclases, zonal, with Baveno twinnings, in the ground mass biotite, plagioclases and magnetite ($\varkappa = 55.75 \times 10^{-3}$ SI, Q = 0.11). Biotite-amphibole quartz porphyrite *PŠ 21d* is characterized by phenocrysts or aggregates of dark minerals (amphibole and biotite), phenocrysts of automorphic zonal plagioclases, very fine-grained ground mass composed of feldspar, quartz, titanite and magnetite ($\varkappa = 37.85 \times 10^{-3}$ SI, Q = 0.32). Amphibole biotite quartz diorite up to granodiorite *PŠ 21a* in addition contains orthite, zircon and ample magnetite ($\varkappa = 21.71 \times 10^{-3}$ SI, Q = 0.26). Amphibole gabbro with phenocrysts of altered plagioclases *PŠ 20c* has a high content of magnetite ($\varkappa = 57.58 \times 10^{-3}$ SI, Q = = 0.11). Of the collected samples paragneiss with association of biotite, muscovite, plagioclases, quartz, magnetite (*PŠ 20d* – $\varkappa = 96.58 \times 10^{-3}$ SI, Q = 0.29) exhibited the highest magnetization. In the southernmost corner of the Mirovice islet southwest of Sedlice the rocks with highest magnetization are leucocratic and biotite orthogneisses (*PŠ 42a* – $\varkappa = 9.76 \times 10^{-3}$ SI, Q = 0.92; *PŠ 42b* – $\varkappa =$ $= 12.67 \times 10^{-3}$ SI, Q = 0.21) and fine-grained amphibolites with association of green amphibole (up to 40%), plagioclases, rare quartz and ample magnetite (*PŠ 42c* – $\varkappa = 41.25 \times 10^{-3}$ SI, Q = 0.26; *PŠ 42d* – $\varkappa = 35.24 \times 10^{-3}$ SI, Q = = 2.24). Magnetite is the carrier of anomalous magnetization of the Mirovice islet rocks. Majority of the mentioned rocks, both acid and basic, showed characteristic features of originally volcanic structures (porphyritic, very fine

-grained ground mass). They had undergone recrystallization of various degrees, most intensive in the southern corner of the islet (*PŠ 42*).

4. Some Moldanubian crystalline schists, namely of the varied units south of Klatovy, in the broader environment of Sušice, Strakonice, and finally southwest of Písek are the sources of continuous anomalous zones and of numerous minor and major isolated anomalies. Passing again from west to east, within the Strážov unit the main source of local intensive anomalies in the vicinity of Radimovy and Běšiny are metabasic rocks (*PŠ 44b* – banded amphibolites with magnetite – $\varkappa = 76.79 \times 10^{-3}$ SI, Q = 0.17; *PŠ 61a* – feldspar amphibolites with ample magnetite and highest magnetic susceptibility within the entire study area – $\varkappa = 249.72 \times 10^{-3}$ SI, Q = 0.07). However, we also encountered leucocratic biotite orthogneisses with association of chlorite, biotite, plagioclases, microcline, quartz, magnetite, macroscopically resembling erlans (*PŠ 44a* – $\varkappa = 38.15 \times 10^{-3}$ SI, Q = 0.11).

The zone of anomalies north of Nemilkov, of NW–SE direction parallel with elongated minor intrusions of Červená granodiorite remains petrophysically not well explained in spite of very detailed ground geophysical verification. Although samples were collected on all profiles, particularly in their parts crossing zones of anomalies, only one of them exhibited weakly anomalous magnetization: erlan in association with biotite, amphibole, pyroxene, basic plagioclases, titanite, pyrrhotite (*PŠ 39a* – $\varkappa = 1.30 \times 10^{-3}$ SI, Q = 8.21). This is not sufficient for adequate petrophysical explanation – the source of anomaly is probably deep. The belt of anomalies in the Kolinec Moldanubicum near Vidhošť, so far unexplained, is presumably due to the effects of intercalations of erlan with amphibole, diopside, quartz, plagioclases, titanite, pyrrhotite (*PŠ 62* – $\varkappa = 7.67 \times 10^{-3}$ SI, Q > 20).

The minor and major isolated anomalies and continuous zones of anomalies in the Sušice varied group between Sušice and Kašperské Hory have various sources. They are predominantly paragneisses and migmatite gneisses in association with sillimanite, cordierite, biotite, K-feldspar, magnetite, sporadically garnet and hercynite (*PŠ 33, 35c, 36b, 37b, 37d*). The sillimanite-cordierite paragneisses reach magnetic susceptibility values up to 44.4×10^{-3} SI, Q = 0.33 (*PŠ 35c*) and often high mineralogical density values – $\sigma_m = 2.88$ g . cm^{-3} (*PŠ 33* – garnet-sillimanitic paragneiss with hercynite and magnetite). Anomalous magnetization is also exhibited by some migmatites of orthogneiss appearance, with amphibole, biotite, titanite, chlorite, quartz, plagioclases, magnetite and orthite (*PŠ 35b*) as well as rocks of the nature of leptynites and erlans in association with diopside, amphibole, biotite, titanite, garnet, quartz, K-feldspar, and magnetite (*PŠ 35a*). Similar may be the source of another group of striking anomalies, forming an almost continuous NW–SE trending belt between Strašín, Maleč and Přečín NNE of Javorník. The rocks there are cordierite-sillimanite-biotite paragneisses containing quartz, plagio-

clases, K-feldspar, garnet, zircon and magnetite, often migmatitized and muscovitized (*PŠ 27a, 27d, 29b, 29c, 26d, 26b*). Magnetic susceptibility values vary from $\varkappa = 9.45 \times 10^{-3}$ SI to $\varkappa = 71.05 \times 10^{-3}$ SI at Q = 1, exceptionally Q = 2.23. Densities attain $\sigma_m = 2.80$ g . cm^{-3}. Moreover, anomalous magnetic values are exhibited by quartz and migmatitized amphibolites in association with amphibole, biotite, pyroxene, epidote, titanite, plagioclases, quartz, magnetite (*PŠ 27b* – $\varkappa = 21.88 \times 10^{-3}$ SI, Q = 0.13; *PŠ 26a* – $\varkappa = 43.04 \times 10^{-3}$ SI, Q = 3.35) and finally by pyroxene-amphibole erlan gneisses, often strongly quartzitic with pyroxene, amphibole, garnet and magnetite (*PŠ 25a, 25b, 25c, 25d* – $\varkappa_{max} = 31.99 \times 10^{-3}$ SI). A relatively isolated zone of anomalies ENE of Soběšice is again due to sillimanite-cordierite-biotite paragneisses with magnetite (*PŠ 30b* – $\varkappa = 82.61 \times 10^{-3}$ SI, Q = 0.29; *PŠ 30c* – $\varkappa = 3.70 \times 10^{-3}$ SI, Q = 0.08) and to migmatites of orthogneiss appearance, i.e. amphibole-biotite trondhjemites with magnetite (*PŠ 30a* – $\varkappa = 56.13 \times 10^{-3}$ SI, Q = 0.4; *PŠ 30d* – $\varkappa = 47.17 \times 10^{-3}$ SI, Q = 0.08). W of Radomyšl leucocratic amphibole orthogneisses with epidote, clinozoisite, titanite, orthite and magnetite (*PŠ 41a* – $\varkappa = 5.65 \times 10^{-3}$ SI, Q = 0.31) together with fine-grained amphibolites (*PŠ 41b* – $\varkappa = 15.61 \times 10^{-3}$ SI, Q = 1.18) occur. To the NW of the zone, an isolated anomaly near Katovice is caused by biotite migmatites with high susceptibility (*PŠ 31a* – $\varkappa = 126.23 \times 10^{-3}$ SI, Q = 0.53; *PŠ 31b* – $\varkappa = 62.96 \times 10^{-3}$ SI, Q = 2.89). These samples were strongly weathered and therefore the thin sections could not be made from them. High σ_m values (up to 2.88 g . cm^{-3}) indicate that these rocks are cordierite-sillimanite paragneisses as in many already mentioned cases.

Relatively most samples were collected in the eastern NE–SW trending chain of magnetic anomalies, the so called Písek zone. Only its north-easternmost part could not be verified because of lack of outcrops due to thick cover. First indication in the form of skelet outcrops south of Cehnice are occurrences of leucocratic amphibole-biotite orthogneisses with magnetite, plagioclases, microcline, quartz, apatite, orthite, zircon and epidote (P3 1a, 1b, 1d with maximum magnetic susceptibility $\varkappa = 28.32 \times 10^{-3}$ SI, Q = 0.19) and diopside amphibolites with magnetite (*PŠ 1e* – $\varkappa = 68.90 \times 10^{-3}$ SI, Q = 0.11, $\sigma_m = 3.0$ g . cm^{-3}). In the further continuation of the Písek zone contrast rocks can be encountered: leucocratic biotite-amphibole orthogneisses with magnetite (*PŠ 2b* – $\varkappa = 24.42 \times 10^{-3}$ SI, Q = 0.26) and amphibole-pyroxene leptynites with titanite, orthite and magnetite (*PŠ 2a* – $\varkappa = 24.02 \times 10^{-3}$ SI, Q = 0.19) on the one hand, and amphibolites with magnetite on the other hand (*PŠ 2c* – $\varkappa = 87.36 \times 10^{-3}$ SI, Q = 0.07). At the next locality predominate the biotite-amphibole gneisses with apatite and magnetite (*PŠ 4a* – $\varkappa = 59.96 \times 10^{-3}$ SI, Q = 0.26) and fine-grained biotite paragneisses with magnetite (*PŠ 4c* – $\varkappa = 22.76 \times 10^{-3}$ SI, Q = 0.16). The same rocks occur east of Litochovice (*PŠ 2b* – $\varkappa = 30.48 \times 10^{-3}$ SI, Q = 0.30) and not far from there again migmatitized and quartz amphibolites with magnetite (*PŠ 6b* – $\varkappa = 45.22 \times 10^{-3}$ SI, Q = 0.20) together with biotite orthogneisses (*PŠ 6e*). In the

centre of the Písek zone prevail biotite paragneisses with magnetite (*PŠ 7* – $\varkappa = 60.94 \times 10^{-3}$ SI, Q = 0.10), various migmatites of orthogneiss appearance (*PŠ 8* and *9*). The contrasts in composition of rocks with anomalous magnetic values can be observed also in the south-western linear termination of the Písek zone where acid biotite-amphibole orthogneisses to leptynites (*PŠ 10a*, *11c*) and amphibolites and pyroxene amphibolites (*PŠ 10a* – $\varkappa = 46.66 \times 10^{-3}$ SI, Q = 4.92; *PŠ 12b* – $\varkappa = 52.74 \times 10^{-3}$ SI, Q = 0.49; *PŠ 12c* – $\varkappa = 111.14 \times 10^{-2}$ SI, Q = 0.20) both contain ample magnetite. Near Vlachovo Březí similarly as in the Strakonice varied group occur biotite-cordierite gneisses extremely highly magnetized containing abundant magnetite (*PŠ 13c* – $\varkappa = 203.59 \times 10^{-3}$ SI, Q = 1.3). In its southern termination the Písek zone crosses a NW–SE trending zone, similarly as the northernmore Strakonice zone. The sources of anomalies there are analogous: leucocratic orthogneisses (*PŠ 17b* – $\varkappa = 5.49 \times 10^{-3}$ SI, Q = 25.0) and quartz amphibolites with garnet (*PŠ 17e* – $\varkappa = 95.29 \times 10^{-3}$ SI, Q = 0.7). Unfortunately, the high remanent magnetization of the rock was not explained because in thin section any ferromagnetic ore mineral was not found. Noteworthy is the occurrence of garnet-amphibole skarn containing pyrrhotite (*PŠ 15b* – $\varkappa = 3.24 \times 10^{-3}$ SI, Q = 2.08) near Husinec and of dynamically compressed biotite porphyrite to kersantite at the locality Skařez near Šumavské Hoštice (*PŠ 18* – $\varkappa = 5.88 \times 10^{-3}$ SI, Q = 1.28).

Taking into account the given observations it is possible to conclude two interpretational facts: firstly, the clearly zonal, though often irregular, trend of magnetic anomalies and secondly, the defined lithology of rocks occurring in the zones. The dominating trend of seven zones of magnetic anomalies in the entire study area is NE–SW, while part of the Kdyně-Štěnovice zone displays an azimuthal deviation (NNE-SSW). The source of the Kdyně-Štěnovice zone is doubtlessly associated with products of Proterozoic basalt volcanism, more precisely with pyrrhotite genetically connected with it. Moreover, pyrrhotite mineralization occurs also in contact-metamorphic paleobasalts (spilites) at the northern margin of the Klatovy apophysis, in some rocks of the Kasejovice metamorphic islet and rarely in the Moldanubian rocks (e.g. near Nemilkov, Husinec).

The zones of magnetic anomalies in the Moldanubicum are, as a rule, characterized by the presence of magnetized rocks of three kinds: 1. the sillimanite-cordierite-biotite paragneisses containing magnetite and exhibiting the highest mineralogical density within the paraseries; 2. rocks of a relatively very acid nature which may be leucocratic orthogneisses or migmatites of orthogneiss appearance or leptynites with a low content of mafic minerals (amphiboles, pyroxenes, garnet, titanite) and with magnetite, most probably representing metamorphic products of acid volcanic or subvolcanic trondhjemite rocks; and 3. amphibolites with magnetite, sometimes pyroxene-bearing, rarely garnet-bearing often with mineralogical densities only rarely attaining the value of 3.0 g . cm^{-3} typical of amphibolites. The educt of these amphibolites are presumably mafic volcanites in which the content of the

light component can be either primary or a product of migmatitization or mutual interaction of products of volcanism of bimodal chemism on linear tectonic zones. The occurrences of both these bipolar types of rocks can be observed, as a rule, at majority of studied localities. It is especially remarkable along the entire Písek belt of anomalies assumed to be a linear zone of contrast volcanites in the NE fringing the Podolsko complex of the Moldanubicum. Occurrences of contrast anomalous rocks can be encountered also in the islet zone, particularly in the Mirovice islet where these rocks evidently have volcanic nature. It is noteworthy (all over the entire study area) that almost all NE–SW trending zones of anomalous magnetization at their southern termination "spread" into perpendicular (NW–SE) anomalous areas, representing some belts of crossing from the southern end of the Kdyně-Štěnovice anomaly to the southern end of the Písek zone. Unfortunately, this perpendicular zone is located at the boundary of the surveyed area and therefore it cannot be accurately delimited.

It can be concluded that in the study area aeromagnetometry indicated several NE–SW trending tectonic zones with occurrences of non-metamorphic and metamorphic paleovolcanites exhibiting anomalous magnetization. The westernmost of them (the Kdyně-Štěnovice zone), according to petrological and petrophysical results, is due to the presence of pyrrhotite genetically connected with products of Upper Proterozoic basalt volcanism. The zone correlates with the linear discontinuity indicated by geophysical data (Pokorný, Šťovíčková, Beneš, 1985) corresponding to the Kladno deep fault (Röhlich, Šťovíčková, 1968). The neighbouring Žinkovy zone of anomalies, on the contrary, strikes from ENE to WSW and according to petrophysical and petrological results is also due to the presence of Proterozoic paleobasalts (mainly contact-metamorphic "spilites"), containing not only pyrrhotite, but also magnetite. This zone correlates with the northern border of the Klatovy apophysis of the Central Bohemian Pluton, and above all with the fault discontinuity detected by geophysics (Pokorný, Šťovíčková, Beneš, 1985), i.e. with the Klatovy deep fault (Röhlich, Šťovíčková, l.c.). Both discontinuities are important gravity linear structures of the Bohemian Massif and in part form the boundary between the Teplá-Barrandian and the Moldanubian blocks. It can be assumed that the significant transport of material from subcrustal portions took place in the Upper Proterozoic. Then the Kladno deep fault evidently acted as an important linear zone of the spreading of the ocean floor with all its attributes including hydrothermal, especially sulphidic mineralization. Pyrrhotite, obviously the primary carrier of anomalous magnetization, is recently regarded as sulphide which might originate at great depths within the Earth body (Anderson, Ahrens, 1986).

Another NE–SW striking linear zones, indicated by magnetometry, occur in the Moldanubian block, but they do not particularly correlate with gravity indication, and, therefore, can be regarded as intra-block zones. They doubtlessly indicate the paleovolcanic linear zones, in some cases several tens of kilometers long. The

volcanism is, according to petrological and petrophysical studies, of bimodal character and shows that the crustal (and maybe also subcrustal) structure of this block differs from that of the Teplá-Barrandian block. The anomalous magnetization of this block is, with only few exceptions, due to the presence of magnetite (see Table 3) in metamorphic paleovolcanites, acid or basic. The volcanics of intermediate composition are present with a high probabiljty, too. Their metamorphic equivalents can be the rocks described as paragneisses containing sillimanite, cordieri e, hercynite etc. and revealing besides anomalous magnetization higher values of mineralogical densities. They can represent a specific type of high alumina intermediate volcanism, recently described from yong volcanic belts. It is noteworthy that e.g. the zone delimited by anomalies $s-r-q$ (Fig. 6), in the Moldanubicum more or less links up with the distinct zone of anomalies in the Mirovice metamorphic islet. This again draws attention to the recently newly raised problem of stratigraphic classification of the Bohemian Moldanubicum. The most striking of the zones delimited by magnetometry and petrophysics is the Písek zone, the easternmost NE–SW striking linear zone within the study area.

Conclusion

The airborne geophysical survey in southwestern Bohemia was carried out within an investigation of selected parts of the Bohemian Massif.

The quality of measurements and data processing surpassed the previous airborne surveys in Czechoslovakia. In the field was used the verification system based on the Olivetti M 20 computer which enables an immediate check of obtained data. The computer was used on site for processing of check measurements (stability of the instrument, background, test profiles), which also contributed to an increased quality of field works.

Data processing in the computing centre of Geofyzika Brno included a new way of complex data adjustment throughout the entire area of interest, which succeeded in eliminating the differences in measured field levels for individual flight days. Derived maps proved helpful for regional interpretation of the magnetic field.

Ground verification focused on the geological character of the anomalies. Interpretation yielded a lot of information. In some cases the contribution of magnetometry and gamma spectrometry is so important that it can result in changes in the concepts of the structural-geological image of individual parts of the studied area.

In the westernmost part of the area of interest, i.e. in the southern corner of the Teplá-Barrandian block, an expressive zone of magnetic anomalies can be observed, forming the southern part of the so-called Kdyně-Štěnovice first rate anomaly. It consists of several anomalous belts corresponding with decreased K, U, Th concentration zones and mostly correlating with morphological elevations built up by the products of Proterozoic basalt volcanism (the so-called "spilites"). Petrophysical and petrological studies proved that pyrrhotite is the main carrier of

anomalous magnetization in these rocks, regardless of the degree of regional or contact metamorphism. Similar character and source has the anomalous belt at the northern boundary of the Klatovy apophysis. In this belt, magnetite in metabasalts also manifests as carrier of magnetization.

The Klatovy apophysis exhibits anomalous radioactivity values. The course of the anomaly indicates that the boundary between the Kozlovice type and the marginal type is different from that shown in previous geological maps.

In the Moldanubicum, south of the Central Bohemian Pluton there are several NE–SW trending zones of anomalous magnetization. They are associated with the so called varied group of the Moldanubicum (Strážov, Sušice, Strakonice units). According to petrophysical and petrological studies the source of these zones are metamorphic products of volcanism of bipolar character. Regardless of their acid or mafic chemism they contain magnetite. Magnetite is also present in rocks of the type of cordierite-sillimanite paragneisses with high mineralogical densities, the educt of which may be also volcanic. Most striking of the magnetic zones of this kind is the Písek zone, which is also due to belt of metamorphic bipolar volcanics, fringing the north-western boundary of the Podolsko complex. In the radiometric pattern, the Podolsko complex is manifested by an increased Th-concentration and the boundary so characterized coincides with the anomalies in the northern part of the Písek zone. In the southern part of the Písek magnetic anomaly the boundary is veiled by the presence of E–W trending anomalies of Th, U and K concentrations. These anomalies are associated with acid dykes obviously indicating younger disjunctive tectonics of regional significance.

In the south-western margin of the study area the orientation of magnetic and some radiometric anomalies radically turns to the NW–SE (direction). It may indicate a linear zone of regional significance, almost over the entire area.

The study area comprises a whole range of metamorphic islets indicated by both magnetometry and radiometry. They are either minor enclaves in the Hory Matky Boží and Střelské Hoštice apophyses of the Central Bohemian Pluton, or the major metamorphic islets (Kasejovice, Sedlčany, Krásná Hora, Mirovice). There again the acid and mafic metamorphic volcanites containing magnetite are the sources of magnetic anomalies.

Airborne gamma spectrometry revealed zones of increased U-concentrations with numerous local anomalies in the Central Bohemian Pluton, in the Moldanubicum between Mirotice and Putim, in the West Bohemian Proterozoic between Blovice and Čížkov.

It should be noted that further occurrences of ore mineralizations may be anticipated not only in the zones of anomalies themselves, but also in some transverse structures disrupting them or even dislocating them. It concerns NW–SE lines as well as E–W lines.

K tisku doporučil Z. Mísař
Přeložila D. Maliková

References

Anderson, W. W.—Ahrens, T. Y. (1986): Shock wave experiments on iron sulfide and sulfur in planetary cores. — LPSC, 17, *11—12*, LPI. Houston.

Benda, V. (1973): Geofyzikální podklady pro prognózní ocenění Českého masívu — Nové Mitrovice, magnetometrie. — MS Geofyzika, s. p., Brno. Praha.

Čejchanová, B. (1971): Petrofyzikální charakteristika spilitového vulkanismu a výzkum příčin kdyňsko-štěnovické magnetické anomálie. (Rigorózní práce.) — MS přírodověd. fak. Univ. Karl. Praha.

Dědáček, K. et al. (1985): Letecký geofyzikální výzkum a geologická interpretace jižní části středočeského plutonu a přilehlé části moldanubika. — MS Geofond. Praha.

Hron, J. (1963): Ověřování aeromagnetických anomálií. — MS Geofond. Praha.

Chlupáčová, M. et al. (1984): Petrofyzikální výzkum pro rudní geofyziku. — MS Geofyzika, s. p., Brno. Praha.

Každan, A. B. (1983): Prognozirovanie, poiski i razvedka mestoroždenij urana. — Ènergoatomizdat. Moskva.

Kovalová, M.—Mrázek, P. (1986): Minoritní prvky v proterozoických horninách mezi Trnčínem a Struhadlem u Klatov. — Čas. Mineral. Geol., 31, 2, *153—171*. Praha.

Krasnov, A. I. et al. (1980): Aérogeofizičeskie metody prognozirovanija mestoroždenij urana. — Atomizdat. Moskva.

Krsová, M. (1976): Výzkum příčin kdyňsko-štěnovické anomálie. — MS Geofyzika, s. p., Brno. Praha.

Krsová, M.—Šťovíčková, N. (1975): Petrofyzikální charakteristika geofyzikálně anomálních oblastí — II. etapa. — MS Geofyzika, s. p., Brno. Praha.

Matolín, M. (1970): Radioaktivita hornin Českého masívu. — Academia. Praha.

Pokorný, L.—Šťovíčková, N.—Beneš, L. (1975): Geologické projevy strukturně geologických deformací. (Závěrečná zpráva za etapu 1974.) — MS Geofond. Praha.

— (1986): Geofyzikálně indikované zlomové struktury Českého masívu a jejich význam pro metalogenezi. — Sbor. geol. Věd, užitá Geofyz., 19,*127—150*. Praha.

Röhlich, P.—Šťovíčková, N. (1968): Die Tiefenstörungs-Tektonik und deren Entwicklung im zentralen Teil der Böhmischen Masse. — Geologie, 17, 6/7, *670—694*. Berlin.

Šalanský, K.—Čejchanová, B. (1973): Geofyzikální výzkum spilitového vulkanismu barrandienského proterozoika. — MS Geofyzika, s. p., Brno. Praha.

Šalanský, K.—Manová, M. (1966): Zpráva o leteckém geofyzikálním měření v letech 1962—1964. V. Jižní Čechy. — MS Geofyzika, s. p., Brno. Praha.

— (1974): Letecké geofyzikální mapování — XIII — Jihozápadní Čechy. — Geofyzika, s. p., Brno. Praha.

— (1976): Letecké geofyzikální mapování — XIV — Šumava. — Geofyzika,s. p., Brno. Praha.

Vorobjev, V. P. et al. (1977): Aérogamma-spektrometričeskij metod poiskov rudnych mestoroždenij. — Nedra. Leningrad.

Letecké geofyzikální měření v jihozápadních Čechách (Pošumaví) a jeho interpretace

(Résumé anglického textu)

Karel Dědáček–Jan Mašín–Naděžda Šťovíčková–Zdeněk Vejnar – Václav Veselý

Předloženo 22. září 1988

V šedesátých letech a počátkem 70. let proběhla na našem státním území etapa podrobného leteckého geofyzikálního měření – magnetického a radiometrického (úhrnná radioaktivita), která byla po řadu let interpretována v oblasti Českého masívu kolektivem vedeným K. Šalanským.

V rámci nového leteckého geofyzikálního mapování s magnetometrem G801/3B fy Geometrics a gamaspektrometrem DiGRS 3001 fy Exploranium, prováděného s. p. Geofyzika Brno, byla proměřena v roce 1983 oblast Pošumaví.

Do oblasti Pošumaví spadaly z regionálně geologického hlediska jz. cíp středočeského barrandienského proterozoika a přilehlé domažlické krystalinikum s částí kdyňského bazického komplexu, jz. část středočeského plutonu (tj. klatovská a chanovická apofýza), dále metamorfované ostrovy nebo jejich část (kasejovický a jižní část mirovického a sedlčansko-krásnohorského) a konečně krystalinikum českého moldanubika, přesněji jeho pestré jednotky strážovská, sušická a strakonická a v jeho nejvýchodnější části podolský komplex.

Výsledky měření byly zpracovány ve výpočetním středisku s. p. Geofyzika Brno a prezentovány ve formě map izolinií anomálií magnetického pole, úhrnné aktivity gama a koncentrací K, U a Th v měřítku 1 : 50 000 a 1 : 200 000. Počítačové zpracování umožnilo sestavit odvozené mapy magnetometrie (přepočty do různých úrovní) a gamaspektrometrie (poměry koncentrací radioaktivních prvků).

Na základě získaných mapových podkladů byla provedena komplexní interpretace s použitím terénní rekognoskace území a pozemních ověření významnějších magnetických a gamaspektrometrických anomálií. Na řadě magnetických anomálií byly odebrány vzorky hornin a určeny jejich petrofyzikální a petrologické charakteristiky.

Magnetické pole v oblasti Pošumaví je dosti členité a jednotlivé geologické celky se odlišují specifickým charakterem magnetických anomálií.

V nejzápadnější části území je výrazná kdyňsko-štěnovická anomálie tvořena několika více nebo méně pravidelnými zónami (*a* až *e* na obr. 6). Výsledky pozemních geofyzikálních měření i petrofyzikálního ověřování některých anomálií v tomto prostoru jednoznačně ukazují, že magnetické anomálie jsou vázány na proterozoické bazalty, tzv. spility, s vysokým obsahem pyrhotinu, event. na horniny, které jsou s nimi geneticky spjaté, tj. tufy a tufity.

Severozápadní okraj klatovské apofýzy sleduje žinkovská magnetická zóna. Anomálie v jz. části této zóny (g_1) mohou být vyvolány pyrhotinem, vzniklým kontaktní metamorfózou proterozoických kyzových břidlic. V severovýchodní části žinkovské zóny (g_2) jsou vázány na výskyty metabazitů (kontaktních amfibolických rohovců) s magnetitem.

Ve středočeském plutonu v j. výběžku chanovické apofýzy vystupuje anomální zóna *l*, která odpovídá vložkám amfibolitů, a u Březan nevýrazná zóna *m*, pravděpodobně vyvolaná zbytky pláště plutonu.

Intenzívní anomálie vyvolávají horniny kasejovického (*i*) a mirovického ostrova (*o*). Méně výrazný je projev starosedelských ortorul v j. cípu sedlčansko-krásnohorského ostrova (*u*).

V moldanubiku vystupují jednotlivé zóny magnetických anomálií (*h*, *k*, *n*, *g*, *r*, *t*), které jsou orientovány přibližně ve směru SV–JZ. Nejvýraznější z nich je tzv. písecká zóna (*t*). Severní část této zóny sleduje velmi přesně rozhraní nižších koncentrací K, U a Th na SZ a vyšších na JV. Dále k JZ nelze toto rozhraní sledovat, protože pole koncentrací je komplikováno lokálními anomáliemi. Tato situace nasvědčuje, že písecká zóna sleduje hranici podolského komplexu, který má vyšší radioaktivitu, a ostatního moldanubika.

V jižní části měřeného území se objevují anomálie spíše subekvatoriálních až sz.–jv. směrů. U takové nejrozsáhlejší anomální zóny (*s*) tvoří její z. část jakýsi uzel, ze kterého anomálie vybíhají všemi směry.

Směrově se také odlišuje zóna nevýrazných anomálií (*j*), která sleduje pásmo výstupů drobných granodioritových těles mezi j. výběžky chanovické apofýzy.

Zóny *y* a *z* kopírují kontakt granulitového tělesa.

Z hlediska radioaktivity náleží Pošumaví k oblastem s členitým polem přirozené radioaktivity, přítomné jednotky se vzájemně odlišují distribucí radioaktivních prvků. Zatímco většina magmatitů středočeského plutonu náleží ke kyselým diferenciátům s relativně vysokými koncentracemi K a s tím do značné míry souvisejícími koncentracemi Th a U, náleží slabě metamorfované sedimenty a vulkanity proterozoika k horninám se sníženými koncentracemi těchto prvků. Radioaktivita metamorfitů moldanubika šumavské větve je pak ve srovnání se středočeským plutonem v průměru nižší a ve srovnání s proterozoikem naopak vyšší.

V oblasti proterozoika převládají horniny s nízkými koncentracemi K a Th. Rovněž průměrná koncentrace U je nižší než v oblasti moldanubika a středočeského plutonu. Distribuce radioaktivních prvků v obou zastižených částech proterozoika (v z. okolí Klatov a v okolí Blovic) je přesto poněkud rozdílná.

Západní okolí Klatov mezi klatovskou apofýzou středočeského plutonu, kdyňským a stodským masivem se vyznačuje nejnižším polem koncentrací K, U a Th. Zjištěné extrémní koncentrace odpovídají bazickým proterozoickým vulkanitům. V okolí Blovic je vyšší diferenciace pole koncentrace U, kde se kromě celkového zvýšení nad průměr proterozoika vyskytla řada lokálních anomálií.

Většina granodioritů středočeského plutonu má průměrné koncentrace K,

U i Th blízké. V oblasti klatovské apofýzy se od ostatních granitoidů odlišují vyšším polem koncentrací K, U i Th granity až granodiority okrajového typu. Koncentrace odpovídající anomálie se odchyluje od hranic geologicky předpokládaného rozšíření tohoto typu, a to zejména v místech připojení klatovské apofýzy ke středočeskému plutonu, kde se podle interpretace leteckých map koncentrací již okrajové granity neuplatňují.

Oba kontakty klatovské apofýzy i sz. kontakt chanovické apofýzy se od svého okolí poměrně výrazně odlišují. Podobně jako v magmatitech klatovské apofýzy, jsou i v blatenském granodioritu koncentrace K, U a zejména Th vyšší než v okolí a jejich rozdíly proti moldanubiku jsou dostatečně kontrastní pro stanovení průběhu hranice. Naproti tomu hranici červenského typu, který se uplatňuje v kolineckém výběžku a dále podél j. okraje středočeského plutonu až k Písku, není v polích koncentrací možné jednoznačně interpretovat. Příčinou je pozvolné snižování koncentrací ve středočeském plutonu směrem k jeho j. okraji. Blatenský granodiorit se kontrastně odlišuje od metamorfovaných ostrovů mezi Kasejovicemi a Uzeničkami i od z. okraje mirovického ostrova.

Vysokými koncentracemi se jednoznačně odlišuje durbachit typu Čertova břemene u Soběděraže. Výskyt stejného typu u Vráže se rovněž projevuje anomálními koncentracemi K, U i Th, které však podle leteckých map přesahují rozsah odpovídajícího geologicky předpokládaného tělesa.

Koncentrace radioaktivních prvků ve většině moldanubických hornin je velmi blízká, a proto není možné na základě leteckých radiometrických map odlišit pararuly od ortorul a migmatitů. Směrem od SZ k JV se radioaktivita para- i ortosérií pozvolna a mírně zvyšuje. Ve v. části je zřejmá souvislost vyšších konších koncentrací s migmatity ortorulového vzhledu podolského komplexu.

Výrazné v.—z. lineární anomálie v oblasti mezi Kašperskými Horami, Volyní, Bavorovem a Vimperkem jsou způsobeny akumulací paralelních žil, resp. i jednotlivými žílami porfyrů a porfyritů s vysokou radioaktivitou.

Hlavní proterozoický vulkanitový pruh sz. křídla Barrandienu, tzv. domažlicko-kralupský, resp. jeho jz. část, koinciduje zcela přesně s nejintenzívnější magnetickou zónou této oblasti — kdyňsko-štěnovickou magnetickou anomálií. Prostorově koreluje tato anomálie (i její jednotlivé dílčí zóny) přesně s morfologicky nápadnými elevacemi bazaltových paleovulkanitů, a to jak v jejich téměř nemetamorfovaném vývoji v jz. cípu Barrandienu, tak i v metamorfním vývoji v domažlickém krystaliniku. Jsou to tedy jednak velmi slabě regionálně metamorfované bazalty, tj. zelené břidlice s výraznými reliktními strukturami bazaltů a jejich tufů, jednak intenzívně regionálně i kontaktně metamorfované bazalty, tj. pyroxen-amfibolické rohovce bez reliktů původních lávových a pyroklastických struktur. V obou typech je přítomen pyrhotin, udílející jim často vysoké hodnoty remanentní magnetizace (při relativně nízkých hodnotách $\varkappa$ bývá $Q > 20$; tab. 3). Pyrhotin je přítomen nejen jako integrální rudní minerál přímo ve vulkanitech, ale i jako samostatné sulfidické zrudnění na tento vulkanismus nepochybně vázané. Pyrhotin tedy před-

stavuje povrchový zdroj anomální magnetizace samotných vulkanitů, ale podle intenzity a charakteru anomálie nelze vyloučit přítomnost subvulkanických i hlubších těles obsahujících i jiná feromagnetika, především magnetit. U této zóny tedy magnetometrie, ale i gamaspektrometrie zřejmě zobrazuje významnou zónu lineární extenzní tektoniky rozpínání proterozoického mořského dna, tj. tehdejší oceánské kůry. Produkty vulkanismu vázané na tuto zónu mají tholeiitový charakter potvrzený deficitem všech tří gamaspektrometricky sledovaných prvků (U, Th, K). Hustoty paleobazaltů jsou dosti jednotné, kromě tufů nikdy neklesají pod hodnotu 3,0 g . cm^{-3}. Nejjižnější anomální zóna v proterozoiku, tzv. žinkovská, sledující z. kontakt klatovské apofýzy středočeského plutonu, koinciduje opět s pruhem kontaktně metamorfovaných paleobazaltů, v nichž je dominantním feromagnetickým minerálem magnetit.

Horniny středočeského plutonu anomální magnetizaci nevykazují. Pokud se v oblasti budované granitoidními horninami vyskytují lokální anomálie, jsou vždy vyvolávány magnetizovanými enklávami amfibolitů, erlanů a leptynitů (zejména v chanovické apofýze a střelskohoštickém výběžku plutonu).

Horniny metamorfovaných ostrovů jsou jedním z nejvýraznějších anomálních zdrojů v oblasti Pošumaví. V kasejovickém ostrovu to jsou kvarcity s magnetitem, dvojslídné a leukokratní ortoruly, rohovcovité biotitické pararuly, amfibolity s magnetitem, pouze v j. části ostrova s pyrhotinem. V jižní části mirovického ostrova jsou to jednak mirotické ortoruly, namnoze leukokratní, jednak horniny dioritového až gabrového složení vesměs s magnetitem. Struktury většiny uvedených hornin jak kyselých tak bazických mají rysy původních vulkanických struktur.

Anomální zóny sv.—jz. směru i jednotlivé anomálie v prostoru strážovské, sušické a strakonické pestré jednotky moldanubika lze vesměs objasnit povrchovými zdroji, tj. anomální magnetizací některých specifických typů krystalických břidlic. Jsou to tyto horninové typy: sillimanit-cordieritické pararuly s magnetitem, místy i hercynitem o vysokých hodnotách $\varkappa = 126 . 10^{-3}$ SI i vysokých hodnotách σ_m (2,90 g . cm^{-3}), migmatity ortorulového vzhledu až leptynity a erlany a konečně amfibolity, pro něž je příznačný vyšší obsah živců a křemene (tím i relativně nízké hustoty). U všech těchto typů lze předpokládat předmetamorfní vulkanogenní původ. Toto zjištění platí pro všechny anomální zóny, především pro nejvýraznější z nich — píseckou. Je tedy velmi pravděpodobné, že u všech těchto sv.—jz. zón jde o lineární vulkanická pásma hornin kontrastního chemismu od křemenem bohatých trondhjemitických až po bazické, přičemž podíl bazické složky stoupá směrem k JZ. Nositelem magnetizace je magnetit.

Porovnáme-li kontrastní charakter vulkanismu bloku moldanubického s tholeiitovým charakterem vulkanismu sousedního tepelsko-barrandienského bloku, dospějeme znovu nutně k závěru, že tento blok se vyznačuje jinou korovou a pravděpodobně i podkorovou stavbou. Jak skutečnost, že v moldanubickém bloku magnetické anomální zóny vcelku nekorelují s význačnými tíhovými prvky, tak i kontrastní charakter vulkanismu svědčí pro vnitroblokový rozsah a menší hlu-

binný (nejspíše korový) dosah tektonických struktur leteckou magnetometrií indikovaných. Navíc i tento strukturní pohled opětovně motivuje úvahy o stratigrafickém zařazení pestrých skupin moldanubika v současné době znovu živě diskutované. Především je tím, byť nepřímo, dokumentována větší mocnost kůry v prostoru moldanubického bloku, o které přímo svědčí gravimetrické a seizmické údaje.

Vysvětlivky k tabulkám

Tabulka 1. Střední chyba jednoho měření.

Tabulka 2. Výsledky statistického zpracování pozemní spektrometrie gama. p — aritmetický průměr, σ — směrodatná odchylka aritmetického průměru.

Tabulka 3. Přehled anomálně magnetizovaných hornin a jejich základních fyzikálních vlastností.

Vysvětlivky k obrazkům v textu

1. Zjednodušená geologie a přehled odběru vzorků pro petrofyzikální výzkum.
   1 — moldanubikum, *2* — proterozoikum, *3* — KI — kasejovický ostrov, MI — mirovický ostrov, *4* — bazické vulkanity a plutonity: β' — proterozoické bazalty (spility), σ — kdyňský masív (KM), A — amfibolity, *5* — kyselé a intermediární plutonity, CBP — středočeský pluton, SGM — stodský masív, *6* — lokality odběru vzorků (symbol *PŠ* v textu).
2. Letecká magnetometrie, přepočet pole ΔT do výšky 200 m nad úrovní letu.
3. Letecká gamaspektrometrie, koncentrace draslíku.
4. Geofyzikální profily nad štolou u Tetětic.
   1 — profil A — zdánlivý specifický odpor a vynucená polarizace, *2* — metoda VDV (reálná složka), *3* — magnetometrie, *4* — susceptibilita měřená ve štole a na jádrech z vrtu SP-1, *5* — geologický profil, *6* — spility a amfibolitické metabazity, *7* — drobové břidlice a prachovce, *8* — grafitické břidlice s polohami metabazitů, *9* — stratiformní zrudnění, *10* — pásma drcení.
5. Přehledné geofyzikální schéma radiometrie.
   1 — anomálie bez geologického opodstatnění, *2* — anomálie odpovídající známým objektům, *3* — regionální anomálie vícekomponentní, *4* — regionální anomálie K, *5* — regionální anomálie U, *6* — regionální anomálie Th, *7* — regionální gradienty koncentrací — vícekomponentní, *8* — regionální gradienty K, *9* — regionální gradienty U, *10* — regionální gradienty Th, *11* — lokální anomálie vícekomponentní, *12* — lokální anomálie K, *13* — lokální anomálie U, *14* — lokální anomálie Th, *15* — regionální anomálie nízkého poměru Th/U, *16* — lokální anomálie nízkého poměru Th/U. Šrafováno vždy na straně vyšší koncentrace.
6. Přehledné geofyzikální schéma magnetometrie a gravimetrie.
   1 — anomální magnetické zóny — $\Delta T < 200$ nT, *2* — anomální magnetické zóny — $\Delta T > 200$ nT, *3* — vymezení jednotlivých magnetických zón, *4* — interpretované tektonické linie, *5* — izolinie tíhového pole, *6* — osy záporných tíhových anomálií, *7* — osy kladných tíhových anomálií, *8* — hranice aerogeofyzikálního mapování 1 : 25 000.

АЭРОГЕОФИЗИЧЕСКИЕ ИЗМЕРЕНИЯ В Ю.-З. ЧЕХИИ (ШУМАВСКАЯ ОБЛАСТЬ) И ИХ ИНТЕРПРЕТАЦИЯ

В баррандиенском протерозое в исследуемой области было обнаружено, что главным источником четких зональных магнитных аномалий является пирротин, присутствующий в продуктах палеобазальтового вулканизма, которые по данным радиометрии однозначно проявляются минимумом K, U и Th.

Область Среднечешского плутона по данным магнитометрии не проявляется. В поле концентраций радиоактивных элементов отчетливо наблюдаются с.-з. контакты частичных апофиз. В метаморфизованных островах плутона выступают крупные магнитные аномалии, обусловленные продуктами кислого и основного вулканизма, содержащими магнетит. Радиометрические аномалии свидетельствуют о значительной изменчивости пород островной зоны.

Область Молданубикума характеризована региональными аномальными зонами намагниченности преимущественно с.-в.—ю.-з. направления, источники которых представляют метаморфизованные вулканиты контрастного химизма, содержащие магнетит. Аномалии радиоактивности в в.-з. направлении могут наблюдаться длиной до десятков км. Они сопровождают жильные системы порфиров и порфиритов.

Přeložila H. Kuksová

Sbor. geol. věd	Užitá geofyz., 24	Pages 51–69	7 figs.	5 tabs.	– pl.	Praha 1990 ISSN 0036-5319

Interactive program for kinematic problems in laterally heterogeneous media

Program pro interaktivní řešení kinematických úloh v laterálně nehomogenních prostředích

Petr Firbas[1]–Marta Skorkovská[1]

Received September 14, 1988

Computer program
Refraction methods
Velocity models
Interactive program

Firbas, P.–Skorkovská, M. (1990): Interactive program for kinematic problems in laterally heterogeneous media. – Sbor. geol. Věd, užitá Geofyz., 24, *51–69*. Praha.

Abstract: An interactive program system for modelling velocity distribution of seismic waves in 2-D laterally heterogeneous stratified media with curved interface is described. The inverse kinematic problem can be solved by means of the method of successive approximations. Applied to ray equations, the method assumes piecewise linear approximation of the medium. The program system enables fast computation of rays or fans of rays, interruption of the computation in real time, and interactive change of all parameters of the velocity model within one passage of the program. All these features make an efficient shell for the inverse problem solution. The program system was written in BASIC for the desk-top computer Hewlett–Packard HP 9845 for full use of HP graphics software and graphics peripheral devices. An example is given of computation for a 2-D laterally heterogeneous stratified model. It is a test model suggested by W. D. Mooney for the Symposium of the Commission on Controlled Source Seismology at Einsiedeln, Switzerland, 1983. The program system was also tested on real data, but these results will be published in a following paper.

[1] *Geofyzika Brno, s. p., Brno, Podnikový výzkumný ústav, Ječná 29a, 612 46 Brno 12*

Introduction

During the last fifteen years the increasing volumes of data forced the development of interpretational methods which would enable construction of sufficiently accurate mathematical models for areas with complicated structure, which in

recent years have been in the focus of seismic investigations. The assumption of a laterally homogeneous stratified medium cannot elucidate the numerous characteristic features of the measured data, or may lead to erroneous conclusions. All the investigated real media are laterally heterogeneous and therefore methods have been developed for finding the distribution of real velocities in the depth section for laterally heterogeneous media, i.e. for solving both the direct and inverse problem.

One way of constructing a velocity model of laterally heterogeneous medium is the "trial and error" method. It is a method of successive approximations for solving the inverse kinematic problem. For this purpose interactive modelling seems to be optimum. Therefore the desk-top computer HP 9845 was chosen for computations. It makes it possible to use the HP graphics software and it is equipped with appropriate graphics peripherals (graphics screen, matrix printer, four-colour plotter A3).

Solution of the inverse problem using desk-top computer

The aim was to develop a fully interactive program system for fast construction of an accurate velocity model, using refraction data or combined refraction and reflection data by the "trial and error" method.

Two approaches to calculation of rays have been successively applied. First an approach solving seismic ray equations for laterally heterogeneous media (Červený–Molotkov–Pšenčík 1977) by the 4th order Runge–Kutta method was used. The developed program was based on programs of the Mathematical-Physical Faculty of Charles University (Červený–Pšenčík 1981) written in FORTRAN, where the velocity model and interfaces are given by a relatively dense grid of points. The interactive program was written for media without interfaces only as its expansion for media with interfaces became cumbersome and demanding for the computer memory.

The other approach of calculating seismic waves assumes piecewise linear approximation of the velocity distribution in the medium. Then the solution of ray equations is analytical and results are given by explicit expressions. This approach is based on the method (Aric–Gutdeutsch–Sailer 1980) which was further developed (Firbas–Skorkovská 1984). On its basis a fully interactive program system for the desk-top computer HP 9845 was written in BASIC, assuming full use of graphics HP software and graphics peripherals. The system was tested. Despite the limitations of the computer's internal memory capacity (64 Kb) it was feasible through extensive program segmentation to implement all changes of the velocity model in the main segment of program RAY. The program segmentation was done in such a way that every task of the program was coded in one segment only so the program speed in interactive mode was not lowered.

Description of the model

From the top the medium is bounded by a curved relief, from the bottom by a curved interface, and from the sides by two vertical boundaries. The model can consist of up to ten layers separated by curved interfaces. Each interface must intersect the whole area delimited by vertical boundaries. The interfaces must not mutually intersect, but may touch, or overlap. The model can therefore contain layers of zero thickness. The interfaces and layers are numbered downwards.

The whole studied area must be covered with vertical grid lines and the whole first layer with horizontal grid lines as well. The first vertical line coincides with the left boundary of the model, the last with the right boundary. The program works with a maximum of 19 vertical and 20 horizontal grid lines. Distances between all lines can be non-equidistant.

The velocity model enables a more detailed description of the first layer. The velocity distribution of the first layer is given by velocities at the grid points of non-equidistant rectangular grid formed by horizontal and vertical grid lines. The depths of the interfaces and the heights of the relief are given on all vertical lines. The velocity distribution of any deeper-seated layer is given by velocities below its upper and above its lower interface on all vertical lines. The program internally divides the medium into triangles where the analytical formulae for ray and travel-time are applied.

Description of waves

Program RAY can be used for computation of ray diagrams and times of arrivals of rays to the surface for multiple-reflected and reflected P and S waves, and for transformed waves. The refracted ray is a ray which refracts upon incidence on all interfaces. This type of rays can be computed automatically without additional information. If the refracted ray hits the interface under an over-critical angle, then its computation is prematurely terminated.

The behaviour of a multiple-reflected ray is given by a code. The code contains information about the layers through which the ray successively passes. It therefore implies on which interfaces the ray is reflected or refracted. The code is formed by a sequence of integer numbers corresponding to numbers of layers through which the ray passes. The part of the ray between two subsequent points of reflection or refraction is called "ray element". If the end points of the ray elements lie on different interfaces, the element is called "simple ray element" and one number (the number of the layer in which the ray element lies) in the code corresponds to it. If the end points of the ray element lie on the same interface, two equal numbers in the code (numbers of the layer in which the element lies) correspond to it and such an element is called "compound element". The compound element

is therefore given as two single ray elements corresponding to a ray reflected in the given layer. The code definition is very close to that used in SEIS81 (Červený–Pšenčík 1981), but its use is expanded by the possibilities outlined later in this paper.

Short description of the program system

The program system consists of three segmented program units:

1. Program for constructing the input and for input of experimental traveltime curves.
2. Program for interactive computation of rays and for velocity model changes.
3. Program for selection and plotting of ray diagrams and corresponding experimental traveltime curves along with computed traveltimes.

The generalized scheme of the program system is outlined in fig. 1.

Program MODEL

The program MODEL is used for construction and testing of input velocity model and for input of experimental traveltime curves. The program is segmented and consists of the main program and 14 subroutines.

Input data are arranged as follows:

1. Each profile that is to be processed by the program RAY is named by four alphanumeric characters and name is recorded in the catalogue of profiles. The catalogue of profiles provides complete information about the profiles which can be further processed.
2. For each profile a set of files is used:
   a) catalogue of model files,
   b) catalogue of files of experimental traveltime curves,
   c) catalogue of rays,
   d) ray file.

The catalogue of model files provides complete information about files with the velocity models which are available for processing by the program RAY. Each velocity model is stored in one file and its name is written in the catalogue of model files. There may be a maximum of nine files with velocity models for each profile.

The catalogue of files of experimental traveltime curves contains complete information about files of experimental traveltime curves, including the number of traveltime curves. The maximum number of such data files for each profile is nine.

The program MODEL is used for creating a file with a velocity model. Another function of the program is to modify such an existing file. If a new profile is input,

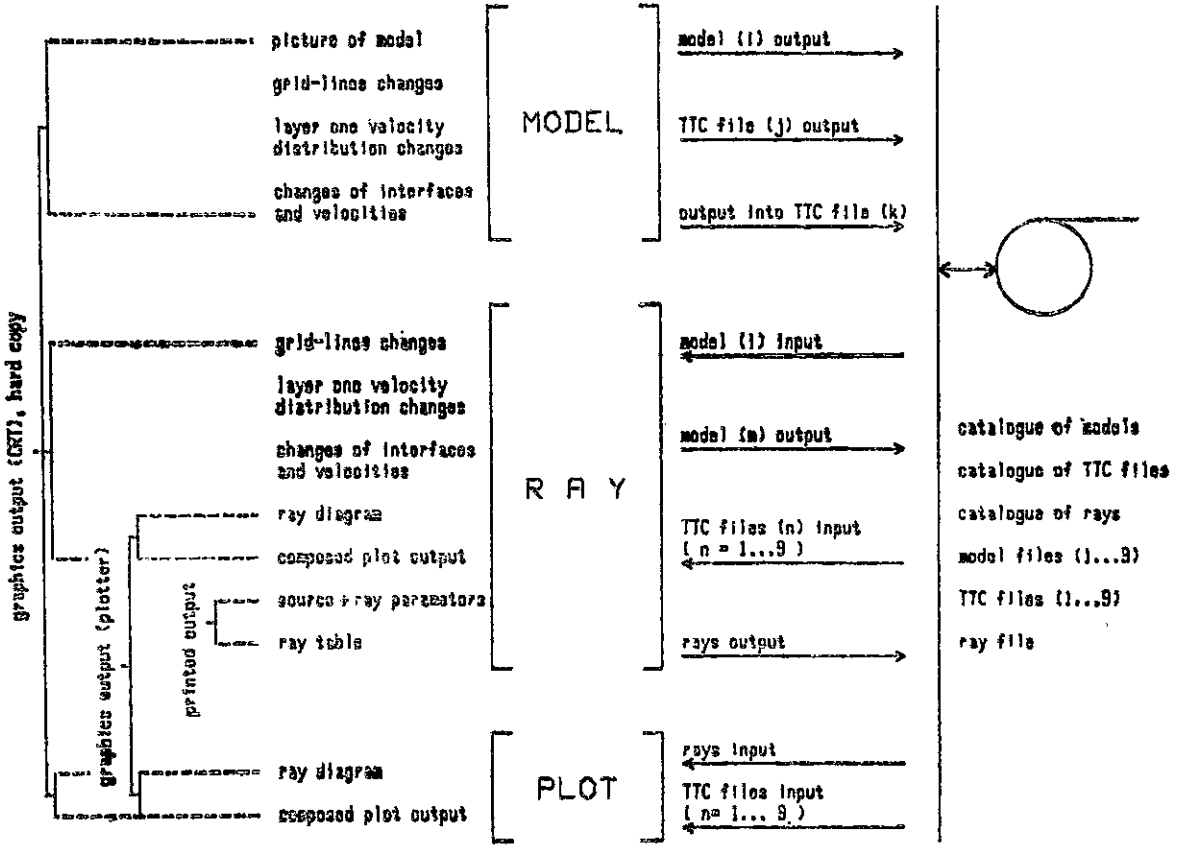

1. Generalized flow-diagram of the computation and input-output operations of the program system (programs MODEL, RAY, PLOT)

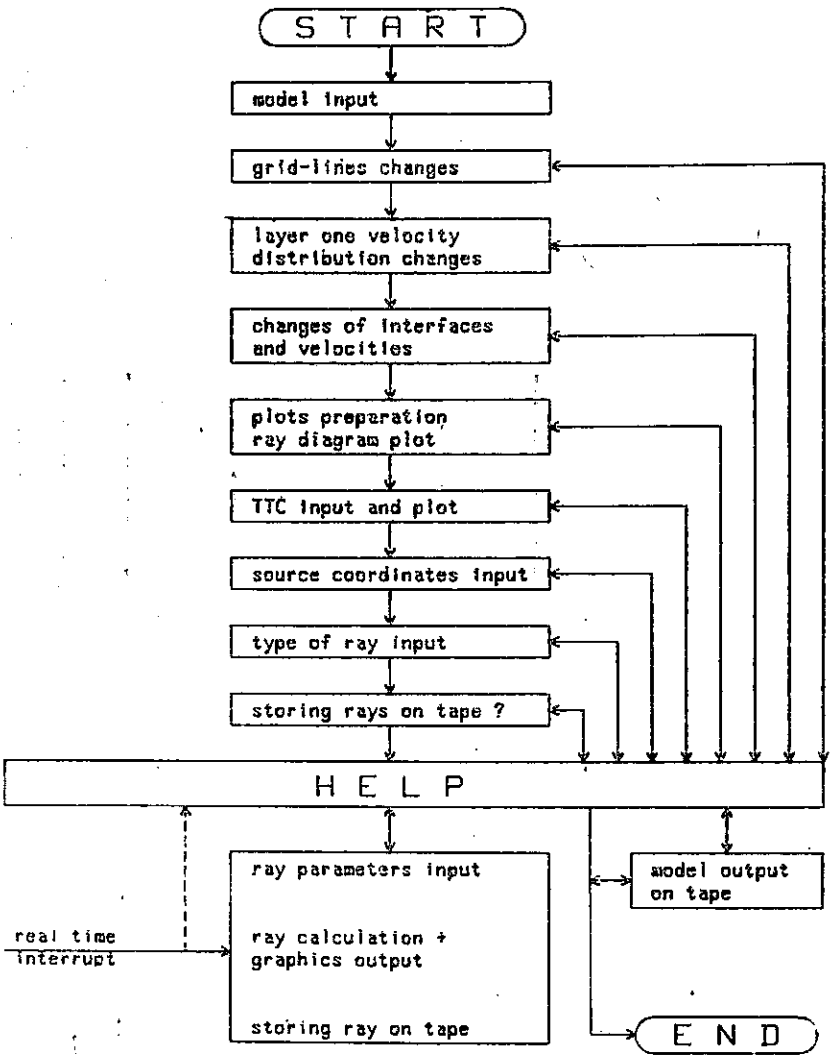

2. Simplified diagram for the program RAY

```
SELECT FUNCTION:

0          SHIFT OF A X-GRID LINE
1          DELETION OF A X-GRID LINE
2          INSERTION OF A X-GRID LINE
3          TABLE OF X-GRID LINES
4 OR CONT  SHOW PICTURE OF THE MODEL
5          ESCAPE

NUMBER OF THE X-GRID LINES IS 11 (MAXIMUM VALUE 19)
```

Table 1

Table of program branching as displayed at the point of change of vertical grid lines

its name is recorded in the catalogue of profiles. Subsequently, catalogues of models, traveltime curves, and rays are created.

The program enables interactive changes of all input values at the input stage of both the model and traveltimes. All data is tested at the input whether it is in reasonable limits.

Program RAY

The program RAY is the core of the program system. The program is segmented, consists of the main routine and 32 subroutines which form nine segments. The program can be used by an interpreter little acquainted with computers as in case of error the operator is instructed how to proceed.
The computation consists of six basic steps:

1. Input of the model and experimental traveltimes.
2. Changes of the model (if required).
3. Input of plotting parameters, selection and plotting of experimental traveltime curves.
4. Input of ray parameters.
5. Computation of rays with raypath plotting (interruption in real time possible).
6. Recording of the modified model on magnetic tape.

A simplified flow-diagram is in fig. 2. The computation starts with choice of a profile and of the appropriate velocity model. The choice is very simple as the table of existing velocity models available for the chosen profile is shown on the display.

As soon as the velocity model is stored in the internal memory, the model can be changed in three steps:

1. Changes of grid lines.
2. Changes of velocities in the first layer.
3. Changes of interfaces including changes of corresponding velocities under and over them.

The program enables to delete, add or shift any horizontal or vertical grid line and simultaneously tests on allowed input values. For instance, if a change of vertical grid line is required, the program prints a table of allowed actions (tab. 1).

If a grid line is to be shifted, the whole picture of the model is plotted (fig. 3) and the interpreter places the cursor near the line which is to be shifted. The program answers with the sequence number and the current coordinate of the grid line and expects the cursor input of a new grid line coordinate. The digitized new value is printed. If it is a non-acceptable value, it is automatically substituted with the nearest acceptable value. This coordinate can be changed from the key-

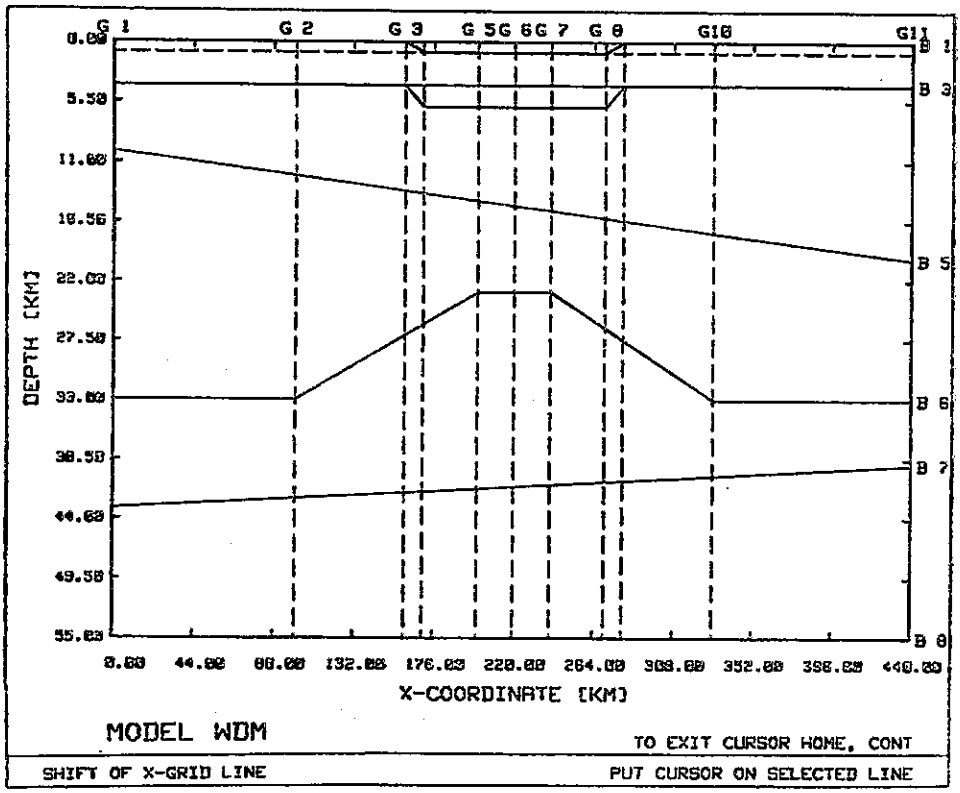

3. Model WDM (grid lines and interfaces) as shown on the display at the point of vertical grid lines changes, see table 1. Graphics cursor (not shown) serves for a vertical grid line selection and subsequently for digitization of its new coordinate

board, or the started shift of the grid line can be interrupted and the program control returned to the beginning of the program branch (changes of vertical grid lines). If the new grid line coordinate is accepted, the velocities in the first layer are automatically interpolated for this new grid line. The z-coordinates of all lower interfaces and velocities below and above them are also automatically interpolated. In this way the changes of horizontal and vertical grid lines can proceed.

In next step the velocities in the first layer can be changed. The program can display the first layer velocity model for up to ten vertical grid lines simultaneously. An example of graphics output for changing the first layer velocities is in table 2. The cursor is placed in the rectangle in which the velocity to be changed is located. The coordinates of the corresponding grid point are digitized, the original velocity value in the rectangle is erased and the value is offered for change together with information about the grid point coordinates. The new input value is plotted in the place of the old one. After the changes in the displayed part of the first

layer of the velocity model are completed, another part of the velocity grid can be plotted and changes may proceed.

Individual interfaces can also be changed interactively. The allowed branching of the program at the changes of interfaces is shown in table 3.

Table 2

Example of a velocity grid section for the first layer (model TEST) displayed at the point of velocity changes. Graphics cursor for x, y point picking is not shown

DEPTH [KM]	1	2	3	4	5	6	7	8	9	10	
0.00	3.90	4.10	4.05	3.80	3.80	3.70	3.65	3.65	3.72	3.90	1
1.00	4.70	4.70	4.65	4.50	4.40	4.39	4.30	4.20	4.32	4.24	2
2.00	5.30	5.40	5.40	5.12	5.02	5.02	4.45	4.40	4.92	5.00	3
3.00	5.85	5.85	5.70	5.40	5.20	5.20	4.72	4.70	5.42	5.55	4
4.00	6.10	6.00	6.10	5.65	5.50	5.40	4.85	4.80	5.53	5.75	5
5.00	6.15	6.10	6.15	6.05	5.80	5.65	5.02	5.03	5.64	5.85	6
6.00	6.20	6.20	6.29	6.10	6.00	5.80	5.40	5.40	5.70	5.92	7
7.00	6.25	6.25	6.35	6.32	6.20	5.90	5.65	5.65	5.96	6.04	8
8.00	6.30	6.30	6.42	6.40	6.20	6.03	5.75	5.72	6.10	6.10	9
9.00	6.35	6.35	6.43	6.42	6.33	6.15	5.80	5.80	6.15	6.30	10
10.00	6.45	6.36	6.43	6.42	6.42	6.30	6.10	6.10	6.22	6.42	11
12.00	6.40	6.40	6.42	6.42	6.49	6.35	6.30	6.25	6.35	6.46	12
14.00	6.30	6.30	6.30	6.40	6.55	6.46	6.42	6.30	6.42	6.49	13
16.00	6.30	6.30	6.30	6.30	6.65	6.55	6.55	6.55	6.55	6.55	14
18.00	6.35	6.35	6.35	6.35	6.65	6.60	6.60	6.60	6.60	6.60	15
20.00	6.45	6.45	6.45	6.45	6.65	6.65	6.65	6.65	6.65	6.65	16
24.50	6.65	6.65	6.65	6.65	6.70	6.70	6.70	6.70	6.70	6.70	17
25.00	7.04	7.04	7.04	7.04	7.04	7.04	7.04	7.04	7.04	7.04	18
30.00	7.21	7.21	7.21	7.21	7.21	7.21	7.21	7.21	7.21	7.21	19
40.00	7.60	7.60	7.60	7.60	7.60	7.60	7.60	7.60	7.60	7.60	20

0.0 50.0 100.0 150.0 200.0 250.0 300.0 350.0 400.0 450.0

X-COORDINATE [KM]

MODEL TEST

VELOCITY DISTRIBUTION

LOCATE CURSOR, PRESS CONT TO EXIT THIS BLOCK LOCATE CURSOR HOME

SELECT FUNCTION:

1 OR CONT THE PICTURE OF THE MODEL
2 SHIFT AN INTERFACE AND VELOCITY, CHANGE
3 DELETE AN INTERFACE
4 INSERT AN INTERFACE
5 END OF CHANGES

Table 3

Table of program branching as displayed at the point of interface changes

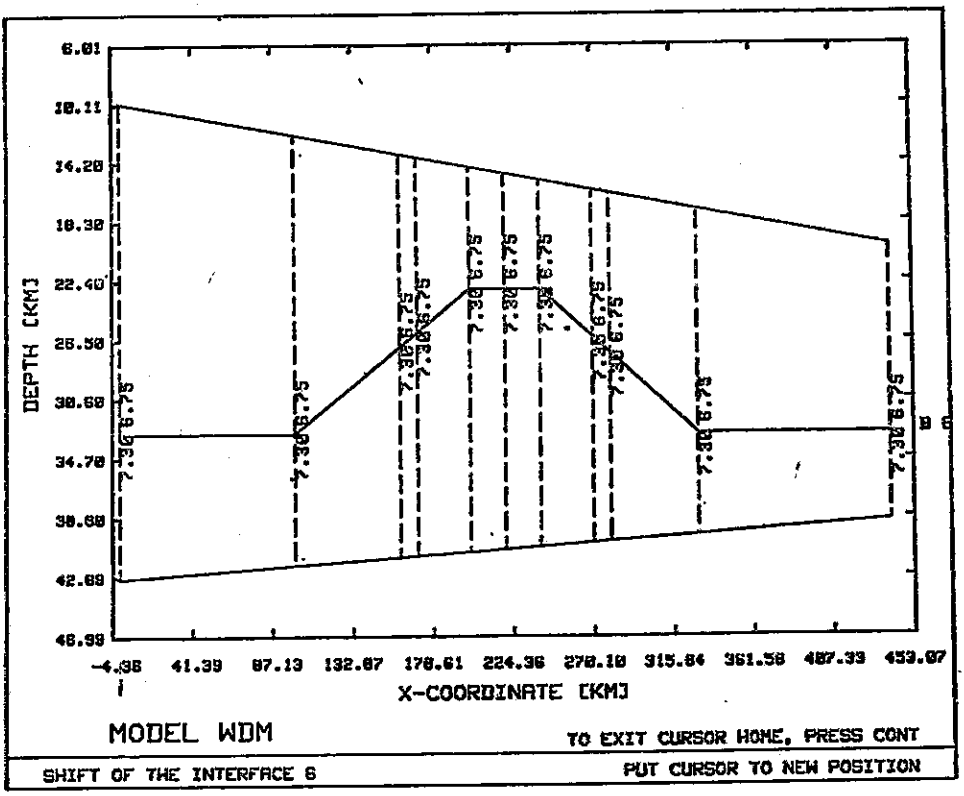

4. The picture shown on the display when the sixth interface is shifted. For convenience the velocities above and below the shifted interface are shown as well. Graphics cursor (not shown) serves for selection of the shifted grid point and for digitization of its new coordinate

If, for instance, a shift of the sixth interface is required, only the part of the model is displayed corresponding to the first and to the second layer. The velocity values are plotted along the interface to be changed. An example of graphics output for the shift of the sixth interface is in fig. 4. The choice of a new z-coordinate and of a vertical grid line where the interface is to be changed is performed simultaneously. The selected z-coordinate of the cursor represents the new z-coordinate of the interface. The cursor must be in close vicinity of the grid line for which the shape of the interface is to be changed. The old and the new coordinate are shown together with the coordinate of the vertical grid line and the operator is given the opportunity to accept it, or to modify it from the keyboard. After the new interface coordinate is accepted, the changed part of the interface and the corresponding velocities are erased from the picture. The corresponding velocities above and below the interface can be changed from the keyboard. In this way the whole interface or its part can readily be shifted.

Before changing the picture in the display, if it is required, a hard copy of the picture can be done. Thus information about all successive changes of the model can be preserved.

Next step is input of ray diagram parameters. All parameters have default values which can be changed according to the user's requirements. The output device is a four-colour plotter HP 9872A or graphics display. The program makes it possible to choose either a ray diagram plot only or to produce a composed graphics output, i.e. plot the ray diagram along with experimental traveltime curves and computed times of ray arrivals. The latter alternative seems to be more suitable as it makes it possible to simultaneously follow the computation of rays and directly compare the experimental traveltimes with the computed times of ray arrivals.

The traveltime curves for plotting in the composed graphics output can be interactively chosen from all available files with experimental traveltime curves corresponding to the chosen profile. The traveltime curves from a file can easily be chosen from the displayed list of traveltime curves. Immediately after the choice is completed, the chosen traveltime curves are plotted. Examples of composed graphics outputs are in figs. 6 and 7.

The next program step is the input of source coordinates and choice of the type of rays which will be computed. According to the behaviour of the rays at the interface the following types of rays can be selected:

a) refracted rays,
b) single reflected rays,
c) multiple reflected rays,
d) rays interactively controlled in the course of computation.

The difference between a single reflected and a multiple reflected ray is useful for the user's convenience. Rays of both types are internally code controlled but the code of the ray single reflected from an interface is automatically computer generated after the sequence number of the reflecting interface is input.

The interactive control of the ray in the course of computation means that after each incidence of the ray on an interface the interpreter can decide whether the ray will refract or reflect.

If a multiple reflected ray is required, the code of the ray must be given from the keyboard, but the computer assists at this task. After an inquiry whether it is an upward- or downward-pointing ray, the end point of the first ray element is automatically set. The display shows information about the interface which the ray should hit and another element of the ray can be chosen. At any stage of the code input it is possible to cancel the code input and return to a new source selection, a new type of ray, or to restart the code selection.

If the initial point of the ray element lies on an internal interface, choice can be made between a simple and a compound ray element (up- or down-oriented from the interface). For every ray element input the table of allowed functions is repeated-

ly shown on the display. The input of the code is successfully completed if the last ray element hits the surface of the model and no back reflection is requested.

As the last step the inquiry follows whether the rays to be computed should be stored on magnetic tape for later processing by the PLOT program or not.

At this point the first program pass is ended. Now, at the main branching point HELP the program is waiting for the interpreter's command. The possible program branching is displayed, see table 4. Either individual rays or fans of rays can be computed. In the latter case the number of rays in the fan, the initial angle at the source, the step of this angle and the step reduction factor must be given. In the course of computation of a ray or a fan or rays the passage of the ray through the medium in real time can be followed. The computation can be interrupted by a function key, the computed ray deleted, erased from the screen and the program control returned to the branching point HELP. If a composed graphics output has been chosen, the arrival time of the successful ray can be immediately plotted.

Table 4

Table of program branching at the point HELP, see fig. 2

1	NEW RAY DIAGRAM PLOT
2	ADDITIONAL TTC PLOT
3	CHANGES OF GRID-LINES IN THE FIRST LAYER
4	CHANGES OF THE VELOCITY DISTRIBUTION IN THE FIRST LAYER
5	CHANGES OF INTERFACES IN THE MODEL
6	NEW SHOT POINT
7	RAY COMPUTATION CONTROL
8	STORING-OF RAYS ON THE TAPE - ENABLE-DISABLE
9 OR CONT	RAY COMPUTATION
10	SAVE THE MODEL ON THE TAPE
11	END OF COMPUTATION (HARD COPY, SAVE THE MODEL ON THE TAPE)

Table 5

Example of a printer output for rays reflected at the seventh interface in the WDM model

```
X SOURCE =  50.000[KM]                          RAY CONTROLLED BY CODE
Z SOURCE =   0.000[KM]                          RAY ORIENTED DOWNWARDS
                                          CODE 1 2 3 4 5 6 6 5 4 3 2 1

RAY TABLE

RAY NO        X END      Z END       T END    PHI INIT    ERROR INDICATION
    12         2.869      0.000      14.600    -25.0000
    13        23.349      0.000      13.379    -15.0000
    14        41.012      0.000      12.825     -5.0000
    15        57.790      0.000      12.791      5.0000
    16        75.235      0.000      13.268     15.0000
    17        95.165      0.000      14.385     25.0000
    18       120.959      0.000      16.531     35.0000
    19       161.291      0.000      20.873     45.0000
```

If recording on magnetic tape is required, the computed ray is recorded in the ray file. One line is printed for each ray, containing the number of the ray, the angle at the source, the coordinates of the ray end point, the arrival time, and optionally the error message. An output is exemplified in table 5. After the computation of a ray or a fan of rays has been completed, the program returns to the branching point HELP.

Before the end of the computation it is checked whether the model has been changed. In such a case the new model can be stored as a new model variant.

Program PLOT

The program PLOT serves for selection and plotting of rays recorded by the program RAY on magnetic tape.

The rays can be repeatedly selected according to various criteria:

a) name of velocity model,
b) coordinates of the source,
c) chosen ray code,
d) refracted rays only,
e) sequence numbers of rays in the ray file.

The output graphics device is plotter or graphics display. Either a simple ray diagram can be plotted or a composed graphics output can be chosen. When the experimental traveltimes are to be plotted, their selection is the same as in the program RAY. The picture can be plotted also by parts, which enables plotting of long profiles or plotting in selected scale.

Model example and tests

The program function is exemplified by computation for the model o W. D. Mooney (U.S. Geological Survey, Menlo Park) which was prepared for the Symposium of the Commission on Controlled Source Seismology at Einsiedeln, Switzerland, 1983. This model named WDM consists of seven layers (fig. 5). It is laterally inhomogeneous because both the velocity distribution and shapes of the interfaces vary along the profile. The layers are numbered with roman figures. Velocities ($km \cdot s^{-1}$) below the upper and above the lower interfaces bounding individual layers are shown. The coordinates of the interfaces are given on all vertical grid lines. The positions of the lines can be seen in fig. 3. Computations were done for two reflected waves from the sixth (code 1234554321) and the seventh (code 123456654321) interface. The composed graphics output for the wave reflected on the sixth interface is in fig. 6 and for the wave reflected on the seventh interface in fig. 7. Computation of 10 rays in the fan where the rays are

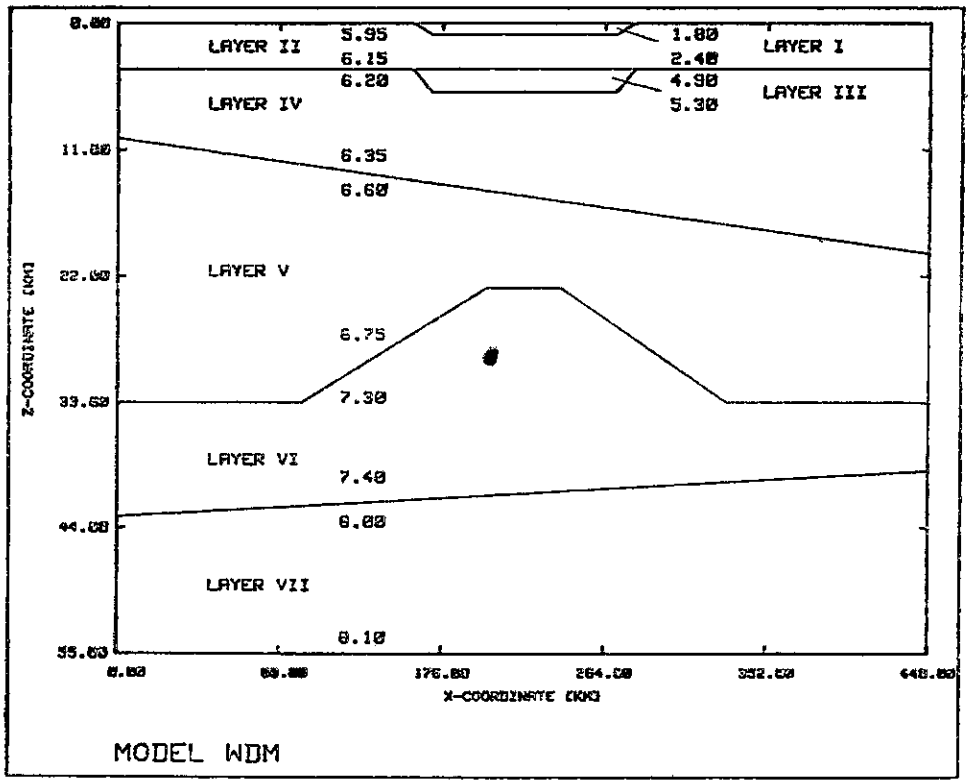

5. Two-dimensional laterally inhomogeneous velocity model suggested by W. D. Mooney. Velocities in km . s^{-1}

on average 25 points long including the graphics output on plotter lasts four minutes 18 seconds. For comparison, the traveltimes computed for the WDM model by the program TRIANGL (Červený–Jánský 1985) were used in the role of experimental traveltime curves. The "experimental" traveltime curves and the computed times have been plotted with reduction velocity 6 km/s. The results produced by the program RAY are in good agreement with the traveltime curves computed by the program TRIANGL.

In the period 1986–1987 the program was also tested on real refraction data. The present version is based on the gained experience. The examples will be published in a following paper.

Conclusion

The program system for solving the direct kinematic problem and the inverse kinematic problem by the "trial and error method" for laterally inhomogeneous medium with curved interfaces was developed. The system is fully interactive and

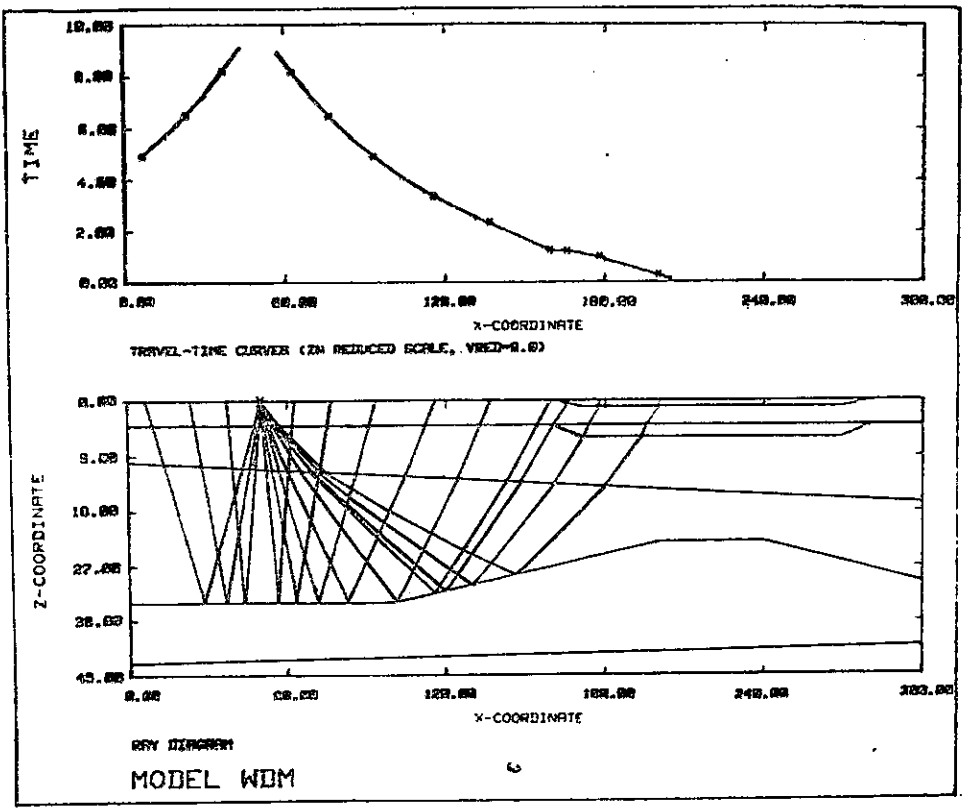

6. Example of a composed graphics output for the WDM model. The rays reflected from the sixth interface are shown. Traveltimes are plotted with the reduction velocity of 6 km . s^{-1}

so enables fast and precise modelling on any velocity distribution consisting of several layers separated by curved interfaces. The system is formed by three programs – MODEL, RAY and PLOT. The core of the whole system is the program RAY for fast computation of rays and fans of rays.

Within one run of the program RAY interactive and fast changes of all parameters of the velocity model can be performed. The program RAY can be applied for verification of velocity models, using various types of waves from different shotpoints as well.

The program system was written in BASIC for the desk-top computer HP 9845. Owing to the interactive operation the time needed for construction of a velocity model was many times reduced as compared with batch-processing. The system was successfully tested on model refraction data and its possibilities were verified for real field data.

K tisku doporučil I. Pšenčík
Přeložila D. Malíková

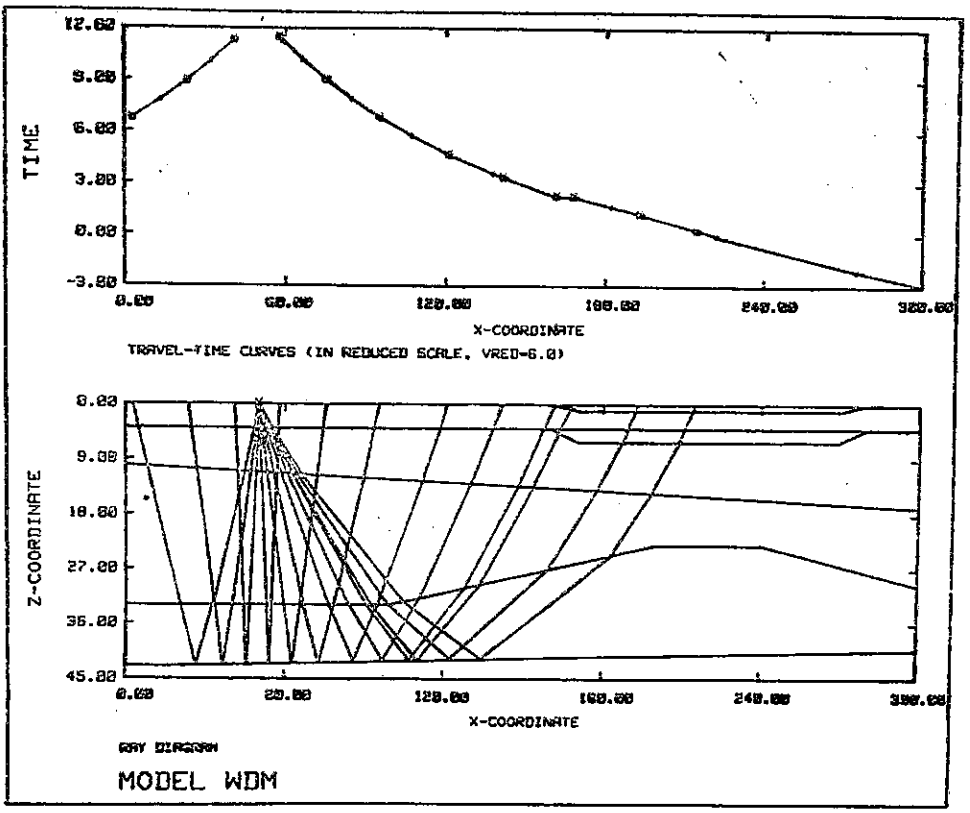

7. Example of a composed graphics output for the WDM model. The rays reflected from the seventh interface are plotted with the reduction velocity of 6 km . s^{-1}

References

Aric, K.–Gutdeutsch, R.–Sailer, A. (1980): Computation of traveltimes and rays in a medium of 2-D velocity distribution. – Pageoph., 118, *796–805.*

Červený, V.–Janský, J. (1985): Rychlé řešení kinematických úloh ve dvoudimensionálních prostředích, založené na trojúhelníkové aproximaci prostředí, program TRIANGL. Dílčí zpráva 70. – MS mat.-fyz. fak. Univ. Karl. Praha.

Červený, V.–Molotkov, I. A.–Pšenčík, I. (1977): Ray method in seismology. – MS Univ. Karl. Praha.

Červený, V.–Pšenčík, I. (1981): Program SEIS81. Dílčí zpráva. – MS mat.-fyz. fak. Univ. Karl. Praha.

Firbas, P.–Skorkovská, M. (1986): Velocity distribution modelling in laterally heterogeneous media (program for a desk-top computer). – Sbor. geol. Věd, užitá Geofyz., 20, *139–153.* Praha.

Program pro interaktivní řešení kinematických úloh v laterálně nehomogenních prostředích

(*Résumé anglického textu*)

Petr Firbas—Marta Skorkovská

Předloženo 14. září 1988

t Byl vyvinut plně interaktivní programový systém, který umožňuje rychle a s dostatečnou přesností určit rychlostní rozložení seizmických vln pro dvourozměrné v stevnaté laterálně nehomogenní prostředí. K účelu byla zvolena metoda postupných aproximací při řešení obrácené kinematické úlohy (metoda "trial and error"). Pro výpočet paprsků pak byla rozvinuta metoda, která předpokládá po částech lineární aproximaci prostředí, pro kterou pak řešení paprskových rovnic je dáno analytickými výrazy.

Programový systém byl vyvinut pro stolní počítač HP 9845, je plně interaktivní a využívá grafický HP software a grafické periférie (grafická obrazovka, čtyřbarevný plotter A3, maticová tiskárna). Systém sestává ze tří segmentovaných programů MODEL, RAY a PLOT. Program MODEL vytváří a testuje vstupní rychlostní model a dále slouží ke vstupu experimentálních hodochron. Program PLOT slouží k výběru paprsků, uložených programem RAY na magnetickou pásku, a jejich následnému vykreslení. Základem celého systému je program RAY, který umožňuje rychle počítat paprsky, vějíře paprsků, sledovat šíření paprsků v prostředí v reálném čase, výpočet přerušit a zároveň v rámci jednoho průchodu programu interaktivně a rychle měnit všechny parametry rychlostního modelu.

Program RAY umožňuje prověřovat rychlostní modely od povrchu do hloubky, používat různé typy vln a časy šíření se vlnění od různých odpalovacích bodů. Dále program umožňuje do výpočtu zahrnout apriorní informace.

Programový systém je napsán v jazyce BASIC pro stolní počítač HP 9845. Využívá se tedy malá výpočetní technika, která je cenově dostupná ve srovnání s velkými počítači. Zároveň díky interaktivnímu přístupu byla doba potřebná k vytvoření rychlostního modelu několikanásobně zkrácena ve srovnání se zpracováním na počítači, pracujícím v režimu dávkového zpracování dat. Programový systém byl úspěšně testován na datech řídké refrakce a jeho praktické možnosti při tvorbě nehomogenních rychlostních modelů byly ověřeny. Popis použití programu při řešení obrácené úlohy na reálných datech je obsahem připravovaného článku.

Vysvětlivky k tabulkám

Tabulka 1. Tabulka možných činností programu, jak se zobrazuje na obrazovce při změnách vertikálních čar mříže.

Tabulka 2. Příklad výřezu rychlostní sítě 1. vrstvy (modelu TEST), jak se zobrazí na obrazovce při změnách rychlostí 1. vrstvy. Grafický kursor, sloužící k výběru měněné hodnoty rychlosti, není zobrazen.

Tabulka 3. Tabulka možných činností programu, jak se zobrazí na obrazovce při změnách rozhraní.

Tabulka 4. Tabulka možného větvení programu RAY v rozhodovacím bodě HELP, jak se zobrazuje na obrazovce (srov. s obr. 2).

Tabulka 5. Příklad výstupního tisku na tiskárně při výpočtu paprsků odražených od sedmého rozhraní pro model WDM.

Vysvětlivky k obrázkům

1. Zobecněné schéma výpočtu a vstupních/výstupních operací programového systému (programy MODEL, RAY a PLOT).
2. Zjednodušený blokový diagram programu RAY.
3. Celkový obrázek modelu WDM (síťových čar a rozhraní), jak se zobrazí na obrazovce při posunu vertikálních čar (viz tab. 1). Grafický kursor (není zobrazen) slouží k volbě posouvané vertikální síťové čáry a následně k digitalizaci její nové x-souřadnice.
4. Obrázek, který se zobrazí na obrazovce, je-li posouváno 6. rozhraní. Pro usnadnění změn jsou znázorněny i rychlosti pod a nad posouvaným rozhraním. Grafický kursor (není zobrazen) slouží současně k volbě posouvaného bodu rozhraní a digitalizaci jeho nové souřadnice.
5. Dvourozměrný laterálně nehomogenní sedmivrstevný rychlostní model, který předložil W. D. Mooney. Rychlosti jsou uvedeny v $km \cdot s^{-1}$.
6. Příklad složeného grafického výstupu pro model WDM. Pro zvolený zdroj (50 km, 0 km) jsou vykresleny paprsky odražené od šestého rozhraní. Časy příchodu paprsku stejně jako experimentální hodochrony jsou vykresleny v redukovaném měřítku s redukční rychlostí $6 km \cdot s^{-1}$.
7. Složený grafický výstup pro paprsky odražené od sedmého rozhraní. Model, zdroj i použitá redukční rychlost jsou stejné jako pro grafický výstup na obrázku 6.

Программа для решения кинематических задач в латерально-неоднородных средах диалоговым способом

В докладе описана диалоговая программная система, предназначенная для моделирования распределения скоростей сейсмических волн в двумерной неоднородной слоистой среде с криволинейными границами раздела. Программа предназначена для решения обратной кинематической задачи методом постепенных аппроксимаций. Метод, используемый для решения уравнений луча, предполагает линейную по частям аппроксимацию среды. Программная система обеспечивает быстрое вычисление лучей или веера лучей, прерывание расчета в реальном времени и диалоговое изменение всех параметров скоростной модели в рамках одного прохода программы. Программная система написана на языке BASIC для настольного калькулятора Hewlett-Packard HP 9845 и предполагает полное использование графи-

ческого программного матобеспечения и соответствующих графических периферийных устройств. Приведен пример расчета для двумерной латерально-неоднородной слоистой модели. Эта проверочная модель была предложена В. Д. Муным на симпозиуме Комиссии по управляемым сейсмическим источникам в 1983 г. во Швейцарии. Программная система была проверена по реальным данным и приобретенные результаты подготовляются к опубликованию.

Přeložila H. Kuksová

Sbor. geol. věd	Užitá geofyz., 24	Pages 71–89	11 figs.	1 tab.	– pl.	Praha 1990 ISSN 0036-5319

Presentation of results of the IP field measurements in maps and sections

Представление результатов полевых измерений ВП на картах и разрезах

Miloš Karous[1]

Received June 12, 1987

Induced polarization
Pseudosections
Electrical methods
Polarizability

Karous, M. (1990): Presentation of results of the IP field measurements in maps and sections. – Sbor. geol. Věd, užitá Geofyz., 24, *71–89*. Praha.

Abstract: New ways of processing of area and profile measurements by the IP method in the time and frequency domains by means of modified values of apparen polarizability are suggested. The configuration of modified polarizability anomalies in maps and sections better corresponds to the actual distribution of anomalous polarizability, thus making it possible to obtain a more reliable geoelectric model of the investigated region. In a similar manner it is possible to process also simultaneous resistivity measurements. The interpretation of both resistivity and polarizability data arranged into the suggested schemes is less ambiguous, simpler and more illustrative than that based on resistivity and polarizability pseudoschemes constructed in "classical" ways as pseudosections.

[1] *Katedra užité geofyziky přírodovědecké fakulty Univerzity Karlovy, Albertov 6, 128 43 Praha 2*

Introduction

This paper is dedicated to the possibility of determining the position and extension of anomalously polarized geological bodies. This problem is the one most frequently solved by the IP method. However, unambiguous procedures have not yet been developed for interpretations of buried anomalous bodies. In majority of cases we have been satisfied with the qualitative interpretation when on the basis of our experience in interpreting and using a limited set of theoretical model curves some geometrical parameters (shape and position of anomalous body)

have been estimated directly from a particular graphical presentation of apparent polarizability data or other parameters derived from the IP measurements. As it will be shown in the paper, the classical graphical presentation of the measured parameters has not always been suitable, for the extremes (maxima) of the apparent polarizability do not appear directly above the anomalous object. The shift of the maximum depends on the electrode configuration used, on the shape, dimensions and depth of the anomalous object as well as on other factors. An anomalous object is frequently manifested by numerous local extremes which could be misinterpreted as caused by other objects. The possibilities of constructing more illustrative schemes – maps and vertical sections – will be shown, which better correspond to the actual distribution of polarizability than the "classical" ones, so that dimensions and the space distribution of investigated anomalously polarized bodies can be directly interpreted from them. The ways suggested in this article for processing the data obtained by the IP method can analogically be used also for processing the resistivity measurements taken simultaneously with the IP measurements.

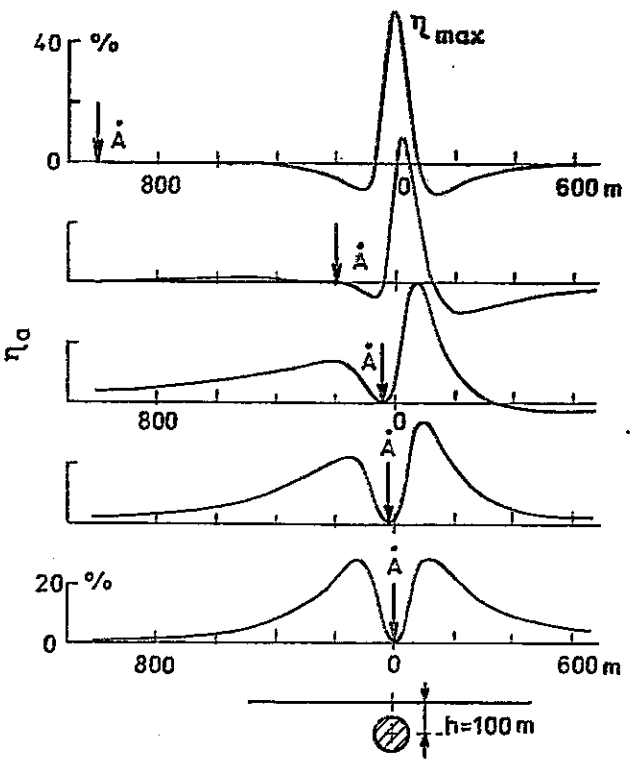

1. Apparent polarizability curves above a polarizable sphere for the three-electrode gradient configuration *AMN* with fixed current electrode *A* for various positions of grounding

Profile curves and polarizability maps

Maps of isolines of measured or simply transformed data represent, to various (mostly small) extent, the actual distribution of polarizability. They have usually been constructed from values obtained from measurements along parallel profiles the distance of which is defined by the scale of a particular survey to cover the

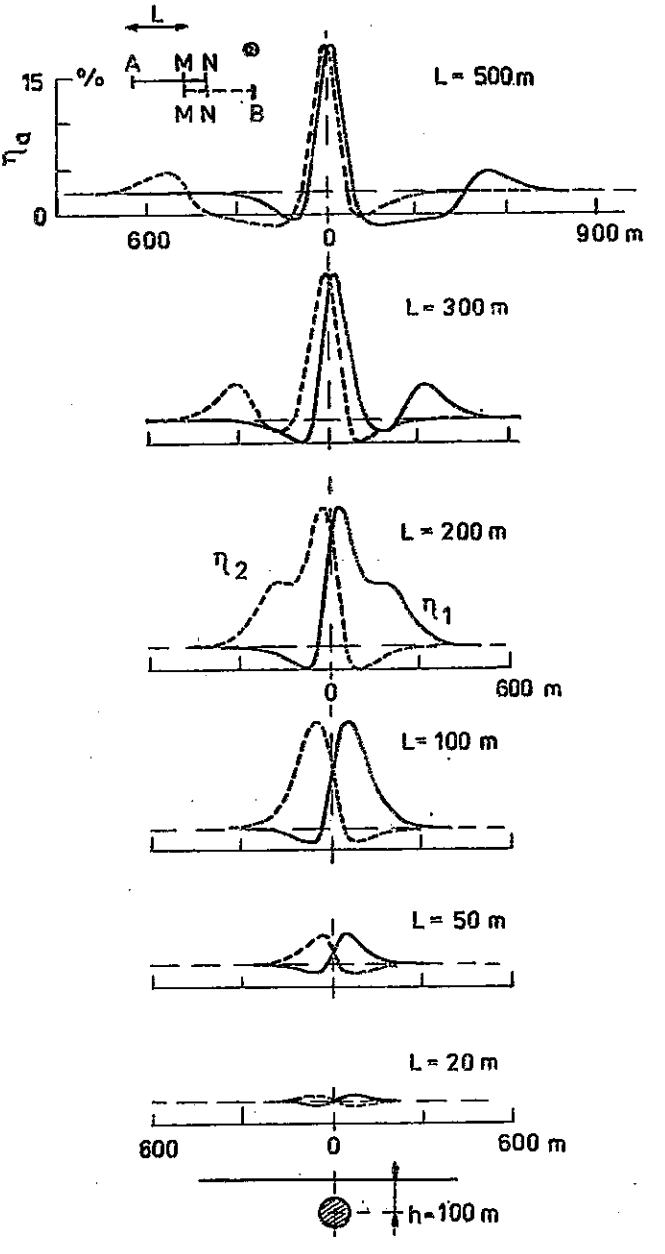

2. Apparent polarizability curves above a polarizable sphere for the combined profiling of various lengths $L = AB/2$

study area. Using different electrode configuration above the same anomalous object, different profile curves are obtained. Above one object, profile curves exhibit, in majority of cases, several extremes corresponding to the passage of individual electrodes or dipoles over the object at depth.

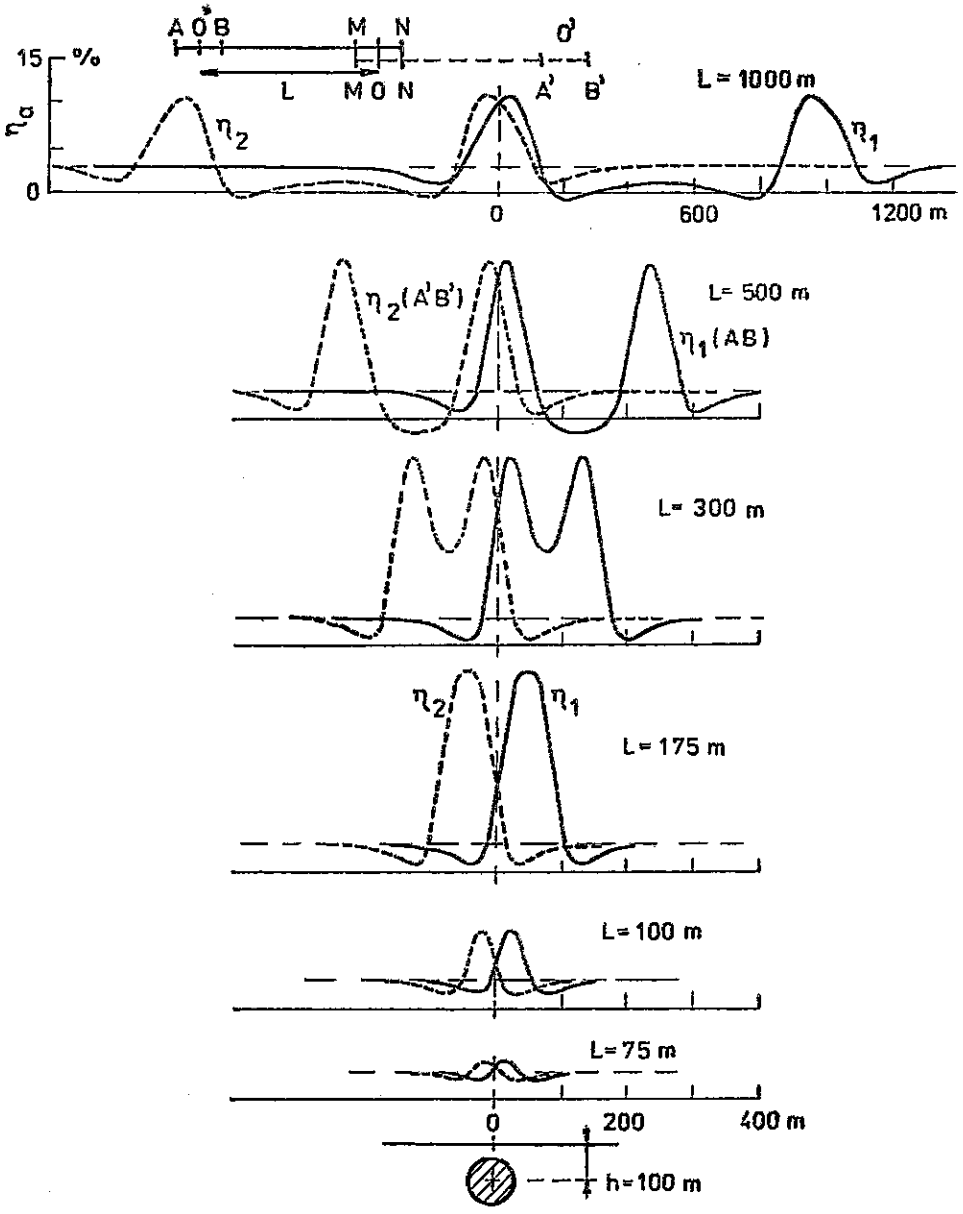

3. Apparent polarizability curves above a polarizable sphere for the dipole-dipole profiling of various lengths $L = OO'$

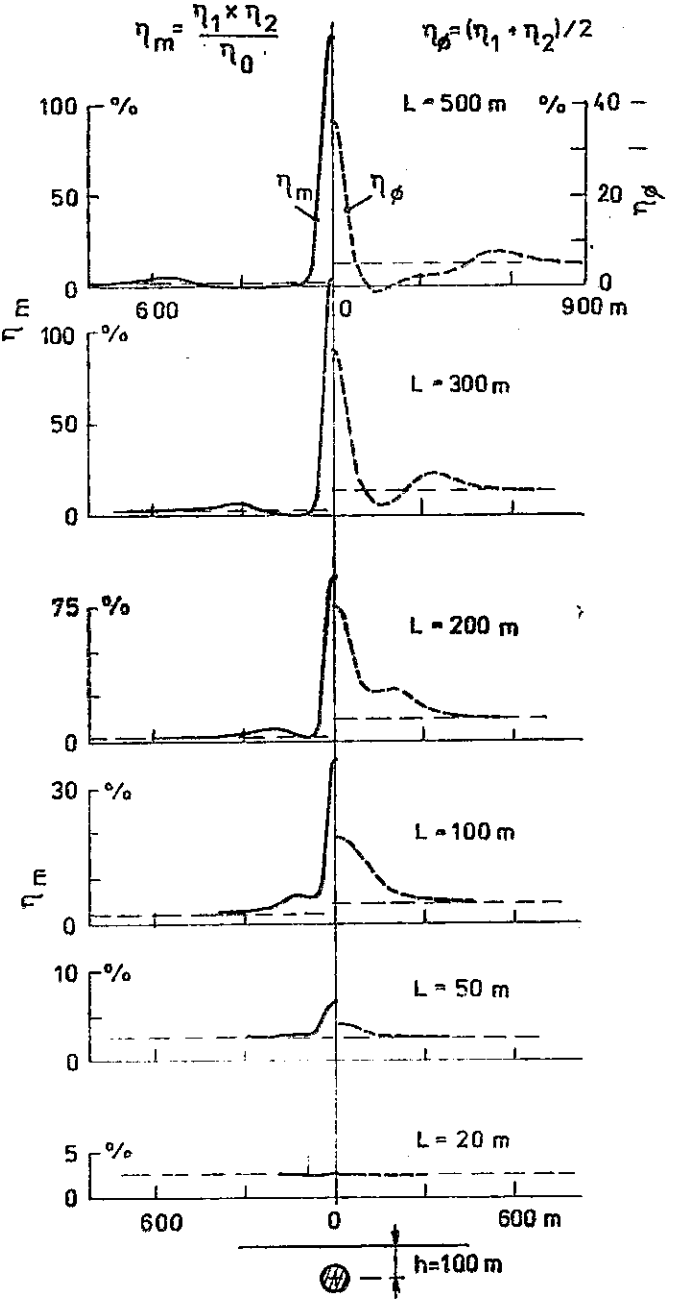

4. Modified polarizability η_m and mean polarizability η_ϕ curves above a polarizable sphere for the combined profiling

In order to map polarized bodies it is more suitable to use an electrode configuration with fixed grounding of current electrodes for which extremes are to be formed only when the moved potential dipole passes over an anomalous body. Among these configurations the most frequently applied is the one called the gradient

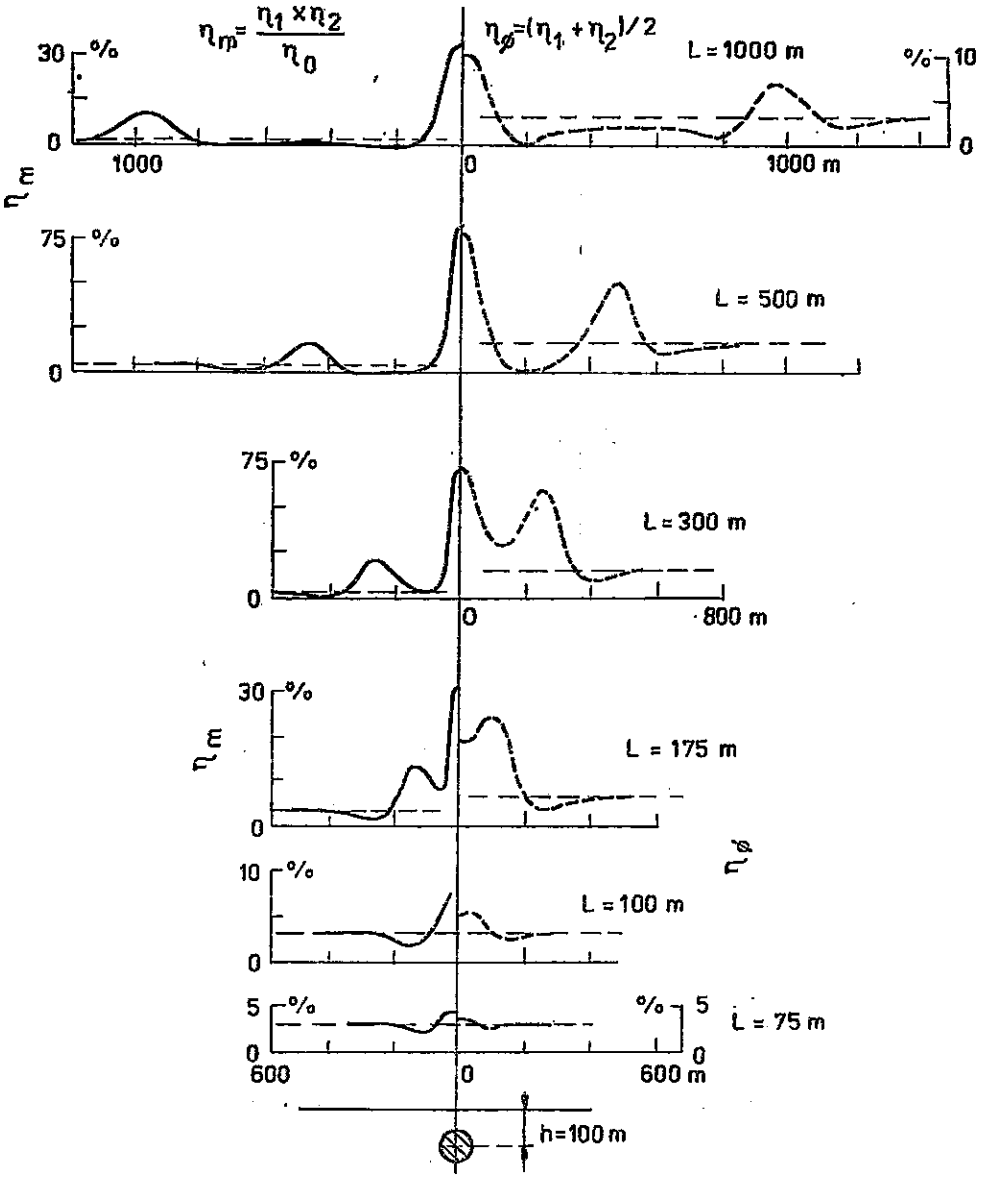

5. Modified polarizability η_m and mean polarizability η_ϕ curves above a polarizable sphere for the dipole-dipole profiling

array (GA) and/or the so called combined gradient array (CGA) represented by two pole-dipole arrays in which the third current electrode is situated at a relatively long distance. Considering the justification of using particular arrays to explore anomalous objects and taking into account the depth of their investigation it is most suitable to analyze the profile curves above a locally limited object, preferably of an isometric form (e.g. a sphere). Using the GA modification apparent polarizability curves η_a exhibit maximum directly above the object of increased polarizability, similarly as in the CGA modification for the current electrode A grounded at a relatively long distance from the object (upper part of Figure 1). The anomalous object being close to one of the groundings in the GA modification the maximum is shifted similarly as in the CGA modification because the influence of the second grounding is negligible (Figure 1). If the grounding is very close to the epicentre of the object or even directly above the object, two maxima of apparent polarizability appear on both sides of the grounding (lower part of Figure 1). The magnitude of the shift of the extreme is proportional to the depth of the object h.

In the case of symmetrical configuration with moving current electrodes (i.e. the Schlumberger and Wenner profilings) the anomalous curve above the sphere shows three maxima. The central (the largest) one corresponds to the position of the polarized sphere. Asymmetric electrode configurations (i.e. dipole-dipole and combined two pole-dipole arrays) yield two curves of apparent polarizability η_1 and η_2, each of them exhibiting two maxima (figures 2 and 3). In the case of objects at greater depths both maxima can merge into a broader one. Then, in such a case, there is a problem to construct maps of isolines. It is usual to plot the mean values of polarizability $\eta_\varnothing$ (figures 4 and 5 – broken line):

$$\eta_\varnothing = \frac{1}{2}(\eta_1 + \eta_2). \tag{1}$$

Particularly in the case of dipole-dipole profiling the curves of mean polarizability $\eta_\varnothing$ exhibit expressive false maxima on both sides of the object at distances that equal the length L, i.e. the electrode separation. In the map of isolines, the number and positions of anomalous objects can be incorrectly interpreted.

In the case of asymmetric electrode configuration out of the two maxima of both curves, however, only one is located above the object. It is therefore suitable to substitute the mean values of polarizability with the simplest correlation, i.e. with the product of values of both polarizabilities divided by normal value of polarizability η_0 typical of the nonanomalous parts of the region investigated. Let the value obtained in this way be called a modified polarizability η_m:

$$\eta_m = \frac{\eta_1 \times \eta_2}{\eta_0}. \tag{2}$$

Curves of modified polarizability do not show such expressive false maxima away from the anomalous object (figures 4 and 5 – left-hand part, solid line).

Vertical sections of polarizability

It has been said that for the mapping of polarizable objects the GA modification is most suitable as the maximum of the curve is located directly above the object. A disadvantage of the GA is in its low ability to differentiate the sources of anomaly at depth. For more detailed investigations of depth relations of polarizable objects it is necessary to apply an electrode configuration with controlled extent of the depth of investigation, e.g. by a change of length L of the electrode configuration (for the Schlumberger and combined profilings $L = AB/2$, in the case of the dipole-dipole profiling L is the distance $00'$ between the centres of the potential and current dipoles). In the case of these configurations vertical pseudosections of the apparent polarizability have been constructed, so that the measured values of apparent polarizability have been plotted at points P in the vertical section beneath the investigated profile. Positions of points P are given by the centre of the electrode configuration used and the length $L/2$ (Figure 6). The values at points P have then been interpolated. In this way a map of isolines of apparent polarizability has been obtained. Thus the construction has been quite simple. The value of this construction is, despite its simplicity, considerably reduced because the courses of isolines in the section do not correspond to the shape of the anomalous body (Figure 6). For example, above the studied objects of isometric form false "shadows" occur in the section, extending downward from the position of the object under the angle of 45°. At the crossing of two false "shadows" due to two different objects an intensive unreal anomaly develops which could be erroneously interpreted as caused by another object. "Classical" pseudosections can thus be interpreted correctly only with the use of a large set of model pseudosections.

By using the different shifts of two curves of asymmetric electrode configuration measurements it is possible to construct vertical pseudosections from the IP profiling with only one electrode spacing. It is necessary, however, to carry out bilateral measurements by two asymmetric configurations, i.e. measurements at the position of current pole or dipole on both sides of the measuring dipole. It has been discovered (Komarov 1980) that in the CGA modification the maxima of apparent polarizability are located at points M which are equally distant from the current grounding A as is the centre S of the polarizable sphere from the grounding A, i.e. $AM = AS$. This has also been proved theoretically (Karous 1983). In order to determine the position of the sphere and its depth two measurements should be performed for two different positions of current groundings A_1 and A_2. The centre of the sphere is directly at the intersection of two arcs plotted through points M_1 and M_2 corresponding with the maxima of polarizability $\eta_{1\,max}$ and $\eta_{2\,max}$, with centres at groundings A_1 and A_2.

The interpretation method of Komarov has been generalized and extended for

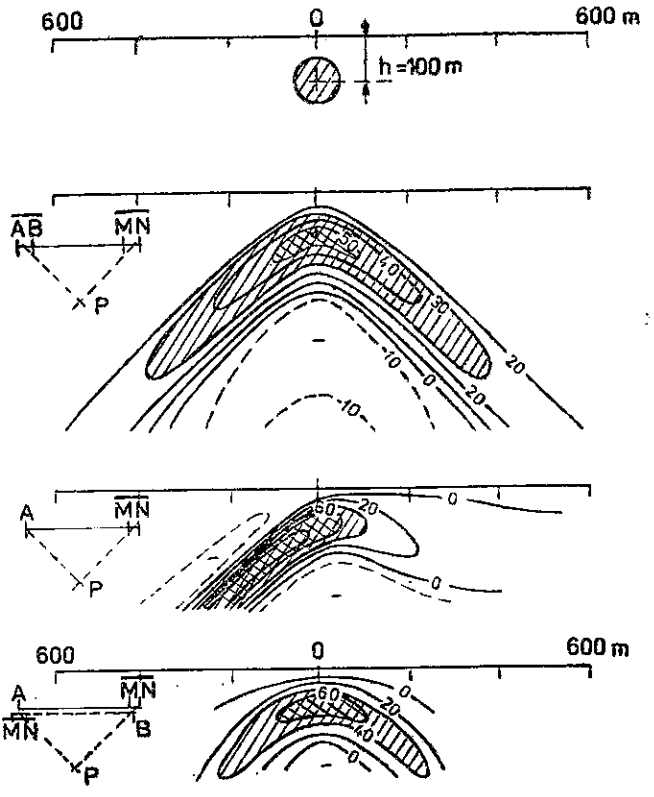

6. "Classical" pseudosections of apparent polarizabilities above a polarizable sphere for the dipole-dipole profiling with several lengths of separation of electrode configuration *ABMN* for the three-electrode configuration *AMN*, and for the combined profiling *AMN*, *MNB*

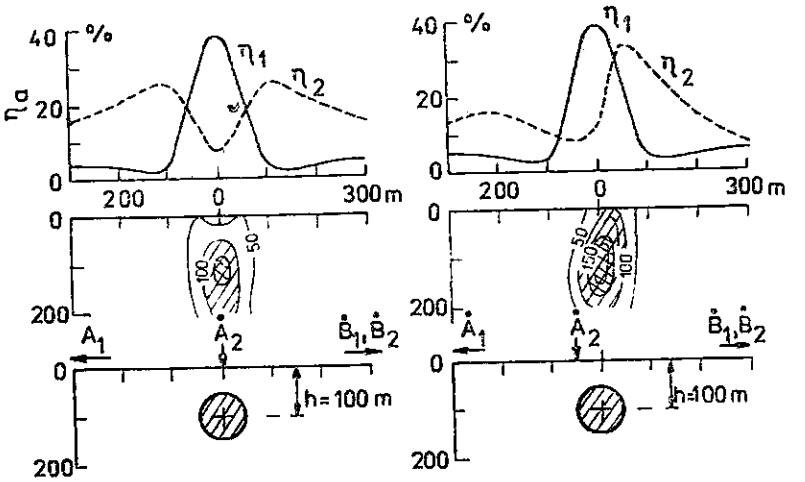

7. Vertical modified pseudosections constructed from the model curves of polarizability above a polarizable sphere for the asymmetric configuration *AMN* with fixed current grounding *A* in two different positions A_1 and A_2

construction of vertical pseudosections from two measurements with fixed current groundings (Karous 1983, 1985). The method of construction is very simple. To each intersection P_{ij} of two arcs with centres at A_1 and A_2 which pass through the points of measurements x_i and x_j the value of modified polarizability can be assessed according to the expression:

$$\eta_m(P_{ij}) = \frac{\eta_1(x_i) \times \eta_2(x_j)}{\eta_0}, \tag{3}$$

which can then be used for construction of isolines. In this way the so called modified pseudosection will be obtained. It is obvious that the modified polarizability reaches its maximum if the point P_{ij} lies at the intersection of arcs passing through the maxima $\eta_{1\,max}$ and $\eta_{2\,max}$. Thus the extreme values of η_m in the section correspond to the position of polarizable objects.

Examples of sections constructed in this way from the model curves above the polarizable sphere are shown in Figure 7. Contrary to "classical" pseudosections the modified pseudosections exhibit extreme values without false "shadows" and in the position of the anomalous object only. As it has been verified for models of other shapes (i.e. sheetlike, ellipsoidal etc.), also in these cases the form of isolines in modified sections corresponds to the shape of the polarizable object.

Analogically, vertical pseudosections can be constructed also from measurements taken using asymmetric configurations with current electrodes moving in one spacing only. From the model and theoretical curves obtained above the sphere using dipole-dipole and combined profilings, the relation has been studied between the centre of isometric body position and the position of maximum of measured apparent polarizabilities. Beneath the maximum the position of the centre can lie on the curve (the so called depth curve) which is plotted in Figure 8 for the combined (CP) and dipole-dipole (DP) profilings. The search for a sphere to depths smaller than the length of separation L is justified only because spheres at greater depths manifest themselves by very weak anomalies. The position of an isometric object at the intersection of two depth curves corresponds to both positions of the current pole or dipole.

Two depth curves can be drawn through each point of measurements (corresponding to the left and right current source). These depth curves form a network of intersecting points P_{ij} to which values of the modified polarizability are positioned according to relation (3). By interpolating the resulting isolines the modified pseudosections are obtained for the combined or dipole-dipole profilings. Examples of such pseudosections for the polarized sphere are shown in figures 9 and 10. Positions of points P_{ij} need not be determined graphically. In order to enable the automatic data processing it is advantageous to make tables of coordinates x_{ij} and h_{ij} of points P_{ij} in the section. For the coordinates the following relation

Table 1

Depth coefficients α_n^m for constructing vertical modified pseudosection from combined and dipole-dipole profilings

Combined profiling						Dipole profiling					
m	n					m	n				
	3	4	5	6	7		3	4	5	6	7
0	0.00	0.00	0.00	0.00	0.00	0	0.00	0.00	0.00	0.00	0.00
1	0.54	0.47	0.42	0.39	0.36	1	0.38	0.32	0.28	0.25	0.23
2	0.77	0.66	0.60	0.54	0.50	2	0.54	0.46	0.42	0.38	0.34
3	0.99	0.82	0.73	0.66	0.62	3	0.92	0.58	0.59	0.46	0.42
4	1.24	0.99	0.85	0.77	0.72	4		0.91	0.62	0.54	0.49
5		1.18	0.99	0.88	0.80	5			0.91	0.66	0.56
6		1.42	1.15	0.99	0.89	6				0.92	0.68
7			1.34	1.11	0.99	7					0.91
8				1.24	1.10						
9				1.43	1.22						
10					1.35						

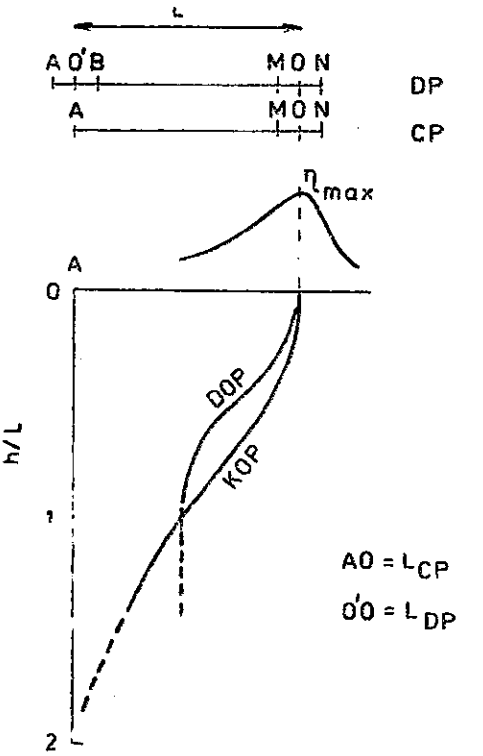

8. Depth curves for a polarizable sphere (i.e. the curves on which the centre of sphere is located for the given position of the apparent polarizability maximum) for the dipole-dipole (DP) and combined (CP) profilings

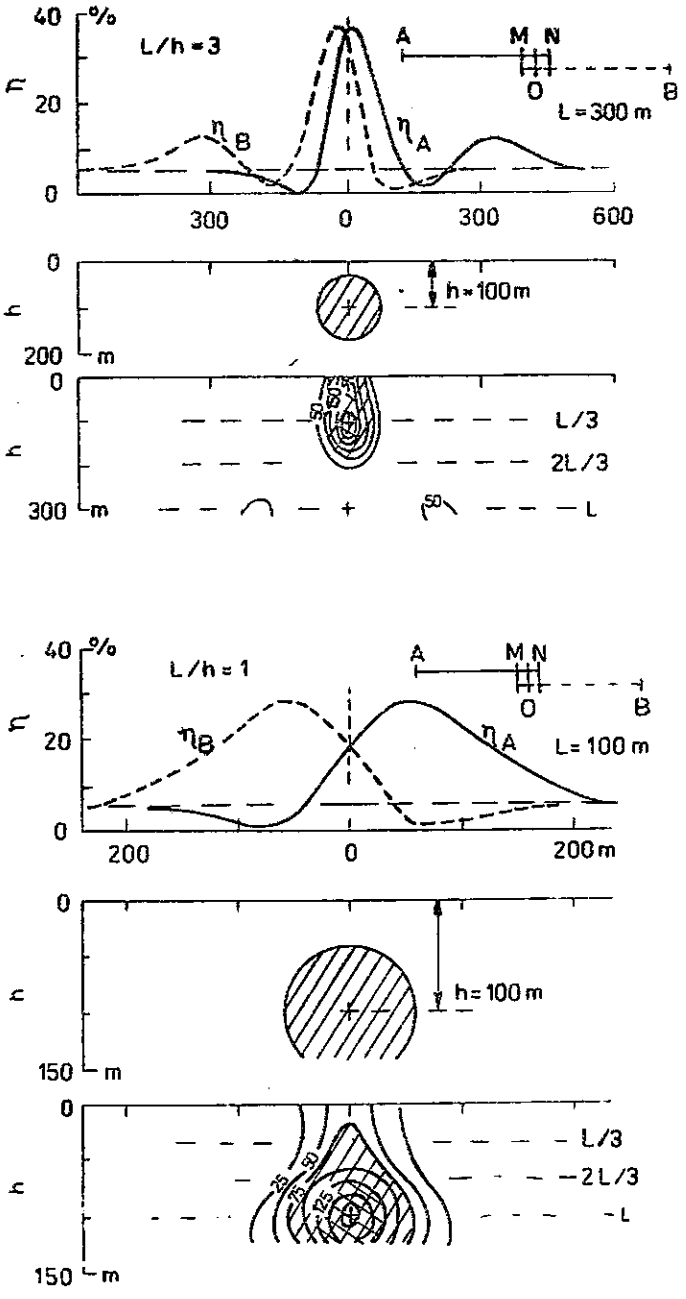

9. Modified vertical pseudosections of polarizability derived from the combined profiling measurements with two different separations above a polarizable sphere

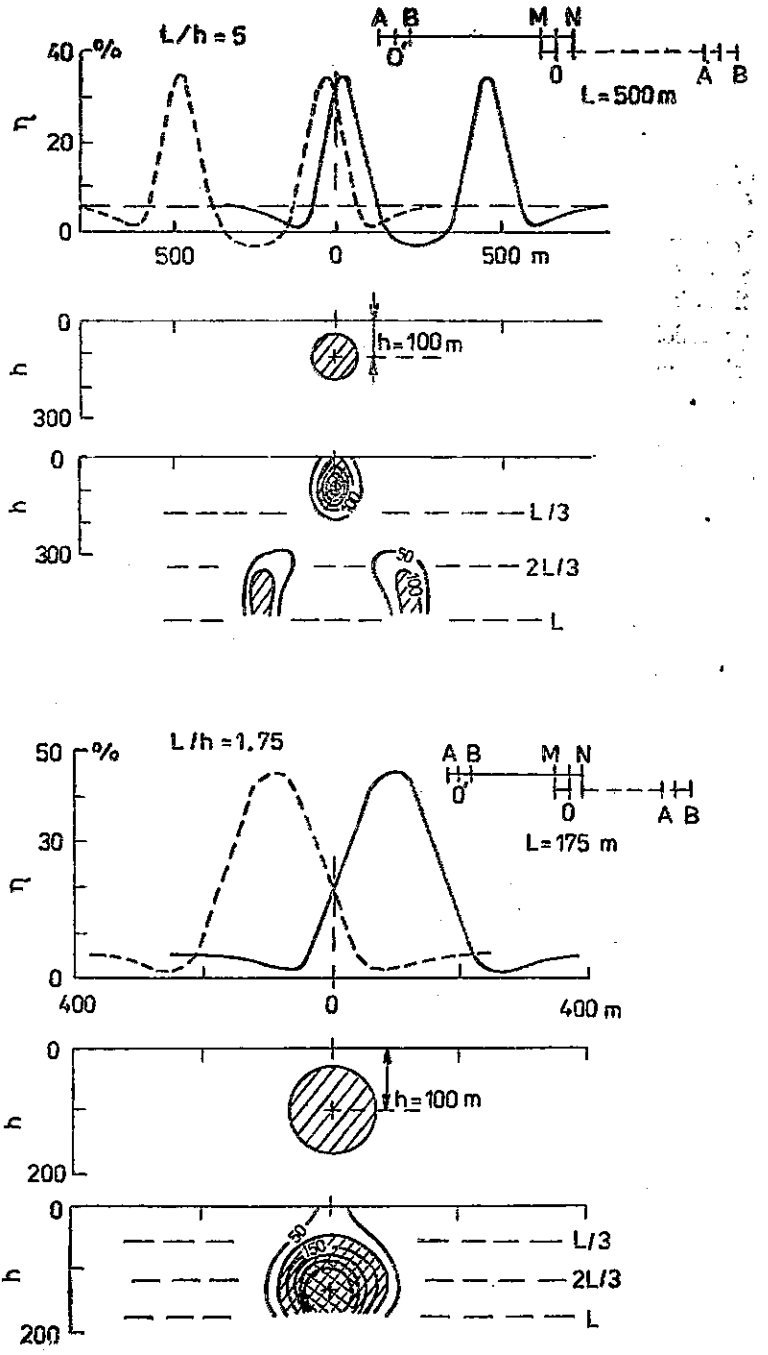

10. Modified vertical pseudosections of polarizability derived from the dipole-dipole profiling above a polarizable sphere for various lengths of electrode separations $L = 00'$

is valid:

$$x_{ij} = \frac{1}{2}(x_i + x_j) = \frac{i+j}{2}\Delta x, \tag{4}$$

$$h_{ij} = h_m = L \,.\, \alpha^n_{|i-j|} = L \,.\, \alpha^n_m, \tag{5}$$

where $n = L/\Delta x$ is the ratio of the length of separation L to the measurement interval Δx, $x_i = i.\ \Delta x$ and $x_j = j\,.\,\Delta x$ are points of measurements, $m = |\,i - j\,|$ is the relative distance of points of measurements. It is equal to $m = |\,x_i - x_j\,|/\Delta x$. The depth coefficients α^n_m derived from the depth curves for isometric inhomogeneities for various m and n are presented in Table 1. Despite the fact that in Table 1 the depth coefficients α^n_m are larger than 1.0, it is justified to construct the sections only to depths smaller than the length L.

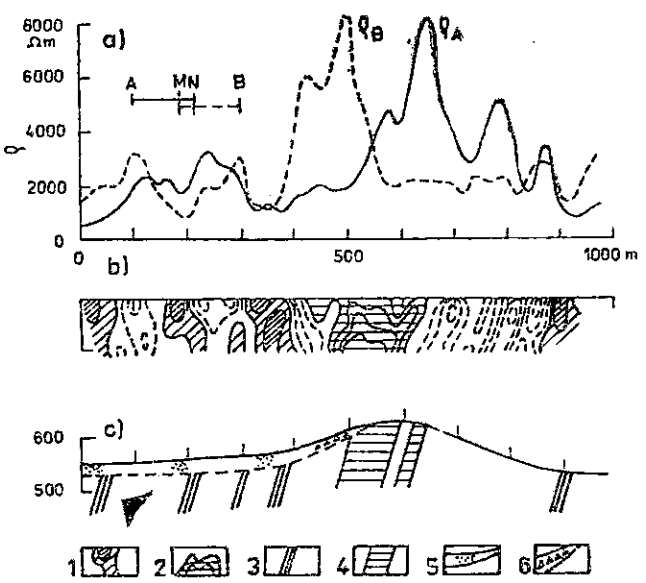

11. An example of the modified vertical resistivity pseudosection derived from the field measurements using the combined profiling method at the locality Rejvíz in the Jeseníky Mts.
a – resistivity profiling curves, *b* – vertical modified resistivity pseudosection, *c* – interpreted geological section; *1* – conductors in the isoohm section, *2* – nonconductors in the isoohm section, *3* – interpreted conductive zones (graphitized rocks), *4* – interpreted non-conductive zones (quartzite rocks), *5* – solid products of weathering of graphitized rocks in the eluvium, *6* – screes of quartzite rocks

The verification of the vertical modified pseudosections obtained above models of bodies of other shapes, including irregular ones, proves a relatively higher effectiveness of the suggested construction method. In a similar manner the resistivity data can also be displayed. An example of a resistivity section and the resulting interpretation of resistivity measurements obtained by the combined profiling is shown in Figure 11.

K tisku doporučil J. Hanzlík

Přeložil autor

References

Baudoin, B. (1968): Etude au laboratoire de la methode de polarisation provoquee. – Bull. BRGM, Sect. Orléans.

Bertin, J.–Loeb, J. (1976): Experimental and theoretical aspects of induced polarization. – Geoexploration Monographs, 1, 7, Gebrüder Borntraeger. Stuttgart–Berlin.

Cole, K. S.–Cole, R. H. (1941): Dispersion and absorption in dielectrics. – J. Chem. Phys., 9, *341–351*. London.

Collet, L. S. (1959): Laboratory investigation of overvoltage. In J. R. Wait: Overvoltage research and geophysical application. – Pergamon Press. New York.

Csorgei, J. et al. (1983): Time domain IP equipment and method for source discrimination. – Geophys. Transactions, 29, 4, *21–32*. Budapest.

DeWitt, G. W. (1978): Parametric studies of induced polarization spectra. – M. Sc. thesis, Univ. of Utah. Salt Lake City.

Erkel, A. et al. (1979): Measurements and interpretation of the dynamic characteristics of induced polarization decay curves. – Geophys. Transactions, 25, *65–81*. Budapest.

Gennadinik, B. I.–Melnikov, V. P.–Gennadinik, G. B. (1976): Teorija vyzvannoj élektrochimičeskoj aktivnosti gornych porod. – Jakutskoe knižnoe izdatelstvo. Jakutsk.

Grissemann, C. (1971): Examination of the frequency-dependent conductivity of ore-containing rock on artificial models. – Sci. Rep. 2, Electr. Lab. Univ. of Innsbruck. Innsbruck.

Hallof, P. G. et al. (1979): The use of the Phoenix IPV-2 phase IP receiver for discrimination between sulphides and graphite. – Paper presented at the SEG Ann. Meeting in New Orleans. Tulsa.

Joffe, L. M. et al. (1979): Metodika raboty s geoélektričeskoj apparaturoj SVP-74. – Naučno-proizvodnoe ob"edinenie Geofizika. Leningrad.

Kanasewich, E. R. (1975): Time sequence analysis in geophysics. – The Univ. Alberta Press. Alberta.

Karous, M. (1983): Induced polarization anomaly above a sphere. – Geoexploration, 21, *49–63*. Amsterdam.

– (1985): Zpracování geoelektrických měření v geologickém mapování v rudní prospekci a hydrogeologickém a inženýrskogeologickém průzkumu. – D. Sc. thesis, Charles Univ. Praha.

Kněz, J. (1985): Určení dynamických parametrů vyzvané polarizace. – Sbor. prací 8. celost. konf. geof. Č. Budějovice.

Komarov, V. A. (1965): Vremennye charakteristiki vyzvannoj poljarizacii. – Metod. Techn. Razv., 49, *29–62*. Leningrad.

– (1980): Élektrorazvedka metodom vyzvannoj poljarizacii. – Nedra. Leningrad.

Komarov, V. A.–Šubnikova, K. G. (1976): O svjazi vremennych parametrov vyzvannoj poljarizacii s razmerom poljarizuemych tel. – Met. Razvit. Geofiz., 26, *103–114*. Leningrad.

Lee, T. (1981): Short note on the Cole-Cole model in time-domain induced polarization. – Geophysics, 46, *932–938*. Tulsa.

Lemec, V. I. et al. (1973): K metodike rabot po metodu INFAZ-VP s ustanovkoj gradienta. – – Vopr. rud. Geofiz., 5, *42–48*. Alma-Ata.

Ljachov, L. L.–Melnikov, V. P. (1968): O vozmožnostjach ispolzovanija fazovočastotnych charakteristik VP dlja klassifikacii anomalij poljarizuemosti. – Izd. Vuzov, Ser. Geof. Razv., 7, *153–154*. Moskva.

Major, J.–Silic, J. (1981): Restrictions on the use of Cole-Cole dispersion models in complex resistivity interpretation. – Geophysics, 46, 6, *916–931*. Tulsa.

Olhoeft, G. R. (1982): Electrical properties of rocks and minerals. – University course notes. Golden.

Pelton, W. H. (1977): Interpretation of induced polarization and resistivity data. – Ph. D. thesis, Univ. of Utah. Salt Lake City.

Pelton, W. H. et al. (1978a): Inversion of two-dimensional resistivity and induced polarization data. – Geophysics, 43, 4, *788–803*. Tulsa.

– (1978b): Mineral discrimination and removal of inductive coupling with multifrequency IP. – Geophysics, 43, 3, *588–609*. Tulsa.

– (1983): Interpretation of complex resistivity and dielectric data, Part I. – Geophys. Transactions, 29, 4, *94–99*. Budapest.

Verö, L. et al. (1985): Comparsion of interpretation methods for time domain spectral induced polarization data. – Geophys. Transactions, 31, *1–3, 182–188*. Budapest.

Wait, J. R. (1984): Relaxation phenomena and induced polarization. – Geoexploration, 22, *345–355*. Amsterdam.

Wong, J. (1979): An electrochemical model of the induced polarization phenomenon in disseminated sulfide ores. – Geophysics, 44, 7, *1245–1265*. Tulsa.

Представление результатов полевых измерений ВП на картах и разрезах

(Резюме английского текста)

Miloš Karous

Представлено 12-го июля 1987 г.

В этой статье предложен новый способ презентации результатов полевых измерений величины вызванной поляризации (ВП) в виде т. наз. модифицированных карт изолиний и вертикальных разрезов, позволяющих быстро и объективно интерпретировать положение, форму и размеры аномально поляризуемых геологических объектов в виде горизонтальной плоскости и вертикальном разрезе под измеряемым профилем. Современное состояние разработки автоматической интерпретации на вычислительных машинах пока не позволяет эффективно использовать обработку данных профилей на ЭВМ в обыкновенных рабочих условиях геофизических исследований, поэтому предложенный способ может пополнить пробел в интерпретационных приемах метода вызванной поляризации.

До сих пор результаты метола ВП представляются в виде кривых кажущейся поляризуемости (рис. 1—3). Максимумы кривых кажущейся поляризуемости, однако, часто не совпадают с расположением аномально поляризуемых тел, в связи с чем карты изолиний не могут дать полное представление о расположении аномальных зон. Поэтому были введены т. наз. модифицированные данные поляризуемости (формулы 2 и 3), кривые которых имеют экстремумы над поляризуемыми телами (рис. 4 и 5).

Результаты профилирования методом ВП, использующего несколько различных расстановок питающих электродов, изображаются часто в виде „классических" псевдоразрезов, но характер изолиний в них не отвечает истинной форме аномального тела (рис. 6). Поэтому в этой статье предлагается строить модифицированные разрезы с использованием модифицированных данных поляризуемости. Эти данные вписываются в разрезах в точки пересечения кривых, в которых на различных глубинах лежат сферы со совпадающими максимумами кажущейся поляризуемости (рис. 8). Форма изолиний в модифицированных разрезах отвечает приблизительно форме вертикального разреза аномально поляризуемого геологического тела (рис. 7, 9 и 10).

Сходно с тем строятся вертикальные модифицированные разрезы по данным модифицированных сопротивлений, измеряемых при применении метода ВП вместе с кажущимися поляризуемостями (рис. 11).

Přeložil autor

Sbor. geol. věd	Užitá geofyz., 24	Pages 91–105	10 figs.	1 tab.	– pl.	Praha 1990 ISSN 0036-5319

Magnetic fabric of sedimentary formations of the Strážovské vrchy Mts., sedimentological and tectonic implications

Magnetická vnitřní stavba sedimentárních formací Strážovských vrchů, sedimentologická a deformační interpretace

František Hrouda[1]–Jaromír Hanák[1]

Received April 15, 1988

1 : 50 000
25–44
26–33, 34

Magnetic anisotropy
Krížna nappe
Sedimentological interpretation
Tectonic interpretation

Hrouda, F.–Hanák, J. (1990): Magnetic fabric of sedimentary formations of the Strážovské vrchy Mts., sedimentological and tectonic implications. – Sbor. geol. Věd, užitá Geofyz., 24, *91–105*. Praha.

Abstract: The magnetic fabric in the sedimentary rocks of the Cover Formation is deformational in origin. In sedimentary rocks of the Krížna nappe (sandstone, marlstone), it is partially sedimentary and partially depositional in origin. The magnetic lineations in rocks with sedimentary magnetic fabric agree with palaeocurrent directions determined by Jablonský (1978) using sedimentological methods.

[1] *Geofyzika, s. p., Brno, Ječná 29a, 612 46 Brno*

Introduction

The Strážovské vrchy Mts. create one of the so-called core mountains of the Central West Carpathians (see Fig. 1). They are characterized, as any core mountains, by the crystalline core covered by sedimentary rocks of the Cover Formation and overthrust by the Subtatric nappes among which the Křížna nappe, the Choč nappe and Strážov nappe are the most important. Their geology has been comprehensively treated by Maheľ (1985).

In the Strážovské vrchy Mts. the Krížna nappe crops out on a relatively large area, being represented by deep-sea sediments of the Zliechov series and in the uppermost part also by flysch sediments Albian in age. The palaeogeographical

situation has been studied by sedimentological methods (Jablonský 1978) mostly on sandstone (see Fig. 2).

The purpose of the present paper is to extend this study using the method of magnetic anisotropy, which enables the preferred orientation of magnetic minerals in a rock to be determined. This method can be applied not only to the investigation of sandstone, but also marlstone and claystone. In addition, it is also able to detect very sensitively weak ductile deformation modifying the sedimentary fabric. We used this method, in combination with sedimentological methods, in the study of the sedimentary rocks of the Strážovské vrchy Mts. Though also the Cover Formation and the Choč nappe were investigated, the paper is essentially devoted to the Krížna nappe, because in this nappe sufficient number of suitable outcrops of marlstone and sandstone have been found, while in the Cover Formation and in the Choč nappe only non-magnetic quartzite and limestone may have been sampled.

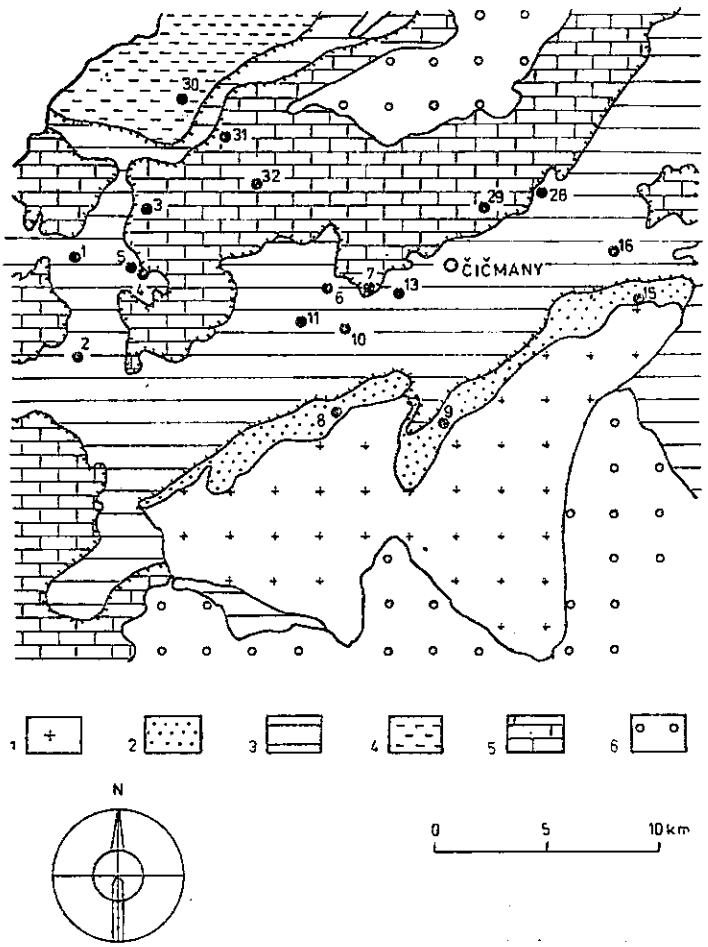

1. Geological scheme of the Strážovské vrchy Mts. with the sampling sites plotted (closed circles with numbers) *1* – metamorphic and granitoid rocks, *2* – Cover Formation, *3* – Krížna nappe, *4* – Manín Unit, *5* – Choč and Strážov nappe, *6* – Palaeogene and Neogene. Simplified from M. Maheľ (1985)

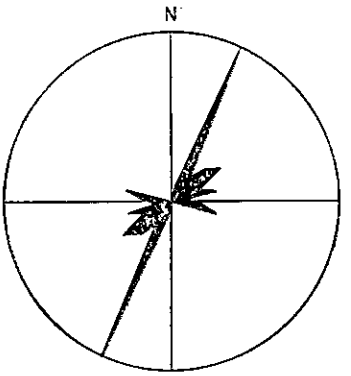

2. Rose diagram of the orientations of the palaeocurrents in the Alb of the Křižna nappe, determined by sedimentological methods. Compiled from the data of J. Jablonský (1978)

Measurement and processing techniques, data presentation

The magnetic anisotropy of oriented specimens was measured by the KLY-2 Kappabridge (Jelínek 1973, 1982) and computed using the ANISO 11 program (Jelínek 1977). In order to obtain a statistical evaluation of the magnetic anisotropy in individual localities, recourse was had to the RESEA and ANS 21 programs (Jelínek 1978), which enable a complete statistical evaluation of a group of specimens to be carried out. The RESEA program transforms the susceptibility tensors of specimens from the geographical coordinate system to the so-called paleogeographical system (defined by the magnetic north and the horizontal bedding plane). Then, the ANS 21 program computes the mean tensor in the latter coordinate system and its variance (for details see Jelínek 1978; Hrouda–Stránik 1985).

The results of measurements are summarized in Table 1 and Figs. 3–10. The first column of the table contains the locality number (corresponding to that in Fig. 1), the second the petrographical type of the rock investigated, the third the stratigraphical position of the locality investigated, the fourth the totals of the specimens measured in each locality (n) and the fifth the arithmetical means of the mean magnetic susceptibility $k_m = (k_1 + k_2 + k_3)/3$, where $k_1 \geq k_2 \geq k_3$ are the principal susceptibilities. The k_m values are given in the order of 10^{-6} (SI units are used). In the sixth to tenth columns there appear pairs of values of the magnetic lineation $L = k_1/k_2$, magnetic foliation $F = k_2/k_3$, magnetic anisotropy degree $P' = \exp \sqrt{\{2[(\eta_1 - \eta)^2 + (\eta_2 - \eta)^2 + (\eta_3 - \eta)^2]\}}$, shape factor $T = 2(\eta_2 - \eta_3)/(\eta_1 - \eta_3) - 1$ ($\eta_1 = \ln k_1$, $\eta_2 = \ln k_2$, $\eta_3 = \ln k_3$, $\eta = (\eta_1 + \eta_2 + \eta_3)/3$, and $q = (k_1 - k_2)/[(k_1 + k_2)/2 - k_3]$ parameter. The values given in the upper line are the arithmetical means of the values for individual specimens, while those given in the lower line represent the parameters derived from the mean tensor for a locality as a whole (calculated using the RESEA and ANS 21 programs). For the simplicity's sake the former parameters will hence-

forth be called the specimen parameters, while the latter the locality parameters. In the eleventh column there are the mean values of the angle (f) between the minimum susceptibility direction and the bedding pole. In the last column the abbreviation of the magnetic anisotropy pattern is given. It consists of two letters, one capital and one small. The capital letter characterizes the relation of the magnetic lineation to the magnetic foliation: P – the magnetic lineation is parallel to the dip line of magnetic foliation, T – the magnetic lineation is transverse to the dip of magnetic foliation, N – the magnetic foliation is parallel to the bedding or the magnetic foliation or lineation are largely scattered spatially so that the above relationship cannot be established. The small letter indicates the orientation of partial girdle in magnetic foliation poles with respect to the trend of magnetic lineation: p – the girdle is parallel, t – the girdle is transverse, o – the girdle is oblique to the trend of magnetic lineation.

Origin of magnetic fabric

In order to understand the magnetic fabric generation under different deposition regimes, many laboratory deposition experiments have been made by experimentalists of the British school (represented by Hamilton, Rees and their co-workers), simulating the natural deposition conditions as closely as possible (see, for example, Rees and Woodall 1975; Rees 1983). It has been shown that during grain by grain deposition (or from thin suspension) from still or running water onto a flat or sloping bottom the q parameter value is less than 0.5 and the magnetic foliation dips less than 15° from the bedding towards the origin of flow. The magnetic lineation is parallel to the direction of flow and to the dip of magnetic foliation. During deposition from very concentrated grain dispersion onto a sloping bottom the q value is higher, reaching 0.7, the magnetic foliation dips 25–30° towards the origin of flow, and the magnetic lineation is parallel to the flow (to the dip of the slope) and to the dip of magnetic foliation. During deposition from medium-concentrated suspension (ca 8 % in Rees' 1983, experiments) the q value is less than 0.3, the magnetic foliation dips less than 15° towards the origin of flow, and the magnetic lineation is perpendicular to the flow direction and to the dip of magnetic foliation. The transverse orientation of magnetic lineation, as shown by Rees' (1983) experiments, can originate also due to synsedimentary pure shear deformation, but the q value is high (0.5–1.0). In all experiments having produced the magnetic lineation parallel to the dip of magnetic foliation the magnetic foliation poles create an embryonic girdle which is parallel to the trend of magnetic lineation. On the other hand, during ductile deformation this girdle is perpendicular to the magnetic lineation. If all the properties mentioned are regarded as characteristic of sedimentary magnetic fabric, they can be used as criteria for distinguishing rocks with sedimentary magnetic fabrics from those with deformational fabrics.

Table 1

Magnetic anisotropy parameters of the sedimentary rocks of the Strážovské vrchy Mts.

Loc.	Rock	Strat.	n	k_m	L	F	P	T	q	f	Ch
	Cover Formation										
8	quartzite	T_1	5	15	1.012	1.014	1.027	0.11	0.61		T_t
					1.010	1.017	1.027	–	0.46		
9	sandstone limy	K_{2a1}	13	107	1.011	1.013	1.025	−0.03	0.73		T_t
					1.009	1.013	1.022	0.15	0.51		
15	quartzite	T_1	10	30	1.014	1.016	1.030	−0.15	0.88		T_t
					1.007	1.002	1.009	−0.70	1.38		
	Křížna nappe										
1	sandstone	K_{2a1}	10	113	1.011	1.031	1.043	0.45	0.33	14	P_p
2	sandstone	K_{2a1}	11	154	1.007	1.019	1.026	0.44	0.38	38	T_t
					1.004	1.010	1.013	0.27	0.34		
3	sandstone	K_{2a1}	12	221	1.002	1.012	1.014	0.70	0.17	12	T_t
					1.001	1.012	1.013	0.85	0.07		
4	sandstone	K_{2a1}	8	168	1.007	1.013	1.020	0.08	0.41	21	P_t
					1.006	1.012	1.018	0.44	0.42		
5	silty sandstone	K_{2a1}	8	195	1.003	1.023	1.027	0.75	0.14	2	N_t
					1.002	1.024	1.026	0.83	0.09		
6	limy sandstone	K_{2a1}	16	115	1.008	1.032	1.043	0.53	0.30	5	N_p
					1.006	1.031	1.037	0.13	0.18		
10	marlstone	J	9	95	1.014	1.036	1.051	0.42	0.35	76	T_t
					1.011	1.035	1.047	0.16	0.28		
11	marlstone	J	11	78	1.006	1.024	1.030	0.58	0.24	7	P_p
					1.004	1.024	1.029	0.72	0.16		
13	marlstone	J	9	18	1.010	1.003	1.013	−0.41	1.15	–	–
					1.004	1.001	1.005	−0.67	1.41		
16	marlstone	J	11	196	1.013	1.036	1.049	0.35	0.43	40	T_p
					1.013	1.016	1.028	0.43	0.58		
30	sandstone	K_{a1}	10	182	1.003	1.009	1.012	0.38	0.40	39	N_o
					1.001	1.004	1.005	0.28	0.26		
31	sandstone	K_n	12	113	1.011	1.030	1.041	0.41	0.38	14	P_p
					1.006	1.029	1.036	0.76	0.20		

As clear from Table 1, in the Cover Formation the mean susceptibility of quartzite is very low, in sandstone it is an order of magnitude higher. (From locality No. 8 only specimens with $k_m > 10 \times 10^{-6}$ were used for interpretation, because less magnetic specimens display unreliable values of magnetic anisotropy parameters arising from the compensation effect of ferromagnetic and diamagnetic fractions – Hrouda 1986.) In all localities of the Cover Formation the specimen anisotropy degree is very low and the locality anisotropy degree is even lower. The magnetic fabric is planar in some specimens and linear in the others. The locality magnetic fabric is planar in localities Nos. 8 and 9 and linear in locality No. 15. The magnetic foliation makes a large angle with the bedding in all specimens in localities Nos. 8 and 15 and in many specimens in locality No. 9. The partial girdles in magnetic foliation poles are oriented in general transversely to magnetic lineation. From these observations we can conclude that the magnetic fabric of the sedimentary rocks investigated in the Cover Formation is undoubtedly deformational in origin.

In the Krížna nappe, as seen from Table 1, the specimen anisotropy degree of both sandstone and marlstone is low, while the locality degree is even lower. The specimen magnetic fabric and the locality magnetic fabric are mostly planar, only in locality No. 13 they are linear. In the majority of localities all three principal susceptibilities are well defined; only in localityNo. 13 they are widely scattered.

After applying the criteria for distinguishing the sedimentary from deformational magnetic fabrics following the observations described in the beginning of this chapter, the magnetic fabric can be classified as sedimentary in localities Nos. 1, 6, 11, 31 and deformational in localities Nos. 2, 3, 4, 5, 10, 13, 16, 30. From Table 1 it is clear that sandstone localities exhibit both types of the magnetic fabric, while the marlstone ones show mostly deformational fabrics.

We realize that we were perhaps too severe in regarding only those rocks which fit all the criteria described in the beginning of this chapter as displaying the sedimentary magnetic fabric. For example, the rocks exhibiting the magnetic lineation transverse to the dip of magnetic foliation may originate not only through deformation, but also through the deposition from medium-concentrated dispersion. However, as this kind of deposition takes place relatively rarely, in a bounded deposition regime corresponding to that in the A division of the Bouma flysch sequence (see Tiara and Scholle 1979; Rees 1983), it seems to us that we make smaller error if we include these rocks into those with deformational magnetic fabric than if they were regarded as depositional.

Fig. 3 shows the orientations of magnetic foliation and lineation in the palaeogeographical coordinate system, Fig. 4 the relation between P' and T parameters and Fig. 5 the relation between f and $P'(T)$ parameters for rocks with sedimentary fabric. It is clear from Fig. 3 that the magnetic foliation poles create an embryonic girdle parallel to the magnetic lineation, the T value increases with increasing P' (Fig. 4) and the T value decreases with decreasing f (Fig. 5). These

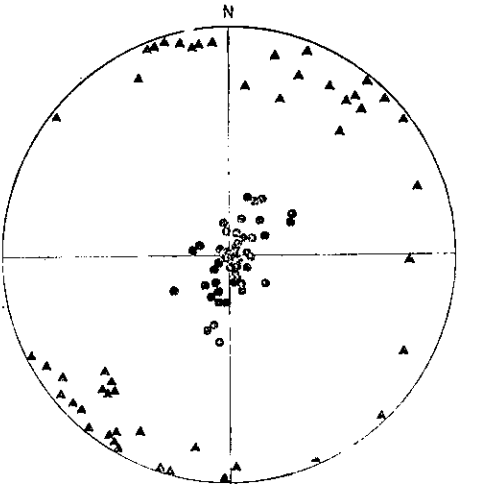

3. Orientations of magnetic lineation (*triangles*) and poles of magnetic foliation (*circles*) in the rocks with sedimentary magnetic fabric in the Krížna nappe in the palaeogeographic coordinate system. Equal-area projection on lower hemisphere

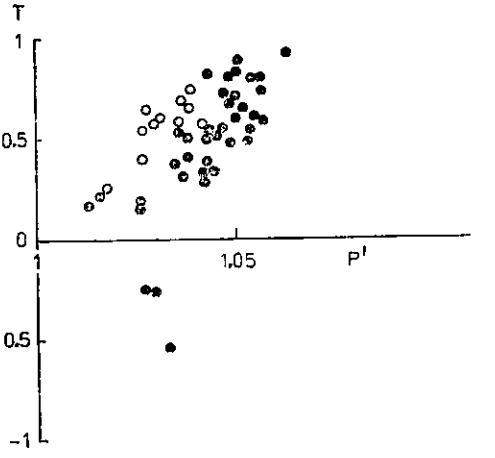

4. Magnetic anisotropy plot of sediments with sedimentary magnetic fabric in the Krížna nappe
Closed circles – sandstone, *open circles* – marlstone

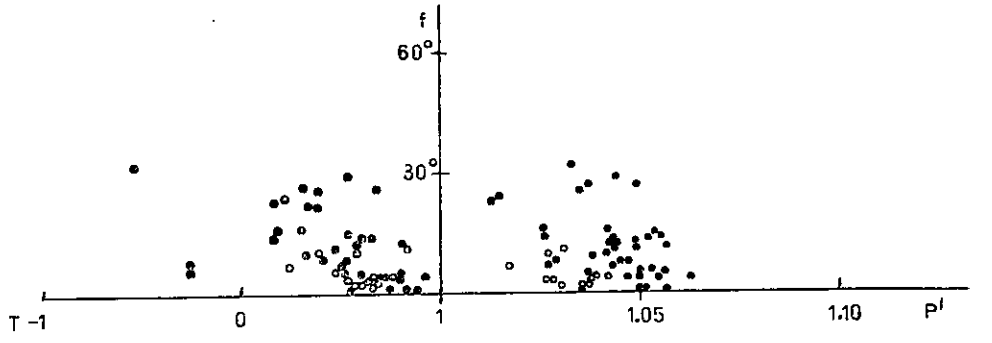

5. The f vs $P'(T)$ plot of rocks with sedimentary magnetic fabric in the Krížna nappe

relationships convince us that the magnetic fabric in localities 1, 6, 11, 31 is really sedimentary in origin. The correlation between T and f parameters reflects variation in the strength of the flow (tangential shear along the bed).

Sedimentological implications

It is clear from Table 1 that in localities with sedimentary magnetic fabrics (in the Krížna nappe) f angle is less than 15° and mean q values less than 0.5. These values imply that the rocks in these localities were not deposited from concentrated grain dispersion. Except for locality No. 6 the magnetic lineations are parallel to the dip of magnetic foliation and q values are relatively high. This magnetic fabric corresponds to that generated during the deposition from thin suspension. The orientation mechanism of grains in such rocks is a rotation of grains in a sheared (flowing) fluid.

In the locality No. 6 the magnetic foliation is virtually parallel to the bedding and it is therefore impossible to deduce whether the magnetic lineation is parallel or transverse to the dip of magnetic foliation. The parallelism of the magnetic foliation to the bedding implies the idea that the deposition of limy sandstone in this locality was from thin suspension and that the orienting mechanism of grains was almost ideal shear flow.

The orientations of magnetic lineation and foliation in localities with sedimentary magnetic fabric are presented in a synoptic diagram in Fig. 3 in the palaeogeographical coordinate system. It can be seen in Fig. 3 that the magnetic lineations are mostly oriented NE–SW, but there are also some specimens oriented NNW–SSE to NW–SE. The magnetic foliation poles create an embryonic girdle oriented NE–SW, i.e. parallel to the magnetic lineation and, consequently, the magnetic lineations can be regarded as representing the directions of the near-bottom water currents. It can be concluded from the orientation of magnetic lineation that the near-bottom currents operating in the sedimentation basin of the Krížna nappe formations were mostly oriented NE–SW and subordinately also NNW–SSE. However, it is necessary to realize that these directions are related only to the today's configuration of the nappe. As the nappe may have rotated during its movement, the actual directions of the currents in respect to the ancient north may have been different. As the palaeogeographical situation in the time of deposition has not yet been clearly known, it can hardly be decided whether the directions indicated by magnetic anisotropy represent the directions of the transport of the clastic material into the basin or those transporting the clastic material along the basin.

Fig. 2 gives an approximate information of the orientations of the palaeocurrents determined by sedimentological methods.

Fig. 2 was compiled from the data contained in the Supplement 1 in the

paper by Jablonský (1978). The palaeocurrent determinations are based on the measurement of flute casts, prod marks, groove casts, cross lamination, ripple marks. In Fig. 2 all the determinations are presented together. The maximum between 20 and 30° (200–210°) comes mostly from flute casts and prod marks, the other maxima come from the other fabric elements. It is clear from the comparison of Figs. 2 and 3 that the palaeocurrents determined magnetically are compatible with those determined non-magnetically. Only the NNW–SSE directions determined magnetically have no correspondence with the directions determined sedimentologically.

The investigation of the palaeocurrent directions confirms Jablonský's (1978) conclusion that the transport directions in the Krížna nappe basin were mostly NE–SW.

Tectonic implications

The magnetic fabrics in all three localities investigated in the Cover Formation have been classified as deformational in origin. In Fig. 6 showing the orientation of magnetic lineation, poles of magnetic foliation in the palaeogeographical coordinate system we can see that the magnetic foliation poles create an imperfect NE–SW girdle and the plunge of the magnetic lineations varies from virtually horizontal to virtually vertical, while the magnetic lineations trend mostly NNW–SSE. The magnetic anisotropy degree is relatively low and the specimen magnetic fabric ranges from clearly linear to clearly planar (see Table 1). The angle between the magnetic foliation and bedding ranges from virtually zero to almost 90°. From all these observations one can conclude that the deformational overprint of the sedimentary magnetic fabric has not been complete and that the magnetic fabric of individual specimens represent different stages of the superposition of the deformational magnetic fabric on the sedimentary one.

In localities with deformational magnetic fabric in the Krížna nappe the anisotropy degree P' in sandstone is lower than in the localities with sedimentary fabric and varies only slightly (Table 1). The shape parameter T varies widely, ranging from slightly linear to almost perfectly planar magnetic fabric, and, unlike to the localities with sedimentary magnetic fabric, there is obviously no correlation between the P' and T parameters (Fig. 7). In marlstone the anisotropy degree P' ranges from very low ($P' < 1.01$) to relatively high ($P' > 1.1$) and the T parameter ranges from -0.9 to $+0.8$; a positive, even though not too close, correlation exists between the P' and T parameters (Fig. 7). As it is clear from Fig. 8, there is apparently no correlation between the anisotropy degree P' and the magnetic foliation/bedding angle (f) in sandstone. As for the T and f parameters, the correlation does not seem to exist at first sight as well (see Fig. 8), but after a more detailed inspection we can see that for the lower values of T the higher values of f are

characteristic and vice versa. In marlstone there are two groups of specimens, one displaying high f values (50–80°) and one showing low f values (less than 20°). In both groups the P' and T values vary largely and there is apparently no correlation between the f and P' or T parameters (see Fig. 8).

In sandstone both the poles of bedding and those of magnetic foliation create imperfect girdles oriented NW–SE and the magnetic lineation is mostly horizontal, but exhibits large azimuthal scatter (see Fig. 9). In marlstone the poles of bedding and those of magnetic foliation again create imperfect NW–SE oriented girdles. The magnetic lineation plunges gently to moderately and its scatter is smaller than sandstone; the predominating direction is NE–SW (Fig. 10).

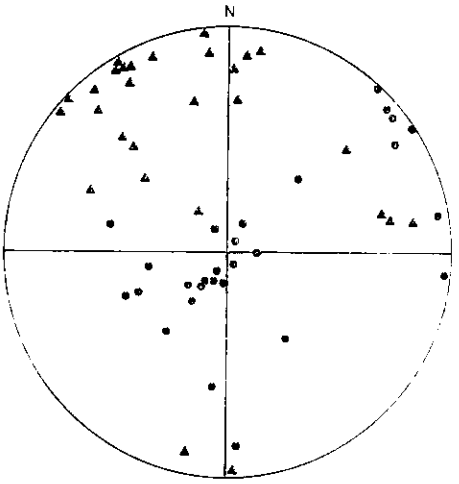

6. Orientations of magnetic lineation (*triangles*), poles of magnetic foliation (*closed circles*) and poles of bedding (*open circles*) in the Cover Formation in the palaeogeographical coordinate system. Equal-area projection on lower hemisphere

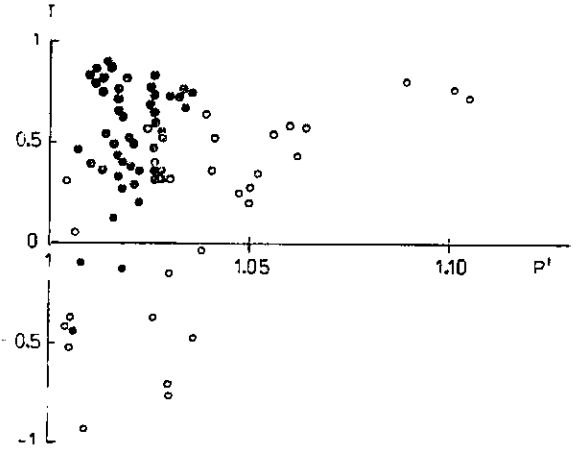

7. Magnetic anisotropy plot of rocks with deformational magnetic fabric in the Krížna nappe
Closed circles – sandstone, *open circles* – marlstone

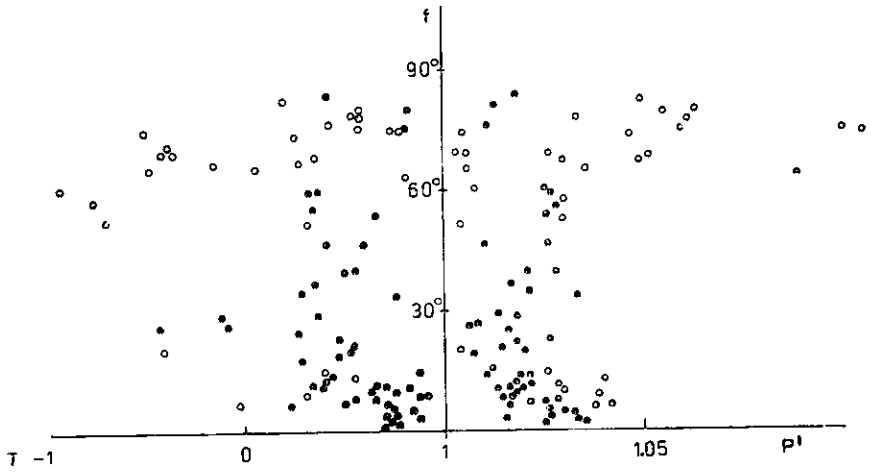

8. The f vs $P'(T)$ plot of rocks with deformational magnetic fabric in the Krížna nappe
Closed circles — sandstone, *open circles* — marlstone

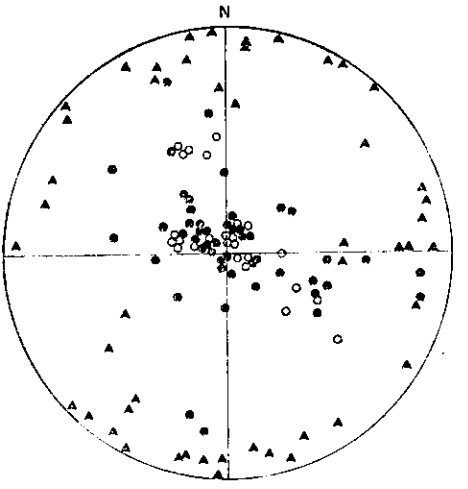

9. Orientations of magnetic lineation (*triangles*), poles of magnetic foliation (*closed circles*), and poles of bedding (*open circles*) in sandstone with deformational magnetic fabric in the Krížna nappe in geographical coordinate system. Equal-area projection on lower hemisphere

From the above observations we may deduce that the magnetic fabric in sandstone reflects a weak overprinting of the sedimentary fabric by the deformational fabric and that the deformation is represented by a combination of simple shear with the shortening parallel approximately to the bedding. During this deformation the sedimentary magnetic fabric was modified in such a way that the anisotropy degree of a rock and the planarity of the magnetic fabric were lowered. The magnetic foliation rotated from the bedding to various degree about the axis

NE–SW and the magnetic lineation may have remained in the original orientation if the deformational magnetic fabric was coaxial with the sedimentary magnetic fabric, while it may have been deflected strongly, if the superposition was non-coaxial.

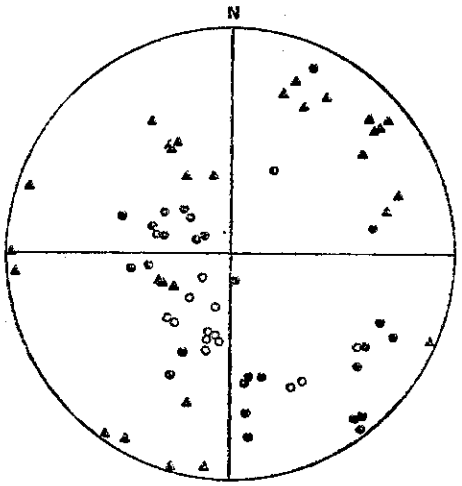

10. Orientations of magnetic lineation (*triangles*), poles of magnetic foliation (*closed circles*), and poles of bedding (*open circles*) in marlstone with deformational magnetic fabric in the Krížna nappe. Equal-area projection on lower hemisphere. Geographic coordinate system

In marlstone, probably due to its higher ductility, the overprint of deformational fabric on the sedimentary one was in general stronger. In those specimens in which the overprint was relatively weak the anisotropy degree decreased, like in sandstone, but in those where the overprint was strong it increased. The increasing planarity of magnetic fabric with increasing anisotropy degree probably indicate that the overprint may have been very strong in some specimens. The orientation of the girdle of magnetic foliation poles being NW–SE and the orientation of the magnetic lineation NE–SW suggest that the deformation mentioned may have been represented by a combination of a simple shear and shortening parallel to the bedding (shortening in the direction NW–SE).

Conclusions

The magnetic fabric in the Cover Formation and in the Krížna nappe of the Strážovské vrchy Mts. has been investigated. From the investigation the following conclusions have been drawn:

1. The magnetic fabric in the Cover Formation is strongly influenced by ductile deformation. The influence is higher in quartzite than in sandstone.

2. The magnetic fabric in the Krížna nappe, both in sandstone and marlstone, is composite, i.e. partially sedimentary and partially deformational in origin.

3. In localities with predominantly sedimentary magnetic fabric the magnetic lineations are oriented in a compatible way with the orientation of palaeocurrents determined by sedimentological methods by Jablonský (1978). The palaeocurrent directions determined by both magnetic and sedimentologic methods are NE–SW.

4. The ductile deformation having affected the Krížna nappe rocks is represented by a combination of simple shear and pure shear. The pure shear is represented by a shortening in the NW–SE direction.

Acknowledgement

The work was supported by the Dionýz Štúr Institute of Geology, Bratislava (Project Principal Investigators Dr. B. Leško and Dr. T. Koráb).

K tisku doporučil O. Orlický

Přeložil F. Hrouda

References

Hrouda, F. (1986): The effect of quartz on the magnetic anisotropy of quartzite. – Stud. geophys. geod., 30, *39–45*. Praha.

Hrouda, F.–Stráník, Z. (1985): The magnetic fabric of the Ždánice thrust sheet of the Flysch Belt of the West Carpathians: sedimentological and tectonic implications. – Sedimentary Geol., 45, *125–145*. Amsterdam.

Jablonský, J. (1978): Príspevok k poznaniu albu zliechovskej série Strážovských vrchov. *In*: Paleogeografický vývoj Západných Karpát, *175–187*. – Geol. úst. D. Štúra. Bratislava.

Jelínek, V. (1973): Precision A. C. bridge set for measuring magnetic susceptibility of rocks and its anisotropy. – Stud. geophys. geod., 10, *58–78*. Praha.

– (1977): The statistical theory of measuring anisotropy of magnetic susceptibility of rocks and its application. – Geofyzika, s. p. Brno.

– (1978): Statistical processing of anisotropy of magnetic susceptibility measured on groups of specimens. – Stud. geophys. geod., 22, *50–62*. Praha.

– (1982): Kappabridge KLY-2. – Geofyzika. Brno (Leaflet).

Mahel', M. (1985): Geologická stavba Strážovských vrchov. – Geol. úst. D. Štúra. Bratislava.

Rees, A. I. (1983): Experiments of the production of transverse grain alignment in a sheared dispersion. – Sedimentology, 30, *437–448*. Amsterdam.

Rees, A. I.–Woodall, W. A. (1975): The magnetic fabric of sand and sandstones. – Earth planet. Sci. Lett., 25, *121–130*. Amsterdam.

Tiara, A.–Scholle, P. A. (1979): Deposition of resedimentated beds in the Pico Formation, Ventura Basin, California from magnetic fabric measurements. – Geol. Soc. Amer. Bull., 90, *952–962*. New York.

Sbor. geol. věd	Užitá geofyz., 24	Pages 107–132	9 figs.	2 tabs.	— pl.	Praha 1990 ISSN 0036-5319

Earthquake activity in the north part of the Socialist Republic of Vietnam during the period from 1976 to 1984

Activité des tremblements de terre dans le Nord du Viêt-Nam pendant la période de 1976—1984

Nguyen Kim Lap[1]

Received May 4, 1987

Vietnam (northern part)
Seismic activity
Magnitude scales
Tuangiao earthquake

Nguyen Kim Lap (1990): Earthquake activity in the north part of the Socialist Republic of Vietnam during the period from 1976 to 1984. – Sbor. geol. Věd, užitá Geofyz., 24, *107–132*. Praha.

Abstract: Data related to more than 1 000 earthquakes which occurred in the north part of Vietnam from 1976 to 1984 were collected. The northwest area of the country is characterized by Tuangiao earthquake (M = 6.7) being the consequence of regional tectonic activity in the northwest-southeast direction. Earthquake activity in the north part of Vietnam was studied qualitatively by showing the space distribution of earthquakes, seismic activity A_{10}, maximum expected earthquakes and the main characteristics of the Tuangiao earthquake.

[1] *Institute of Geophysics National Centre for Scientific Research of Vietnam, Nghia do – Tu liem – Hanoi*

Introduction

The territory of the north part of Vietnam is situated along the contact of two strongest earthquake belts of the world: the Mediterranean and West Pacific belts. These features partly determine the seismic activity of the territory of Vietnam. Seismic data show that in the north part of Vietnam large earthquakes have occurred with heavy human and material losses (Xuyen–Lap, 1985). Earthquake observations in the north part of Vietnam started as early as 1924. Since that time, Phulien seismological station is in active operation and exchanges earthquake data

with international data centres. Rapid development in seismological technology and the increased distribution of seismological stations, especially after 1975, has resulted in precise location of earthquakes of magnitude as small as 3.5. The Tuangiao earthquake of magnitude $M = 6.7$ occurred along the Sonla fault adjacent to the Red river fault system extending northwest-southeast from Yunnan province in China. The Tuangiao earthquake caused considerable damage, a number of brick building were either destroyed or damaged and a considerable amount of rice fields was damaged by falling rocks. The purpose of this paper is to investigate the main characteristics of earthquake activity in the north part of Vietnam, which are the basis of predictions at different stages.

Data

Seismological stations

Seismological stations have been established successively in the north part of Vietnam after 1975 (fig. 1). From these stations, data on the earthquake activity in this region are obtained. Generally speaking, it has been possible to monitor

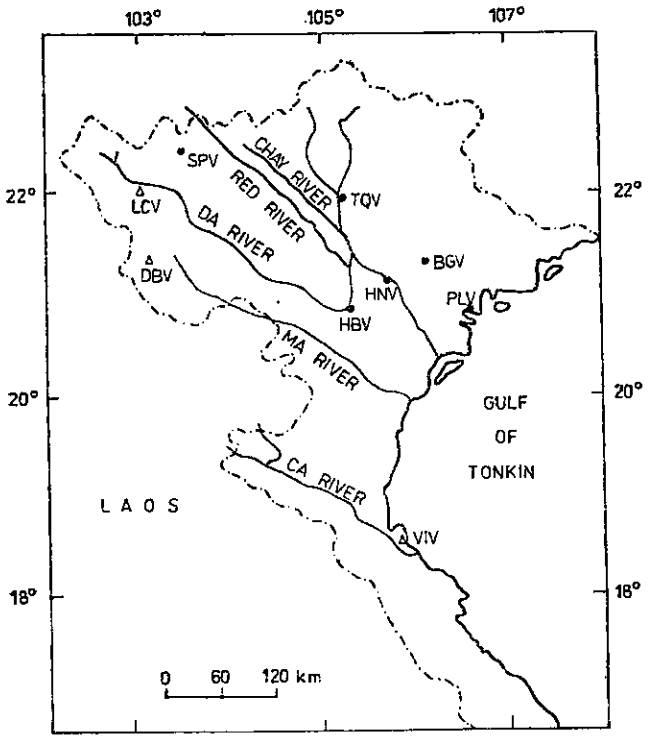

1. Seismograph stations in Vietnam, solid dots are permanent seismic stations
Open triangles are stations proposed for the future

earthquakes of $M \geq 3.5$ since 1976. The list of seismological stations is given in table 1. The location of earthquakes is estimated using travel times of Central Asia.

Table 1

List of seismic stations in the north part of Vietnam

Station name and code	Coordinates		Type of instrument	Component	Siesmometer period T_s(S)	Galvanometer period T_g(S)	Maximum magnification V_{max}
	N	E					
Phulien PLV	21°42′21″	106°37′44″	SKM	NS	12	1.1	1165
				EW	12	1.25	1277
				Z	12	1.25	1920
			SM-3	NS	1.8	0.30	16130
				EW	1.8	0.30	15800
				Z	1.8	0.30	19150
Bacgiang BGV	21°17′38.9″	106°13′42.9″	Kharin	NS	1.0	0.30	42242
				EW	1.0	0.30	42020
				Z	1.0	0.30	47144
Hoabinh HBV	20°49′33.3″	105°21′06.9″	Kharin	NS	1.0	0.49	55788
				EW	1.0	0.46	43000
				Z	1.0	0.33	51124
Tuyênquang TQV	21°49′42″	105°12′30″	SU-59	NS	1.0	0.30	43957
				EW	1.0	0.30	47425
				Z	1.0	0.30	49193
Sapa SPV	20°20′08.9″	103°49′51.8″	SP-1	NS	1.2	0.14	13313
				EW	1.2	0.14	14492
				Z	1.2	0.14	14355

Magnitude scales

Earthquake magnitude is a measure of the elastic strain energy released during earthquakes in the form of elastic waves. In this work, the adopted formulas for surface wave magnitudes are as follows (Thuc, 1979).

$$M_H = \log \frac{A_H}{T} + 1.33 \log \Delta\,[\text{km}] + 1.43, \qquad (1)$$

$$M_Z = \log \frac{A_Z}{T} + 1.66 \log \Delta \text{ [km]} + 0.44, \qquad (2)$$

where A_H and A_Z are the maximum horizontal and vertical amplitudes in micrometers.

Another formula for magnitude scale, elaborated from the duration of seismic records, is also used (Xuyen, 1972):

$$M_D = 2.67 \log (F - P) - 2.49, \qquad (3)$$

where $F - P$ is the duration of seismic record in seconds, F is beginning of seismic record, P is end of seismic record. Magnitude was determined by formulas 1, 2 and 3 almost equal with magnitude of Gutenberg and Richter (Xuyen and Lap, 1985).

Regional distribution of earthquakes in the north part of Vietnam

In the north part of Vietnam, the earthquakes are distributed in narrow bands along tectonic faults which are the boundaries of the geological blocks. The distribution of earthquake epicentres is shown in fig. 2, where their magnitudes are also marked.

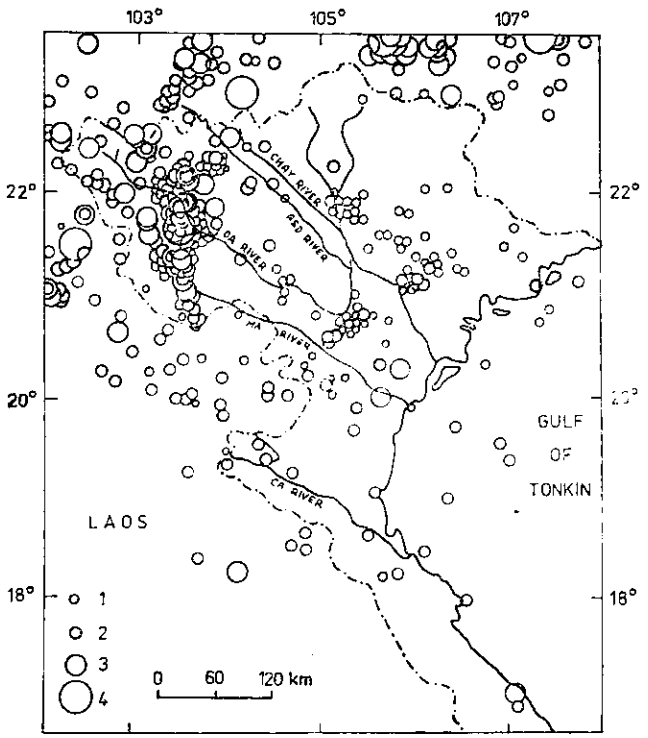

2. Epicentral distribution of earthquakes in North Vietnam during the period 1976 to 1984
Magnitude: 1. M < 3;
2. M = 3÷4;
3. M = 4.1÷5.0;
4. M ≥ 5.1

The earthquake density is higher in northwestern Vietnam, and relatively low in southern part of the studied region. In the north part of Vietnam, the earthquakes usually lie along a recently active fault zone and seismic activity is increasing in the studied period. It should be mentioned that all earthquakes are shallow and their foci are considered to be within the crust (crustal thickness about 35 km). From earthquakes in the north part of Vietnam, for which the depth could be determined, we observe that about 90 % of earthquakes have hypocentres in the depth from 5 km to 20 km.

Cumulative strain release

Benioff assumed that the strain state of the medium around a hypocentre is directly proportional to the square root of earthquake energy. To study seismicity as a function of time, a strain release curve was computed. In evaluating the energy (E) of an earthquake, the formula by Gutenberg was used:

$$\log E = 4.3 + 1.8\,M, \tag{4}$$

where M is the surface wave magnitude and E is the energy of the shock in Joules.

The time variation of the strain release in the north part of Vietnam during the period 1976 to 1984 is presented in fig. 3. This curve shows that the major earthquakes ($M \geq 5$) occurred in 1983. From the strain release curve the yearly strain release can be estimated to be approximately $3.5 \cdot 10^7$ Joules$^{1/2}$.

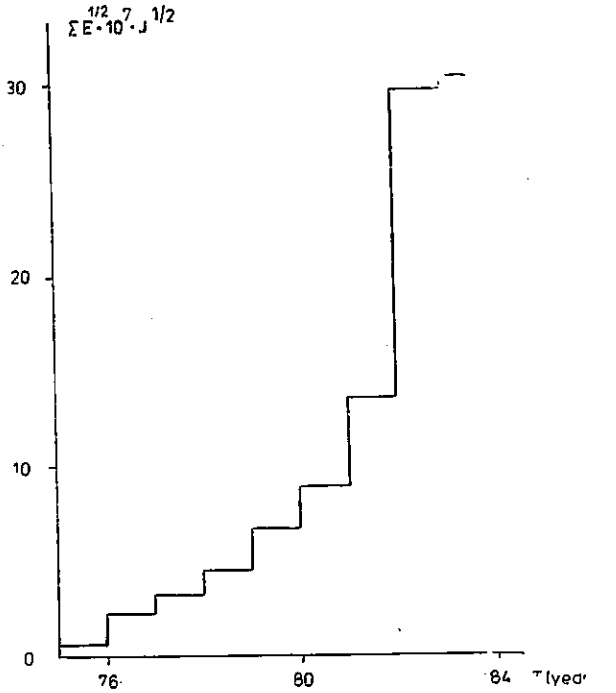

3. Cumulative strain release for earthquakes in North Vietnam during the period 1976 to 1984

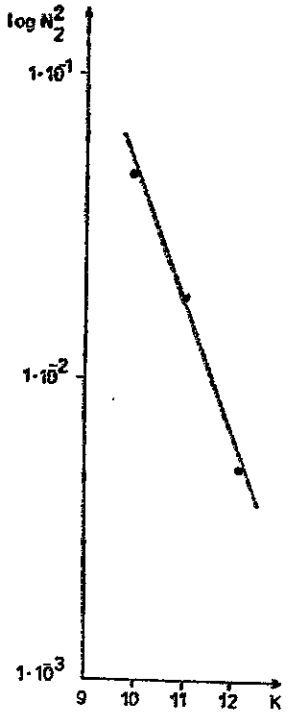

4. Earthquake reccurrence graph of North Vietnam during period from 1976 to 1984

Seismic activity in the north part of Vietnam

Earthquake frequency law

The seismicity of this region was analysed using the method proposed by Riznichenko (1960). This method is based on the earthquake frequency law expressed by the frequency-energy relation (Riznichenko, 1960):

$$\log N = \alpha - \gamma K, \tag{5}$$

where: N – cumulative number of earthquakes,
α – parameter related to the level of activity,
γ – slope of frequency graph,
K – energy class.

Seismic activity A equals α for a certain value of K, e.g. K = 10, according to Riznichenko (1960). The coefficients in equation (5) are calculated using the least squares method. The application of equation (5) to the earthquakes which occurred in the north part of Vietnam within an area of about 426 000 km^2 during the period 1976 to 1984, led to the following relation

$$\log N = 2.27 - 0.38\,K. \tag{6}$$

The graph of equation (6) is given in fig. 4.

Table 2

List of earthquakes with M ≥ 3.0 which occurred in the north part of Vietnam during period from 1976 to 1984

N°	Date			Origin time (GMT)			Epicentre		H	M
	D	M	Y	h	m	s	N	E	(km)	
1	19	01	1976	13	07	07	22.4	103.1	15	3.3
2	29	01		08	56	22	23.6	106.4	10	3.6
3	26	02		11	59	46	22.9	105.4	15	3.0
4	09	03		10	16	11	20.9	103.5	20	3,0
5	09	03		10	58	00	20.1	103.2	15	3.1
6	25	03		18	16	26	21.9	106.7	20	4.0
7	26	03		07	05	50	22.0	103.2	15	3.1
8	07	04		05	34	32	20.3	103.3	15	3.1
9	12	07		20	30	00	18.5	104.9	15	3.4
10	13	07		21	59	48	21.3	102.3	15	3.7
11	19	08		11	44	34	22.6	101.9	10	3.8
12	09	09		17	55	11	19.8	104.0	15	3.1
13	04	10		16	23	06	21.7	103.9	10	3.0
14	08	11		08	09	13	21.1	107.3	10	3.0
15	09	11		06	09	49	23.7	102.4	10	3.7
16	09	11		06	11	35	23.6	102.7	15	5.1
17	23	11		02	00	43	18.6	104.7	15	3.6
18	31	11		14	28	26	21.9	105.1	6	3.6
19	11	01	1977	14	56	05	21.2	102.9	10	3.4
20	04	02		11	12	50	22.1	102.6	13	3.6
21	05	02		04	33	00	19.9	104.0	20	3.4
22	21	02		13	32	59	22.3	105.1	15	3.3
23	24	02		20	33	00	23.3	104.5	10	3.4
24	28	02		09	41	00	19.7	106.4	20	3.1
25	19	03		18	28	32	19.4	104.0	20	3.5
26	03	04		16	38	40	21.2	106.0	10	3.1
27	07	04		04	07	31	19.3	106.7	20	3.6
28	08	04		11	48	39	20.9	102.6	10	3.3
29	09	04		14	02	43	26.6	106.9	10	4.1
30	13	04		00	08	32	18.6	104.9	10	4.0
31	13	04		02	33	41	23.3	104.1	10	3.8
32	24	04		02	16	09	23.6	106.9	20	3.4
33	26	04		08	45	23	23.3	107.6	20	4.0
34	14	05		13	37	00	20.1	105.2	20	3.0
35	02	06		16	48	31	21.0	102.0	25	3.6
36	29	06		19	15	14	22.3	102.2	15	3.3
37	06	07		12	27	00	20.8	105.3	15	3.3
38	15	07		14	16	46	22.5	102.9	10	3.4
39	12	08		06	02	35	20.2	102.8	20	3.3
40	19	09		09	51	52	21.1	103.5	25	3.5

Table 2 (continued)

N°	Date			Origin time (G M T)			Epicentre		H	M
	D	M	Y	h	m	s	N	E	(km)	
41	20	09	1977	11	09	56	20.7	103.3	20	3.1
42	21	09		03	03	00	20.6	103.3	25	3.0
43	29	09		21	18	06	23.5	102.4	25	5.0
44	09	09		05	55	23	19.3	103.6	20	4.0
45	19	10		02	44	38	23.5	107.3	20	5.2
46	19	10		03	55	00	23.5	107.5	25	4.6
47	19	10		21	39	04	23.5	107.0	20	3.5
48	25	10		05	29	58	21.2	105.8	10	3.0
49	16	12		18	20	00	21.8	102.5	20	3.5
50	19	01	1978	19	25	36	23.1	107.6	10	3.9
51	02	02		20	36	26	22.1	103.8	15	3.2
52	06	02		06	08	59	21.4	102.4	10	3.9
53	08	03		18	21	47	23.5	103.5	20	3.5
54	12	03		20	36	54	21.1	102.4	10	3.9
55	06	04		18	12	54	22.5	104.3	10	3.6
56	26	04		11	52	27	22.9	102.9	10	3.3
57	29	04		12	08	10	21.2	107.4	10	3.1
58	03	05		22	01	35	19.0	106.4	15	3.5
59	08	05		08	48	00	23.0	106.9	25	3.1
60	19	05		03	13	19	22.8	107.4	10	3.6
61	16	07		16	53	51	23.4	106.9	20	3.2
62	29	07		22	33	17	22.6	102.2	15	4.2
63	10	08		09	38	58	21.9	102.7	20	3.7
64	19	08		21	17	59	22.4	103.0	10	3.2
65	06	09		22	41	08	21.3	102.8	10	3.3
66	10	09		11	57	00	21.9	101.8	25	3.5
67	10	09		14	04	00	22.2	103.2	15	3.2
68	10	09		14	39	08	22.2	102.6	10	3.2
69	11	09		18	42	31	22.8	104.1	10	3.5
70	28	09		07	33	23	21.2	103.3	15	3.0
71	28	09		08	23	03	22.4	102.4	15	4.5
72	01	10		20	50	38	21.5	103.6	10	3.4
73	04	10		01	56	33	20.8	102.8	25	3.6
74	07	10		12	25	43	22.5	102.6	10	3.2
75	09	10		21	42	36	24.1	104,1	10	4.2
76	09	10		22	55	14	22.1	104.3	10	3.8
77	13	10		04	54	48	22.1	102.0	10	3.4
78	21	10		06	39	11	21.3	106.2	15	3.1
79	01	11		01	47	17	23.2	102.3	10	3.5
80	04	11		06	31	00	21.6	101.9	20	3.7
81	06	11		00	21	03	20.0	104.7	10	3.2
82	11	11		22	32	07	21.5	104.4	10	3.3

Table 2 (continued)

N°	Date			Origin time (G	M	T)	Epicentre		H	M
	D	M	Y	h	m	s	N	E	(km)	
83	15	11	1978	09	24	25	21.2	106.0	10	3.2
84	16	11		01	22	32	23,2	101.9	10	4.2
85	28	11		12	03	23	23.0	106.9	10	3.1
86	28	11		17	53	11	23.0	107.0	10	3.3
87	11	12		13	42	09	22.1	105.0	10	3.2
88	13	12		18	21	09	22.8	101.5	20	3.4
89	19	12		02	01	50	21.4	104.1	10	3.2
90	22	12		05	56	58	22.3	103.8	15	3.7
91	23	12		08	15	40	22.3	103.8	15	3.1
92	09	01	1979	23	29	00	21.6	102.3	10	5.1
93	09	01		23	34	00	21.0	102.8	10	4.8
94	13	01		06	41	30	20.7	102.8	10	4.5
95	24	02		10	15	57	20.2	105.1	15	3.2
96	03	03		10	28	24	23.3	103.9	20	3.3
97	24	03		19	05	12	23.0	103.5	15	3.1
98	26	03		22	24	09	21.0	102.1	15	3.8
99	04	04		17	12	32	20.2	104.0	15	3.4
100	06	04		19	18	00	23.0	106.3	13	4.6
101	14	04		08	00	25	19.4	104.4	10	3.4
102	20	04		19	22	35	22.9	102.0	20	3.8
103	01	05		10	29	04	21.3	102.1	20	3.6
104	07	05		07	59	34	22.6	103.8	15	3.5
105	20	05		20	58	06	22.9	103.2	10	3.2
106	13	06		12	43	00	22.7	102.7	10	3.5
107	28	06		18	29	41	21.3	102.2	10	3.9
108	30	06		03	01	17	23.0	105.7	15	3.6
109	17	07		18	40	47	21.3	106.2	7	3.6
110	05	08		21	29	42	18.7	105.5	15	3.6
111	14	09		12	55	52	19,7	105.3	15	3.2
112	20	10		19	03	22	21.8	102.9	15	3.7
113	22	01	1980	01	21	00	20.0	103.6	10	4.0
114	22	01		14	07	00	20.1	103.6	15	3.5
115	03	04		20	38	00	20.2	104.9	10	3,0
116	07	04		05	04	00	22.6	102.0	15	3.9
117	17	06		21	46	00	23.0	104.1	15	5.7
118	17	06		22	16	00	22.3	103.0	10	4.2
119	17	06		23	02	00	21.8	103.1	10	4.6
120	18	06		00	57	00	23.4	103.8	10	4.0
121	18	06		03	43	01	22.4	103.0	10	3.7
122	18	06		05	13	01	23.4	103.7	10	3.7
123	18	06		07	33	00	22.8	103.2	10	3.2
124	18	06		12	55	00	23.9	104.2	10	4.3

Table 2 (continued)

N°	Date			Origin time (GMT)			Epicentre		H	M
	D	M	Y	h	m	s	N	E	(km)	
125	18	06	1980	20	40	00	23.5	103.6	10	4.5
126	19	06		07	11	00	23.2	103.6	10	4.0
127	21	06		10	58	00	22.6	103.1	15	4.3
128	22	06		07	22	00	23.3	103.7	15	4.3
129	22	06		19	06	00	23.5	103.8	15	3.6
130	23	06		06	42	00	23.0	103.4	15	3.8
131	23	06		15	04	00	23,3	103.6	15	3.8
132	06	08		10	20	55	23.6	104.3	15	3.7
133	06	08		20	44	24	23.7	104.5	15	3.4
134	10	08		14	28	48	23.8	104.1	15	3.3
135	10	08		21	45	00	23.2	103.6	20	3.2
136	10	12		01	43	00	22.9	103.3	15	3.7
137	10	12		11	47	00	22.9	103.3	15	3.7
138	29	12		08	45	00	21.1	102.1	20	4.2
139	14	01	1981	04	30	03	22.1	104.3	15	3.3
140	14	01		11	40	41	23.7	104.8	20	4.0
141	16	01		22	23	28	23.2	103.4	15	3.0
142	31	01		00	13	37	21.6	102.8	10	3.4
143	04	02		06	26	10	23.0	103.3	20	3.3
144	19	02		21	21	34	20.7	101.1	15	3.7
145	23	03		18	58	32	22.3	101.1	10	3,3
146	27	03		14	39	04	20.8	104.9	15	3.0
147	21	04		19	05	50	22.7	103.0	20	4.3
148	21	04		19	11	14	21.9	102.7	15	3.1
149	27	05		21	10	38.1	20.3	102.7	10	3.3
150	28	05		15	09	42	23.3	105.1	20	3.0
151	08	06		00	37	00	22.5	103.1	25	4.3
152	16	06		14	04	03	22.5	108.4	10	3.3
153	18	06		13	32	20	23.3	105.8	15	3.3
154	11	07		03	01	38	20.6	108.4	10	3.7
155	18	07		10	55	12	21.2	103.2	15	3.8
156	23	07		05	47	23	22.8	101.8	15	3.7
157	01	08		00	44	57	24.1	102.7	20	3.5
158	18	08		15	17	03	20.0	101.2	20	4.2
159	18	08		17	13	23	20.5	102.9	15	4.0
160	19	09		06	50	56	23.1	101.3	3	5.4
161	06	07		14	59	09	23.4	103.8	10	3.2
162	18	12		10	10	44	23.3	103.4	10	3.2
163	23	12		20	47	19	22.6	103.0	15	3.2
164	26	12		08	00	26	23.5	107.9	20	3.5
165	08	04	1982	12	23	15	21.6	103.1	15	4.4
166	24	06		14	01	45	22.5	102.2	20	4.4

Table 2 (continued)

N°	Date			Origin time (GMT)			Epicentre		H	M
	D	M	Y	h	m	s	N	E	(km)	
167	07	06	1982	02	12	26	21.6	101.9	20	4.3
168	23	10		10	40	11	20.9	102.2	20	3.9
169	25	01	1983	12	16	54	23.7	105.3	15	3.9
170	17	02		04	24	55	25.6	105.1	15	4.6
171	07	03		06	55	00	20.6	105.2	10	3.1
172	08	03		10	03	04	22.2	102.3	15	3.5
173	30	04		09	16	19	20.3	105.7	10	3.0
174	04	05		11	59	48	19.4	107.0	15	3.6
175	24	06		06	54	24	21.5	103.4	10	3,5
176	24	06		07	18	22	21.7	103.4	23	6.7
177	24	06		08	15	12	21.6	103.5	15	5.0
178	24	06		09	05	08	21.7	103.5	10	3.0
179	24	06		09	44	24	21.8	103.4	5	3.0
180	24	06		09	52	28	22.2	103.4	5	3.4
181	24	06		10	46	31	21.4	103.3	10	4.0
182	24	06		11	23	21	20.5	103.6	15	4.0
183	24	06		11	33	56	21.8	103.4	10	3.3
184	24	06		11	38	52	21.7	103.3	15	3.6
185	24	06		13	02	12	21.7	103.4	5	3.6
186	24	06		13	44	41	22.0	103.5	10	3.5
187	24	06		13	52	56	21.6	103.5	5	3.5
188	24	06		14	03	44	21.8	103.7	10	4.0
189	24	06		14	49	08	22.1	103.7	15	4.1
190	24	06		15	39	01	21.8	103.4	10	3.6
191	24	06		16	46	27	21.7	103.4	5	3.5
192	24	06		16	48	46	21.7	103.4	5	3.5
193	24	06		17	37	44	22.2	103.5	10	3.6
194	24	06		20	12	32	21.6	103.4	5	3.2
195	24	06		21	02	13	22.0	103.4	7	3.7
196	24	06		22	02	02	22.0	103.4	5	4.0
197	25	06		01	47	37	22.0	103.4	5	3.8
198	25	06		03	42	20	22.2	103.4	2	3.3
199	25	06		03	51	59	21.3	103.4	5	4.6
200	25	06		05	02	44	21.6	103.4	5	4.1
201	25	06		05	18	45	21.4	103.4	2	3.5
202	25	06		08	07	53	21.5	103.5	1	3.7
203	25	06		08	18	24.3	21.8	103.4	5	4.1
204	25	06		08	31	12.2	21.3	103.5	5	4.5
205	25	06		09	23	00	21.6	103.4	5	3.6
206	25	06		09	47	09	21.8	103.5	7	3.6
207	25	06		10	04	17	21.6	103.4	5	3.1
208	25	06		10	53	08	22.2	103.5	7	3.4

Table 2 (continued)

N°	Date			Origin time (G M T)			Epicentre		H	M
	D	M	Y	h	m	s	N	E	(km)	
209	25	06	1983	12	55	24	21.7	103.4	6	4.2
210	25	06		13	16	21	21.8	103.4	5	4.2
211	25	06		14	48	21	21.6	103.4	10	3.9
212	25	06		16	09	40	21.5	103.4	15	3.5
213	25	06		16	13	04	21.6	103.4	15	3.4
214	25	06		16	52	02	21.6	103.5	20	3.5
215	25	06		18	39	00	21.8	103.5	20	3.2
216	25	06		19	20	22	22.0	103.5	20	3.3
217	25	06		20	27	33	21.7	103.4	15	3.7
218	25	06		20	28	54	21.8	103.4	15	4.2
219	25	06		22	34	59	21.6	103.4	5	3.5
220	26	06		00	21	44	21.6	103.4	10	4.2
221	26	06		02	05	04	21.7	103.3	5	3.3
222	26	06		03	36	14	21.8	103.4	7	3.8
223	26	06		04	40	15	21.8	103.4	8	3.2
224	26	06		04	47	57	21.5	103.8	5	3.3
225	26	06		05	30	00	21.7	103.4	4	3.8
226	26	06		16	12	04	22.0	103.5	5	3.2
227	26	06		17	36	50	21.9	103.5	15	3.6
228	26	06		17	55	46	21.8	103.5	15	4.1
229	26	06		19	37	46	21.6	103.4	15	3.4
230	26	06		19	40	38	21.2	103.4	15	3.3
231	26	06		20	03	16	21.9	103.4	15	3 3
232	26	06		20	15	24	21.6	103.4	10	3·2
233	27	06		01	51	42	22.0	103.5	15	3·3
234	27	06		02	15	12	21.8	103.4	15	3·9
235	27	06		02	43	31	21.9	103.6	15	3·6
236	27	06		11	18	16	21.9	103.8	10	4·1
237	27	06		13	38	27	21.6	103.4	5	4·2
238	27	06		14	54	32	21.3	103.5	5	3·3
239	27	06		15	44	25	21.4	103.4	5	4.7
240	27	06		20	11	07	21.8	103.5	2	3.4
241	27	06		20	54	36	21.7	103.4	1	3.7
242	28	06		02	38	32	21.7	103.5	2	4.0
243	28	06		07	12	19.3	21.4	103.4	2	3.2
244	28	06		11	19	09	28.4	103.5	10	3.3
245	28	06		20	35	04	21.6	103.4	15	3.7
246	28	06		22	23	07	21.5	103.5	10	3.4
247	29	06		13	13	21	21.2	103.3	5	3.6
248	30	06		01	31	01	21.5	103.5	2	3.0
249	30	06		16	44	06	21.2	103.5	5	3.9

Table 2 (continued)

N°	Date			Origin time (GMT)			Epicentre		H	M
	D	M	Y	h	m	s	N	E	(km)	
250	02	07	1983	03	58	03	21.2	103.4	5	3.9
251	02	07		15	30	55	20.9	103.6	2	3.7
252	03	07		05	17	19	21.6	103.5	5	3.6
253	03	07		09	26	22	21.0	103.5	3	4.5
254	03	07		09	33	54	21.5	103.5	7	3.5
255	03	07		12	26	04	21.7	103.5	5	3.5
256	03	07		15	14	50	21.5	103.5	7	4.3
257	05	07		00	52	34	22.1	103.4	5	3.7
258	05	07		05	09	12	21.8	103.5	5	3.2
259	05	07		15	26	53	21.4	103.5	7	3.5
260	05	07		17	58	49	22.2	103.5	5	3.0
261	06	07		21	52	13	21.7	103.4	5	3.3
262	07	07		09	31	12	21.3	103.4	2	3.6
263	07	07		11	16	37	22.2	103.5	5	4.3
264	07	07		14	04	24	21.7	103.5	5	3.3
265	08	07		12	15	00	21.2	103.5	7	3.6
266	08	07		15	21	51	21.6	103.5	5	3.1
267	08	07		21	29	20	21.5	103.5	5	3.5
268	09	07		14	09	52	21.8	103.4	10	3.1
269	11	07		10	32	02	22.2	103.5	5	4.3
270	12	07		02	10	49	21.6	103.4	5	3.9
271	15	07		02	02	23	21.2	103.4	7	4.1
272	15	07		04	48	53	21.2	103.4	7	5.4
273	15	07		05	44	20	21.2	103.5	10	3.4
274	24	07		05	49	26	21.9	103.6	5	3.2
275	01	09		09	50	38	23.4	103.4	5	4.9
276	01	09		15	37	49	21.4	103.4	2	3.4
277	04	09		16	39	47	21.7	103.6	5	4.4
278	05	09		20	48	40	21.7	103.4	5	3.2
279	09	09		18	17	02	21.9	103.4	7	3.5
280	13	09		00	39	45	21.8	103.4	7	3.2
281	16	09		09	54	55	21.8	103.4	5	3.5
282	16	09		22	58	12	21.9	103.5	5	3.6
283	26	09		04	28	59	21.8	103.5	5	3.8
284	26	09		22	11	29	21.9	103.5	10	3.4
285	29	10		13	29	49	23.2	103.5	5	3.5
286	19	12		00	30	20	22.0	103.4	10	3.5
287	24	12		19	45	45	21.2	103.5	5	3.2
288	03	01	1984	13	17	05	21.3	103.4	7	3.4
289	04	01		22	00	34	22.9	103.4	7	3.3
290	10	01		16	57	57	18.4	103.9	7	3.5
291	14	01		09	39	43	19.6	104.3	5	3.5

Maximum expected earthquake

Knowledge of the maximum expected energy is of importance for the seismic zoning of the territory of Vietnam. To determine the maximum expected energy of earthquakes, the correlation between the possible earthquake with maximum energy class K_{max} and average seismic activity $\bar{A}$ was also used (Riznichenko 1964):

$$\log \bar{A} = \bar{2}.84 + 0.21(K_{max} - 15). \tag{9}$$

The map of expected origin zones was covered by a mesh $0.2° \times 0.2°$, and values of K_{max} were determined from each knot. A map K_{max} was computed using the programme by Zacharova (1972), Nuoi and Lap (1985). The maximum value of K_{max} is found in the northwest of Vietnam. The largest expected earthquake with $K_{max} = 17$ will take place only at the contact between the Dienbien-Laichau fault and the fault system of Sonla, River Da and of the River Ma. At the northeast of the Hanoi depression, earthquakes with $K_{max} = 16$ are considered as the possible maximum earthquakes. A zone of the River Ca has $K_{max} = 15$. The map of maximum expected earthquake in the north part of Vietnam is shown in fig. 6.

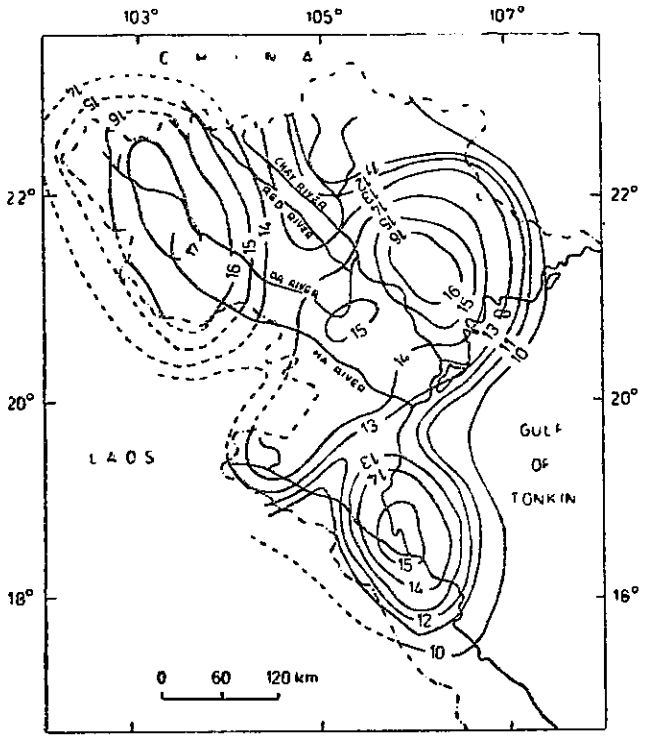

6. Map of maximum expected earthquake K_{max} in North Vietnam during the period from 1976 to 1984

The main characteristics of the Tuangiao earthquake

On June 24, 1983 at 07h 18m 22.3s an earthquake of magnitude M = 6.7 occurred near Tuangiao town in the mountainous Laichau province in northwest Vietnam. Its epicentre located by Vietnamese determination is $\varphi = 21.71$ °N, $\lambda = 103.43$ °E, H = 23 km (Xuyen–Lap 1985). It is the largest known earthquake that has taken place in the area. The Tuangiao earthquake caused considerable damage.

Aftershocks

. The main earthquake was followed by a number of aftershocks and field micro-earthquake survey conducted in May 1984 revealed quite a high level of micro-aftershock activity still in progress, eleven months after the occurrence of the Tuangiao earthquake. During the first 12 months after occurrence of earthquake in Tuangiao, 350 aftershocks of magnitude $M = 3 \div 5.4$ were recorded by Vietnamese stations: Tuyenquang, Bacgiang and Hoabinh. The largest aftershock with M = 5.4 occurred later in sequence, on July 15, 1983 at 04h 48m 52.6s, three weeks after the main shock. The length of aftershock zone is 100 km, and the width is 20 km. The hypocenters were located at a depth of 3 to 20 km. A preliminary investigation indicated that the earlier aftershocks were attached to the north-western end of the surface rupture, and later they moved to the central and south-eastern part of the fault. The aftershocks might be subdivided into two groups. The first group was located near the main shock hypocenter, in the central part of the fault zone. The second group was located near the margin of the fault zone with depth $H = 3 \div 10$ km (Lap 1985; Xuyen–Lap 1985).

The magnitude-frequency relation of aftershocks of the Tuangiao earthquake is given by the expression:

$$\log N_\Sigma = 4.1 - 0.71\, M. \tag{10}$$

The value of the coefficient b = 0.71 ($\gamma = 0.39$) shows that the aftershocks occurred in a relatively homogeneous and tectonically symmetric medium (Gibowicz 1985). The maximum expected magnitude $M_{max,a}$ of aftershocks sequence, expressed by the relation:

$$M_{max,a} = \frac{a}{b} = 5.7 \tag{11}$$

is close to the maximum observed magnitude $M_{max,a} = 5.4$.

The aftershocks activity is indicated by the ratio of energies released by aftershocks (E_a) and the main shock (E_0) (Bracinac 1976). The total energy of the aftershocks is $E_a = 2.854 \cdot 10^{14}$ Joules and the energy of the main shock is $E_0 = 1 \cdot 10^{16}$ Joules. So, the total energy of aftershocks represents 3 % of the energy of the main shock.

Microaftershocks

In May 1984 a Joint Polish-Vietnamese field expedition was organized to the mountainous epicentral area to study the microaftershocks of the Tuangiao earthquake (Gibowicz 1985). Three portable seismic stations were operated at Bancang, Tuangiao and Phadin. The stations were equipped with Portacorder RV-320 ink-recording systems manufactured by Teledyne Geotech, and with Soviet SM-3 seismometers. Altogether over 250 small aftershocks were recorded, but only 22 events were located. They occurred either at the southeast end of the surface rupture or further away in the southeast direction. Their depth could roughly be estimated as very shallow, between 1 and 7 km. The largest magnitude of microaftershock is 2.9. The frequency-magnitude relation was calculated by the maximum likelihood method and is given by the expression (Gibowicz 1985):

$$\log N = 2.42 - 0.83\,M. \tag{12}$$

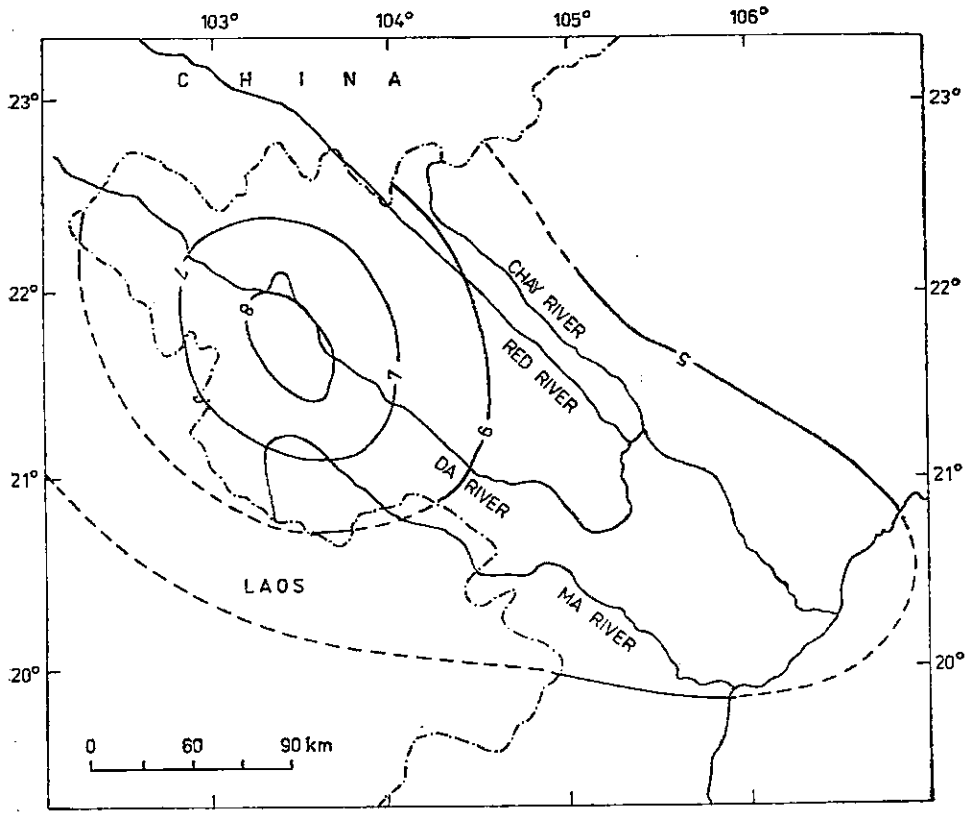

7. Isoseismal map – MSK scale (1964 – version) of the Tuangiao earthquake

Effects of the Tuangiao earthquake

Using the MSK-64 scale, effects of the Tuangiao earthquake on the considered region were drawn in the form of isoseismal contour lines around their epicentre (fig. 7). A map of isoseismals of an intensity from V to VIII on the MSK-64 macroseismic scale was elaborated (Xuyen and Lap 1985). The maximum intensity VIII was felt up to a distance of 25 km from the centre of the elongated isoseismal and intensity was felt up to a distance of 350 km. The earthquake was associated with a surface rupture, a fresh surface rupture was found and mapped along the 23 km long segment of the Sonla fault, striking N 130 °E, with a horizontal displacement of about 16 cm, corresponding to right-lateral motion (fig. 8).

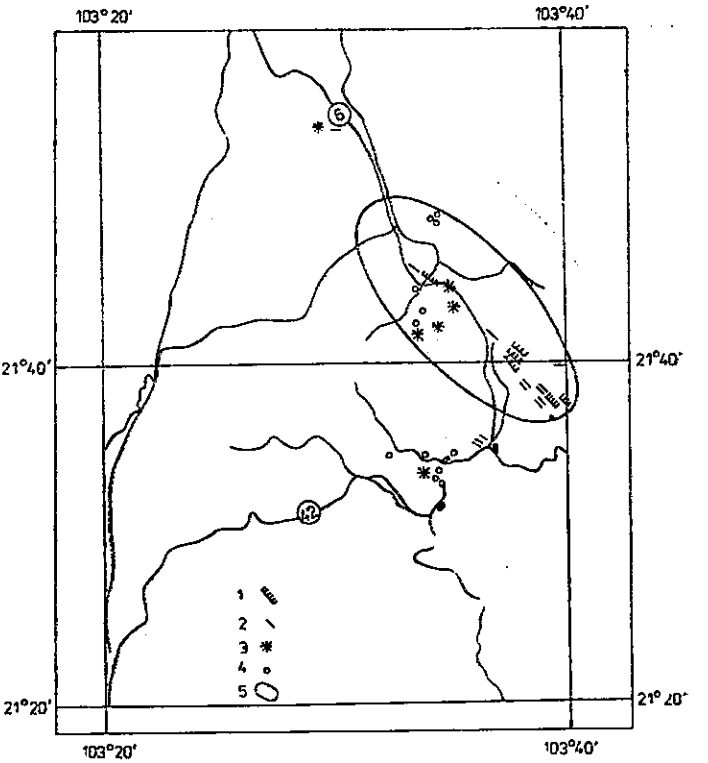

8. Scheme of surface deformations in Tuangiao
1 — Observed fault traces of Tuangiao earthquake with length larger than 100 m, *2* — Observed fault traces of Tuangiao earthquake with length over 10 m, *3* — Thunder — like booming noises, *4* — The wells observed immediately after the Tuangiao earthquake, *5* — Boundary of the area of the surface deformation; 6 and 42 are the road numbers

The variations in groundwater level for wells located in the Laichau district were observed, well-water level had a tendency to lower to 0.5 m until the occurrence of the Tuangiao earthquake, after which it recovered. The unusual behaviour of fish, dogs, rats, snakes, cats, boa reached its climax in the two days immediately before the Tuangiao earthquake. This is very interesting and may be of use in forecasting the time of earthquakes.

Source parameters

In order to determine the focal mechanism, we used the method of A. V. Vvedenskaia (1969). The first motion data were obtained from the seismograph station network of the USSR, Vietnam and contributing stations of neighbouring countries. The focal mechanisms of the Tuangiao earthquakes are shown in fig. 9. The distribution of compression and dilatation of the main shock and aftershock shows focal mechanism:

Focal mechanism of the main shock (fig. 9a): A strike-slip mechanism with a NE–SW striking nodal plane (1) dipping 60° towards NNW (azimuth 313°) with oblique sinistral lateral slip (slip vector az/dip: 224°/18°) and NW–SE striking plane (2) dipping 72° towards NE (az: 54°) with oblique dextral lateral slip (slip vector: 133°/30°). The compression axis (i) dips 35° towards S (az: 187°). The dilatation axis (K) dips 16° towards E (az: 93°) (Lap 1985).

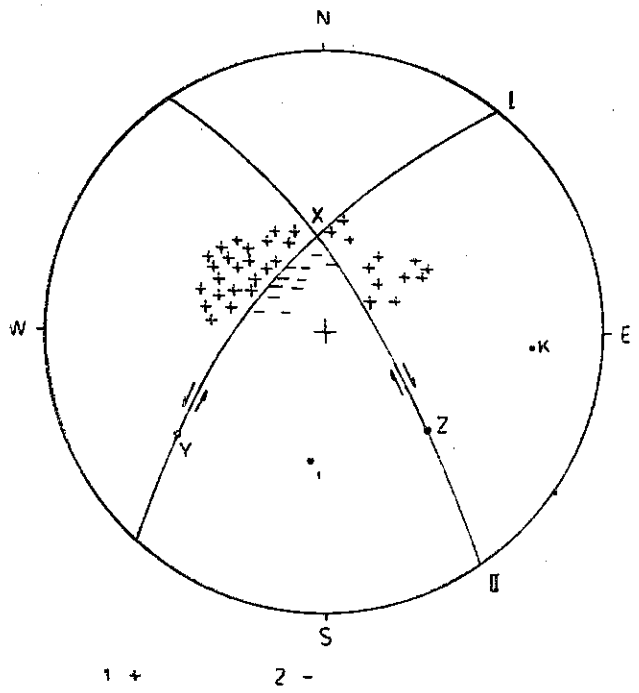

9a. Focal mechanism from P-wave first motion data shown on an equal-area lower hemisphere projection of the Tuangiao earthquake (June 24, 1983)
1 – compression,
2 – dilatation

Focal mechanism of aftershock (July 15, 1983) (fig. 9b): One of the planes (1) dips to the E (az/dip: 82°/72°), the other (2) to the NW (342°/64°). i – axis (i): 213°/21°, K – axis (K): 123°/6° (Lap 1985).

Focal mechanism of microaftershocks: A tentative composite fault – plane solution from the first-motion data of 21 microaftershocks was determined. It

indicates right – lateral strike – slip motion with a distinct normal faulting component on a fault dipping at 50° and striking at 314°, with the pressure axis plunging at about 40°. Such a mechanism could be explained by the locking of the northwestern end of the fault, where no microaftershocks were located (Gibowicz 1985).

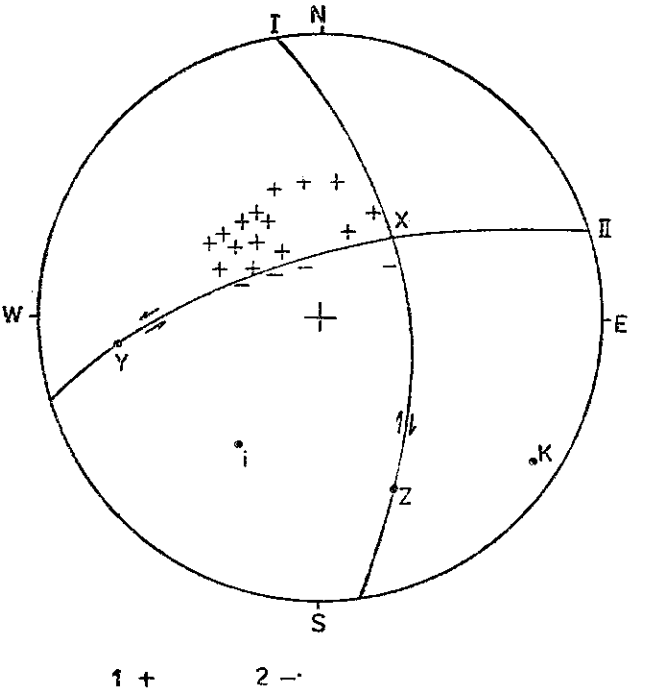

9b. Focal mechanism from P-wave first motion data shown on equal-area lower hemisphere projection of the aftershocks of Tuangiao earthquake (July 15, 1983)
1 – compression,
2 – dilatation

The Tuangiao earthquake source is characterized by the following overall parameters: the static seismic moment $M_0 = 3.5 \cdot 10^{25}$ dyne . cm, fault length $L = 23$ km, fault width $W = 25$ km, process time $\tau_0 = 12$ s, rupture velocity $V_r = 2$ km/s; average displacement $D_0 = 28$ cm, stress drop $\Delta\sigma = 11$ bars, dynamic stress drop $\Delta\sigma_d = 7$ bars and apparent stress $\sigma_{ap} = 2$ bars. A multiple unilateral rupture, composed of two subevents, moving horizontally in the southeast direction from the epicenter along a vertical square section of the right – lateral Sonla fault seems to be a reasonable model of the source processes, deduced from the available field and seismological evidence (Gibowicz 1985).

Conclusions

From the investigation of earthquake activity in the north part of Vietnam, the following conclusions can be derived:

– The territory of the north part of Vietnam is seismically active. During the last

9 years, about 1 000 earthquakes have occurred in this region, including the large Tuangiao earthquake.

- The earthquake density is higher in northwestern Vietnam, almost all hypocenters in this region were in the Earth's crust.
- The earthquakes in the north part of Vietnam are related to the tectonic faults and geological structures in the northwest–southeast directions.
- The maximum expected values of $A_{10} = 0.2 \div 0.5$ and $K_{max} = 17$ are found in the northwest Vietnam.
- The Tuangiao earthquake of magnitude $M = 6.7$ occurred along the Sonla fault and caused considerable damage. The shock was associated with a surface rupture and aftershocks.

Acknowledgements

The author wishes to thank Dr. K. Cidlinsky for reading the manuscript critically and for providing useful suggestions.

K tisku doporučil V. Schenk

Přeložila D. Maliková

References

Bracinac, Z. et al. (1976): Seismological characteristics of the Rudnik area according to the analysis of aftershocks of the earthquake of 15 May 1927. – Proceedings of the seminar on seismic zoning maps, 27 October–4 November 1975. Skopje.

Gorbunova, I. V. (1964): Mapping of seismic activity with a constant accuracy. (In Russian.) – Trudy Inst. Fiziki Zemli, Akad. Nauk USSR, 32, *40–47*. Moscow.

Gibowicz, S. J.–Thuc, P. V. (1985): Source study of the Tuangiao Vietnam earthquake of June 24, 1983. – Acta geophys. pol. 33, *85–100*. Warszawa.

Lap N. K. (1983): Seismic regime and strain field in South-East of Asia. (In Vietnamese.) – Contu. Centre Geophys. Res. Vietnam, *60–75*. Hanoi.

– (1985): Seismicity of the territory of Vietnam and the neighbourhood (1981–1984). (In Vietnamese.) – Contr. Centre Geophys. Res. Vietnam, 4, *15–25*. Hanoi.

– (1985): Focal mechanism of Tuangiao earthquake. (In Vietnamese.) – Scientific report of NCSR of SRV, 1. *15–22*. Hanoi.

– (1985): Aftershocks of Tuangiao earthquake. (In Vietnamese.) – Scientific report of NCSR of SRV, 2. *90–97*. Hanoi.

– (1986): Seismicity of the territory of Laos. (In Vietnamese.) – Contr. Centre Geophys. Res. Vietnam, 5, (1985–1986), 80–97. Hanoi.

Nuoi, N. D.–Lap, N. K. (1985): Computation of parameters A_{10} and K_{max}. (In Vietnamese.) – Seminar on Geophysics. 20–21 December 1985. *15–22*. Hanoi.

Riznichenko, Yu. V. (1960): Methods of detailed study of seismicity. (In Russian.) Moscow.

– (1964): On relation between the energy of maximum earthquakes and seismic activity. (In Russian.) – Izv. Akad. Nauk USSR, Fiz. Zemli, 7, *869–877*. Moscow.

– (1974): Crustal seismic activity and maximum expected earthquakes in the Carpathian – Balkan region. (In Russian.) Regionalnye issledovanie seismicheskogo rezhima. Stinta, Kishinev.

Thuc, P. V.–Lap, N. K. (1979): Some properties of the seismicity in the North part of Vietnam from instrumental data. (In Vietnamese.) – Contr. Inst. Earth Sci., Geophysics, *32–45*. Hanoi.

– (1981): Seismicity of South-East Asia. – Acta geophys. pol., XIX, *63–73*. Warszawa.

Thuc, P. V.–Luong, N. V.–Yem, N. L. (1979): Seismological magnitude scale in Vietnam. (In Vietnamese.) – Contr. Centre Geophys. Res. Vietnam. *64–78*. Hanoi.

Xuyen, N. D. (1972): Seismological magnitude scale for local earthquakes in Vietnam. (In Vietnamese.) – Biology and Earth Sci., X. *10–16*. Hanoi.

Xuyen, N. D.–Lap, N. K. (1985): The Tuangiao earthquake, June 24, 1983. (In Vietnamese.) – Contr. Centre Geophys. Res., IV, *61–72*. Hanoi.

Zacharova, A. J. (1974): Computation of parameters of seismic regime. (In Russian.) – FAN. Tashkent.

Activité des tremblements de terre dans le Nord du Viêt-Nam pendant la période de 1976—1984

(*Résumé du texte anglais*)

Nguyen Kim Lap

Présenté le 4 mai 1987

Le territoire de la partie Nord du Viêt-Nam est situé à la proximité des deux zones de tremblements de terre les plus fortes du monde: celle de la Méditerranée et celle de l'Océan pacifique occidental. Les dates séismiques montrent de lourdes pertes en vies humaines et en biens causées par de grands tremblements de terre dans la partie Nord du Viêt-Nam. Pendant la période 1976—1984 on a observé dans cette région 800 tremblements de terre à peu près, y compris un immense tremblement de terre à Tuangiao ($M = 6,7$ et $I_0 = 8 \div 9$). Les tremblements de terre sont situés le long de grandes failles comme suit: rivière Rouge, rivière Chay, Dien Bien-Lai Chau, Son La, rivière Ma, rivière Da, rivière Ca et le Nord-Est de la plaine de Hanoi. La densité des tremblements de terre est la plus importante au Nord-Ouest du Viêt-Nam, leur fréquence est relativement basse dans la partie du Sud de la région récherchée. On considère que tous les focus du tremblement de terre se trouvent dans la croûte terrestre à une profondeur de moins de 40 km. La loi de la fréquence de tremblements de terre est exprimée par la rélation: $\log N = 2,27 - 0,38\,K$. L'activité séismique A_{10} (le nombre moyen de tremblements de terre de l'échelle d'énergie $K = 10$ se déroulant dans l'unité spatiale de temps) dans la partie Nord du Viêt-Nam était de 0,01 à 0,5. Les valeurs maximales A_{10} étant égales à $0.1 \div 0,5$ furent observées au Nord-Ouest du Viêt-Nam où se croisent de différentes failles de profondeur, telles que Dien Bien-Lai Chau, Son La, rivières Da et Ma. Dans cette zone mentionnée s'est produit le plus grand tremblement de terre avec $I_0 = 8 \div 9$ (MSK-64). Dans le delta de la rivière Rouge on a déterminé la zone de l'activité séismique de $A_{10} = 0,02 \div 0,2$. Les zones plus basses $A_{10} = 0,05$ sont observées dans la faille de la rivière Ca. Le plus grand tremblement de terre attendu ($K_{max} = 17$) se déroulera justement au contact entre la faille de Dien Bien-Lai Chau et le système de la faille de Son La, des rivières Da et Ma. Comme les tremblements de terre maximaux sont prévus ceux au Nord-Est de la plaine de Hanoi ($K_{max} = 16$). Dans la zone de rivière Ca on attend un tremblement de terre maximal avec $K_{max} = 15$. Le 24 juin 1983 s'est produit le plus grand tremblement de terre à la proximité de la région Tuangiao

($\varphi = 21{,}71°$ N, $\lambda = 103{,}43°$ E, H = 23 km). Le tremblement de terre à Tuangiao est arrivé le long de faille de Son La. La solution de la faille plane montre un mouvement du côté droit sur la faille presque verticale passant sous l'angle de 140° ± 10°. L'intensité maximale (8 ÷ 9) s'est abaissée à la distance de 25 km du centre de l'isoséisme prolongé et l'intensité s'est abaissée à la distance de 350 km. Le tremblement de terre à Tuangiao a eu lieu près de la surface, on a constaté et dressé la carte de certaines ruptures fraîches le long du segment de faille Son La à la longueur de 23 km passant sous l'angle de 130°, au déplacement horizontal de 16 cm à peu près. On a observé la variation du niveau de la nappe aquifère dans un puits de la région de Lai Chau; le niveau d'eau dans le puits avait la tendance d'être plus bas avant le tremblement de terre à Tuangiao, après lequel il est remonté. On constate de même certains symptômes caractéristiques en ce qui concerne le comportement des animaux avant le tremblement de terre. La plupart des animaux se trouvant dans la zone séismique deviennent très inquiets, plusieurs d'entre eux sentant une grande angoisse. L'endommagement total causé par le tremblement de terre à Tuangiao présente 30 millions de dongs viêtnamiens. La détérioration de si grande importance avait des influences néfastes sur l'économie dans plusieurs régions de la partie Nord du Viêt-Nam.

Přeložila P. Kellnerová

Légendes des tableaux

Tableau 1. Liste des stations séismiques dans la partie de Nord du Viêt-Nam.
Tableau 2. Liste des tremblements de terre avec M ≥ 3.0 qui se sont produits dans la partie du Nord du Viêt-Nam pendant la période des années 1976–1984.

Légendes des figures

1. Stations séismographiques au Viêt-Nam; les points plains représentent les stations séismiques permanentes. Le triangle ouvert montre les stations proposées pour l'avenir.
2. Distribution des épicentres des tremblements de terre au Viêt-Nam du Nord pendant le période des années 1976–1984.
   Magnitude: 1. M < 3; 2. M = 3÷4; 3. M = 4,1÷5,0; 4. M ≥ 5,1.
3. Relaxation cumulative de la tension pour les tremblements de terre du Viêt-Nam du Nord pendant la période des années 1976–1984.
4. Graphe des tremblements de terre répétés au Viêt-Nam du Nord au cours de la période 1976–1984.
5. Carte de l'activité séismique A_{10} au Viêt-Nam du Nord dans les années 1976–1984.
6. Carte du tremblement de terre maximal K_{max} attendu au Viêt-Nam du Nord pour les années 1976–1984.
7. Carte isoséismique – l'échelle MSK (1964 – version) du tremblement de terre à Tuangiao.
8. Schème des déformations de surface à Tuangiao.
   1-les traces observées des failles du tremblement de terre de Tuangiao étant plus longues que 100 m, *2* – les traces observées des failles du tremblement de terre de Tuangiao étant

plus longues que 10 m, *3* – l'orage – comme le bruit croissant, *4* – les trous observées immédiatement après le tremblement de terre à Tuangiao, *5* – les bornes de surface des déformations superficielles; *6* et 42 – le numéro de la route.

9a. Mécanisme de focus des données du premier mouvement de la vague P montré sur la projection de l'hémisphère inférieure à la conservation de surface du tremblement de terre à Tuangiao (le 24 juin 1983).
1 – compression, *2* – dilatation.

9b. Mécanisme de focus des données du premier mouvement de la vague P montré sur la projection de l'hémisphère inférieure à la conservation de surface au cours des chocs suivants aprés le tremblement de terre à Tuangiao (le 15 juillet 1983).
1 – compression, *2* – dilatation.

Активность землетрясений в северной части Социалистической Республики Вьетнам за 1976—1984 гг.

В представленной работе составлен каталог землетрясений в северном Вьетнаме за 1976 до 1984 гг., магнитуда которых превышала $M \geq 3{,}0$. Для северо-западной части страны характерно землетрясение Туанзао ($M = 6{,}7$), происшедшее на глубине 30 км в глубинном разломе Шонла, простирающемся в с.-з. направлении. Качественное изучение активности землетрясений занималось пространственным распределением землетрясений, сейсмической активностью A_{10}, максимумом возможных землетрясений K_{max} и основными характеристиками землетрясения Туанзао.

Přeložil A. Kříž

Sbor. geol. věd	Užitá geofyz., 24	Pages 133–157	8 figs.	4 tab.	– pl.	Praha 1990 ISSN 0036-5319

Paleomagnetism of selected Quaternary, Cainozoic, Jurassic, and Proterozoic to Lower Paleozoic volcanic rocks from Nigeria

Paleomagnetizmus vybraných kvartérnych, kenozoických, jurských a proterozoických až spodnopaleozoických vulkanických hornín z Nigérie

Oto Orlický[1]

Received August 25, 1987

Magnetic minerals
Oxidized titanomagnetites
A. C. demagnetization tests
Computed pole positions

Orlický, O. (1990): Paleomagnetism of selected Quaternary, Cainozoic, Jurassic, and Proterozoic to Lower Paleozoic volcanic rocks from Nigeria. – Sbor. geol. Věd, užitá Geofyz., 24, *133–157*. Praha.

Abstract: Paleomagnetic results have been obtained from seventeen localities (30 sites) in volcanic (mostly basaltic) rocks of Quaternary, Younger Cainozoic, Jurassic, and Proterozoic to Lower Paleozoic age from the Jos plateau, Biu plateau, Samunaki locality, and Runka locality, northern and north-eastern Nigeria. A complex of physico-analytical methods and laboratory procedures was used to obtain information on the carriers of the magnetism, paleomagnetic stability, and the distribution of the direction of the RMP in the mentioned geological complexes.

Oxidized (cation-deficient) titanomagnetites are the most frequent magnetic minerals in the studied rocks, but ilmeno-hematite solid solutions, ferroilmenite, and magnetite-hematite solid solutions also were revealed in some petrographical types of rocks. The *RMP* of studied rocks is a secondary one, probably of chemical (C.R.M.) origin. Most of the diabases, olivine basalts, and nepheline basanites under study (samples of rocks from 19 sites) are unstable with respect to the A.C. demagnetization tests. Quaternary (or Younger Cainozoic) olivine basanites from the Jos plateau (JP-2) give a stable direction of *RMP*. The paleomagnetic data are as follows: $I = 21.4°$, $D = 17.3°$; $\varphi_p = 72.9$ °N; $\lambda_p = 92.2$ °E. Three acceptable sites from the Biu plateau represented by a Quaternary (or Younger Cainozoic) olivine basalts (BP-2, BP-3), and albitized olivine basalts (BP-4) give a mean direction of the *RMP*, $I = -3.9°$; $D = 186.5°$, and virtual poles $\varphi_p = 79.2$ °N; $l_p = 154.9$ °E. Computed pole positions of the Jurassic alkali granite porphyry from the Jos plateau (JP-9), ($\varphi_p = 70.7$ °N; $\lambda_p = 259.0$ °E) are very close to those published by McElhiny et al. (1968 *in* Piper–Richardson 1972) for Mesozoic rocks from Africa.

No detectable movement of the African plate was revealed by the results of Quaternary or Younger Cainozoic age. But the shift of the African plate has been detected on the base of the direction of the *RMP* and computed pole positions of Jurassic alkali granite porphyry from the Jos plateau.

[1] *Geofyzika, s. p., Brno, závod Bratislava, Geologická 18, 825 52 Bratislava*

Introduction

Piper and Richardson (1972) realized the paleomagnetic investigations of the Gulf of Guinea volcanic provinces (West Africa, fig. 1). They employed the computed pole positions of individual volcanic structures (age: 18.4 to 0.5 m.y.) of the Gulf of Guinea and from the western part along the volcanic line in Cameroun for the detection of the movement of the African plate. The above-mentioned authors presented in their work also poles computed for the Upper Tertiary and younger lavas of the East African Rift (Piper–Richardson 1972). The authors have demonstrated no detectable movement of the African plate relative to the geographic pole for about 25 m.y., according to the analysis of the Upper Tertiary paleomagnetic results.

This paper presents the results of paleomagnetic study of volcanic rocks from the following areas of northern and north-eastern Nigeria (fig. 1): basaltic rocks from the Jos plateau, Biu plateau (Quaternary and Cainozoic age), Runka locality (mid-Jurassic age), Samunaki locality (unknown age), alkali granite porphyry from Jos locality (JP-9, Jurassic age) and migmatized amphibolite from Runka locality (RK-Gr, Proterozoic to Lower Paleozoic age). The presented results are not the consequence of a systematic investigation, but they only point out partial problems concerning the convenience of the volcanic rocks under study for paleomagnetic investigations and for the detection of the movement of the volcanic complexes.

Geological outline

The Jos plateau is a restricted volcanic sequence paralleled by a similar larger volcanic area in Cameroun. The Jos plateau and the Cameroun highlands are part of a complex crustal dome, transected by the Benue trough and Cameroun rift, the whole constituting the Gulf of Guinea magmatic province (Le Bas 1971 *in* Kogbe 1976). The Biu basalt plateau lies on the axis of NE–SW direction which connects the volcanoes Annobon, Sao Tomé, Principe Fernando Poo in the Gulf of Guinea and Mt. Cameroun which were investigated by Piper and Richardson (1972) (fig. 1).

The Jos plateau is one of the Neogene uplifts tangential to the Chad basin believed to result from local partial melting of the asthenosphere. Its axis is marked

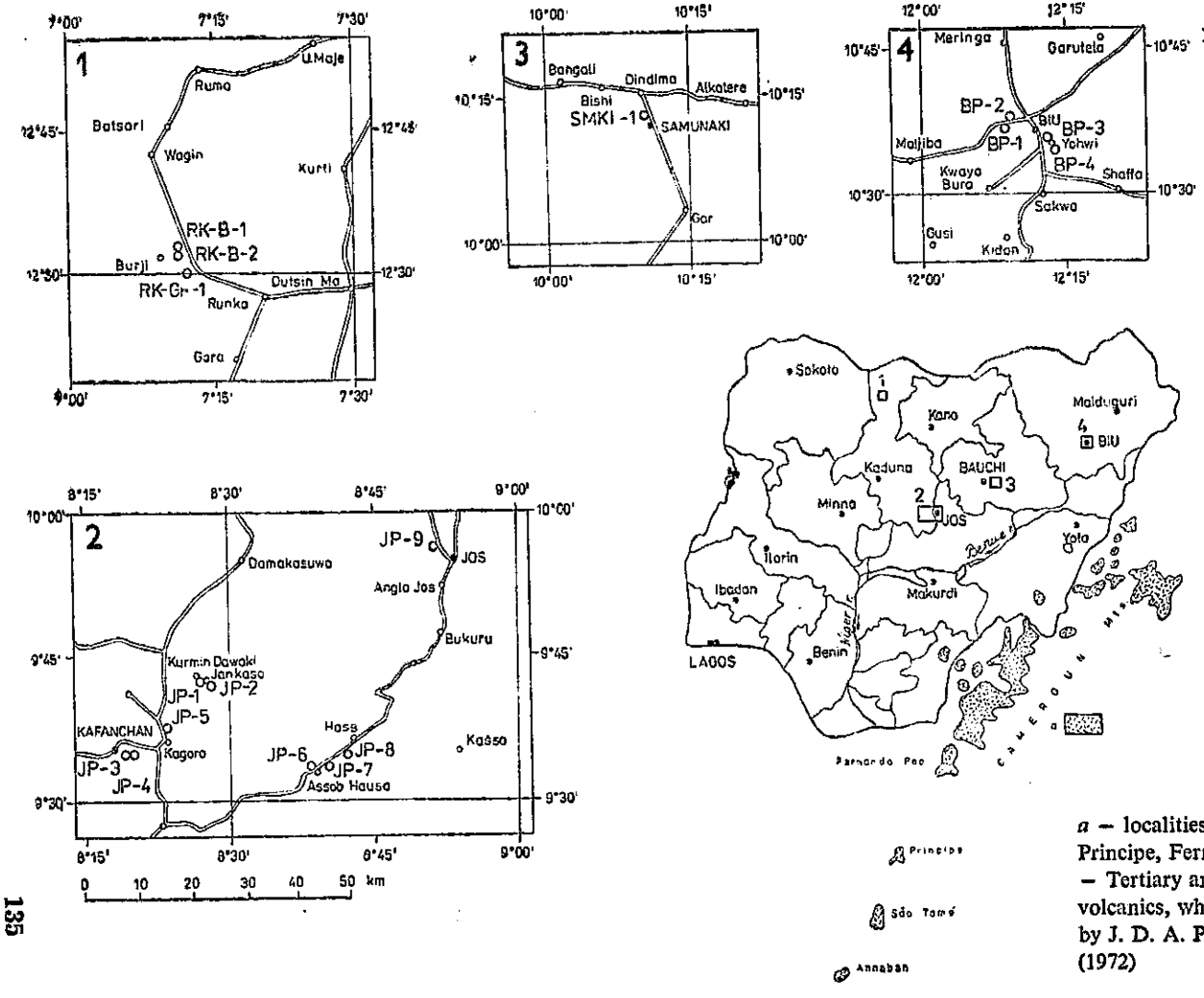

1. Schematic map of Nigeria, including selected areas 1, 2, 3, 4 — sampling localities *1* — Runka: outcrops RK-B-1 and RK-B-2 — mid-Jurassic nepheline basanites; RK-Gr-1 — Proterozoic to Lower Paleozoic migmatized amphibolite; *2* — Jos plateau: JP-1—JP-8 — Cainozoic basaltic rocks, JP-9 — Jurassic alkali granite porphyry; *3* — Samunaki locality (olivine basalts); *4* — Biu basalt plateau: BP-1—BP-4 — Cainozoic olivine basalts; *a* — localities: Annobon, São Tomé, Principe, Fernando Poo, Cameroun — Tertiary and recent volcanics, which were investigated by J. D. A. Piper and A. Richardson (1972)

the influence on the magnetic needle of the compass by an anomalous local magnetic field was detected. (It was influenced by a very intensive *NRMP* of basaltic rocks – see tables 1 and 2. Jos plateau 5 places, Biu plateau 1 place, Samunaki locality 1 place, Runka southern facies 5 places).

All rock samples were shaped by a diamond saw to the cube of 20 mm edge.

Remanent magnetic polarization (*RMP*) of the rocks was measured with the spinner magnetometer JR-4, and with the astatic magnetometer LAM-24. All samples were subjected to progressive demagnetization in alternating fields up to 48 or 64 kA . m^{-1} in steps 2, 4 and 8 kA . m^{-1}. The external magnetic field was compensated by the Helmholtz coils and controlled by a flux-gate magnetometer or by a ROCOMA system.

Magnetic susceptibility ($\varkappa$) measurements were performed using A. C. KLY-2 bridge. This instrument was employed also for the measurements of the change

Table 2

Magnetic characteristics of rock samples

Number of outcrop (region)	Number of samples	$\varkappa \times 10^6$ (SI)	*NRMP* (nT)	*Q*
Jos plateau				
JP-1	5	10 028	74 292	148.2
JP-2	21	25 113	5 740	4.6
JP-3	3	12 294	15 610	25.4
JP-4	6	17 948	80 702	89.9
JP-5/2	2	16 319	20 983	25.7
JP-5/1a, 3a, 4, 4a, 6b	19	22 486	126 908	112.9
JP-6-3/1	2	14 457	30 962	42.8
JP-6-4	8	92 902	4 721	1.02
JP-6-6	4	12 744	1 215	1.91
JP-7	4	11 544	110 703	191.8
JP-8	5	9 455	131 783	278.8
JP-9	14	1 769	64.5	0.73
SMKI-1	3	18 496	182 188	197.0
SMKI-2	4	21 000	2 042	1.9
Biu plateau				
BP-1	2	20 957	166 873	159.3
BP-2	17	28 355	4 390	3.1
BP-3	19	26 317	4 369	3.3
BP-4	6	21 756	7 627	13.0

For explanation see table 1

of the $\varkappa$ of powdered rocks during their Curie temperature (T_C) measurements. The complete apparatus for the T_C measurements consists of a special device (nonmagnetic furnace and cooling system) of our own construction. This device serves for the gradual heating of the powdered sample. The nonmagnetic furnace is gradually supplied by automatically controlled electrical power. Continual and regular increasing of the temperature within the furnace was 10 °C . min^{-1}.

Using several methods, petrographic description of rocks, identification of main chemical components, and determination of the magnetic minerals as the carriers of *RMP* of rocks were carried out. Petrographic analyses and ore microscopy were performed in the laboratories of the Dionýz Štúr Geological Survey, Bratislava. X-ray spectroscopy by Philips PW 1420 X-ray spectrometer and PW 1150 diffractometer were executed mostly in the laboratories of the Geological Institute of the Slovak Academy of Science in Bratislava. Mössbauer spectroscopy was performed in the laboratory of the Department of Nuclear Physics and Technology of the Slovak Technical University in Bratislava (Lipka et al. 1983, 1988). The additional electron microprobe analyses were performed by means of the JEOL electron microscope with the EDAX system in the laboratory of the Dionýz Štúr Geological Survey, Bratislava. Several samples of magnetic fraction of basaltic rocks were investigated by X-ray and Mössbauer spectroscopy, also in the Laboratory of Applied Physics II, Technical University, Lyngby, Denmark (Lipka et al. 1988). The magnetic fraction of rocks for both X-ray and Mössbauer spectroscopy was obtained by their crushing, grinding, cleaning by alcohol and subsequent separation.

The results of individual laboratory methods

Brief petrographical description of rocks (according to microscopical analyses made by A. Mihalíková, written report):

- the rocks of the Jos plateau (JP): JP-1, JP-7 diabase with olivine; JP-2 olivine basanite; JP-3 to JP-6 and JP-8 olivine basalts; JP-9 alkali granite porphyry;
- the rocks of the Biu basalt plateau (BP): BP-1 olivine basalt; BP-2, BP-3 olivine basalts; BP-4 albitized olivine basalt (spilite ?);
- the rocks of the Samunaki locality (SMKI): SMKI-1, SMKI-2 olivine basalts;
- the rocks of the Runka localities (RK): RK-1, RK-2 nepheline basanites;
- the nonbasaltic rocks of the outcrop near Runka village (RK-Gr): migmatized amphibolite.

Brief outline of the presence of magnetic minerals in the rocks according to the results of individual methods:

Ore microscopy (J. Beňka and Š. Suchý, written report): Hematite was identified in all studied samples of rocks. Magnetite is present (except of the hematite) in the olivine basalts from the localities JP-4, JP-5, JP-8, BP-2, BP-3, also in the olivine

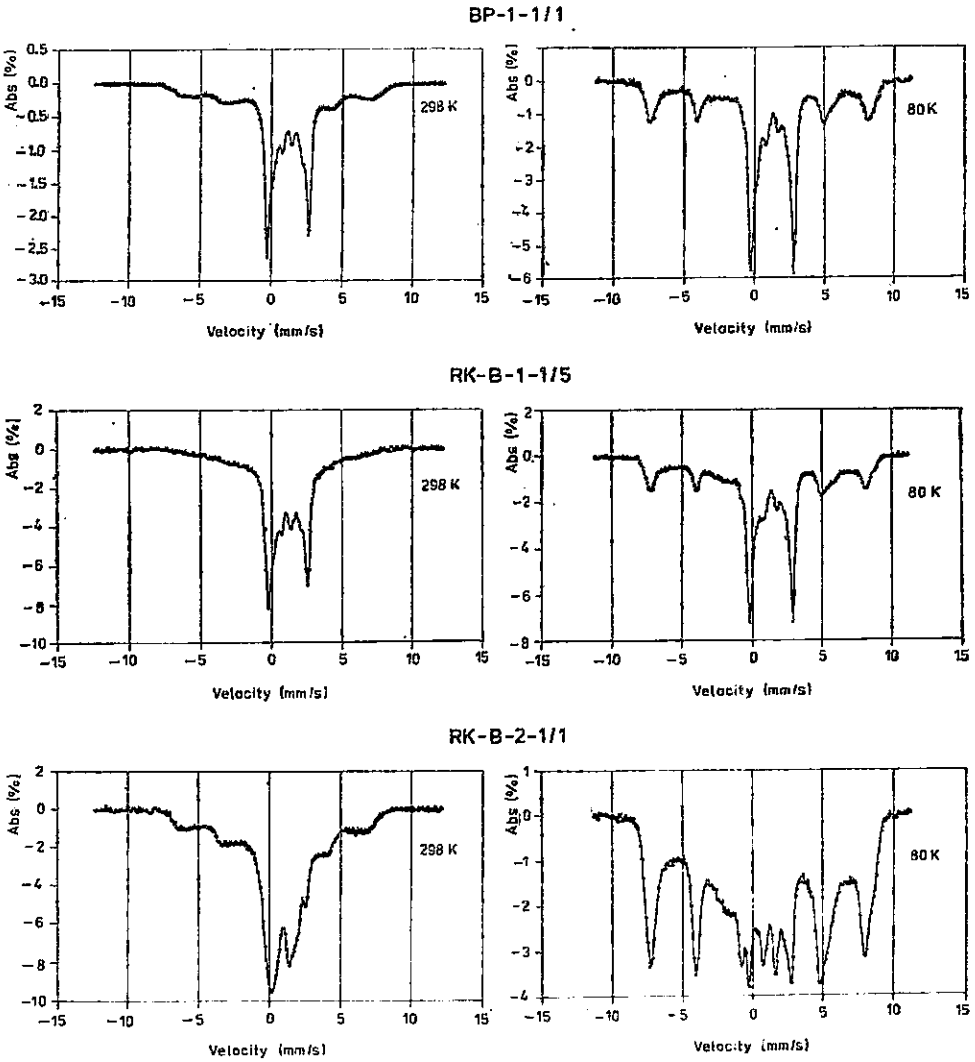

2. Mössbauer spectra of samples BP-1-1/1, RK-B-1/5, RK-B-2-1/1 obtained at room temperature (298 K) and at the temperature of liquid nitrogen (80 K)

basanite from the locality JP-2, and in the nepheline basanites from the localities RK-1 and RK-2.

X-ray spectroscopy: Two groups of basaltic rocks were investigated by X-ray powder diffraction. The results of one group of basaltic rocks were published by Lipka et al. (1988). The results of second group were reported by B. Toman (written report). The results of analyses made by B. Toman are as follows:

– titanomagnetites ($Fe_{3-x}Ti_xO_4$) with hematite (α-Fe_2O_3), and ilmenite ($FeTiO_3$) are present in the investigated olivine basalts from the locality BP-3,

– hematite (α-Fe_2O_3), and magnetite (Fe_3O_4) are present in the albitized olivine basalt from the locality BP-4,
– titanomagnetites ($Fe_{3-x}Ti_xO_4$), with hematite (α-Fe_2O_3), ilmenite ($FeTiO_3$), brookite (TiO_2), and pseudobrookite (Fe_2TiO_5) are present in the nepheline basanites from the localities RK-1, and RK-2.

Titanomagnetites ($Fe_{3-x}Ti_xO_4$) were identified in all studied samples according to Lipka et al. (1988). The unit cell parameters of the titanomagnetites are as follows: $a = 0.852\,4$ nm, and $a = 0.846\,3$ nm in the samples of the nepheline

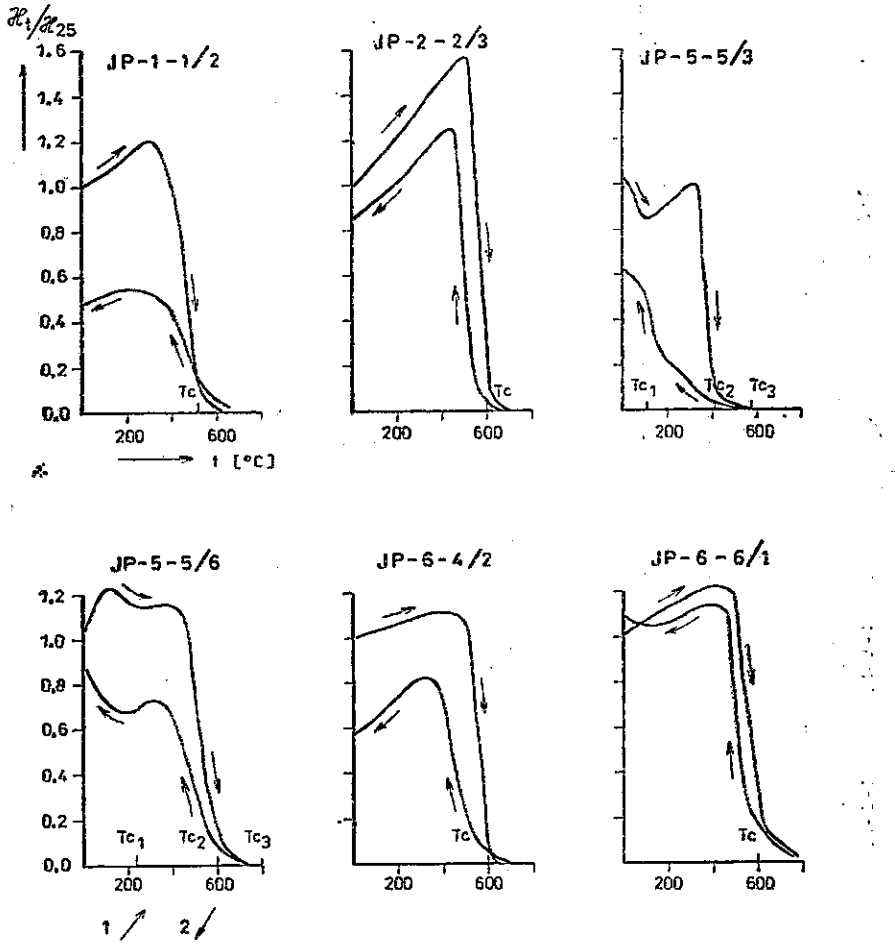

3. The results of the Curie temperature measurements of powdered rock samples
$\varkappa_t$, $\varkappa_{52}$ – magnetic susceptibility of the sample – after heating to the temperature $t(\varkappa_t)$, without the heating effect ($\varkappa_{25}$); *1*, *2* – Curie temperature, curve registered during the heating (*1*) and the cooling (*2*) of the sample; T_c – Curie temperature of magnetic mineral of rock sample

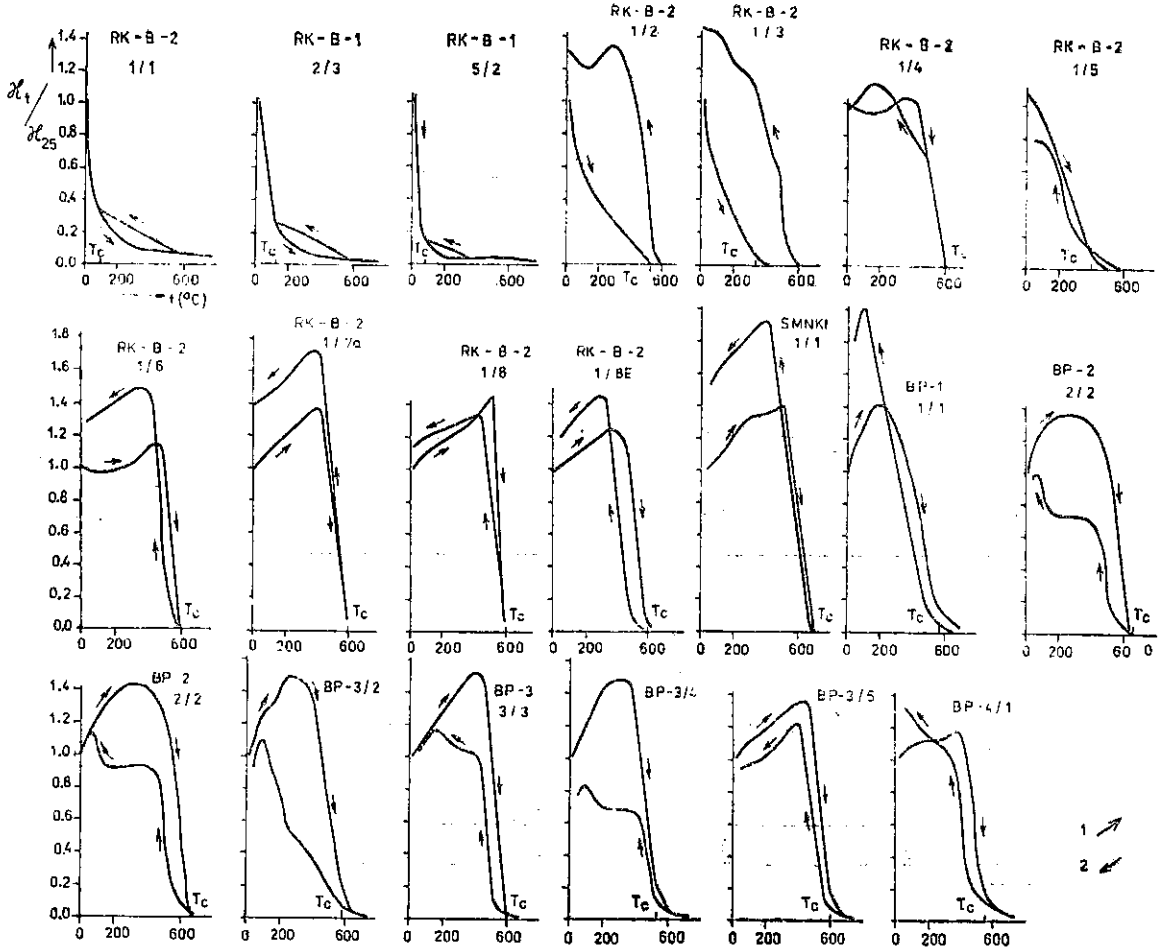

4. The results of the Curie temperature measurements of powdered rock samples $\varkappa_t, \varkappa_{25}$ – magnetic susceptibility of the sample – after heating to the temperature $t(\varkappa_t)$, without the heating effect ($\varkappa_{25}$); *1, 2* – Curie temperature curve registered during the heating (*1*) and the cooling (*2*) of the sample; T_C – Curie temperature of magnetic mineral of magnetic mineral of rock sample

basanite (RK), and in the sample of the olivine basalt (BP-1), respectively. A mineral intermediate between α-Fe_2O_3 and $FeTiO_3$, i.e. hematite-ilmenite solid solution was identified in the samples JP-2, BP-1, BP-2 and SMKI-1.

Mössbauer spectroscopy of magnetic fraction was mostly applied at room temperature, but in several cases also at the temperature of liquid nitrogen (see fig. 2). Mössbauer spectra of samples were measured also after heating of magnetic fraction. Sixteen samples of the studied rocks were analysed by this method. Volume portion of the Fe-Ti oxides was determined in the magnetic fraction on the base of the results of Mössbauer spectroscopy. The composition of the titanomagnetites in the samples was estimated from their unit cell parameters. It is as follows: BP-1 $Fe_{2.4}Ti_{0.6}O_4$; BP-2 $Fe_{2.5}Ti_{0.5}O_4$; SMKI-1 $Fe_{2.9}Ti_{0.1}O_4$; RK-1 $Fe_{2.3}Ti_{0.7}O_4$; RK-2 $Fe_{2.4}Ti_{0.6}O_4$.

Mössbauer spectroscopy and X-ray diffraction showed that heating of the samples RK-1, RK-2 and BP-1 causes a transformation of titanomagnetites into almost titanium-free magnetite, hematite, brookite and ilmenite (Lipka et al. 1988).

Electron microprobe analyses were realized on the samples of four petrographical types of studied rocks. The content of both Fe and Ti components (according to the analyses made by F. Caño, written report) is as follows:

	FeO(%)	TiO_2(%)
– olivine basalt (BP-2, BP-3)	74.48	23.30
– olivine basanite (JP-2)	72.54	26.01
– albitized olivine basalt (BP-4)	89.33	8.66
	45.39	54.46
– nepheline basanite (RK-1)	74.83	24.41
	48.06	51.60
– nepheline basanite (RK-2)	75.27	24.30
	48.45	51.23

Curie temperature measurements: It is well known that a quite successfull identification of magnetic constituents of rocks can be obtained by determining their Curie temperature. We have applied the method of change of magnetic susceptibility of a powdered sample with the temperature. The applied method was worked out by the author of this article. Curie temperature curves of the samples are shown in figs. 3 and 4. We see that the main carriers of magnetism within the rocks of Jos plateau are minerals with T_C close to magnetite (fig. 3). Olivine basalts of Biu plateau localities (except loc. BP-1) show T_C – around 600 °C. The albitized olivine basalt of the loc. BP-4 shows T_C close to magnetite, but also the second magnetic phase (T_C about 350 °C) is present in this rock. There is a presence of the mineral with $T_C = 150-250$ °C after heating over 750 °C and cooling up to laboratory temperature in the rocks of the localities BP-2, and BP-3 (fig. 4). Nepheline basanites of the localities RK-1 and RK-2-1/1 show T_C around 200 °C.

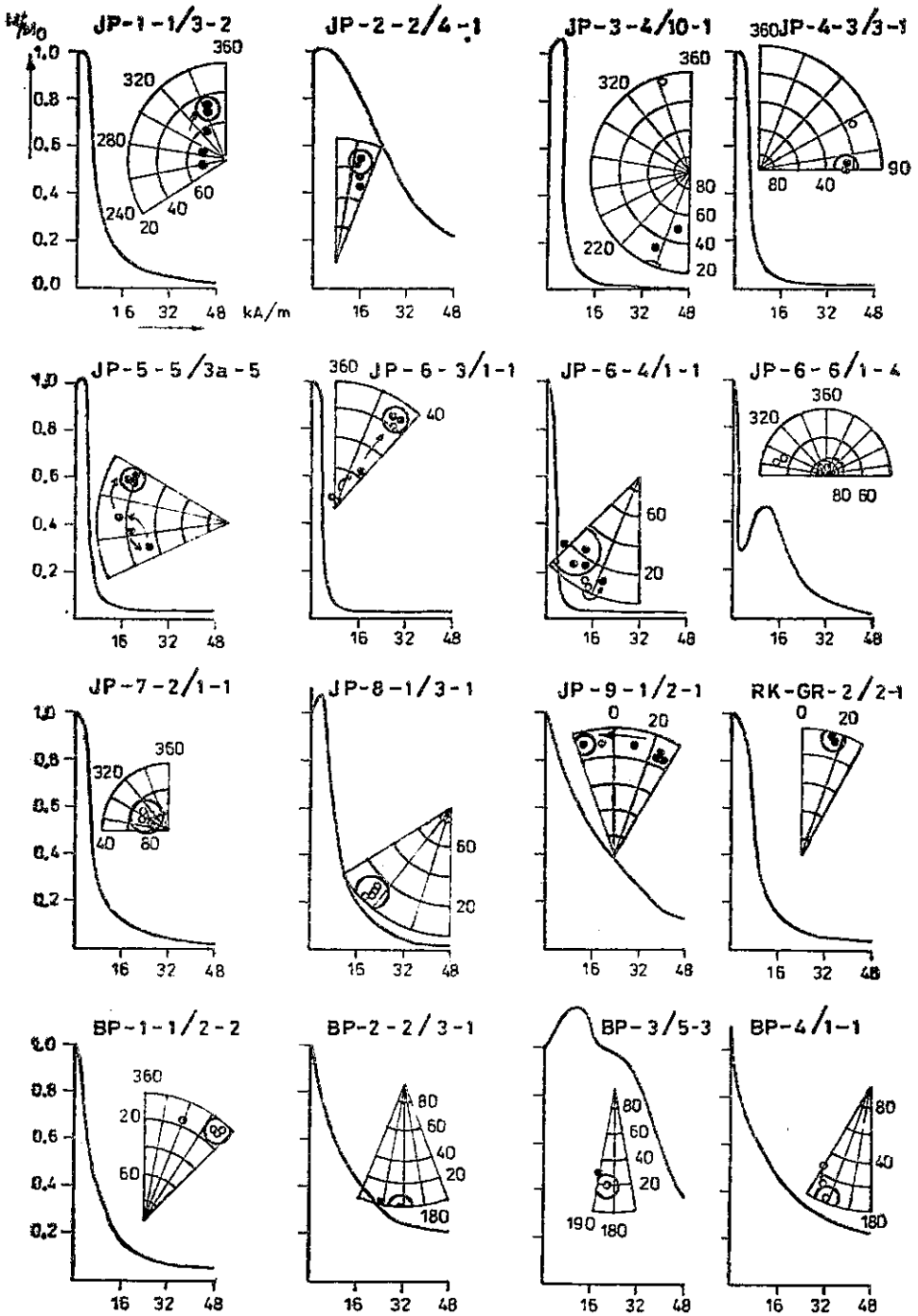

5. A.C. demagnetization in nonmagnetic medium
M – magnetic remanent moment of the specimen demagnetized by field *H*; *full, open circle* – positive, negative *RMP* respectively

The samples of other RK-2 localities and locality SMKI-1 show T_C close to magnetite (except RK-B-2-1/2, 1/3) (fig.4).

Basic magnetic and paleomagnetic results are presented in tables 1, 2, 3, 4. The results of A.C. demagnetization are in figs. 5 and 6. Average directions of *RMP* and computed pole positions of rocks of selected localities are presented in figs. 7 and 8. The results which have been taken over from Piper and Richardson (1972) in fig. 8 are also presented.

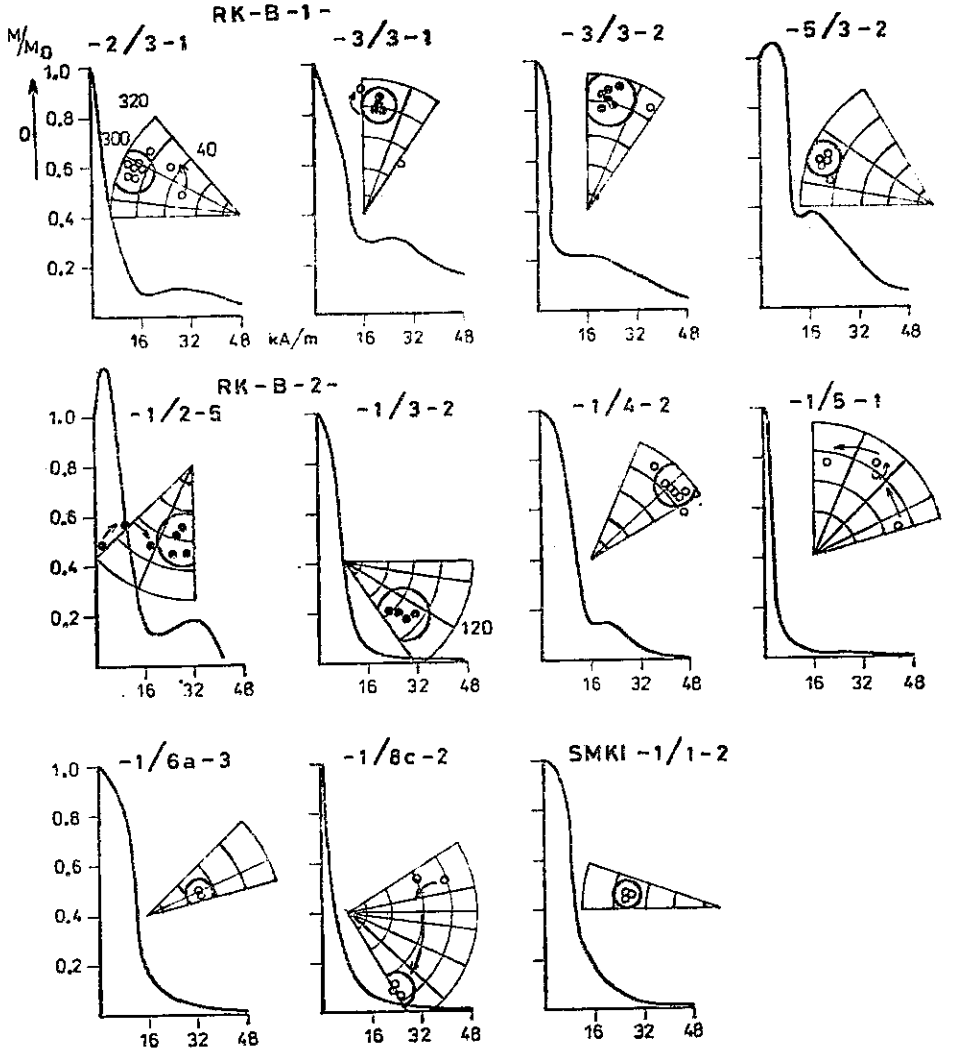

6. A.C. demagnetization in nonmagnetic medium
M – magnetic remanent moment of the specimen demagnetized by field H; *full, open circle* – positive, negative *RMP* respectively

Table 3

Paleomagnetic characteristics of rocks

Region	φ_L	λ_L	D_s	I_s	α_{95}	k	n	$\varphi_{p(N)}$	$\lambda_{p(E)}$	δ_m	δ_p
Runka – loc. 1											
RK-1	12.505	7.186	326.9	13.5	26.5	3.6	12	56.9	270.9	27.1	13.8
RK-Gr	12.500	7.205	18.8	4.9	8.1	69.4	6	69.9	125.8	8.1	4.1
Runka – loc. 2											
1/2	12.503	7.186	161.2	28.9	22.5	9.8	6	56.4	221.4	24.8	13.6
1/3	12.503	7.186	132.3	41.3	9.6	165.8	3	30.9	239.4	11.7	7.1
1/4	12.503	7.186	34.9	−13.4	9.1	760.1	2	50.3	124.3	9.3	4.7
1/5	12.503	7.186	324.6	18.6	36.2	5.4	5	55.1	276.0	37.6	19.6
1/6	12.503	7.186	56.9	−63.4	24.4	7.1	7	22.8	220.0	38.5	30.4
1/7	12.503	7.186	260.0	−51.1	6.7	81.6	7	14.9	67.2	9.1	6.2
1/8	12.503	7.186	129.8	10.7	25.0	6.8	7	37.0	260.5	25.3	12.8
1/2+1/3 +1/8	12.503	7.186	137.0	27.1	19.6	4.5	16	45.1	249.5	21.4	11.6

φ_L, λ_L – geographical coordinates; D_s – mean declination of remanent magnetic polarization I_s – mean inclination of remanent magnetic polarization; α_{95} – semi-angle of the cone confidence for $p = 0.05$; k – precision parameter; n – number of samples; φ_p, λ_p – coordinates of the virtual pole calculated to the north (N), east (E); δ_m, δ_p – dimensions of the reliability oval for pole position

Conclusion and discussion

A complex of physico-analytical methods and laboratory procedures was used during the study of Quaternary, younger Cainozoic, Jurassic, and Proterozoic to Lower Paleozoic volcanic rocks from Nigeria, to obtain information on the carriers of the magnetism, paleomagnetic stability, and the distribution of the direction of the *RMP* in the mentioned geological complexes.

As mentioned previously the Fe-Ti oxides are the main carriers of the magnetism in the studied volcenic rocks. They are in various magnetic state and chemical stages, corresponding to different degrees of their alterations. Also the products of the alterations of the titanomagnetites are present in some rocks. Abundant ilmenite is e.g. present in the nepheline basanites of the northern facies (RK-1), also in the northern part of the southern facies (RK-2), according to the results of microscopical analyses, electron microprobe analyses, and Curie temperatures, except for the non-stoichiometric (cation-deficient) titanomagnetites. The Möss-

Table 4

Palcomagnetic characteristics of rocks

Region	φ_L	λ_L	D_s	I_s	α_{95}	k	n	$\varphi_{p.n.}$	$\lambda_{p.n.}$	δ_m	δ_p
Jos plateau											
JP-1	9.709	8.450	359.6	59.0	17.3	20.5	5	59,9	7.9	25.8	19.3
JP-2	9.700	8.467	17.3	21.4	2.5	161.7	21	72.9	92.2	2.6	1.4
JP-3	9.584	8.318	172.6	45.7	107.3	2.5	3	52.5	199.3	136.8	87.2
JP-4	9.584	8.336	258.6	38.9	131.9	1.2	8	6.8	122.0	157.1	93.5
JP-5	9.627	8.391	334.8	14.0	20.0	3.4	22	64.9	274.6	20.4	10.4
JP-6/3	9.559	8.641	32.8	4.4	10.0	627.3	2	56.5	109.0	10.0	5.0
JP-6/4	9.559	8.641	265.9	−1.4	55.0	2.0	8	4.1	89.3	55.1	27.5
JP-6/6	9.559	8.641	164.6	81.4	46.0	3.1	6	6.6	192.8	89.1	86.3
JP-7	9.559	8.679	249.6	−64.8	13.2	21.9	7	20.9	52.1	21.2	17.1
JP-8	9.580	8.705	212.8	−23.3	54.6	2.2	7	57.7	91.1	58.1	30.9
JP-9	9.936	8.859	341.8	6.4	6.4	40.1	14	70.7	259.6	6.4	3.2
Biu plateau											
BP-1	10.614	12.141	38.4	−15.1	24.4	26.5	3	47.7	126.2	25.1	12.9
BP-2	10.636	12.152	182.9	4.3	13.6	11.2	12	76.9	179.3	13.6	6.8
BP-3	10.600	12.216	184.3	−13.8	11.0	7.3	27	84.4	142.4	11.3	5.8
BP-4	10.573	12.232	197.4	12.8	10.7	24.0	9	65.7	146.0	10.9	5.6
BP-2 + + BP-3 + + BP-4	10.603	12.200	186.5	−3.9	7.8	8.0	48	79.2	154.9	7.8	3.9
SMKI	10.223	10.168	288.3	−14.8	9.5	17.2	15	16.4	269.1	9.8	5.0

For explanation see table 3

bauer spectra of the magnetic fraction from the nepheline basanites (all samples of the locality RK-1, and the samples of northern outcrops of the locality RK-2) are very complicated. The basic spectra probably correspond to non-stoichiometric titanomagnetites. The presence of the ilmenite is also reflected in the samples. The ferroilmenite is probably the main carrier of the magnetism in these rocks, to judge from their magnetic characteristics and all the data mentioned above. Most of these rocks have extreme high magnetic susceptibility.

The cation-deficient titanomagnetites are probably the main carriers of the magnetism in the nepheline basanites of the southern part of the locality RK-2. Most of these rocks have extremely intensive *NRMP*. The cation-deficient titanomagnetites are probably the main carriers of the magnetism in the olivine basalts from the localities of the Jos plateau. The ilmeno-hematites are present in the

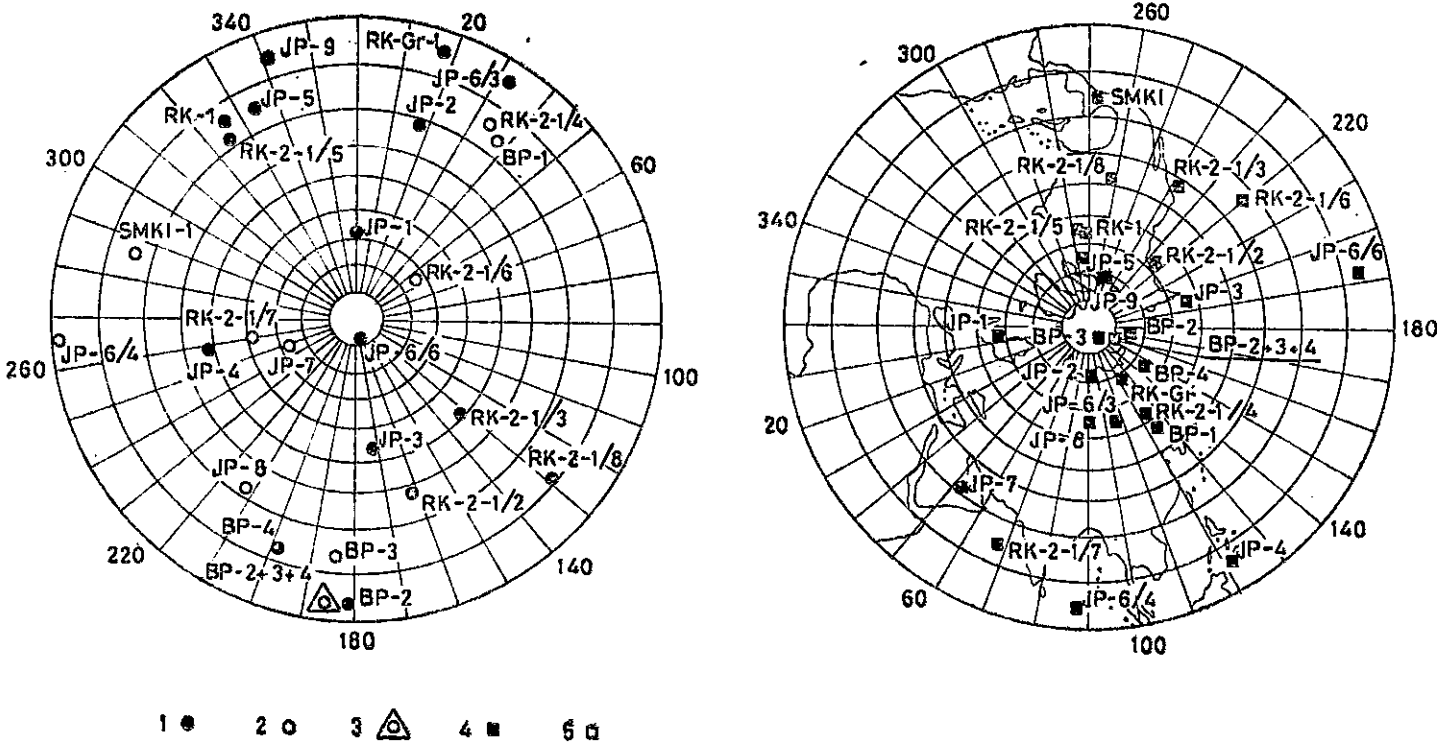

7. Stereographic projections of mean direction of the *RMP* and pole positions of the rocks of individual outcrops under study; *1*, *2* – positive, negative *RMP* respectively; *3* – mean direction of *RMP* of the localities BP-2, BP-3 and BP-4; *4* – mean virtual pole position of the outcrop under study; *5* – mean virtual pole position of the localities BP-2, BP-3, BP-4

olivine basalts of the localities BP-2, BP-3, and in the olivine basanite of the locality JP-2, except the cation-deficient titanomagnetites. The ilmeno-hematites are only present in the albitized olivine basalt of the locality BP-4.

The magnetite-hematite solid solution is probably the main carrier of the magnetism in the olivine basalt of the locality SMKI-1, and in the alkali-granite porphyry of the locality JP-9, also in the migmatized amphibolite of the locality RK-Gr. The ferroilmenite is probably present in the olivine basalt of the locality BP-1.

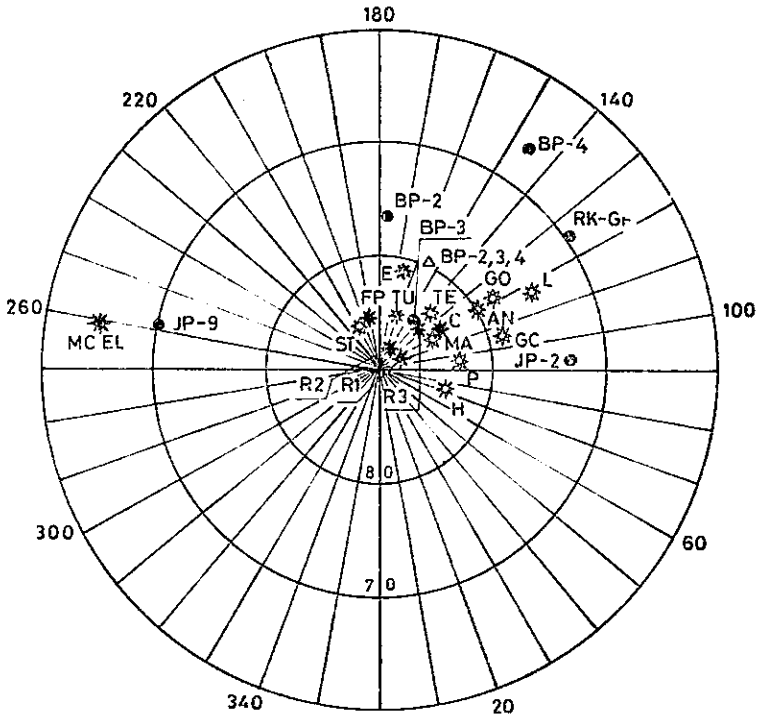

8. Pole positions of the selected localities under study and paleomagnetic pole positions according to J. D. A. Piper and A. Richardson (1972)
JP-2 – olivine basanite from the Jos plateau of Cainozoic age;
JP-9 – alkali granite porphyry of Jurassic age; BP-2, BP-3, BP-4 – olivine basalts from the Biu basalt plateau of Cainozoic age;
RK-Gr – migmatized amphibolite of Proterozoic to Lower Paleozoic age
Explanations according to J. D. A. Piper and A. Richardson (1972):
the continental (*closed stars*) and oceanic (*open stars*) parts of the African plate; FP – Fernando Poo, AN – Annobon, P – Principe, ST – São Tomé, C – Cameroun, E – Ethiopian traps, TU – Turkana lava, MA – Madeira, GC – Gran Canaria, GO – Gomera, H – Hierro, TE – Tenerife, L – La Palma; R1, R2, R3 – African rift valley: 0–2.5 m.y. (R1), 2.5–5.0 m.y. (R2), 5.0–7.5 m.y. (R3); MCEL – the Mesozoic poles from Africa published by McElhiny et al. 1968 (*in* J. D. A. Piper, A. Richardson 1972)

All analysed properties and detected signs indicate that the above-discussed rocks have been altered from the time of their origin. I suppose that their remanence is not a primary one, but that it has been acquired during the alteration processes. It means that the *RMP* is a secondary one, probably of chemical origin (C.R.M.).

The alterations of the magnetic properties of the rocks with regard to an alteration of their Fe-Ti oxides have been described by many authors, e.g. by Ade–Hall et al. (1971); Tarling (1974); Stacey–Banerjee (1974); Pecherskij et al. (1981); Pecherskij (1985); Orlický (1987); Orlický–Lipka (1987). But it is complicated to reconstruct the whole alteration process in the individual rock with regard to detection of the stages of forming of the magnetic fraction from its origin. This means that the considerations concerning the carriers of the *RMP* and their origin in the rocks under study are despite many particular results of analyses not definite in all cases.

It remains to examine whether we can separate the influences of an alteration processes on the *RMP* of volcanic rocks, the reflections of nondipole behaviour of the field and real polar wandering or continental drift in the Jurassic, Middle Jurassic, Upper Tertiary and Quaternary times.

The virtual pole position obtained from Middle Jurassic (Runka localities), Younger Cainozoic (Biu plateau), Quaternary (Jos plateau) basaltic rocks, including nonbasaltic rocks (alkali granite porphry from JP-9 locality and migmatized, amphibolite from RK-Gr locality) are in fig. 7.

The virtual pole of JP-2 locality is derived from the results of olivine basanites, the magnetic minerals of which are believed to be of secondary origin. This means that this virtual pole corresponds to the time of alteration of original magnetic minerals, or to the time after, but not to the time of the origin of the mentioned rocks. The olivine basanite of JP-2 locality belongs to Newer basalts of Jos plateau (age: 2.1 – 0.9 m.y.). As already indicated, there is not always a distinction between the Fluviovolcanic series (age of basalts up to 7.0 m.y.) and Older basalts, and the subdivision between Older and Newer basalts may also be artificial.

The Biu basalt plateau of a Younger Cainozoic age is represented by three virtual poles (BP-2, BP-3, BP-4). There is evident distinction among the carriers of the magnetism of the albitized olivine basalt (BP-4), and those from the olivine basalts of the localities BP-2, BP-3. There are different positions of the virtual poles of these localities in fig. 8. The individual localities differ in the inclinations of the *RMP* of rocks, but the declinations of all three localities are close to each other. I suppose that the differences in the inclinations are probably due to a local irregular slope of concrete volcanic bodies. Unfortunately it has not been corrected due to the lack of detailed geological data. The petrographic signs, magnetic characteristics and Curie temperature curves of the samples of the locality BP-4, and those of the localities BP-2, BP-3 suggest that the process of the origination or postvolcanic development of these rocks has not been uniform. A total sum

of φ_p and λ_p of all three localities is believed to be the probable virtual pole for the Biu basalt plateau of a Younger Cainozoic age.

The alkali granite porphyry of JP-9 locality belongs to the porphyry ring dyke complex of the large Jurassic (160–170 m.y.) Younger Granite massif centered on the Jos plateau, according to Kogbe (1976). It has been reported that the emplacement of the Younger granites was associated with epeirogenic uplift. The ring complexes of the entire Nigeria – Niger provinces lie on a north-south belt which is 1,200 km long. This can be related to two major features of the African continent. First it corresponds to the central part of the north-south trending Pan-African orogenic belt and second, it forms a northerly continuation of the continental margin of southern Africa. These may be inter-related. The rifting and separation of South America from Southern Africa during Jurassic to Cretaceous times was guided by structural trends in the basement. It seems probable that the Younger Granites lie on an extension of this ancient rift structure on a zone of incipient faulting where crustal separation did not take place (Black 1965 *in* Kogbe 1976).

The computed pole position of alkali granite porphyry from JP-9 locality is $\varphi_p = 70.7°$ N; $\lambda_p = 259.6°$ E. The *RMP* is probably a secondary one of C.R.M. origin. It is probable that a stable *RMP* of these rocks was acquired in the times close after the forming of the Jurassic Younger Granite massif. Migmatized amphibolite of the RK-Gr locality belongs to the Older Granite suite of an Upper Proterozoic to Lower Paleozoic age. In north-eastern Nigeria, a group of fine-grained granites is described as being earlier than the migmatites. These granites represent a minor, discordant intrusion of small areal extent occurring as dykes and irregular bodies rarely extending for more than 200 m, according to Kogbe (1976). The magnetism of migmatized amphibolite of RK-Gr locality is believed to be a secondary one, of C.R.M. origin. The origin of the magnetism falls probably into a Brunhes epoch of positive polarity. This means that a stable *RMP* of rocks has been acquired during the recent time, and not in the Proterozoic to Lower Paleozoic.

The other 18 derived poles have been exluded from this discussion due to insufficient paleomagnetic stability, anomalous magnetization or shortage of rocks of individual outcrops.

Piper and Richardson (1972) investigated rocks of 205 sites from the Upper Tertiary to recent lavas and intrusions in the Gulf of Guinea volcanic area of equatorial West Africa. They have presented an idea "that there is no paleomagnetic reason for believing that the African plate has moved relative to the pole in Upper Tertiary times", on the base of their results, supported by the results of other authors (see fig. 8).

The nine Mesozoic poles from Africa group closely at near 65° N and 261° E have been published by McElhiny et al. (1968 *in* Piper–Richardson 1972). The youngest Mesozoic pole is of about 100 m.y. age and the shift of the African

ného titanomagnetitu, ktorý je nositeľom novej pomerne stabilnej *CRMP*. Vedľa neho je v hornine ilmenit, ktorý je magneticky pasívny.

Výsledkami je potvrdené, že extrémne intenzívnú *NRMP* vykazujú nefelinické bazanity Runka lokality a olivinické bazalty Jos plató s jednou Curieovou teplotou (T_C) blízkou T_C magnetitu, pričom nefelinické bazanity s nízkymi hodnotami T_C, u ktorých je potvrdená zároveň prítomnosť $FeTiO_3$, vykazujú výrazne nižšie hodnoty *NRMP*.

V olivinických bazaltoch troch lokalít Biu plató (BP-2, BP-3 a BP-4) je okrem titanomagnetitov zistená aj prítomnosť tuhých roztokov ilmenito-hematitov. Tieto olivinické bazalty vykazujú relatívne nízke hodnoty *NRMP*, reverznú polaritu a stabilný smer *RMP* voči demagnetizácii striedavým poľom.

Olivinické bazanity JP-2 lokality, alkalické granitové porfýry lokality JP-9 a migmatitizované amfibolity lokality RK-Gr obsahujú z magnetických minerálov hlavne nestechiometrický magnetit. Magnetizácia týchto hornín je pravdepodobne sekundárna, avšak magneticky i smerovo pomerne stabilná.

Iba 6 vypočítaných pólov (JP-2, JP-9, RK-Gr, BP-2, BP-3, BP-4) z celkového počtu 25 na obr. 7 bolo využitých pre záverečnú analýzu výsledkov.

Virtuálny pól lokality JP-2 je odvodený z výsledkov olivinických bazanitov, magnetické minerály ktorých sú považované za sekundárne. To znamená, že odvodený virtuálny pól zodpovedá obdobiu alterácie pôvodných minerálov, nie však obdobiu vzniku pôvodných hornín. Vek tzv. „Newer bazaltov", do ktorých sú začlenené i bazanity predmetnej lokality, je ca 2,1 – 0,9 mil. rokov (alebo 7,0 mil. rokov – Fluvio – volcanic serie). Výsledky poukazujú, že alterácie minerálov prebehli v olivinických bazanitoch lokality JP-2 v recentnom období.

Bazalty Biu plató – lokalít BP-2, BP-3, BP-4 – sa vypočítanými hodnotami smeru strednej *RMP* i virtuálnych pólov medzi sebou vzájomne líšia. Deklinácia *RMP* všetkých troch lokalít je veľmi blízka, inklinácia *RMP* je ovplyvnená pravdepodobne nepravidelným zaklesnutím individuálnych telies, z ktorých vzorky pochádzajú. Žiaľ, pre nedostatok ďalších geologických údajov tieto lokálne zmeny polohy telies a ich vplyv na inklináciu *RMP* horniny nie je možné vylúčiť.

Vieme, že všetky tri lokality patria do Biu bazalt plató, vrchnokenozoického veku. Podobné petrografické znaky, magnetické charakteristiky, rovnaké Curieove teploty i ďalšie výsledky analýz poukazujú, že pôvod alebo postvulkanický vývoj týchto hornín boli pravdepodobne rovnaké. Na základe uvedeného predpokladám, že stredné hodnoty φ_p a λ_p vypočítané z individuálnych výsledkov lokalít BP-2, BP-3 a BP-4 sú pravdepodobným virtuálnym pólom olivinických bazaltov vrchnokenozoického veku Biu plató.

Alkalický granitový porfýr lokality JP-9 patrí do porfýrového – „ring-dyke" – komplexu rozsiahleho jurského (160 – 170 mil. rokov) mladšieho granitového masívu, vyskytujúceho se v rámci Jos plató (podľa Kogbeho 1976).

Vypočítaná poloha pólu pre granitový porfýr lokality JP-9 je $\varphi_p = 70{,}7°$ N, $\lambda_p = 259{,}6°$ E. *RMP* týchto hornín je pravdepodobne sekundárna (CRM). Je

pravdepodobné, že stabilná *RMP* granitového porfýru vznikla v období veľmi blízkom po formovaní jurského mladšieho granitového masívu.

Migmatitizovaný amfibolit lokality RK-Gr patrí do „staršej granitovej formácie" proterozoického až spodnopaleozoického veku.

Magnetizmus migmatitizovaného amfibolitu lokality RK-Gr má pravdepodobne sekundárny pôvod. Stabilná zložka *RMP* týchto hornín vznikla v recentnom období, pravdepodobne počas Brunhesovej epochy.

Zo skúmaných hornín poukazujú na možný pohyb a rotáciu africkej litosférickej dosky iba výsledky meraní jurského granitového porfýru lokality JP-9. Ostatné výsledky buď nepoukazujú na pohyb africkej dosky, alebo z dôvodov nestability *RMP*, nedostatočného počtu experimentálneho materiálu sú výsledky pre takúto interpretáciu nevyužiteľné.

Ako je známe z úvodu práce, Piper a Richardson (1972) vyslovili názor, že na základe paleomagnetických výsledkov recentných až vrchnoterciérnych vulkanitov z oblasti Guinejského zálivu a rovníkovej západnej Afriky nie je detegovaný pohyb africkej dosky relatívne voči pólu v období vrchného terciéru.

Mc Elhiny et al. (1968 *in* Piper–Richardson 1972) publikovali deväť mezozoických pólov lokalít Afriky $\varphi_p = 65°$ N, $\lambda_p = 261°$ E. Podľa uvedených autorov došlo k premiestneniu africkej dosky v období od mezozoika do vrchného terciéru (v intervale 100 až 25 m. r.).

Ako vidieť z obr. 8 i z predchádzajúceho textu, pomerne dobrá zhoda je medzi strednou hodnotou pólu vypočítaného pre mezozoické horniny lokalít Afriky podľa Mc Elhinyho et al. (l.c.) a hodnotou pólu pre granitový porfýr jurského veku lokality JP-9. Naše výsledky taktiež poukazujú na okolnosť, že od obdobia vzniku jurského granitového porfýru lokality JP-9 došlo k premiestneniu africkej dosky z jej predošlej polohy.

Paleomagnetické výsledky mladších vulkanických hornín pohyb africkej dosky nedetegovali.

Vysvetlivky k tabuľkám

Tabuľka 1, 2. Magnetické charakteristiky hornín.

$\varkappa$ – objemová magnetická susceptibilita; *NRMP* – prirodzená remanentná magnetická polarizácia; Q – Koenigsbergerov koeficient.

Tabuľka 3, 4. Paleomagnetické charakteristiky.

φ_L, λ_L – geografické súradnice; D_s – stredná deklinácia remanentnej magnetickej polarizácie; I_s – stredná inklinácia remanentnej magnetickej polarizácie; α_{95} – polovičný uhol kužela spoľahlivosti pre $p = 0{,}05$; k – koeficient presnosti; n – počet vzoriek; φ_p, λ_p – súradnice virtuálneho pólu počítaného voči severu (N) a východu (E); δ_m, δ_p – parametre oválu spoľahlivosti pre vypočítaný pól.

Vysvetlivky k obrázkom

1. Schematická mapa Nigérie, včítane vybraných oblastí, z ktorých boli odobrané vzorky.
   1 — oblasť Runka: odkryvy RK-B-1 a RK-B-2 — strednojurské nefelinické bazanity, RK-Gr-1 — proterozoický až spodnopaleozoický migmatitizovaný amfibolit; *2* — Jos plató: JP-1 až JP-8 — kenozoické bazaltické horniny, JP-9 — alkalický granitový porfýr jurského veku; *3* — lokalita Samunaki (olivinické bazalty); *4* — Biu plató (bazaltové): BP-1 až BP-4 — kenozoické olivinické bazalty; *a* — lokality Annobon, São Tomé, Principe, Fernando Poo, Kamerun — terciérne a recentné vulkanity skúmané J. D. A. Piperom a A. Richardsonom (1972).
2. Mössbauerove spektrá vzoriek BP-1-1/1, RK-B-1-1/5 a RK-B-2-1/1 získané pri izbovej teplote (298 K) a pri teplote kvapalného dusíka (80 K).
3. a 4. Výsledky merania Curieových teplôt práškových vzoriek hornín.
   $\varkappa_t$, $\varkappa_{25}$ — magnetická susceptibilita vzorky — po vyhriatí na teplotu $t(\varkappa_t)$, bez tepelného účinku ($\varkappa_{25}$); *1, 2* — krivka merania Curieovej teploty počas vyhrievania (*1*) a počas chladnutia (*2*) vzorky; T_C — Curieova teplota magnetického minerálu vzorky horniny.
5. a 6. Výsledky demagnetizácie vzoriek hornín striedavým poľom, s kompenzovaním geomagnetického poľa.
   M — magnetický moment po demagnetizovaní vzorky poľom H; *plný, otvorený krúžok* — kladná, záporná *RMP*.
7. Stereografické projekcie stredných smerov *RMP* a polôh pólov hornín jednotlivých študovaných odkryvov.
   1, 2 — kladná a záporná *RMP*, *3* — stredný smer *RMP* lokalít BP-2, BP-3 a BP-4; *4* - stredná virtuálna poloha študovaného odkryvu; *5* - stredná virtuálna poloha pólu lokalít BP-2, BP-3 a BP-4.
8. Polohy pólov vybraných študovaných lokalít a paleomagnetické polohy pólov (podľa J. D. A. Pipera a A. Richardsona 1972).
   JP-2 — olivinický bazanit z Jos plató kenozoického veku; JP-9 — alkalický granitový porfýr jurského veku; BP-2, BP-3, BP-4 — olivinické bazalty z Biu-bazaltového plató kenozoického veku; RK-Gr — migmatitizovaný amfibolit proterozoického až spodnopaleozoického veku. Vysvetlivky podľa J. D. A. Pipera a A. Richardsona (1972): kontinentálne (*plné hviezdičky*) a oceánické (*prázdne hviezdičky*) časti africkej dosky; FP — Fernando Poo, AN — Annobon, P — Principe, ST — São Tomé, C — Kamerun, E — etiópske trapy, TU — turkanská láva, MA — Madeira, GC — Gran Canaria, GO — Gomera, H — Hierro, TE — Tenerife, L — La Palma; R1, R2, R3 — africké riftové údolia: 0—2,5 mil. rokov (R1), 2,5—5,0 mil. rokov (R2), 5,0—7,5 mil. rokov (R3); MCEL — mezozoické póly z Afriky, publikované Mc Elhinym et al. 1968 (*in* J. D. A. Piper—A. Richardson 1972).

Палеомагнетизм избранных четвертичных, кайнозойских, юрских и протерозойских до нижнепалеозойских вулканических пород Нигерии

Большинство изученных диабазов, оливиновых базальтов и нефелиновых базанитов является с палеомагнитной точки зрения нестабильным.

Четвертичные (или верхнекайнозойские) оливиновые базаниты из Джос плато (JP-2) имеют стабильное направление остаточной намагниченности (ОН). Основными магнитными минералами являются нестехиометрические магнетиты с небольшим присутствием гематита. ОН горных пород является вторичной, имея вероятно химическое происхождение ($I = 21{,}4°$; $D = 17{,}3°$; $\varphi_p = 72{,}9°$ N; $\lambda_p = 92{,}2°$ E).

Среднее направление ОН четвертичных (или верхнекайнозойских) оливиновых базальтов с трех мест Бию плато (BP-2; BP-3; BP-4) характеризовано следующими величинами: $I = -3{,}9°$; $D = 186{,}5°$; $\varphi_p = 79{,}2°$ N; $\lambda_p = 154{,}9°$ E. Магнитными минералами в этих породах являются титаномагнетиты и твердые растворы ильменито-гематитов.

Юрские щелочные гранит-порфиры из Джос плато (JP-9) имеют малоинтенсивную естественную ОН, вероятно химического происхождения. Исчисленный палеомагнитный полюс ($\varphi_p = 70{,}7°$ N; $\lambda_p = 259{,}9°$ E) очень близок полюсу, исчисленному для мезозойских горных пород Африки авторами Mc Elhiny et al. (1968 *in* J. D. A. Piper—A. Richardson 1972).

Результаты показали, что в течение четвертичного и верхнекайнозойского времени Африканская литосферная плита не перемещалась, но с времени возникновения стабильного компонента ОН юрских щелочных гранит-порфиров она переместилась из ее прежнего положения.

Přeložil autor

Sbor. geol. věd.	Užitá geofyz., 24	Стр. 159—184	14 рис.	3 табл.	— прил.	Praha 1990 ISSN 0036—5319

Изменения удельных сопротивлений и относительных диэлектрических проницаемостей от влажности при частоте f = 80 МГц

Změny měrných odporů a poměrných permitivit s vlhkostí při frekvenci f = 80 MHz

Josef Kozel[1]

Представлено 9-го марта 1988 г.

Resistivity
Relative permittivity
Water saturation
Effect of clay
High frequency

Kozel, J. (1990): Izmenenija udeľnych soprotivlenij i otnositeľnych diėlektričeskich pronicaemostej ot vlažnosti pri častote f = 80 MHz. — Sbor. geol. Věd, užitá Geofyz., 24, *159-184*. Praha.

Экстракт: В представленной работе приводятся теоретические формулы для зависимости удельных сопротивлений и относительных диэлектрических проницаемостей от влажности осадочных, а также изверженных, рудоносных горных пород. Описываются так называемая перколяционная теория, с помощью которой в последнее время объясняются аномальные изменения удельных сопротивлений от влажности, и целый ряд практических определений этих зависимостей в случае горных пород на территории ЧССР. Изучаются также некоторые технические материалы, которые близки к горным породам. В заключении работы с помощью электрической модели порового канала осадочной породы дается объяснение экспериментально установленного нелинейного изменения относительных диэлектрических проницаемостей глинистых пород в зависимости от степени насыщения пор слабоминерализованной водой. Подыскиваются способы аналитического выражения этой зависимости.

[1] *Geofyzika, s. p., Brno, Ječná 29a, 612 46 Brno*

Введение

В последние годы в геофизическую разведку внедряются новые высокочастотные методы, как напр. геофизический радиолокационный метод, который в ЧССР проводится преимущественно с помощью импортного прибора СИР-7.

При исследованиях в скважинах все чаще применяется метод диэлектрического каротажа, который получил большое распространение в СССР (Даев 1980, Карус и др. 1980). Оба названных метода проводятся на частотах порядка 10^7 Гц; частота $f = 80$ МГц — это одна из несущих частот аппаратуры СИР-7.

Накопленный до сих пор опыт свидетельствует о том, что для определения глубинности радиолокационных исследований, для облегчения и уточнения интерпретации результатов полевых работ, в том числе каротажных, очень важно знать изменения удельных сопротивлений и относительных диэлектрических проницаемостей от влажности. На небольших глубинах обычно встречается влажность, значения которой колеблются от степени насыщения $S_w = 0$ вплоть до значений $S_w = 100$ %. Следует заметить, что в порах этих горных пород обычно находится слабоминерализованная вода, удельное сопротивление которой составляет десятки омметров.

Настоящая работа, являющаяся продолжением работы „Относительные диэлектрические проницаемости и удельные сопротивления горных пород в диапазоне частот $10^6 - 10^8$ Гц“ (Kozel 1989), в которой, кроме прочего, приводится детальное описание методов измерения относительных диэлектрических проницаемостей и удельных сопротивлений на образцах горных пород, должна содействовать решению данной проблематики. Необходимо заметить, что измерения проводились с помощью высокочастотного моста Тесла BM 431 E. Средняя погрешность измерения указанных параметров колебалась в пределах от 2 до 5 % в зависимости от точности изготовления образцов.

Некоторые знания об изменениях удельных сопротивлений и относительных диэлектрических проницаемостей от влажности

Изучение зависимости удельных сопротивлений от влажности — это часто встречающееся задание, решение которого нужно для интерпретации данных различных методов электроразведки. В качестве примеров можно назвать работы: Bitterlich—Wöbking (1972), Дахнов (1962), Keller (1966), Kozel (1983, 1985), Пархоменко (1965) и др. Ради иллюстрации можно привести, напр., определение зависимости удельного сопротивления ϱ_h от степени насыщения пор S_w аргиллитов с органическим компонентом (Kozel 1989) (рис. 1). Значение S_w вычисляется по формуле $S_w = \dfrac{m_w - m_0}{m_{100} - m_0}$, где m_w — масса частично насыщенной горной породы, m_{100} — масса горной породы со 100%-ым насыщением и m_0 — масса совершенно сухой горной породы.

Из рис. 1 вытекает, что по мере увеличения влажности происходит понижение удельного сопротивления. Сначала это понижение является довольно быстрым, с $S_w = 30$ % оно становится уже более медленным, а приблизительно с 60 % оно является уже довольно малым. Форма зависимости у обоих образцов U1, U5 в принципе одинакова.

Однако более часто, чем определение зависимости удельного сопротивления от степени насыщения пор, встречается определение удельных сопротивлений или параметров пористости F от пористости p; $\varrho_h/\varrho_w = F = f(p)$, где ϱ_w – удельное сопротивление раствора в порах. В данном случае влажность выражается не посредством процента заполнения порового пространства одного образца

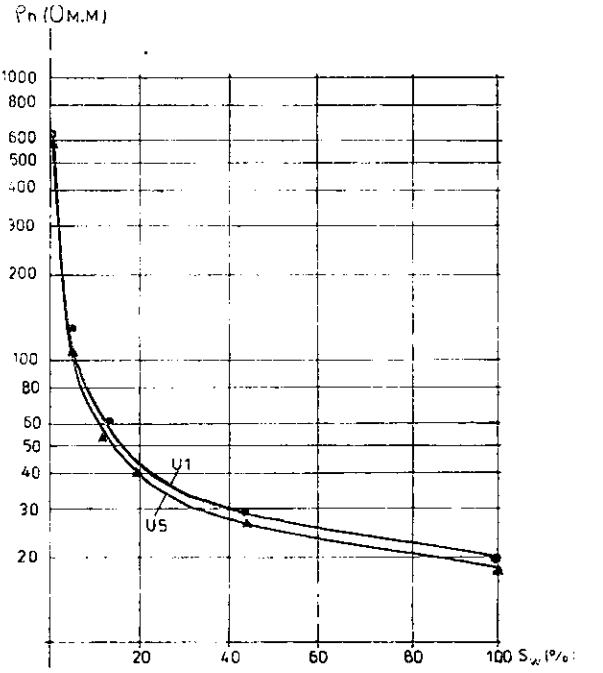

1. Зависимость удельных сопротивлений от степени насыщения водой аргиллитов с органическим компонентом (образцы U1, U5)

породы, а посредством пористости совокупности горных пород (формации пород), в которой находятся горные породы разной пористости. При этом обычно предполагается, что $S_w = 100\ \%$. Одной из наиболее применяемых формул для выражения этой зависимости является эмпирическая формула, введенная Арчи: $F = p^{-m}$, где m – т. наз. коэффициент сцементированности. Впоследствии эта формула была модифицирована разными авторами. Дахновым (1962), напр., для коэффициентов сцементированности вводятся значения m в пределах $m = 1{,}3-2{,}2$. В настоящее время применяется закон Арчи в форме $\varrho_h = a \cdot \varrho_w \cdot p^{-m}$, где константа a может обладать значениями от 0,6 до 3,0 в зависимости от литологии и текстуры горных пород (Handbook of physical properties of rocks, Carmichael, ed., 1986).

В течение прошедшего десятилетия авторы Schante–Kirkpatrick (1971) и Kirkpatrick (1973) опубликовали новую теорию для объяснения сущности электропроводности в неоднородных системах – теорию перколяции (просачивания, протекания). Впервые эта теория была применена для объяснения

электропроводности горных пород, по всей вероятности, в работе авторов Schankl–Waff (1974).

В СССР была аналогично использована теория протекания (Шкловский–Эфрос 1975) для объяснения проводимости сильно неоднородных сред. В 1979 г. Челидзе была опубликована работа „Перколяционная модель электропроводности минералов". Для наглядного объяснения проблематики ниже приводится часть его работы в свободной переработке.

Экспериментальным путем (Пархоменко–Мкртчян 1974) была получена зависимость удельной проводимости минералов от содержания проводящих окислов (рис. 2). Для численного выражения такой зависимости обычно применяются законы для смесей Максвелла, Лихтенеккера и других. Челидзе использовал закон Максвелла–Вагнера–Ханая в форме $\sigma = \sigma_1(1 - V_2)\pi^{-3}$, где σ_1 – удельная проводимость относительно непроводящего скелета (основной массы), V_2 – объем проводящих частиц удельной проводимостью σ_2.

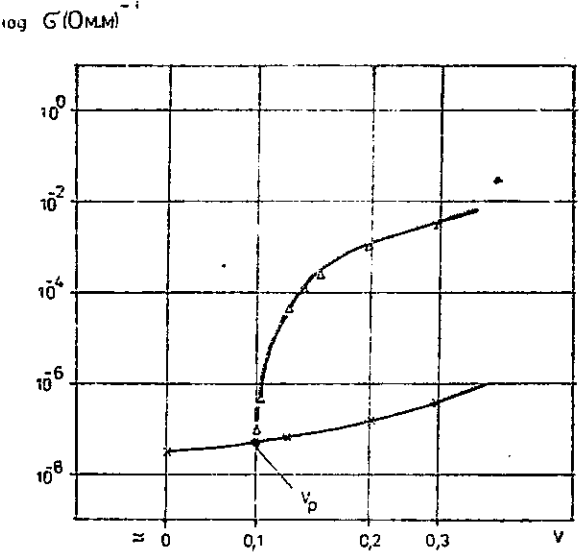

2. Зависимость удельной проводимости минералов от содержания проводящих окислов. Перколяционная модель по Т. Л. Челидзе

Действительно, что σ_1 существенно меньше σ_2. Однако, законом предполагается, что взаимное воздействие друг на друга частиц проводимостью σ_2 не имеет места. Графическое изображение этой зависимости позволило установить, что эта формула соответствует эксперименту лишь до значения V_p, которое называется пороговым значением. В случае более высоких значений ($V_2 > V_p$) проводимость резко увеличивается. Это явление объясняется с помощью теории перколяции (просачивания) тем, что происходит объединение, скапливание проводящих частиц. Для проводимости такой системы по установлению авторов Schante–Kirkpatrick (1971) действительна формула $\sigma(V) \approx (V - V_p)^t$, где t – критический коэффициент; в случае двумерной

модели его значение составляет 1–1,3, в случае трехмерной – 1,5–1,6. Объединив таким образом обе частные формулы, Челидзе находит окончательную формулу

$$\sigma = \begin{bmatrix} \sigma_1(1-V)^{-3} & \text{для } V < V_p \\ k(V-V_p)^t & \text{для } V > V_p \end{bmatrix}.$$

Если ради сравнения взять классический закон Арчи, его можно написать в форме $F = \frac{\varrho_h}{\varrho_w} = p^{-m}$, откуда $\varrho_h = \varrho_w \cdot p^{-m}$ и, следовательно, обратная величина удельного сопротивления $\sigma_h = \frac{1}{\varrho_w} \cdot p^m = \sigma_w \cdot p^m$, где m, как уже было сказано, находится в пределах $m = 1{,}3-2{,}2$. Коэффициент m представляет собой сложную функцию сцементированности, структуры пор или же глигистости пород.

Пористость, как известно, определяется как $p = V_{\text{пор}}/V$ (V – общий объем горной породы). Следовательно, для вышеприведенной части экспоненциального прироста проводимости можно получить близкое функциональное отношение.

Относительные диэлектрические проницаемости

Зависимости относительных диэлектрических проницаемостей ε_r от влажности w изучаются уже в меньшей степени, чем аналогичная зависимость для удельных сопротивлений. В литературе встречаются два вида данных. Часто находят или предполагают линейную зависимость $\varepsilon_r = f(w)$ (Zemčíková 1981; Jašek 1984 и др.), иногда результаты соответствуют нелинейным, степенным зависимостям. Интересные данные по группам пород разной пористости опубликованы, напр., Краевым (1951).

Чтобы можно было лучше изучать характер изменений удельных сопротивлений и переменных диэлектрических проницаемостей от влажности и сформулировать определенное мнение относительно образцов горных пород из наших областей, была выполнена совокупность исследований разных типов горных пород, а с целью сравнения – также некоторых технических материалов.

Результаты исследования зависимости удельных сопротивлений от влажности или же от степени заполнения пор пород слабоминерализованной водой

Кроме приведенного уже примера для аргиллитов с органическим компонентом были проведены исследования мелкозернистого слабоглинистого песка из района карьера Брно-Черновице, в котором параметрически увеличивалось

содержание бентонита (от 10, 25, 50 объемных % до 100 %) вплоть до „чистого" бентонита. Результаты приводятся на рис. 3. Из графиков ясно, что по мере увеличения влажности происходит сначала резкое увеличение проводимости (резкое понижение сопротивления) и что приблизительно с 30 % S_w понижение сопротивления становится более медленным, являясь более или менее линейным. Заметно также, что при 50%-ном содержании бентонита зависимость близка к значениям сопротивлений для 100%-ного бентонита. Однако, в общем характер зависимостей очень близок к уже обсуждавшимся зависимостям для аргиллитов с органическим компонентом (образцы U1, U5).

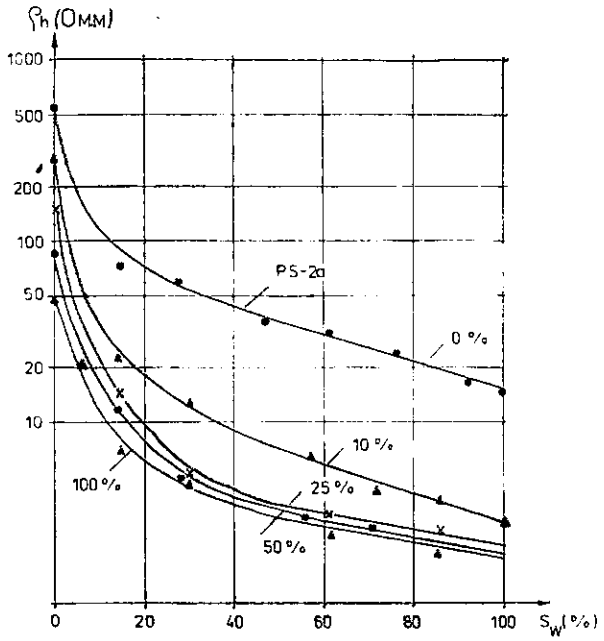

3. Влияние содержания бентонита на изменения удельных сопротивлений песка PS-2a при разной влажности S_w

Если сравнить характер изменений зависимости с предполагаемым изменением по теории перколяции, необходимо отметить, что зависимости не содержат „линейной" части до т. наз. порогового значения, или что порог смещен к значению близкому к $S_w = 0$.

Для проверки воспроизводимости результатов исследований были проведены контрольные исследования второго и третьего образцов из того же района (рис. 4). Графики свидетельствуют о том, что характер изменений такой же, рассеяние точек вызвано несколько другой пористостью, т. е. неточностью при заполнении пор.

Изучались также горные породы из некоторых рудоносных областей, именно из районов Злате Горы (скважина ЗГ-2093) и Суха Рудна (скважина СРВ-4), содержащие разные количества пирита, пирротина, иногда также графита.

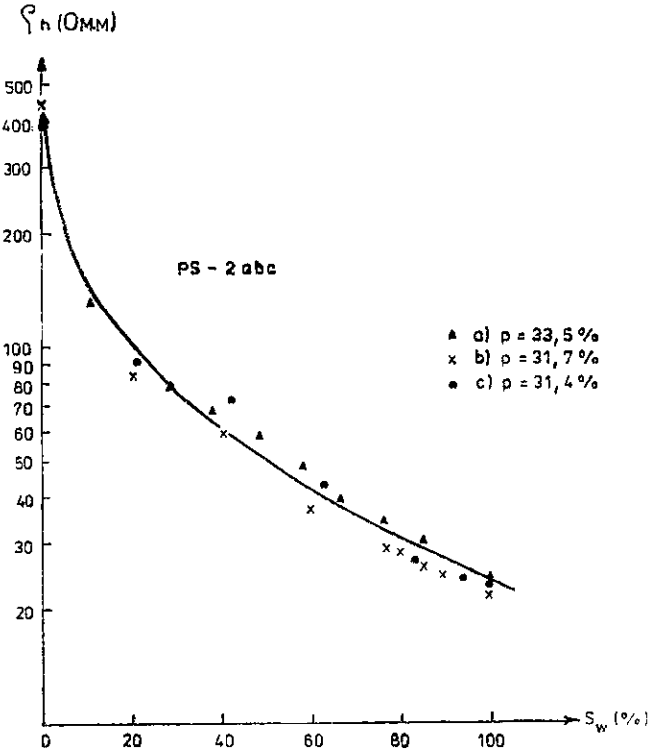

4. Зависимость удельных сопротивлений от влажности образцов слабоглинистых песков PS-2a, PS-2b, PS-2c. Контроль воспроизводимости результатов

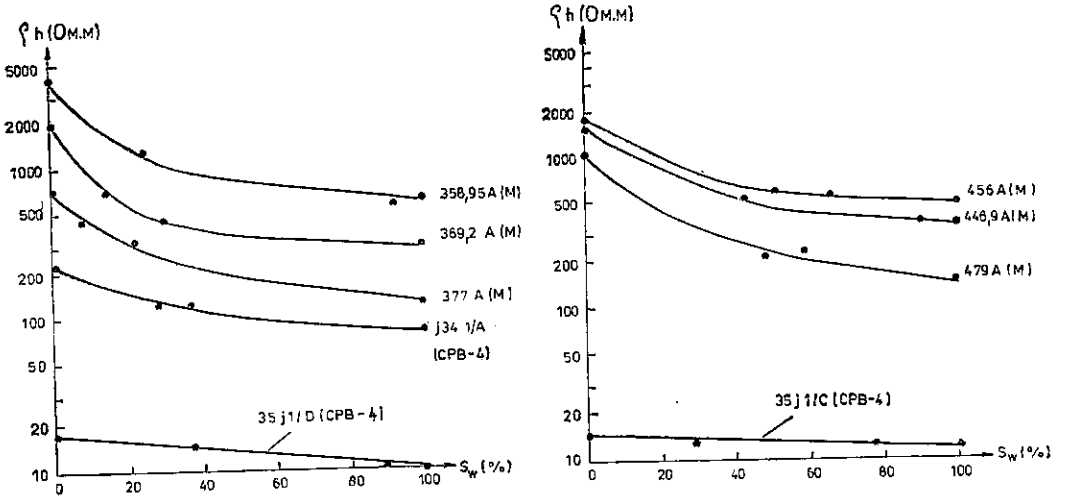

5. Примеры зависимости удельных сопротивлений от влажности некоторых образцов из районов Злате Горы (скважина ЗГ-2093) и Суха Рудна (скважина СРВ-4)

Полученные результаты приводятся на рис. 5. Зависимости удельных сопротивлений от влажности обладают обычным характером, значения ϱ_h понижаются с ростом влажности, сначала быстрее, а при более высокой степени насыщения – медленнее. Необходимо обратить внимание на то, что пористость этих образцов низка и колеблется в пределах $p = 0{,}2-2$ % (Kozel 1985), так что понижение удельных сопротивлений от влажности довольно низко. Далее видно, что высокое содержание графита (см. керны N°N° 35C, D) вызывает существенное понижение удельного сопротивления уже у сухих образцов, так что характер зависимости в данном масштабе нельзя четко различить, однако понижение удельного сопротивления от влажности хорошо заметно. В заключение к этим примерам (рис. 5) хотелось бы еще заметить, что влияние пирита и графита на удельные сопротивления и относительные диэлектрические проницаемости детальнее рассматривается в частном заключительном отчете (Kozel 1985).

Если обобщить результаты названных выше исследований, можно сказать, что „перколяционного характера", т. е. резкого увеличения удельной проводимости с какого-то порога V_p установлено не было, только, допустим, в случае, если бы порог V_p был сдвинут в область значений $S_w = 0$. Однако, мы ни в коем случае не собираемся существование перколяционного характера отрицать. Вполне логично, что при увеличении объема проводящих частиц, находящихся в непроводящей среде, при определенном, пороговом количестве, когда зерна начнут соприкасаться, должно произойти резкое увеличение проводимости. Однако, кажется, что у общераспространенных горных пород, особенно если они частично влажны, нет такого контраста между проводящим и непроводящим компонентами, чтобы перколяционный характер мог проявиться.

Что касается факта, что не слишком сухие породы отличаются удельным сопротивлением близким к сопротивлению совершенно мокрых пород, как об этом говорилось в предыдущей работе автора (Kozel 1989), то легко понять, что этот факт вытекает из общих изменений $\varrho_h = f(S_w)$. Целый ряд полученных результатов свидетельствует о том, что приблизительно с $S_w = 50$ % понижение удельных сопротивлений является довольно низким. Этот факт может иметь большое значение для практики полевых малоглубинных исследований.

Характер изменений относительной диэлектрической проницаемости от влажности разных типов горных пород и технических материалов

В предыдущей работе автора (Kozel 1989) сказано, что изучение зависимостей относительных диэлектрических проницаемостей от влажности будет продолжено с целью объяснения петрофизических условий для существования линей-

ного или нелинейного характера зависимости $\varepsilon_r = f(S_w)$. Для целей решения этого вопроса проводились следующие измерения.

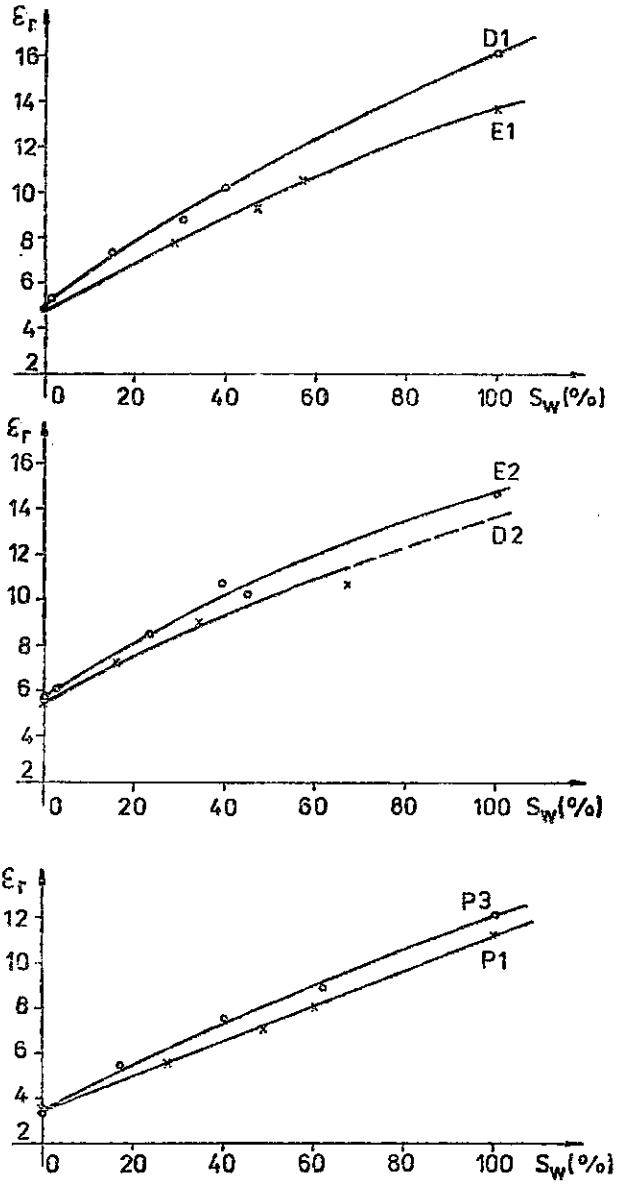

6. Примеры зависимости относительных диэлектрических проницаемостей от степени насыщения туфов и песчаников

пронумерованных X1 – X9. Для целей проверки однородности кирпича у всех образцов определялись параметры плотности. Полученные результаты приводятся в табл. 3, которая дополнена значениями относительных диэлектрических проницаемостей совершенно сухих и полностью насыщенных водой образцов, где $\varrho_w = 7$ омметров.

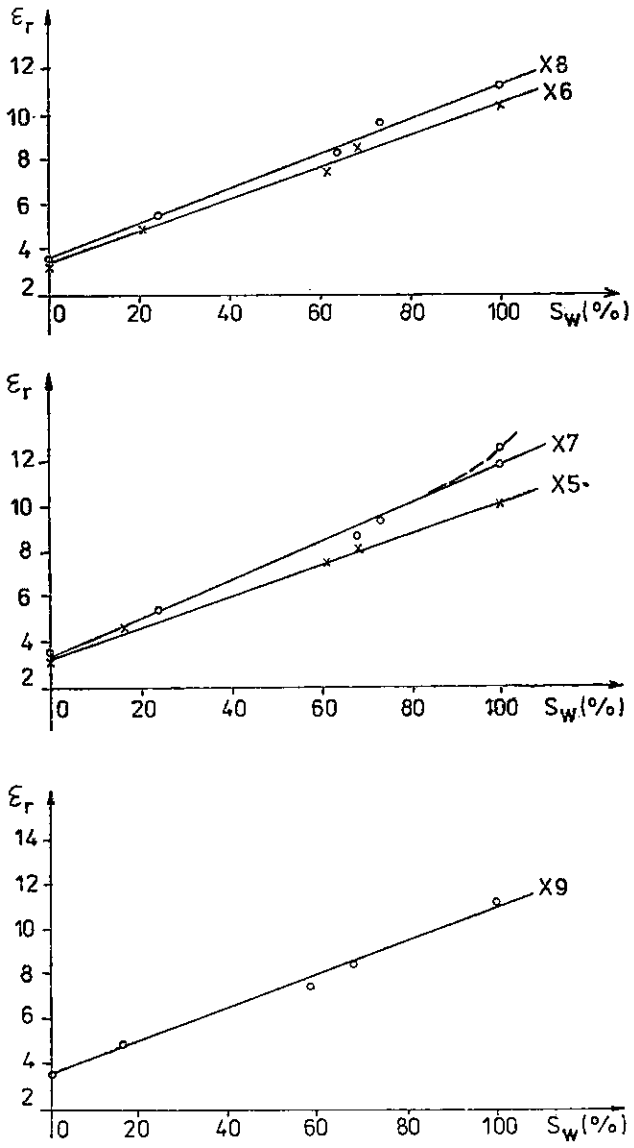

7. Зависимость относительной диэлектрической проницаемости от влажности кирпичного пола

Что касается параметров плотности, видно, что значения плотности друг от друга не слишком отличаются. Пористость этого материала является довольно большой, в большинстве случаев она приближается к значениям $p = 30\ \%$, однако значения относительных диэлектрических проницаемостей при $S_w = 100\ \%$ относительно низки, $\varepsilon_r \doteq 11{,}4$. Это значение гораздо меньше значения, установленного для той же частоты $f = 80$ МГц и приблизительно такой же пористости аргиллитов с органическим компонентом, где $\varepsilon_r = 16$.

Для целей более детального изучения изменений $\varepsilon_r = f(S_w)$ образцы X5–X9 после частичного насыщения порового пространства подверглись более детальным исследованиям. Полученные результаты приводятся на рис. 7. Можно сказать, что в случае всех этих образцов значения относительной диэлектри-

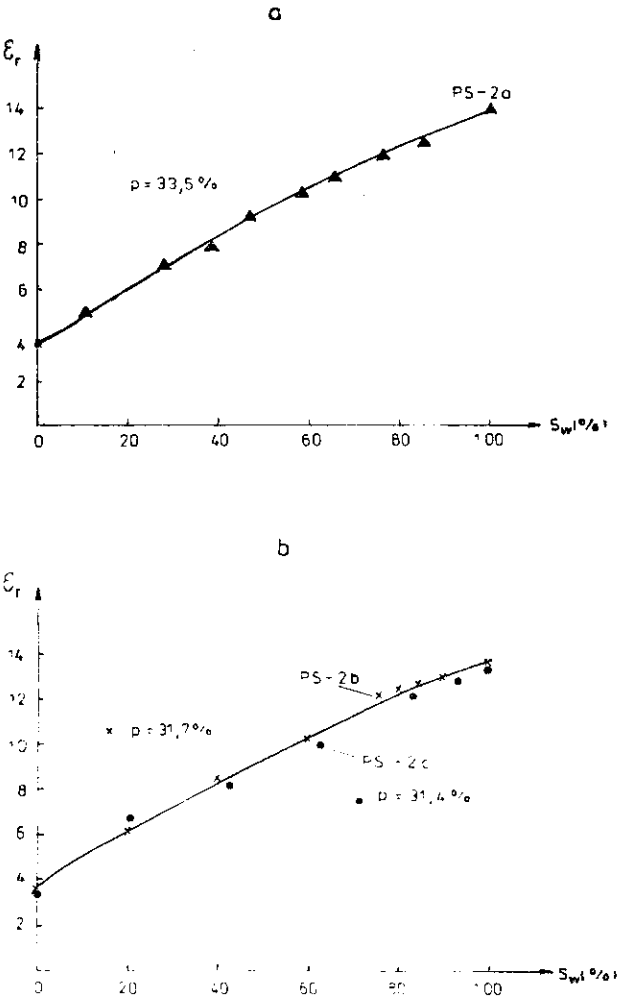

8. *a* — зависимость относительной диэлектрической проницаемости от влажности слабоглинистого песка PS-2a; *b* — контроль воспроизводимости результатов — образцы PS-2b, PS-2c

ческой проницаемости линейно растут с влажностью. Что касается отклонения (обозначено штриховой линией) по образцу X7, то оно вызвано чрезмерной влажностью поверхности образца при измерении при $S_w = 100\ \%$. После удаления этой избыточной влажности значение понизилось и зависимость стала линейной.

В конце настоящей части необходимо коснуться еще результатов измерений песка PS-2a из карьера Брно-Черновице, по которому зависимость удельного сопротивления от степени насыщения S_w уже обсуждалась. Кривая на рис. 8 (*a*) свидетельствует о том, что зависимость является слегка нелинейной. Для контроля воспроизводимости результатов на рис. 8 (*b*) показаны результаты по второму и третьему образцам из того же района (PS-2b, PS-2c). Сравнение обоих рисунков подтверждает, что зависимости являются практически тождественными и что было достигнуто очень хорошей воспроизводимости.

Ради полноты необходимо сказать, что в работе Kozel (1985) изучались также другие образцы рыхлых горных пород, а именно, образцы грунтов с примесью глин, трав, хвои и т. п., а также образцы без этих примесей. Также в этом случае подтвердилось, что примесь глин вызывает нелинейный характер зависимости $\varepsilon_r = f(S_w)$ и повышение значений ε_r для $S_w = 0$.

Анализы зависимости относительной диэлектрической проницаемости от степени насыщения горных пород из наших районов, которые исследовались некоторыми другими авторами

В дипломной работе Яшека (Jašek 1984) описывается большее количество определений зависимости $\varepsilon_r = f(S_w)$. Эти работы проводились в нашей лаборатории. Исследованию подверглись прежде всего технические материалы, как кирпич из терезианской крепости, образцы из дорожного полотна, каменно-керамический материал больших труб и т. п. Результаты приводятся Яшеком в форме таблиц. Некоторые его измерения показаны на рис. 9. Образцы J1 и J6 — это пластинки из терезианского кирпича, K1 и K2 — образцы из каменно-керамической трубы, A1 — образец из битумного слоя и H2 — образец из верхнего слоя бетона автомагистрали.

Кривые на рис. 9 свидетельствуют о том, что в большинстве случаев имеют место приблизительно линейные зависимости ε_r от S_w. Однако, необходимо заметить, что в случае приведенного образца J1 (и то же самое было установлено нами также у других образцов, приведенных в работе Яшека) происходит резкое, фиктивное увеличение ε_r при $S_w \to 100\ \%$. Мы думаем, что это вызвано т. наз. избыточной по сравнению с предположением для $S_w = 100\ \%$ водой на поверхности образца. С этим явлением мы встретились при исследовании кирпичного пола (рис. 7, образец X7). После поправки за это явление линейная зависимость $\varepsilon_r = f(S_w)$ становится еще более четкой.

В заключительном отчете Земчиковой (Zemčíková 1981) основное внимание уделяется определению влияния влажности на поведение относительной диэлектрической проницаемости. Было проведено исследование шести разных образцов пористостью $p = 1{,}3-8{,}5$ % при разной степени насыщения порового пространства. У всех предполагается приблизительно линейная зависимость $\varepsilon_r = f(S_w)$. С помощью обработки результатов этих исследований, которые приводятся нами в виде кривых на рис. 10, Земчикова находит способ определе-

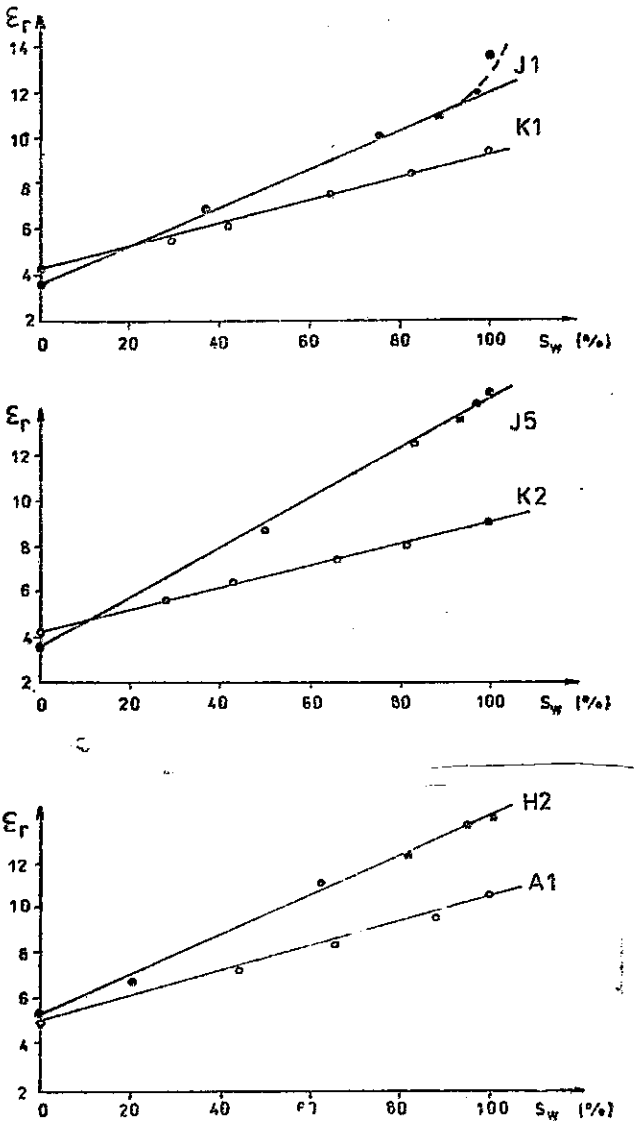

9. Зависимость относительных диэлектрических проницаемостей от влажности некоторых технических материалов (по результатам Г. Яшека)

ния измерений ε_r под влиянием влажности, если известны пористость p, степень насыщения S_w и относительная диэлектрическая проницаемость в сухом состоянии ε_0.

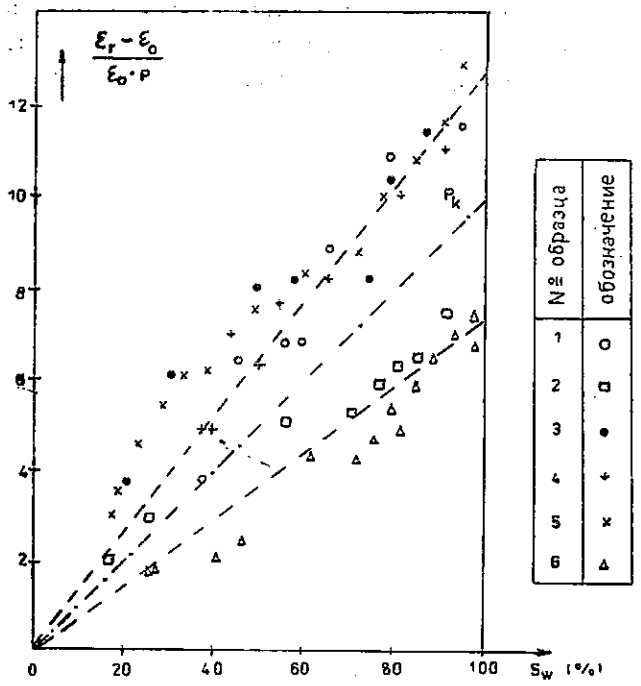

10. Нормированное изменение относительной диэлектрической проницаемости в зависимости от степени насыщения (по данным Я. Земчиковой)

Влияние „глинистости" на изменения относительных диэлектрических проницаемостей в зависимости от влажности

Анализы, проведенные в предыдущей части, имели своей целью накопление данных, которые привели бы к объяснению разного характера зависимости $\varepsilon_r = f(S_w)$. Так как классификация по пористости (см. Краев 1951) может быть проблематичной (аргиллит с органическим компонентом U1 обладает p приблизительно 30 % и той же пористостью отличается также кирпичный пол, образцы X1 – X9), напрашивается возможность заниматься влиянием глинистости. С этой точки зрения приходим к заключению, что для т. наз. неглинистых горных пород или технических материалов будем, как правило, получать линейные зависимости относительных диэлектрических проницаемостей от степени насыщения пор водой. К этой группе можно относить породы и технические материалы, как напр. кристаллические породы с м. Дубрава, измерение которых описано автором (Kozel 1989), разные типы гранитных пород, обожженные глины, кирпич из терезианской крепости Йосефов, образцы из пола собора

в г. Збраслав, образцы из битумного слоя автомагистрали, каменно-керамический материал сточных труб и другие образцы. Можно предполагать, что к этой группе будет относиться большая часть изверженных и метаморфических горных пород.

Ко второй группе т. наз. глинистых горных пород можно отнести прежде всего аргиллиты с органическим компонентом, пески с бентонитом, частично доломитовые туфы, к ней относятся также песчаники с большей степенью глинистости. В работе авторов Uhmann–Kozel (1957) приводятся также примеры резкого увеличения зависимости ε_r от влажности в начальной стадии насыщения аргиллитов из района Лужице. С этим хорошо согласуется также работа, опубликованная Рикитаки (Rikitaki 1951). По результатам его исследований относительная диэлектрическая проницаемость почвы ε_r при увеличении влажности S_w от 0 до 50 % увеличивается по кривой, близкой к параболе, от $\varepsilon_r = 3$ до $\varepsilon_r = 40$.

Необходимо также заметить, что под понятием глинистость в данном случае не подразумевается только содержание частиц, размеры которых меньше 0,01 мм, как это часто имеет место. Глинистость считается физико-химическим проявлением породы, где наряду с содержанием частиц, меньших 0,01 мм, роль играют также качество цемента, степень сцементированности, криволинейность пор и т. д., т. е. понятие глинистости в данном случае соответствует понятию глинистости в электрическом каротаже. Известны также способы количественного определения глинистости (Вендельштейн 1960, Kozel 1969, Schlumberger Corp. 1972a,b).

Электрическая модель порового пространства

Относительно резкое увеличение значений относительных диэлектрических проницаемостей глинистых пород в начальной фазе насыщения (в случае аргиллитов с органическим компонентом это было приблизительно до $S_w = 20$ %) объясняем с помощью следующего представления, опирающегося на модель электрического двойного слоя, образующегося внутри порового канала осадочных пород.

Согласно часто применяемому представлению поровое пространство отложений можно заменить системой капилляров, на стенках которых находится электрический заряд. Этот в большинстве случаев отрицательный заряд компенсируется ионам H^+, Na^+, Ca^{++} ... из порового раствора. Таким образом на границе твердой и жидкой фаз образуется электрический двойной слой.

В случае глинистых горных пород возникновение заряда можно по Гриму (Grim 1959) иллюстрировать на примере мицеллы SiO_2 (рис. 11). В результате диссоциации кремневой кислоты образуются катионы H^+ и анионы SiO_3^{--}. Анионы SiO_3^{--} остаются на поверхности ядра SiO_2 и придают ему отрицатель-

ный заряд; таким образом они образуют внутреннюю оболочку электрического двойного слоя. Внешней оболочкой являются катионы H^+, которые с определенной интенсивностью притягиваются к отрицательной поверхности.

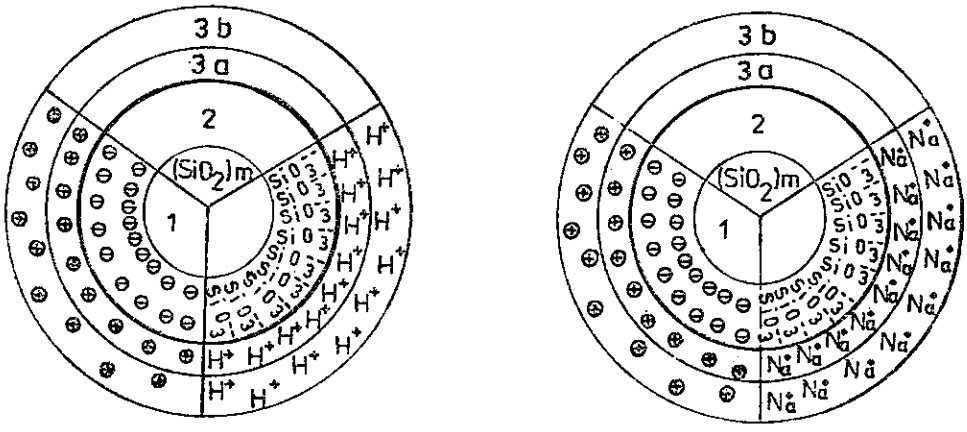

11. Образование электрического двойного слоя на примере мицеллы SiO_2
1 — ядро мицеллы; *2* — внутренняя оболочка электрического двойного слоя; *3a, b* — внешняя оболочка двойного слоя

Таким образом образуется трехслойная модель:

1 — ядро мицеллы, т. е. твердая фаза, которая с электрической точки зрения нейтральна;

2 — слой отрицательного заряда, прилипающий к поверхности ядра и относящийся к твердой фазе породы (внутренняя часть электрического двойного слоя);

3 — слой положительного заряда, образованный катионами, находящимися в контактном растворе (наружная часть электрического двойного слоя); по некоторым представлениям (Buzagh 1958) его можно разделить на две части *3a*, *3b* (рис. 11).

В естественных условиях под влиянием разной минерализации поровых растворов происходят разные ионообменные процессы. Таким образом по Вендельштейну (1960) и Козелу (Kozel 1966) глинистую породу можно перевести на тип Na^+, K^+ или Ca^{++}. Пример электрического двойного слоя с внешней оболочкой, сложившейся из ионов Na^+ приводится также на рис. 11.

Применением приведенных моделей для объяснения возникновения диффузионно-адсорбционных потенциалов занимались Эйдманн (1956), а также Kozel (1966). На основании этих работ электрическую модель порового канала можно себе представить способом, приведенным на рис. 12:

(*a*) При 100 %-ном насыщении пор раствор заполняет пространство внешней части электрического двойного слоя и в середине пор находится т. наз. свобод-

ный раствор, на который электрическое поле двойного слоя уже не действует.

(*b*) При полном (ввиду имеется стандартном) высушивании $S_w = 0$, что у глинистых пород является в определенной степени релятивным (кристаллическая вода), предполагаем, что вода удаляется сначала из мест свободного раствора и затем из обоих слоев внешнего двойного слоя (*3a*, *3b*).

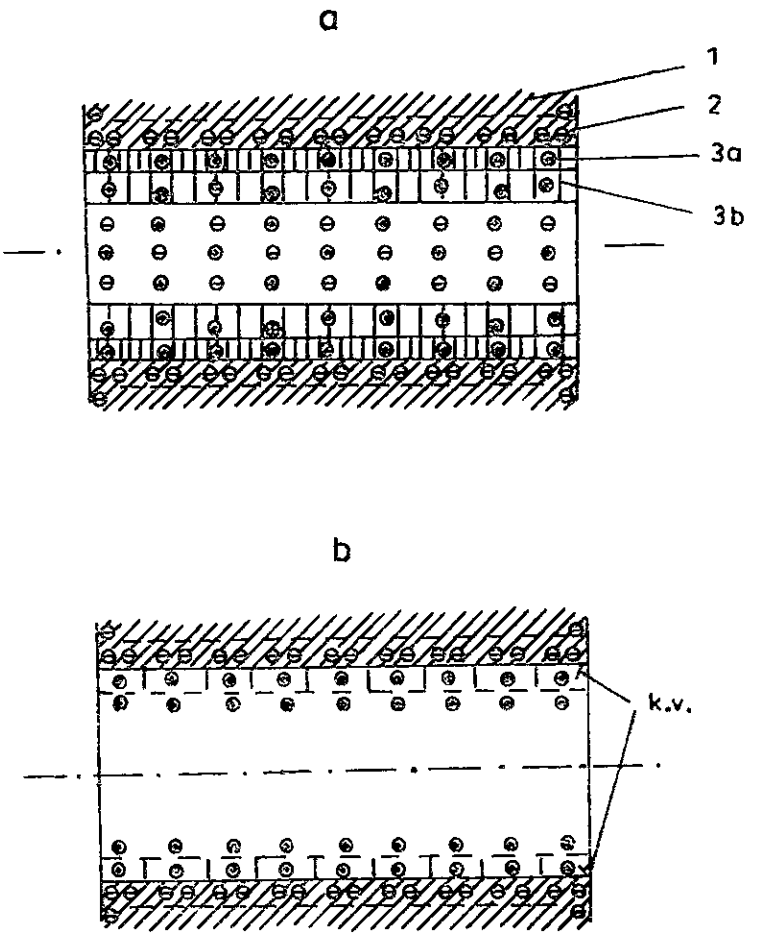

12. Электрическая модель порового канала породы
1 — ядро мицеллы; *2* — внутренняя оболочка электрического двойного слоя; *3a* — адсорбционный слой; *3b* — диффузионный слой; *a* — насыщение $S_w = 100$ %; *b* — насыщение $S_w = 0$ %; *k. v.* — „кристаллическая вода" (при стандартном высушивании)

Для частичного насыщения глинистой породы (в размере единиц S_w) у гидрофильных пород можно предполагать, что влажность распределяется более или менее равномерно по стенкам пор и заполняет пространства слоев *3a* и *3b*

(т. наз. слоев Стерна и Гуйова). Ионы этих слоев по отношению к слою 2 можно себе представить как параллельно расположенные микроконденсаторы, которые существенно содействуют увеличению относительной диэлектрической проницаемости.

После заполнения пространства внешней части электрического двойного слоя происходит постепенное заполнение пространства т. наз. свободного раствора и относительная диэлектрическая проницаемость увеличивается уже практически линейно.

Для случая экстремально глинистых горных пород (мембран) можно предполагать, что пространством т. наз. свободного раствора можно пренебречь и, следовательно, участок с линейным увеличением $\varepsilon_r = f(S_w)$ в форме зависимости не проявится.

Аналитическое выражение зависимости $\varepsilon_r = f(S_w)$

Для неглинистых горных пород можно принять формулу

$$\varepsilon_r = \varepsilon_{r_{100}} \cdot S_w + \varepsilon_{r_0} \cdot (1 - S_w).$$

Для глинистых пород ищутся пути, как долю, которая при частичном и полном насыщении приводит к повышению относительных диэлектрических проницаемостей, учесть в предыдущей формуле. Из разных возможностей было бы, может быть, подходящим введение в формуду т. наз. глинистостей B. В результате этого можно было бы получить:

$$\varepsilon_r = \varepsilon_{r_{100}} \cdot S_w + \varepsilon_{r_0} \cdot (1 - S_w) + B \cdot f(S_w).$$

Однако, в данной стадии работ пока еще нет достаточного материала для количественного определения члена $B \cdot f(S_w)$. Затруднение заключается в том, что в нашем распоряжении имеется лишь небольшое количество результатов измерений глинистых горных пород и их глинистость B в большинстве случаев оценивается по макроскопическому описанию горной породы. Поэтому желательно продолжить работы по этой проблематике, постепенно проводить дальнейшие исследования и на следующем этапе эту формулу уточнить.

Зависимость относительных диэлектрических проницаемостей от пористости горных пород

При полном заполнении порового пространства можно в общем сказать, что относительная диэлектрическая проницаемость будет увеличиваться по мере увеличения пористости. Если полученные результаты выразить графически, можно получить очень свободную связь относительной диэлектрической прони-

цаемости с пористостью (рис. 13). Рассеяние данных обусловлено прежде всего горными породами низкой пористости $p \doteq 1-3\,\%$, минеральный состав которых вызывает относительно высокие значения относительных диэлектрических проницаемостей. Это, напр., изученный автором антимонит (Kozel 1989), из литературы известны мраморы ($\varepsilon_r = 8{,}3$), филлиты ($\varepsilon_r = 13{,}0$), габбро ($\varepsilon_r = 9$ до 10) и т. д. (Пархоменко 1956). Наоборот, значения относительных диэлектрических проницаемостей большинства осадочных пород, особенно неглинистых, находятся в предполагаемом диапазоне пористостей $\varepsilon_r = 3-5$.

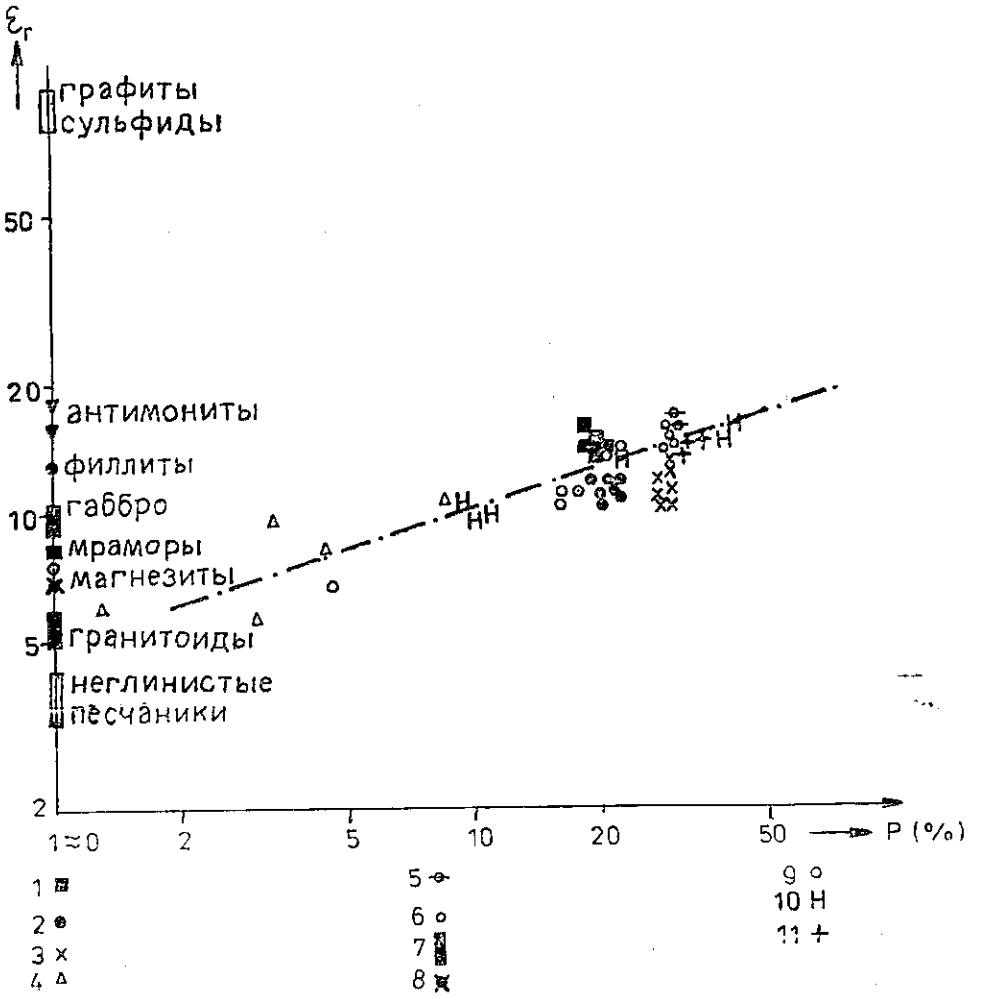

13. Связь относительной диэлектрической проницаемости с пористостью пород
1 — доломитовые туфы; *2* — песчаники P1—P8; *3* — образцы X1—X9; *4* — образцы Я. Земчиковой; *5* — аргиллиты с органическим компонентом; *6* — порцелланиты; *7* — гранодиориты с м. Дубрава; *8* — магнезиты; *9* — графитовые сланцы; *10* — образцы Г. Ящека; *11* — песок из карьера Брно-Черновице

По мере увеличения пористостей (при $S_w = 100\ \%$) происходит увеличение относительных диэлектрических проницаемостей, которые по данным исследований достигают значений $\varepsilon_r \approx 15$, причем для той же пористости (напр. $p \approx 30\ \%$) можно предполагать большее увеличение относительных диэлектрических проницаемостей глинистых пород, чем в случае неглинистых. Однако, и здесь может иметь место целый ряд исключений. Значения, превышающие 81, т. е. ε_r воды, отмечены у графита, некоторых сульфидов и т. д. (Пархоменко 1965).

Для целей более удобной обработки зависимости относительных диэлектрических проницаемостей от пористости мы ввели отношение относительных диэлектрических проницаемостей совершенно насыщенной и совершенно сухой горных пород $\varepsilon_{r_{100}}/\varepsilon_{r_0}$. Таким образом как будто исключается влияние минерального состава. Потом, в отличие от свободной связи (рис. 13), находим зависимость отношения относительных диэлектрических проницаемостей от пористости, которая приводится на рис. 14.

Для частот $f = 80$ МГц, при которых исследовались обсуждаемые образцы, зависимость $\varepsilon_{r_{100}} = \varepsilon_{r_0} \cdot f(p)$ можно выразить также посредством приближенной аналитической формулы. Для пористых рыхлых и уплотненных горных пород и близких к горным породам материалов приблизительно действительно:

$$\varepsilon_{r_{100}} \doteq \varepsilon_{r_0}(1 + 0{,}080 \cdot p);\ p(\%)$$

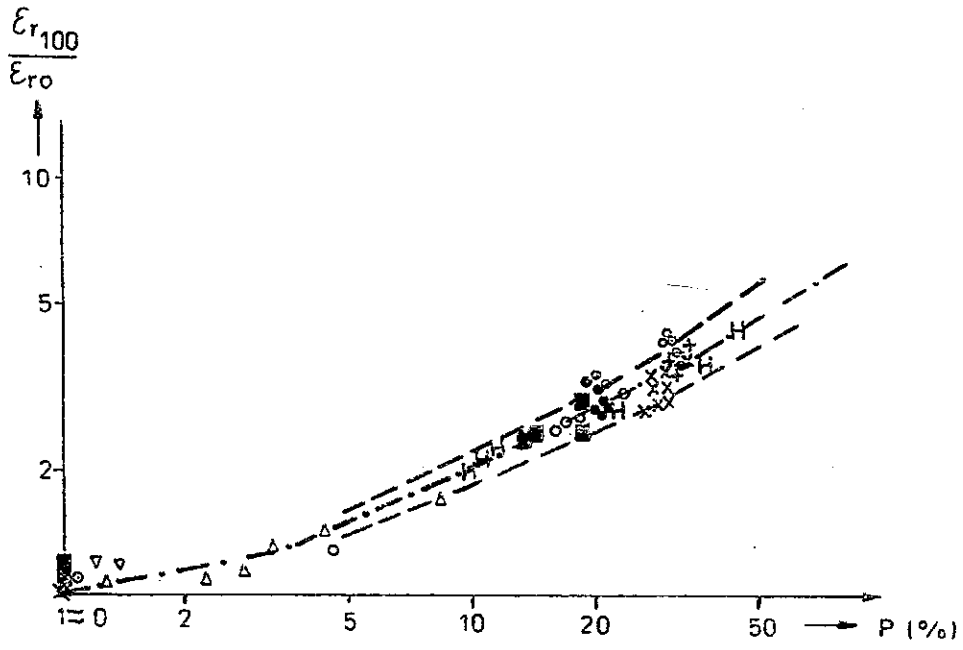

14. Зависимость отношения относительных диэлектрических проницаемостей от пористости горных пород и технических материалов

Результаты исследований, приведенные на рис. 14, целесообразно будет в течение дальнейшего этапа дополнить еще исследованием глинистых пород, почв и других покрывающих материалов и в случае необходимости уточнить, напр., по литологическим типам горных пород и т. д.

Обобщение результатов

В работе обсуждаются теоретические формулы для зависимости удельных сопротивлений и относительных диэлектрических проницаемостей от влажности осадочных, изверженных, рудоносных пород. Описывается т. наз. перколяционная теория, с помощью которой в последнее время объясняются аномальные характеристики изменений удельных сопротивлений в зависимости от влажности. Был проведен целый ряд практических исследований этих зависимостей на выбранных породах ЧССР. Изучались также некоторые технические материалы, близкие к горным породам, как напр. кирпичный пол, каменно-керамический материал сточных труб, образцы из дорожного полотна и т. д. Исследования предоставили целый ряд новых, конкретных данных как по исследовавшимся породам, так и по техническим материалам, которые при частоте $f = 80$ МГц в литературе описываются лишь изредка.

Из изучения зависимости удельных сопротивлений от влажности вытекает, что у исследовавшихся образцов горных пород из разных районов ЧССР лишь с трудом можно говорить о т. наз. перколяционной характеристике зависимости; может быть, лишь тогда, когда порог V_p резкого увеличения проводимости сдвинут в область значений, близких $S_w \approx 0$. Такой же результат можно установить также по модели порового канала осадочной горной породы.

На основании изучения зависимостей $\varepsilon_r = f(S_w)$ разных типов горных пород и технических материалов были получены новые, оригинальные сведения о поведении относительных диэлектрических проницаемостей глинистых пород разной влажности. В случае этих пород с помощью электрической модели порового канала новым способом объяснены нелинейные изменения зависимости $\varepsilon_r = f(S_w)$. Ведутся поиски способов аналитического выражения этой зависимости.

В заключительной части работы проведен анализ зависимости относительных диэлектрических проницаемостей от пористости. Введение отношения $\varepsilon_{r100}/\varepsilon_{ro}$ позволило учитывать и количественно выражать зависимость отношения относительных диэлектрических проницаемостей от пористости глинистых и неглинистых горных пород.

K tisku doporučila M. Laštovičková

Přeložila E. Pešková

Литература

Вендельштейн, Б. Ю. (1960): О природе диффузионно-адсорбционных потенциалов. — Прикл. геофиз., 26. Москва.

Даев, Д. С. (1980): Диэлектрический каротаж. — Труды 25-го междунар. геофиз. симп., 2. Секешфехервар.

Дахнов, В. Н. (1962): Интерпретации результатов геофизических исследований разрезов скважин. — Гостоптехиздат. Москва.

Карус, Е. В. и др. (1980): Выделение и оценка коллекторов нефти и газа. — Труды 25-го междунар. геофиз. симп., 2. Секешфехервар.

Краев, А. П. (1951): Основы геоэлектрики. — Гос. издат. научно-техн. литературы. Москва, Ленинград.

Пархоменко, Э. И. (1965): Электрические свойства горных пород. — Издат. Наука. Москва.

Пархоменко, Э. И.—Мкртчян, С. А. (1974): Химический состав и электропроводность минералов при высоких давлениях и температурах. — Изв. Акад. наук СССР, Физ. Земли, 12. Москва.

Челидзе, Т. Л. (1979): Перколяционная модель электропроводности минералов. — Изв. Акад. наук СССР, Физ. Земли, 11. Москва.

Шкловский, Б. И.—Эфрос, А. Л. (1975): Теория протекания и проводимость сильно неоднородных сред. — Усп. физ. наук, 117. Москва.

Эйдманн, И. Е. (1956): Об электрокаротажных параметрах. — Прикл. геофиз., 14. Москва.

Bitterlich, W.—Wöbking, H. (1972): Geoelektronik. — Springer Verl. Wien, New York.

Buzagh, A. (1958): Koloidika. — Vyd. Slov. akad. vied. Bratislava.

Carmichael, R. S., ed. (1986): Handbook of physical properties of rocks, vol. I. — CRC Press, Inc., Sec. Printing. New York.

Grim, R. E. (1959): Минералогия глин. — Издат. иностр. лит. (перевод с англ.). Москва.

Jašek, H. (1984): Geofyzikální radiolokační metoda. — Dipl. práce, přírodověd. fak. Karl. univ. Praha.

Keller, G. V. (1966): Electrical properties of rock and minerals. — Handbook of physical constants. New York.

Kirkpatrick, S. (1973): Percolation and conduction. — Rev. mod. Phys., 45. New York.

Kozel, J. (1966): Difúzně adsorpční potenciály. — Kand. dis. práce, Úst. užité geofyz. Brno.

— (1969): Зависимость собственных потенциалов от удельной поверхности осадочных горных пород. — Sbor. geol. Věd, užitá Geofyz., 8, *117—138*. Praha.

— (1983): Výzkum měření elektrické permitivity hornin. — MS Geofond. Praha.

— (1985): Výzkum elektrických vlastností hornin s iontovou a elektrickou vodivostí v oblasti 10^8 Hz. — MS Geofond. Praha.

— (1989): Относительные диэлектрические проницаемости и удельные сопротивления горных пород в диапазоне частот 10^6—10^8 Гц. — Sbor. geol. Věd, užitá Geofyz., 23, *85—102*. Praha.

Rikitaki, T. (1951): Electrical properties of soil at radio frequencies. — Bull. Earthquake Res. Inst., 29. Tokyo.

Schankl, T. J.—Waff, H. S. (1974): Conduction in fluid-bearing rock. — J. geophys. Res., 79. Washington.

Schante, V. K.—Kirkpatrick, S. (1971): An introduction to percolation theory. — Advances in Geophys., 20. London, New York.

Schlumberger Corp. (1972a): The essentials of log interpretation practice. — Paris.

— (1972b): Log interpretation, vol. I. Principles. — Washington.

Uhmann, J.—Kozel, J. (1957): Výzkum elektrických vlastností hornin naftonadějných oblastí ČSR. — MS Úst. pro naft. výzk. Brno.

Zemčíková, J. (1981) *in* Záhora, R.—Kunzmann, R. et al. (1981): Geofyzikální radiolokační metoda, část I. — MS Geofyzika, s. p. Brno.

Změny měrných odporů a poměrných permitivit s vlhkostí při frekvenci f = 80 MHz

(*Résumé ruského textu*)

Josef Kozel

Předloženo 9. března 1988

V předložené práci byly diskutovány teoretické vztahy pro závislost měrných odporů a poměrných permitivit na vlhkosti hornin sedimentárních i hornin vyvřelých, rudonosných. Byla popsána tzv. perkolační teorie, kterou se v poslední době vysvětlují anomální průběhy změn měrných odporů na vlhkosti (obr. 2). Byla provedena řada praktických měření těchto závislostí u vybraných hornin z území ČSSR (obr. 1, 3, 4, 5). Rovněž byly zkoumány i některé technické materiály blízké horninám, jako je například cihlová dlažba, cihly, kamenina odpadních rou-, vzorky z dálničního tělesa apod. (obr. 6 až 11). Měření přineslo řadu nových konkrétních poznatků na studovaných horninách i technických materiálech, které při zvolené frekvenci f = 80 MHz jsou v literatuře uváděny jen ojediněle.

Ze studia závislosti měrných odporů na vlhkosti vyplynulo, že u sledovaných vzorků hornin z různých lokalit ČSSR lze stěží hovořit o tzv. perkolačním průběhu závislosti, snad jen tak, že by byl práh V_p pro prudký nárůst vodivosti posunut do hodnot blízko $S_w = 0$. To lze vyvodit i z modelu pórového kanálku sedimentární horniny (obr. 12).

Na základě studia vztahů $\varepsilon_r = f(S_w)$ u různých typů hornin a technických materiálů byly získány nové, původní poznatky o chování poměrných permitivit jílovitých hornin s různou vlhkostí. U těchto hornin byl pomocí elektrického modelu pórového kanálku (obr. 12) originálním způsobem vysvětlen nelineární průběh závislosti $\varepsilon_r = f(S_w)$. Je hledána cesta pro analytické vyjádření tohoto vztahu.

V závěru práce je proveden rozbor závislostí poměrných permitivit na pórovitosti (obr. 13). Zavedením poměru $\varepsilon_{r100}/\varepsilon_{r0}$ se podařilo vystihnout a kvantitativně vyjádřit závislost poměru poměrných permitivit na pórovitosti pro jílovité i nejílovité horniny (obr. 14).

Vysvětlivky k tabulkám

Tabulka 1. Hustotní parametry a poměrné permitivity některých hornin z lokality Bankov.
Tabulka 2. Hustotní parametry a poměrné permitivity některých vybraných pískovců.
Tabulka 3. Hustotní parametry a poměrné permitivity vzorků z cihlové dlažby chrámu ve Zbraslavi.

Vysvětlivky k obrázkům

1. Závislost měrných odporů na stupni nasycení vodou pro uhelné jílovce U1, U5.
2. Závislost měrné vodivosti minerálů na obsahu vodivých oxidů. Perkolační model T. L. Čelidze.
3. Vliv obsahu bentonitu na změny měrných odporů písku PS-2a při různé vlhkosti S_w.
4. Závislost měrných odporů na vlhkosti pro vzorky slabě jílovitých písků PS-2a, PS-2b, PS-2c. Kontrola reprodukovatelnosti měření.
5. Ukázky závislosti měrných odporů na vlhkosti některých vzorků z oblasti Zlatých Hor (vrt ZH-2093) a Suché Rudné (vrt SRV-4).
6. Ukázky závislosti poměrných permitivit na stupni nasycení pro tufy a pískovce.
7. Závislost poměrné permitivity na vlhkosti cihlové dlažby.
8a. Závislost poměrné permitivity na vlhkosti pro slabě jílovitý písek PS-2a.
8b. Kontrola reprodukovatelnosti měření — vzorky PS-2b, c.
9. Závislost poměrných permitivit na vlhkosti pro některé technické materiály (podle měření H. Jaška).
10. Normovaná změna poměrné permitivity v závislosti na stupni nasycení (podle měření J. Zemčíkové).
11. Vznik elektrické dvojvrstvy na příkladu micely SiO_2.
    1 — jádro micely, *2* — vnitřní obložení elektrické dvojvrstvy, *3a*, *b* — vnější obložení dvojvrstvy.
12. Elektrický model pórovitého kanálku horniny.
    1 — jádro micely, *2* — vnitřní obložení elektrické dvojvrstvy, *3a* — vrstva adsorpční (Sternova), *3b* — vrstva difúzní (Gouyova), *a* — nasycení $S_w = 100\,\%$, *b* — nasycení $S_w = 0$, *k. v.* — „krystalická voda" (při standardním vysušení).
13. Vztah mezi poměrnou permitivitou a pórovitostí hornin.
    1 — dolomitické tufy, *2* — pískovce P1 — P8, *3* — vzorky X1 — X9, *4* — vzorky J. Zemčíkové, *5* — uhelné jílovce, *6* — porcelanity, *7* — granitoidy ložiska Dúbrava, *8* — magnezity, *9* — grafitické břidlice, *10* — vzorky H. Jaška, *11* — písek — Brno-Černovice.
14. Závislost poměru poměrných permitivit na pórovitosti hornin a technických materiálů.

Dependences of resistivities and relative permittivities on moisture content at the frequency of f = 80 MHz

The theoretical relations for dependences of resistivities and relative permittivities on the moisture content of ore-bearing sedimentary and igneous rocks are discussed. The so-called percolation theory is described which has recently served for an explanation of anomalous dependences of resistivities on the moisture content. Several measurements of these dependences are studied, which were conducted on the rocks from the Czechoslovak territory as well as for some technical materials. By means of an electric model of the pore channel of a sedimentary rock the detected nonlinear dependence of relative permittivities of argillaceous rocks on the rate of pore saturation with weakly mineralized water is explained. Attempts are made to express this relation analytically.

Přeložil G. Plíva

Sbor. geol. věd	Užitá geofyz., 24	Pages 185–199	8 figs.	1 tab.	– pl.	Praha 1990 ISSN 0036-5319

The influence of electric current transmission through mud on the measurements of self potentials

Vliv propouštění elektrického proudu výplachem na měření vlastních potenciálů

František Ryšavý[1]

Received October 27, 1987

Self-potential methods
Well-logging
Electrical resistance
Mud

Ryšavý, F. (1990): The influence of electric current transmission through mud on the measurements of self potentials. – Sbor. geol. Věd, užitá Geofyz., 24, *185–199*. Praha.

Abstract: In the rocks of higher geological ages exist some permeable beds that we cannot evaluate simply after a record of the specific electrical resistance and of the self potential. Characteristic of them is a relatively high specific electrical resistance of the invasion zone and a higher specific electrical resistance of the mud. The curve of the self potential in such beds is extraordinarily smooth and monotonous in character. It is similar to a curve of the self potential forming in a very salty mud. It seems, that both cases have a common cause – a low electric current transmission through the mud, which influences the self potential curve. We can make use of this fact for a recalculation of the self-potential curve to obtain a more differentiated curve allowing us to evaluate and locate the permeable beds.

[1] *Moravské naftové doly, k. p., Hodonín, Úprkova 6, 695 30 Hodonín*

If we measure by using the method of the self potential, the chemical composition of the mud plays a decisive role there. This has been published in the relevant literature. The author invites you to concentrate on the electric transmission of the mud and is going to attemp to explain this process, that can have an influence on the measurement of the self potential.

The origin of the self potential is based on the existence of a double electric layer forming on the boundary-line of the mud and rock or if need be on the boundary-line of two lithologically different rocks. We shall commit a certain

inaccurancy, when we assume, that an electric current source of self potential was found inside of the rock. Under these conditions, for a point being located inside of the mud, following formula has been accepted (after Dachnov, 1967):

$$U_{SP} = \frac{2R_m R_i}{R_m + R_i} \cdot \frac{I_{SP}}{4\pi r}, \tag{1}$$

where

I_{SP} – an electric current flowing between the rock and the mud [mA],
r – a distance between the electric current source and a point, where the potential U_{SP} is registered [m],
R_m, R_i – the specific electric resistance of the mud and the invasion zone [Ωm].

The formula (1) can be adapted as follows:

$$U_{SP} = \frac{2R_m}{R_m + R_i} \cdot I_{SP} \cdot \frac{R_i}{4\pi r}. \tag{2}$$

Now we shall use the following substitution:

$$E_{SP} = I_{SP} \cdot \frac{R_i}{4\pi r}. \tag{3}$$

Thus we shall obtain the next formula:

$$U_{SP} = \frac{2R_m}{R_m + R_i} \cdot E_{SP}, \tag{4}$$

where

U_{SP} – the self potential being registered by an electrode lying in the mud [mV],
E_{SP} – the self potential situated on the borehole wall [mV].

For E_{SP} the well-known Nernst's formula is accepted:

$$E_{SP} = -\alpha \cdot k_t \cdot \log\left(\frac{R_{mf}}{R_w}\right), \tag{5}$$

where

k_t – the lithological factor for NaCl solution [mV],
α – the shaliness of the rock,
R_{mf}, R_w – the specific electrical resistance of the mud filtrate and the stratum water [Ωm].

inaccurancy, when we assume, that an electric current source of self potential was found inside of the rock. Under these conditions, for a point being located inside of the mud, following formula has been accepted (after Dachnov, 1967):

$$U_{SP} = \frac{2R_m R_i}{R_m + R_i} \cdot \frac{I_{SP}}{4\pi r}, \tag{1}$$

where

I_{SP} – an electric current flowing between the rock and the mud [mA],
r – a distance between the electric current source and a point, where the potential U_{SP} is registered [m],
R_m, R_i – the specific electric resistance of the mud and the invasion zone [Ωm].

The formula (1) can be adapted as follows:

$$U_{SP} = \frac{2R_m}{R_m + R_i} \cdot I_{SP} \cdot \frac{R_i}{4\pi r}. \tag{2}$$

Now we shall use the following substitution:

$$E_{SP} = I_{SP} \cdot \frac{R_i}{4\pi r}. \tag{3}$$

Thus we shall obtain the next formula:

$$U_{SP} = \frac{2R_m}{R_m + R_i} \cdot E_{SP}, \tag{4}$$

where

U_{SP} – the self potential being registered by an electrode lying in the mud [mV],
E_{SP} – the self potential situated on the borehole wall [mV].

For E_{SP} the well-known Nernst's formula is accepted:

$$E_{SP} = -\alpha \cdot k_t \cdot \log\left(\frac{R_{mf}}{R_w}\right), \tag{5}$$

where

k_t – the lithological factor for NaCl solution [mV],
α – the shaliness of the rock,
R_{mf}, R_w – the specific electrical resistance of the mud filtrate and the stratum water [Ωm].

We can use the next substitution:

$$\eta = \frac{2R_m}{R_m + R_i}, \tag{6}$$

where η – the factor of the electric current transmission.
The equation (4) will be modified as follows:

$$U_{SP} = \eta \, . \, E_{SP}. \tag{7}$$

The equation (6) can be transformed into the following form:

$$\eta = \frac{2 \, . \, \frac{R_m}{R_i}}{1 + \frac{R_m}{R_i}} \, . \tag{8}$$

We shall attempt to analyse the two last-mentioned equations. We must distinguish the following cases:

1. $R_m \ll R_i$.

For such a case, there exist two causes. The first and better known can be caused by salting of mud after drilling through a salt bed or a bed of salty clays or shales. The second one which is less known, can occur after drilling through a rock having an outstanding specific electric resistance exceeding the specific electric resistance of the mud. The mud may be characterized by a low salinity.

Both cases lead to a common conclusion. The factor of the electric current transmission through mud is approaching for either cases to zero and with respect to equation (8) $\eta = 0$. Then we are able to record on the measuring electrode in the mud only $U_{SP} = 0$.

2. $R_m = R_i$.

In this case the factor of the electric current transmission is equal to one. $\eta = 1$. Therefore, after the equation (7) we receive

$$U_{SP} = E_{SP}.$$

3. $R_m \gg R_i$.

It is very difficult to realize this case. It can occur only, if a very low-salinity water serves as the mud. Then we can record $\eta = 2$ and after equation (7) we shall receive $U_{SP} = 2E_{SP}$.

The most interesting case of all mentioned cases is the first one. It has a concrete consequence for well-logging, too. The mud having a high salinity is perfectly able to wipe out any information about the bed. Within the electric resistance measurement, the electric current flows largely through a highly conductive mud,

so that the specific electric resistance of rock is not able to assert itself. The electric contrast of either environment is too high and therefore throughout the self-potential measurement the electrically conductive mud does not allow potential E_{SP} to penetrate on the registrating electrode. The curves of the self potential and of the specific electrical resistance of a salty mud are characterized by low values, a low differentiation, and a monotonous character.

The boreholes drilled in rocks having a relatively high specific electric resistance are characterized by similar, but not by the same curves. The electric conductivity of mud is usually low. Therefore the curve of the specific electric resistance is considerably differentiated and has high values. But the electric contrast between mud and rock is high. For the curve of the self potential the same effect is produced as for the curve of the high salinity. The curve of the self potential is monotonous and differentiable to a very low degree.

It might have been worthwile to have used in this case a mud having a higher specific electric resistance. This could have had a positive influence changing the monotonous character of the curve.

Let us go back again to equation (7). This equation still furnishes us with the following information. In case, that any conditions being important for forming of the self potential be not favourable, we receive $E_{SP} = 0$ and on the measuring electrode we register then $U_{SP} = 0$. This may occur if we observe that either $\alpha = 0$, or that the ratio contrast between R_{mf} and R_w equals one. According to equation (7) we obtain $E_{SP} = 0$. It is really difficult to distinguish the conditions under which the factors η and E_{SP} are applied there. The two processes are not mutually excludable, but they rather complete each other. Where $E_{SP} = 0$ we obtain $U_{SP} \doteq 0$. But where $E_{SP} \neq 0$, the process of electric current transmission begins and the mentioned factor will reduce the values of E_{SP}. Therefore, we shall register on the measuring electrode lower values of the self potential than the real values recorded at the wall of borehole. E.g. $U_{SP} < E_{SP}$.

This is of considerable significance for evaluation. Up to now it has been premised, that $\eta = 1$ which meant, that medium was electrically homogeneous. $R_i = R_m$. The consequence thereof was, that $U_{SP} = E_{SP}$. The application of the electric field theory shows, that this premise is not right, because the electric inhomogeneity of the environment influences the self potential. In some cases even, when $\eta = 0$, we observe such an extensive smoothing of the self potential curve that we receive the false line of clay there, where the really permeable beds exist.

Figures 1 to 7 show the measurement of the self potential and of the specific electric resistance from various boreholes.

Figure 1 representes a well-logging record of the so-called formation having been drilled through by borehole Dlhé Klčovo-1. This formation is situated in the depth interval of 1 132 – 1 320 m and has several beds of salt. The total thickness of the salt attains 60 m. The other rocks of that formation consist of anhydrite, gypsum, sandstones, and a calcareous clay. The specific electrical resistance has

low deflections and a monotonous character. The same is observable on the curve of the self potential. Even though we cannot exclude that some of the beds of the illustrated profile have $E_{SP} = 0$, there is a higher probability that the mentioned smoothness of the self-potential curve is evoked by factor η as a consequence of salting of the mud.

A similar situation is at borehole Albínov-7. With respect to the geological profile there is a Karpatian Formation at the depth of 2 895 – 4 000 m there. It has two beds of pure salt, their thickness is 60 m and 80 m. The curve of the specific electric resistance is more differentiated there than in the last example, but altogether

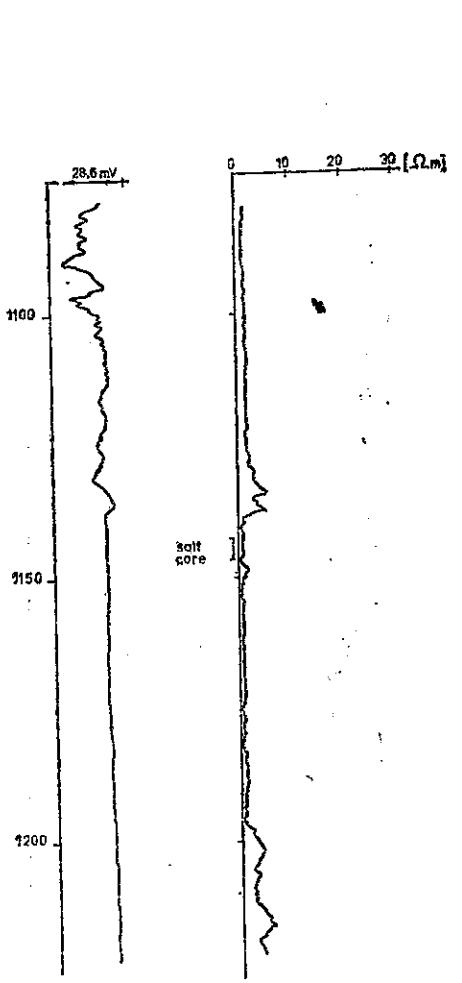

1. Curves of the self potential and the specific electrical resistance of borehole Dlhé Klčovo-1

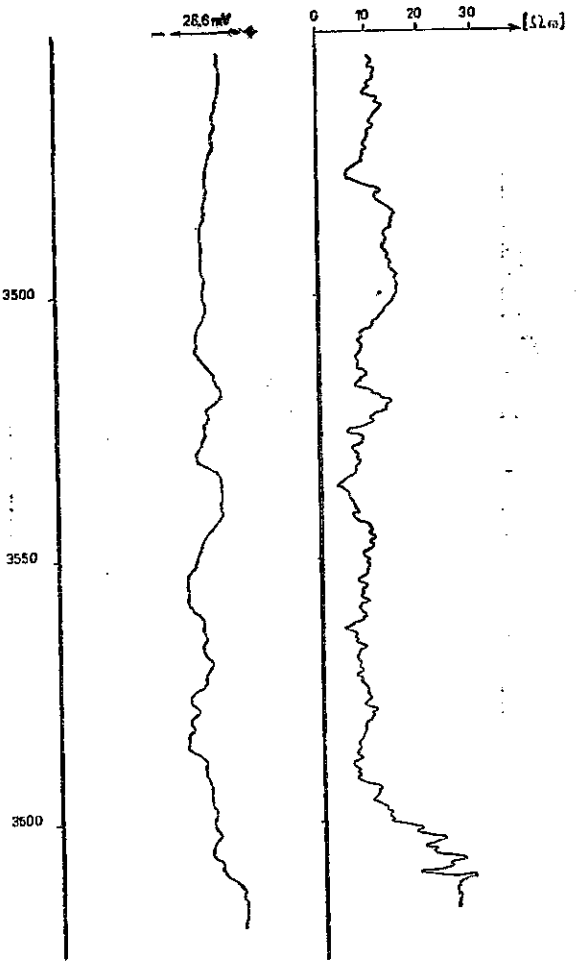

2. Curves of the self potential and the specific electrical resistance of borehole Albínov-7

the values of the specific electric resistance are not high. The curve of the self potential has a more differentiated character, too, but the smoothness of the curve is evident. Also in this case, we rather suppose an influence of the transmission factor η on the registration of the self potential, as the mud was salted.

Figure 3 refers to borehole Ždánice-4. The geological profile is represented by the Ždánice–Hustopeče Formation in the depth interval of 0–915 m. It consists of grey calcareous shales alternating with grey fine-grained calcareous sandstones. The specific electric resistance has relatively high deflections and its character is differentiated. But the record of the self potential has a smooth character. The

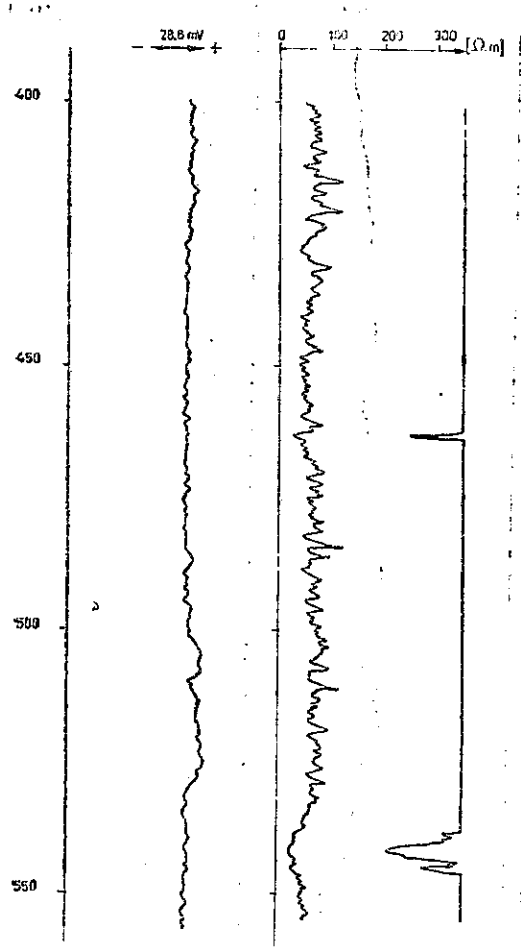

3. Curve of the self potential and the specific electrical resistance of borehole Ždánice-4

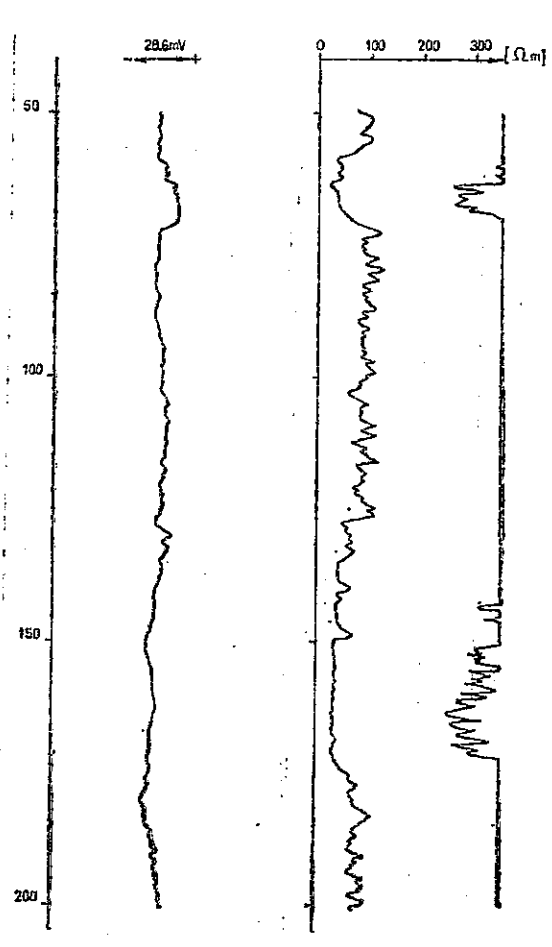

4. Curves of the self potential and the specific electrical resistance of borehole Ždánice-16

mentioned conditions for forming of the self potential may not be favourable there. Nevertheless, some of the sandstones may be fissured and therefore we cannot completely exclude local more favourable conditions.

The other illustration, figure 4, belongs again into the Ždánice – Hustopeče Formation. This formation was found in the depth of 0 – 653 m. The well-logging record is characterized by a differentiable curve of the specific electrical resistance and the monotonous curve of the self potential. Although favourable conditions for the forming of the self potential are not generally present there, we cannot exclude some fissure zones inside the mentioned formation, where $E_{SP} \neq 0$.

Figure 5 represents borehole Ždánice-18. The biotite granodiorite has been altered by hydrothermal process and mylonitized. The boundary-line begins in the

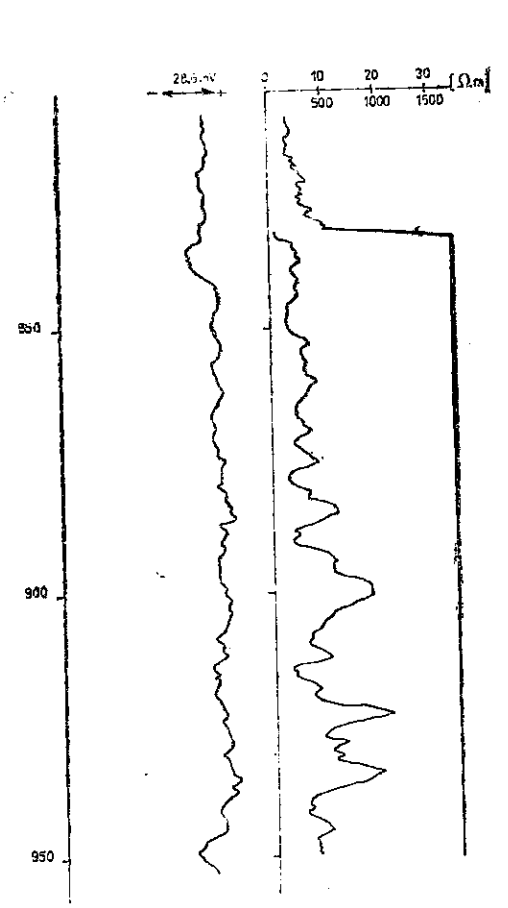

5. Curves of the self potential and the specific electrical resistance of borehole Ždánice-18

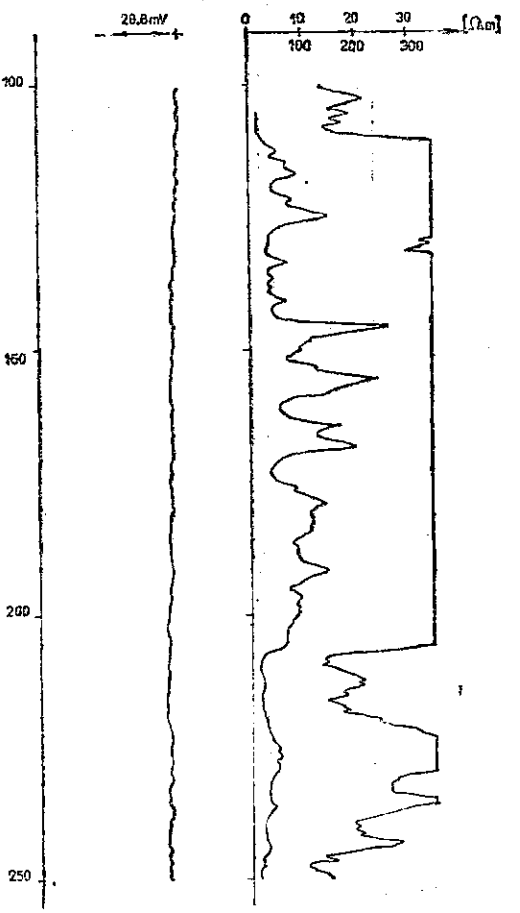

6. Curves of the self potential and the specific electrical resistance of borehole Lubná-5

depth of 834 m. The specific electrical resistance is extraordinarily high. The curve of the self potential – with respect to differentiation – is comparable with the curve of borehole Albínov-7. By this borehole permeable beds have been attained resulting from the mentioned mylonitization. In the upper part of the granodiorite, there is a deposit of oil and gas. Therefore we can expect good conditions for a forming of the self potential.

The next illustration belongs to borehole Lubná-5 (fig. 6). The geological unit is the Magura Flysch Formation there. The specific electrical resistance is characterized by high deflections and its record is differentiated. However, the well-logging record of the self potential is perfectly smooth and comparable with the curve of the borehole Dlhé Klčovo-1. The conditions for the forming of the self potential are not favourable in that formation. But in the flysch there exist local fissure zones, that can have $E_{SP} \neq 0$.

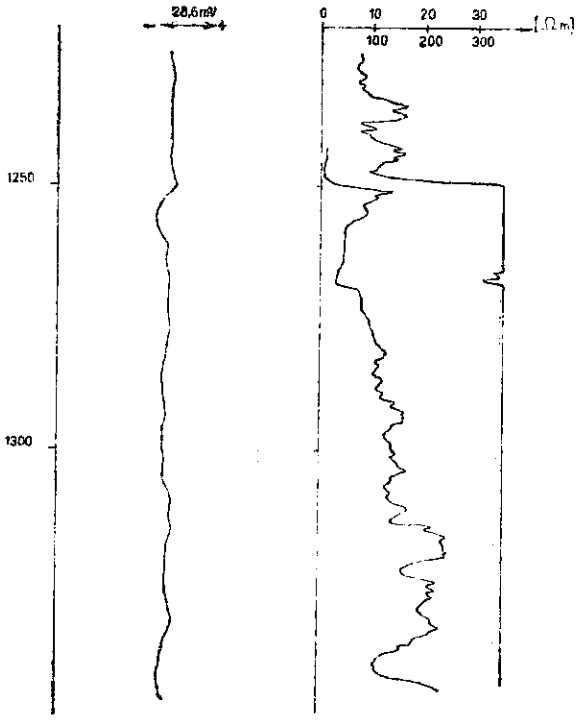

7. Curves of the self potential and the specific electrical resistance of borehole Lubná-6

The last illustration, figure 7, represents borehole Lubná-6 drilled into crumbling kaolinized granite. The specific electrical resistance reaches high values, whereas the curve of the self potential is only sporadically moderately undulated. The upper part of the mentioned granite is easily permeable and we may therefore expect favourable conditions for the forming of the self potential.

I shall now attempt to express the factor of the electric current transmission for every illustration. The results are in table 1.

The specific electrical resistance of the mud was registered by a resistivimeter on the surface of earth for an outside temperature. The specific electrical resistance of the mud having been registered on the surface of the Earth, is in column 2. It is marked as $R_m(t_0)$. The temperature characterizing the ohmic measurement has been marked as t_0 and we can find it in column 3. Table 1 shows a depth interval and the respective temperature.

The mentioned temperature marked as t is in column 5. It has been determined from a temperature well-logging registration.

The specific electrical resistance of the mud in the determined depth interval was calculated after Dachnov (1985).

$$R_m(t) = \frac{R_m(t_0)}{1 + 0.021\,6\,.\,(t - t_0) + 0.000\,008\,.\,(t - t_0)}\,. \tag{9}$$

The mentioned resistance is marked as $R_m(t)$ (see column 6, table 1). The specific

Table 1

Evaluation of the mud electric current transmission in boreholes situated in the regions Dlhé Klčovo, Albínov, Ždánice and Lubná

Borehole	$R_m(t_0)$ [Ω m]	t_0 [°C]	Interval [m]	t [°C]	$R_m(t)$ [Ω m]	R_1 [Ω m]	η
Dlhé Klčovo-1	0.07	18	1 150 – 1 195 1 200 – 1 220	48	0.04	1 4	0.077 0.020
Albínov-7	0.30	20	3 505 – 3 590 3 600 – 3 620	105	0.11	8 25	0.027 0.009
Ždánice-4	5.00	18	440 – 470 470 – 530	23	4.50	50 75	0.165 0.113
Ždánice-16	5.20	10	128 – 170 70 – 128	17	4.50	40 90	0.202 0.095
Ždánice-18	4.50	20	845 – 850 898 – 905	30	3.70	175 950	0.041 0.008
Lubná-5	3.60	12	128 – 132 145 – 148	18	3.20	30 260	0.193 0.024
Lubná-6	6.90	24	1 230 – 1 245 1 315 – 1 335	72	3.40	16 225	0.351 0.030
Column	1	2	3	4	5	6	7

electrical resistance of the invasion zone was not accurantly determined. I have applied for calculation the value of the electric lateral as the value lying near the real value. For this electrical resistance, symbol R_i has been used (see column 7).

Now we may compare the results. All illustrations have shown, that the boreholes having a mud of high salinity and those having a fresh mud and an invasion zone of a high specific electrical resistance, have very similar the self-potential records. We may say, that in several cases these records of the self potential are almost identical.

The factor of electric current transmission through the mud varies within the determined interval and sometimes it varies considerably. However, the lower boundary-level of all examples has values lying very close to one another. The nearest comparable values belong the boreholes Albínov-7 and Ždánice-18. The electric current transmission factor of the mud attains at the borehole Albínov-7, that is characterized by a salty mud, the values of 0.009 – 0.027 and at the borehole Ždánice-18 having a fresh mud the values of 0.008 – 0.041. Thus the visual similarity of the self-potential curves is validated by numerical data of the electric current transmission factor.

The electric current of the self potential does not flow through a permeable bed and through the mud only. It flows also over adjacent rocks that are continuous with the mentioned permeable bed. Therefore, their influence must be considered, too. Now let us go back to the equation (6), and with respect to it we write an analogous equation

$$\eta = \frac{2R_m}{R_m + R_i'}. \tag{10}$$

The value R'_i can be expressed in the following way:

$$R_i' = \frac{R_i \cdot R_s}{R_i + R_s}, \tag{11}$$

where

R_i – the specific electric resistance of an invasion zone [Ωm],
R_s – the specific electric resistance of adjacent rocks [Ωm].

After substitution of this formula (11) into the equation (10) we shall receive the following expression:

$$\eta = 2 \cdot \frac{R_m \cdot R_i + R_m \cdot R_s}{R_m \cdot R_i + R_m \cdot R_s + R_i \cdot R_s}. \tag{12}$$

We shall modify this equation into a form that is suitable for an analysis:

$$\eta = \frac{2 \cdot \left[\frac{R_m}{R_i} + \frac{R_m}{R_i} \cdot \frac{R_s}{R_i} \right]}{\left[\frac{R_m}{R_i} + \frac{R_m}{R_i} \cdot \frac{R_s}{R_i} + \frac{R_s}{R_i} \right]}. \tag{13}$$

Now we are able to analyse this equation.

1. For $R_s \ll R_i$ the ratio $\frac{R_s}{R_i} = 0$ and the transmission factor η is independent of the ratio. Its value $\eta = 2$.

2. For $R_s = R_i$ the ratio $\frac{R_s}{R_i} = 1$. We shall obtain this equation:

$$\eta = \frac{4 \cdot \frac{R_m}{R_i}}{1 + 2 \cdot \frac{R_m}{R_i}}. \tag{14}$$

   a) If $R_m \ll R_i$, the ratio $\frac{R_m}{R_i} = 0$ and the transmission factor η is equal to zero, too. $\eta = 0$.

   b) If $R_m = R_i$, the ratio $\frac{R_m}{R_i} = 1$. We shall obtain, that $\eta = \frac{4}{3}$.

   c) If $R_m \gg R_i$, we can write, that $1 + 2 \cdot \frac{R_m}{R_i} = 2 \cdot \frac{R_m}{R_i}$. We shall receive, that $\eta = 2$.

3. For $R_s \gg R_i$ the ratio $\frac{R_s}{R_i} = \infty$. We shall obtain the following equation. It is the equation characterizing an asymptote:

$$\eta = \frac{2 \cdot \frac{R_m}{R_i}}{1 + \frac{R_m}{R_i}}.$$

This is equation (8) which has already been analysed. It is a partial case of the equation (13) on condition that $R_s \gg R_i$. The mentioned equation (13) was solved in the form of the correction chart for these conditions. ($0 \leqq \eta \leqq 1$, $0.001 \leqq \frac{R_m}{R_i} < 1$, $0.01 \leqq \frac{R_s}{R_i} \leqq 100$).

The formula (13) for $R_m \ll R_i$ attains the minimum, when $\eta = 0$. If $R_s \ll R_i$, we shall obtain, on the contrary, a maximum, when $\eta = 2$. Under certain conditions, the equation (13) has one point on inflection. If $R_s \gg R_i$, then the equation (13) has a tendency to pass from its fundamental form to the form of the equation (8), which is the equation of an asymptote.

Segesman (1962) published his results of modeling on the resistor network analog. The published correction charts include not only such parameters as the specific electrical resistance of an invasion zone, of the adjacent beds and of the mud, but also further parameters such as the diameter of the borehole, the diameter of the invasion zone, and the bed thickness. As this is another transformation of the illustrated curves, where the electric current transmission factor still depends

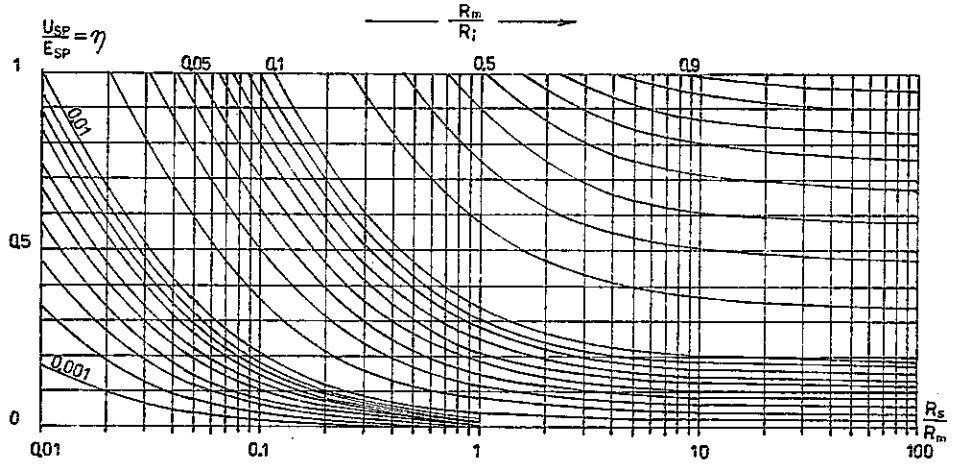

8. Correction chart $\eta = f(R_i, R, R_m)$

on the mentioned further parameters not expressed in equation (13), we cannot directly compare Segesman's correction charts with this equation (13), even though the curves are similar in shape and character to the correction chart constructed after equation (13). But it is necessary to emphasize the fact, that also after Segesman's correction charts, one fundamental phenomenon becomes evident there which has a lot in common with the mentioned equation (13). We can observe, when $R_i \gg R_m$, then $\eta = 0$. Thus, the mentioned correction charts verify the significance of the specific electric resistance of the mud on self-potential measurement.

If we summarize the results of the analysis, we arrive at the following conclusions.

1. The influence of an electric inhomogeneity of the environment on a measurement of the self potential is evident. This influence must be considered when evaluating the self-potential curves. The premise, that the environment is electrically homogeneous, is not right.

2. By means of the influence of the electric current transmission factor on self-potential registration we are able to explain the character of the self-potential curve not only under the conditions of a salty mud, but even in a medium, where

boreholes have been drilled through rocks having a high specific electrical resistance of the invasion zone and where the mud is fresh.

3. After the formulas (13) and (7) we can recalculate the registered data U_{SP} to E_{SP}. For such a recalculation we need a continuous depth-related curve of the electric current transmission factor η. Such a curve can be evaluated, if the parameters R_m, R_s, R_i are known. The mentioned parameter R_m can be directly registered by a continuous well-logging resistivimeter. The remaining parameters R_s and R_i can again be registered by means of the microlog or proximity log. Two depth-related continuous curves indicate the transmission factor η.

During the regressive evaluation of the self-potential curve, we must consider-with respect to equation (7), that in certain cases the self potential on the wall of the borehole can be zero, when $E_{SP} = 0$. Therefore, we should take into account some further methods such as gamma ray log. An information about the specific electric resistance of the stratum water can be obtained, for example, by using the R_{wa} comparison method.

We can expect, that the corrected curve of the self potential after formula (7) will be more differentiated and that the permeable beds will be more easily recognizable. This could be important in a geological profile consisting of rocks having a higher specific electrical resistance and a fresh mud. For well-logging practice, when the interpreter has to determine the permeable beds in the just mentioned rocks, this should certainly be valuable.

K tisku doporučil A. Těžký

Přeložil autor

References

Dachnov, V. N. (1967): Električeskie i magnitnye metody issledovanija skvažin. – Nedra. Moskva.

Dachnov, V. N. (1985): Geofizičeskie metody opredelenija kollektorskich svojstv i neftegazonasyščenija gornych porod. – Nedra. Moskva.

De Witte, L. (1950): Relations between resistivities and fluid contents of porous rocks. – Oil Gas J., 49, 16. Tulsa.

Doll, H. G. (1950): The SP in shaly sands. – J. Petrol. Technol., 2, 7. Dallas.

Komarov, S. G. (1973): Geofizičeskie metody issledovanija skvažin. – Nedra. Moskva.

Kozel, J. (1965): Difúzně adsorpční potenciály a jejich vztah ke kolektorským vlastnostem hornin. Závěrečná zpráva. – MS Geofyzika, s. p. Brno.

Segesman, F. (1962): New SP correction charts. – Geophysics, 27, 6. Tulsa.

Těžký, A. (1961): Praktická použitelnost metod pro interpretaci elektrické karotáže v jílovitých píscích. – Užitá Geofyz., 1, *201–229*. Praha.

Tixier, M. F. (1949): Electric log analysis in the Rocky Mountains. – Oil Gas J., 48, 6. Tulsa.

Vendel'štejn, B. J. (1966): Issledovanie razrezov neftjanych i gazovych skvažin metodom sobstvennych potencialov. – Nedra. Moskva.

Vliv propouštění elektrického proudu výplachem na měření vlastních potenciálů

(Résumé anglického textu)

František Ryšavý

Předloženo 27. října 1987

V předložené práci je vysvětlen způsob, jak se projevuje vliv koeficientu propouštění elektrického proudu na rozhraní výplach—hornina na měření vlastních potenciálů. Ukazuje se, že zhlazení křivky vlastních potenciálů, vzniklé zvýšením obsahu NaCl ve výplachu po provrtání ložiska soli a zhlazení téže křivky v případě výplachu s nízkým obsahem NaCl, ale s poměrně vysokým měrným elektrickým odporem zóny filtrace, může být způsobeno stejným faktorem — nízkou hodnotou koeficientu propouštění elektrického proudu vlastních potenciálů ve výplachu.

Rozborem předložených rovnic jsme dospěli k těmto závěrům:

1. Vliv elektrické nehomogenity okolního prostředí na měření vlastních potenciálů je zcela zřejmý. Proto jej při interpretaci křivek vlastních potenciálů musíme brát v úvahu. Předpoklad, že okolní prostředí může být považováno za elektricky homogenní, je nesprávný.

2. Prostřednictvím koeficientu propouštění elektrického proudu vlastních potenciálů můžeme vysvětlit charakter jejich křivky nejen v podmínkách silně mineralizovaného výplachu, ale i v podmínkách provrtání horniny s poměrně vysokým měrným elektrickým odporem zóny filtrace, přičemž výplach byl jen slabě mineralizován.

3. Měření vlastních potenciálů ovlivňuje nejen měrný elektrický odpor výplachu a zóny filtrace, ale také měrný elektrický odpor okolních hornin. Uplatňuje se zejména tehdy, když platí, že $R_s \ll R_i$.

4. Podle rovnic (13) a (7) můžeme provést přepočet hodnot U_{SP} na hodnoty E_{SP}. Pro zmíněný přepočet potřebujeme získat spojitou křivku koeficientu propouštění η s hloubkou. Tuto křivku můžeme sestrojit podle rovnice (13), známe-li parametry R_m, R_i a R_s. Parametr R_m můžeme přímo registrovat ve tvaru spojité křivky s hloubkou podle údajů hlubinného resistivimetru. Zbývající parametry R_i a R_s můžeme přímo měřit formou spojité křivky s hloubkou na základě údajů Mikrologu nebo Proximity logu. Podle všech těchto údajů můžeme zmíněný koeficient propouštění elektrického proudu vypočítat a později podle rovnice (7) provést přepočet hodnot U_{SP} na hodnoty E_{SP}.

Předtím však je třeba zvážit ty případy, kdy pro vznik vlastních potenciálů nejsou ve vrtu vhodné podmínky. V takových případech platí, že $E_{SP} = 0$. Proto musíme přihlížet i k jiným karotážním metodám, jako je např. metoda gama-karotáže. Informaci o měrném elektrickém odporu vrstevní vody můžeme získat např. podle srovnávací metody R_{wn}.

Soudobé technické prostředky umožňují zkonstruovat spojitou závislost koeficientu propouštění elektrického proudu vlastních potenciálů na hloubce. Tato závislost se dá pak dobře využít pro přepočet naměřených vlastních potenciálů na elektrodě ve výplachu na vlastní potenciály na stěně vrtu. To může mít svůj význam pro vyčleňování propustných vrstev v horninách geologicky starších, vyznačujících se vyšším měrným elektrickým odporem v zóně filtrace a poměrně málo mineralizovaným výplachem.

Vysvětlivky k tabulce a obrázkům

Tabulka 1. Interpretace koeficientu propouštění elektrického proudu výplachem ve vrtech z oblasti Dlhé Klčovo, Albínov, Ždánice a Lubná.

1. Křivky vlastních potenciálů a měrného elektrického odporu z vrtu Dlhé Klčovo-1.
2. Křivky vlastních potenciálů a měrného elektrického odporu z vrtu Albínov-7.
3. Křivky vlastních potenciálů a měrného elektrického odporu z vrtu Ždánice-4.
4. Křivky vlastních potenciálů a měrného elektrického odporu z vrtu Ždánice-16.
5. Křivky vlastních potenciálů a měrného elektrického odporu z vrtu Ždánice-18.
6. Křivky vlastních potenciálů a měrného elektrického odporu z vrtu Lubná-5.
7. Křivky vlastních potenciálů a měrného elektrického odporu z vrtu Lubná-6.
8. Nomogram $\eta = f(R_t, R_s, R_m)$.

Влияние коэффициента пропускания электрического тока в буровом растворе на измерение собственных потенциалов

В горных породах более высокого геологического возраста существуют такие проницаемые пласты, которые нельзя выделить только по удельному электрическому сопротивлению и кривой собственных потенциалов. Их характеризует относительно большое удельное электрическое сопротивление зоны проникновения и более высокое удельное сопротивление бурового раствора. Кривая собственных потенциалов в таких пластах чрезвычайно гладка и имеет монотонный характер. Она похожа на кривую собственных потенциалов, которая возникает в случае соленого раствора. Кажется, что оба случая имеют общий повод — небольшой коэффициент пропускания электрического тока собственных потенциалов границей раздела буровой раствор — горная порода, оказывающий воздействие на кривую собственных потенциалов. Этот факт можно использовать для пересчета кривой собственных потенциалов, чтобы достичь кривой более сложного характера и, таким образом, интерпретировать и выделять упомянутые проницаемые пласты.

Přeložil autor

SBORNÍK GEOLOGICKÝCH VĚD
JOURNAL OF GEOLOGICAL SCIENCES

užitá geofyzika

---

applied geophysics

24

Vydal Ústřední ústav geologický
v Academii, nakladatelství Československé akademie věd
Praha 1990

Vědecký redaktor: RNDr. Karel Cidlinský, CSc.

Obálku navrhl Miloslav Cihelka D
Odpovědná redaktorka: Vlasta Čechová
Překlady: P. Kellnerová, A. Kříž, H. Kuksová, D. Malíková, E. Pešková, G. Plíva
Technická redaktorka: Magdaléna Sokolová

Vydání I. — 200 stran (73 obr.)

Vytiskl Tisk, knižní výroba, n. p., Brno, závod 1
12,86 AA — 13,06 VA
Náklad 600 výtisků — 03/9 — 9442 — 446-427-90

Cena brožovaného výtisku Kčs 24,—
509/827

ISBN 80-7075-011-1